Understanding the effects of hypoxia on spinal cord early myelinating oligodendrocytes *in vitro*

Colin Lindsay Crawford BSc (Hons), MRes

A thesis submitted in fulfilment of the requirements of the
University of Glasgow for the degree of
Doctor of Philosophy

College of Medical, Veterinary and Life Sciences
Institute of Infection, Immunity and Inflammation

September 2021

Abstract

In the developing brain, pre-/early myelinating oligodendrocytes (EMOLs) are particularly vulnerable to hypoxia-ischaemia; however, much less is known about how this impacts spinal cord EMOLs. Indeed, in an *in vivo* mouse model of spinal muscular atrophy, myelinogenesis proceeds normally despite significantly reduced vascularisation of the developing spinal cord. Furthermore, even in the healthy spinal cord, perfusion is up to 60% lower in comparison to the brain. Together, these observations raise the possibility there are anatomically divergent susceptibilities of EMOLs to hypoxia-ischaemia. Thus, this thesis addressed the hypothesis that spinal cord EMOLs are relatively resistant to hypoxia-ischaemia and associated secondary consequences.

To test our hypothesis, we used murine spinal cord mixed glial cultures, which we showed contain EMOLs (indicated by BCAS1 expression), astrocytes, and microglia, but lack neuronal cell bodies, making these suitable for modelling spinal cord white matter. The morphology of DAPI-stained nuclei was confirmed to be a useful indicator of cell survival.

To examine the response of spinal cord EMOLs to hypoxia, cell cultures were subjected to chemical hypoxia for 5 or 24 hours using azide, or to oxygen deprivation for 24 hours. Five hours chemical hypoxia did not cause death of EMOLs (or astrocytes), whereas they failed to survive 24 hours treatment. Surprisingly, oxygen deprivation had little impact on survival, even when glucose was withdrawn, raising doubts about the efficacy of the method. Together, we conclude that spinal cord EMOLs are tolerant of short-term hypoxia.

As neither chemically-induced hypoxia nor oxygen deprivation led to acidosis of the cell culture media, as would occur in the CNS, we next examined the impact of this secondary component of the hypoxic environment. Cells were maintained for 6 days at physiological pH or in increasingly acidic conditions. Reducing pH to 6.8 or lower led to a significant decrease in the densities of EMOLs. Surprisingly, the complete withdrawal of glucose (pyruvate and glutamine) did not compound this and had only a minor effect on cell survival at physiological pH after 6 days. This unexpected observation led us to ask whether our survival assay was sufficiently sensitive. We confirmed this with a lactate dehydrogenase release assay and by further challenging the cells with reintroduction of glucose or complete withdrawal of amino acids and vitamins.

The unexpected survival of EMOLs, and also of astrocytes, in the absence of glucose led us to hypothesise that astrocyte energy reserves might sustain both astrocytes and EMOLs under exogenous energy substrate deprivation. To address this, we explored trans-cellular exchange routes and found EMOLs were dye-coupled to astrocytes by nanotube-like structures: a putative conduit for the transfer of energy substrates.

Recently, it has been demonstrated that astrocytes can accumulate lipid droplets, the β-oxidation of which could potentially provide fuel for cell survival in the absence of exogenous energy substrates. Therefore, we next looked for evidence of lipid droplets in these spinal cord-derived cell cultures and found that lipid droplets were abundant in astrocytes. Consistent with this, lipidomic analyses demonstrated a significant reduction in triglycerides (a lipid droplet-associated species) after 6 days of energy substrate deprivation in mixed glial cultures, but not EMOL-enriched cultures, compared to 5 mM glucose controls.

In all, these data suggest that spinal cord EMOLs are relatively resilient to hypoxia-ischaemia as demonstrated by their tolerance of short-term hypoxia and exogenous energy substrate deprivation in this *in vitro* model. The disease-relevant implications remain to be examined and the source of lipid droplet substrates to be determined.

I dedicate this thesis to my grandparents, Marna and Robert.

Acknowledgements

I would like to express my sincere gratitude to my supervisor Professor Julia Edgar for her mentorship and guidance throughout my PhD. Most of all, I thank Julia for her support, hands-on approach to training, and for always encouraging me to gain the most from my PhD. Her dedication to science, passion for debate, and drive for excellence has set the bar high and I hope to carry these attributes forward in my own career.

I also thank my second supervisor, Prof. Michael Ferguson; my assessors, Prof. James Brewer and Prof. Alain Kohl; friend of the lab, Prof. Chris Linington; our collaborator, Prof. Klaus-Armin Nave; my *viva voce* examiners.

I am grateful for the training and lab space provided by Dr Euan Brown at Heriot-Watt University during my dye-filling experiments. A special thank you to Dr Paul Montague for generously carrying out our genotyping. I also thank Margaret Mullin for processing my electron microscopy samples. Lipidomic analyses were carried out at University Hospital Zurich by Prof. Thorsten Hornemann and Dr Gergely Karsai and I am very grateful for their contribution. Thanks also to the CRF staff who cared for our mice. Finally, I acknowledge the contribution of animal life, which was always carefully considered.

Members of the Edgar lab (past and present), you have all helped me in one way or another. Whether it was discussions at lab meetings, laughs in the office, a sneaky coffee break, or just listening to me whinging. Diana, Katie, Katja, Lina, Lorna, and Shazia, thank you all.

To my fellow PhD colleagues and now forever friends, the whole experience would not have been the same without you. A special mention must go to Clare and Rebecca: our daily renditions of Wicked, outbursts of “oh ya ham!”, and fits of uncontrollable laughter will always be among the best memories of my PhD. To the whole neuro gang, now including Jen, Maddy, Rhona, Susan, Sue, and Verena (but not forgetting those who are gone), you have made this adventure such a laugh with the great times we had. Thank you all.

Thank you to all my friends out of the lab too (apparently there’s an “outside” of the lab). A special mention goes to Kirsty: we started our uni careers together many years ago as we stepped off the train at QMU and look at us now! Thank you for keeping me sane throughout with many laughs, many jaunts, and many routines.

Finally, I thank all my family, including my dogs Bailey and Sandi. I especially thank my grandparents to whom this thesis is dedicated. I would not be where I am today if it was not for your encouragement, endless support, and love. I’m *still* not sure when I’ll be finished at the uni though...

Publications

ORCID iD: 0000-0001-7154-5698

Papers

Schultz, V., Barrie, J. A., Donald, C. L., **Crawford, C. L.**, Mullin, M., Anderson, T. J., Solomon, T., Barnett, S. C., Linington, C., Kohl, A., Willison, H. J., Edgar, J. M. (2021). "Oligodendrocytes are susceptible to Zika virus infection in a mouse model of perinatal exposure: implications for CNS complications". *Glia*, 69, pp. 2023–2036. doi: doi.org/10.1002/glia.24010.

Bijland, S., Thomson, G., Euston, M., Michail, K., Thümmler, K., Mücklisch, S., **Crawford, C. L.**, Barnett, S. C., McLaughlin, M., Anderson, T. J., Linington, C., Brown, E. R., Kalkman, E. R., Edgar, J. M. (2019). "An *in vitro* model for studying CNS white matter: functional properties and experimental approaches". *F1000Research*, 8:117. doi: doi.org/10.12688/f1000research.16802.1.

Abstracts

Crawford, C. L., Smith, R., Yazdani, S. K., Euston, M., Kassmann, C., Kneussel, M., Nave, K.-A., Edgar, J. M. "The myelinic channel system: a highway to the axo-glial junction". *Cold Spring Harbour Glia in Health & Disease*. Online conference. July 16-19, 2020.

Crawford, C. L., Ferguson, M. A. J., Nave, K.-A., Edgar, J. M. "Metabolic characteristics of glia *in vitro*: implications for axonal support?". *Federation of European Neuroscience Societies (FENS2020)*. Glasgow, Scotland, United Kingdom (online). July 11-15, 2020.

Crawford, C. L., Ferguson, M. A. J., Nave, K.-A., Edgar, J. M. "Metabolic characteristics of glia *in vitro*: implications for axonal support?". *7th Molecular Mechanisms of Axon Degeneration Meeting*. Loch Lomond, Scotland, United Kingdom. March 11-14, 2019.

Crawford, C. L., Ferguson, M. A. J., Edgar, J. M. "Metabolic characterisation of oligodendrocytes *in vitro*". *Myelin Netzwerk*. Kassel, Germany. February 28 - March 2, 2019.

Euston, M., **Crawford C. L.**, Smith, R., Marylin, M., Thies, E., Kassmann, C., Brown, E., Kneussel, M., Nave, K.-A., Edgar, J. M. "The myelinic channel: a highway to the axo-glial junction". *7th Molecular Mechanisms of Axon Degeneration Meeting*. Loch Lomond, Scotland, United Kingdom. March 11-14, 2019.

Declaration of authorship

I declare that, except where explicit reference is made to the contribution of others, this thesis is the result of my own work and has not been submitted for any other degree at the University of Glasgow or any other institution.

Signed: Colin Lindsay Crawford BSc (Hons), MRes

Date: 13th December 2021

Contents

List of figures

List of tables

List of abbreviations

4-HT	4-Hydroxytamoxifen
AcCa	Acylcarnitine
ADP	Adenosine diphosphate
ANLS	Astrocyte-neurone lactate shuttle
ATP	Adenosine triphosphate
AZ	Sodium azide
BBB	Blood-brain barrier
BCAS1	Breast carcinoma amplified sequence 1
CACT	Carnitine acylcarnitine translocase
CC3	Cleaved caspase-3
cDNA	Complementary DNA
CNP	2′-3′-cyclic-nucleotide 3′-phosphodiesterase
CNS	Central nervous system
CoA	Coenzyme-A
CPT1	Carnitine palmitoyltransferase 1
CPT2	Carnitine palmitoyltransferase 2
Cx	Connexin
DAG	Diacylglycerol
diH_2O	Deionised water
DIV	Day *in vitro*
DM	DMEM-based media (no glucose, pyruvate, or glutamine unless supplemented)
DMEM	Dulbecco's Modified Eagle Medium
DNase	Deoxyribonuclease

E	Embryonic day
EMOL	Pre-/early myelinating oligodendrocyte
ETC	Electron transport chain
FA	Fatty acid
FAD	Flavin adenine dinucleotide
$FADH_2$	Flavin adenine dinucleotide + 2 hydrogen
GAPDH	Glyceraldehyde 3-phosphate dehydrogenase
gDNA	Genomic deoxyribonucleic acid
GLUT	Glucose transporter
GOI	Gene of interest
HBSS	Hank's balanced salt solution
HDAC	Histone deacetylase
HE	Highly enriched DMEM-based media rich in energy substrates (25 mM glucose, 1 mM pyruvate, 4 mM glutamine)
HI	Heat inactivated
HIF1	Hypoxia-inducible factor 1
IA	Sodium iodoacetate
IFNγ	Interferon-gamma
LCFA	Long-chain fatty acid
LDH	Lactate dehydrogenase
MACS	Magnetic-activated cell sorting
MAG	Myelin-associated glycoprotein
MBP	Myelin basic protein
MCT	Monocarboxylate transporter
MMC	Methanol:methyl *tertiary*-butyl ether:chloroform
MOG	Myelin oligodendrocyte glycoprotein

MS	Multiple sclerosis
mTORC1	Mammalian target of rapamycin complex 1
NAD^+	Nicotinamide adenine dinucleotide
NADH	Nicotinamide adenine dinucleotide + hydrogen
NADPH	Nicotinamide adenine dinucleotide phosphate + hydrogen
NEC	Neuroepithelial cell
nfH_2O	Nuclease-free water
NRT	No reverse-transcriptase
NSC	Neural stem cell
OGD	Oxygen-glucose deprivation
OPC	Oligodendrocyte progenitor cell
P	Postnatal day
PBS	Phosphate buffered saline
PEOT-*Tg*	PLP-$CreER^{T2}$::Cnp-mEos2-PTS1::Ai14(Rosa26-tdT) transgenic
PFA	Paraformaldehyde
PI	Propidium iodide
PLP	Proteolipid protein
PVL	Periventricular leukomalacia
r_p	Pearson correlation coefficient
ROI	Region of interest
ROS	Reactive oxygen species
SEM	Standard error of the mean
SMA	Spinal muscular atrophy
SMN	Survival of motor neuron
SO	Salts-only (cell culture media containing only the inorganic salts of DMEM)

t0	Experimental time zero
TCA	Tricarboxylic acid
TG	Triglyceride (also known as triacylglycerol)
TNF	Tumour necrosis factor
VLCFA	Very-long-chain fatty acid
WMI	White matter injury
WT	Wildtype C57BL/6

Chapter 1

Literature review

1.1 Introduction

This thesis set out to investigate the response of spinal cord pre-/early myelinating oligodendrocytes (EMOLs) to hypoxia-ischaemia and its secondary consequences, such as acidosis, deprivation of energy substrates and/or vitamins and amino acids, and injury by inflammatory factors. Due to the unexpected observation that EMOLs and associated glia survived in cell culture for six days in the absence of glucose and other exogenous energy substrates, the focus moved towards determining the cell-intrinsic factors spinal cord glial cells use for survival in these circumstances. The following literature review provides an overview of the central nervous system (CNS), its energy metabolism, and vulnerability to hypoxia-ischaemia: placing this body of work in the context of developmental myelination.

1.2 An overview of the central nervous system

The CNS is the coordination centre for most of the body's functions, responsible for integrating sensory information from the periphery and directing appropriate responses to regulate such things as temperature, thirst, hunger, motor function, speech, and posture. The brain, spinal cord, and optic nerve comprise the CNS and it is estimated they contain around 86 billion neurons in humans (Azevedo *et al.*, 2009). Highly interconnected neuronal circuits transmit information encoded electrically and chemically, affording coordinated movement, consciousness, memory, and other higher executive function.

The structure and function of neurons are supported by an equal number of non-neuronal cells (Azevedo *et al.*, 2009) called "glia", derived from Greek meaning "glue". Glia are non-vascular, non-epithelial, and do not generate action potentials (Bullock, 2004; Verkhratsky and Butt, 2013). They instead perform house-keeping roles, such as maintaining homeostasis of neurotransmitters, metabolites and ions at the local level, whilst also directing nervous system structure and cell number. Additionally, glia are required for maintaining synapse function and providing metabolic support to neurons (Barres, 2008; Fünfschilling *et al.*, 2012; Fields *et al.*, 2015). Oligodendrocytes and their precursors, astrocytes, microglia, and ependymal cells are the major neuroglia.

Communication between neurons occurs through the rapid and highly organised propagation of action potentials along axons and release of neurotransmitters at synapses. The speed at which signals are conveyed along an axon depends on axonal diameter and myelination. Non-myelinated axons have conductance velocities ranging from 0.5 - 10 m/s (Purves *et al.*, 2001). Much like an electrical wire, large-diameter axons have lower resistance and carry action potentials faster than small-diameter axons. Myelin, which appeared more than 470 million years ago (Bullock *et al.*, 1984), increases the rate of neuronal signalling whilst saving space by eliminating the need for large diameter axons (seminal work by Rushton (1951)).

Myelination of tightly bundled axons within fibre tracts affords the division of the CNS into white and grey matter, defined by the colour of each. White and grey matter have distinct cellular compositions, architecture, and function. Although glia are distributed throughout both, neuronal cell bodies are broadly restricted to the grey matter but extend axons through the white matter forming axonal tracts. Anatomically, white matter is located under grey matter in the brain, *i.e.,* under the cortex, whereas in the spinal cord white matter surrounds most of the grey matter, the latter forming a butterfly-shaped structure (Figure 1.1). The optic nerve is a pure white matter tract.

Despite its complexity and necessity for life, the CNS has little tolerance to injury during development and limited capacity for repair and regeneration in adulthood relative to other organs. Therefore, the brain and spinal cord are highly protected by several anatomical features. For example, the skull bones, vertebrae, and the cerebral spinal fluid in the subarachnoid space protect the brain and spinal cord from physical impact, whereas the blood-brain barrier (BBB) separates this compartment biochemically by acting as a highly selective barrier between the CNS and systemic circulation (Abbott *et al.*, 2006; Banks, 2016).

1.2.1 Development of the central nervous system

The mammalian CNS is formed from neuroepithelial cells (NECs) of the neuroectoderm, which give rise to the neural tube in the third week post-fertilisation in humans (Sadler, 2005) or embryonic day (E) 8 in mice (Gray and Ross, 2011). The formation of the neural

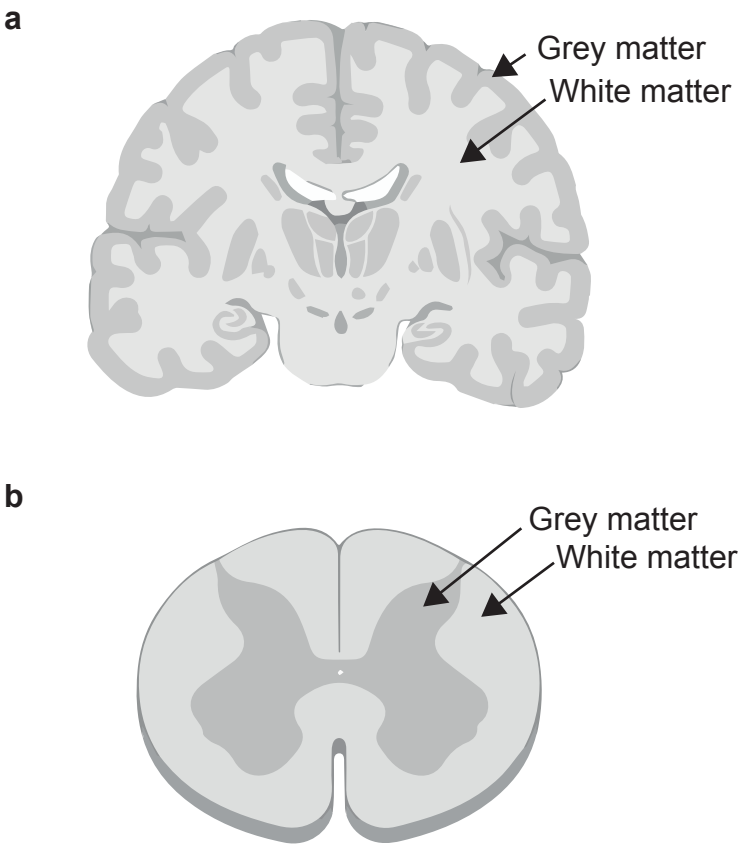

Figure 1.1 | Anatomical arrangement of grey and white matter in the human CNS. Schematics of **(a)** brain and **(b)** spinal cord in coronal and transverse section, respectively. Grey (dark grey) and white matter (light grey) are shown.

tube is a complex process orchestrated by morphogens, such as fibroblast growth factors, retinoic acid, Sonic hedgehog, and bone morphogenetic proteins, secreted in a spatially and temporally controlled pattern (Guérout *et al.*, 2014). The conversion of NECs to neural stem cells (NSCs) is regulated by Notch signalling, which drives neuronal differentiation through intracellular signalling in NSC progeny (Stolfi *et al.*, 2011). The process of neurogenesis begins early in embryonic development and finishes in early postnatal life, with limited neurogenesis in the adult CNS (Paridaen and Huttner, 2014).

Gliogenesis starts later in embryonic development at around 10 weeks in humans (Lee *et al.*, 2000) and E10 in mice (Hinds, 1968), continuing into postnatal life and adulthood in both species. Progenitors derived from NSCs give rise to astrocytes and oligodendroglia, and both are detected from around E12.5-13.5 in mice, first in the spinal cord (Richardson *et al.*, 2006; Hochstim *et al.*, 2008). Microglia are unique as they originate outside of the CNS in the embryonic yolk sac and populate the brain at around 3 weeks of gestation and the spinal cord at around 9 weeks in humans (Hutchins *et al.*, 1990; Rezaie and Male, 1999), and E9 in rodent brain (Morris *et al.*, 1991; Ginhoux and Merad, 2011).

1.2.2 The neuron and its axon

Neuronal cell bodies receive inputs through neurotransmitter receptors on dendrites and generate action potentials at the axon initial segment. These are then transmitted along the axon to convey information to target neurons. Multiples of these form vast neural networks. Neurons receive inputs at multiple synapses on multiple dendrites but most relay information along a single long axon: some of which bifurcate, often multiple times. Most axons in the CNS have a diameter larger than 0.2 µm and are myelinated (reviewed in Faber and Pereda (2018)). At the presynaptic terminal, a neurotransmitter is released and binds to receptors on the postsynaptic/effector neuron. Direct transfer of the action potential can occur in some cases (Faber and Pereda, 2018).

1.2.3 Oligodendrocytes

Oligodendrocytes produce and maintain the myelin sheath. They are distributed throughout the CNS but are most abundant in white matter. Oligodendroglia is a term that encompasses

both immature and mature cells, and in total they are estimated to contribute 20% (17.4 million) of all cells in the adult mouse brain (Valério-Gomes *et al.*, 2018). During gliogenesis, NSCs give rise to oligodendrocyte pre-progenitors that differentiate into oligodendrocyte progenitor cells (OPCs) and migrate from the sites of generation throughout the brain, optic nerve and spinal cord (Pringle and Richardson, 1993; Kessaris *et al.*, 2006). OPCs in the brain and spinal cord originate from different regions of the developing CNS (reviewed in Bradl and Lassmann (2010)). In the spinal cord, most originate from the ventral portion of the neural tube and migrate throughout the spinal cord. In the mouse brain, OPCs are distributed in three distinct waves originating from different areas: the first wave from the medial ganglionic eminence and the anterior entopeduncular area at around E12; the second from the lateral and caudal ganglionic eminence at around E15; the third occurs in postnatal life from the neocortex (Kessaris *et al.*, 2006). OPCs from the first embryonic wave do not contribute to myelination in postnatal life (Kessaris *et al.*, 2006). OPCs are multipotent and can differentiate into oligodendrocytes, astrocytes, neurons, or even Schwann cells in some circumstances (Miron *et al.*, 2011).

During myelination, OPCs exit the cell cycle and become post-mitotic immature oligodendrocytes then pre-myelinating oligodendrocytes (Miller, 2002). The white matter oligodendrocyte population is established in the first years of life. Grey matter is more plastic with oligodendrocyte generation continuing in adulthood (Yeung *et al.*, 2014). Injury to pre-/early myelinating oligodendrocytes (subsequently referred to as *EMOLs*) or to the OPC pool during development severely impacts myelination as discussed in section 1.7

A mature oligodendrocyte can form between 30 and 60 myelinated internodes but rare spinal cord oligodendrocytes myelinate only a single large diameter axon (Matthews and Duncan, 1971; Hildebrand *et al.*, 1993; Chong *et al.*, 2012). Oligodendrocytes were classified into four types by del Río-Hortega (1921) based on morphology (as reviewed in Pérez-Cerdá *et al.* (2015)). Type I oligodendrocytes produce myelin sheaths on small-diameter axons that run in many directions; type II are similar but their myelin sheaths are organised in parallel; type III produce fewer myelin sheaths but wrap larger diameter axons; type IV have their cell bodies close to a single large-diameter axon.

The EMOL is highly metabolically active due to the energy-expensive lipid and protein

synthesis required to form the myelin sheath. The synthesis of myelin lipids is 48 times more energy expensive than the synthesis of myelin proteins (Harris *et al.*, 2012) and a single oligodendrocyte is estimated to generate up to 5,000-50,000 μm^2 of membrane per day. This results in an estimated 2,000,000 μm^2 of myelin membrane per adult oligodendrocyte in the rat brain (Pfeiffer *et al.*, 1993). The process of myelination is discussed in section 1.3.2.

1.2.3.1 Oligodendrocyte markers

The expression of specific protein "markers" is used to define oligodendroglial maturation and is summarised in Figure 1.2. All cells of the oligodendroglial lineage express Olig1, Olig2, and SOX10. Oligodendrocyte pre-progenitors express Olig1/2, A2B5, and PDGFRα (low expression). Committed OPCs express PDGFRα (high expression) and NG2. Post-mitotic (differentiated) immature oligodendrocytes continue to express PDGFRα (low), NG2 (high), A2B5, and sulfatide, the latter of which is recognised by the antibody O4 (Levine *et al.*, 2001; Ghoumari *et al.*, 2005; Kuhn *et al.*, 2019). The EMOL population can be distinguished by expression of the recently identified breast carcinoma amplified sequence 1 (BCAS1) marker (Fard *et al.*, 2017). They, and mature oligodendrocytes, are also positive for adenomatous polyposis coli commonly referred to as CC1 after the antibody clone that recognises it (anti-APC clone CC1 binds to Quaking 7 protein; Bin *et al.* (2016)). Myelin-associated glycoprotein (MAG) is also expressed at this stage, with some expression of 2′-3′-cyclic-nucleotide 3′-phosphodiesterase (CNP). Mature myelinating oligodendrocytes are negative for BCAS1 and express the major myelin-associated proteins, such as myelin basic protein (MBP), proteolipid protein (PLP), and myelin oligodendrocyte glycoprotein (MOG).

1.2.4 Astrocytes

Astrocytes are best known for their role in the formation and maintenance of the BBB (Abbott *et al.*, 2006). However, they have many other well-characterised roles in the CNS, including the regulation of local blood flow (Howarth, 2014), maintenance of CNS homeostasis (Sofroniew and Vinters, 2010), regulating neuronal circuitry function (Haim and Rowitch, 2017), and supporting myelination (Traiffort *et al.*, 2020). During development, astrocytes are generated from NSCs or radial glia (a subset of cells formed from NECs)

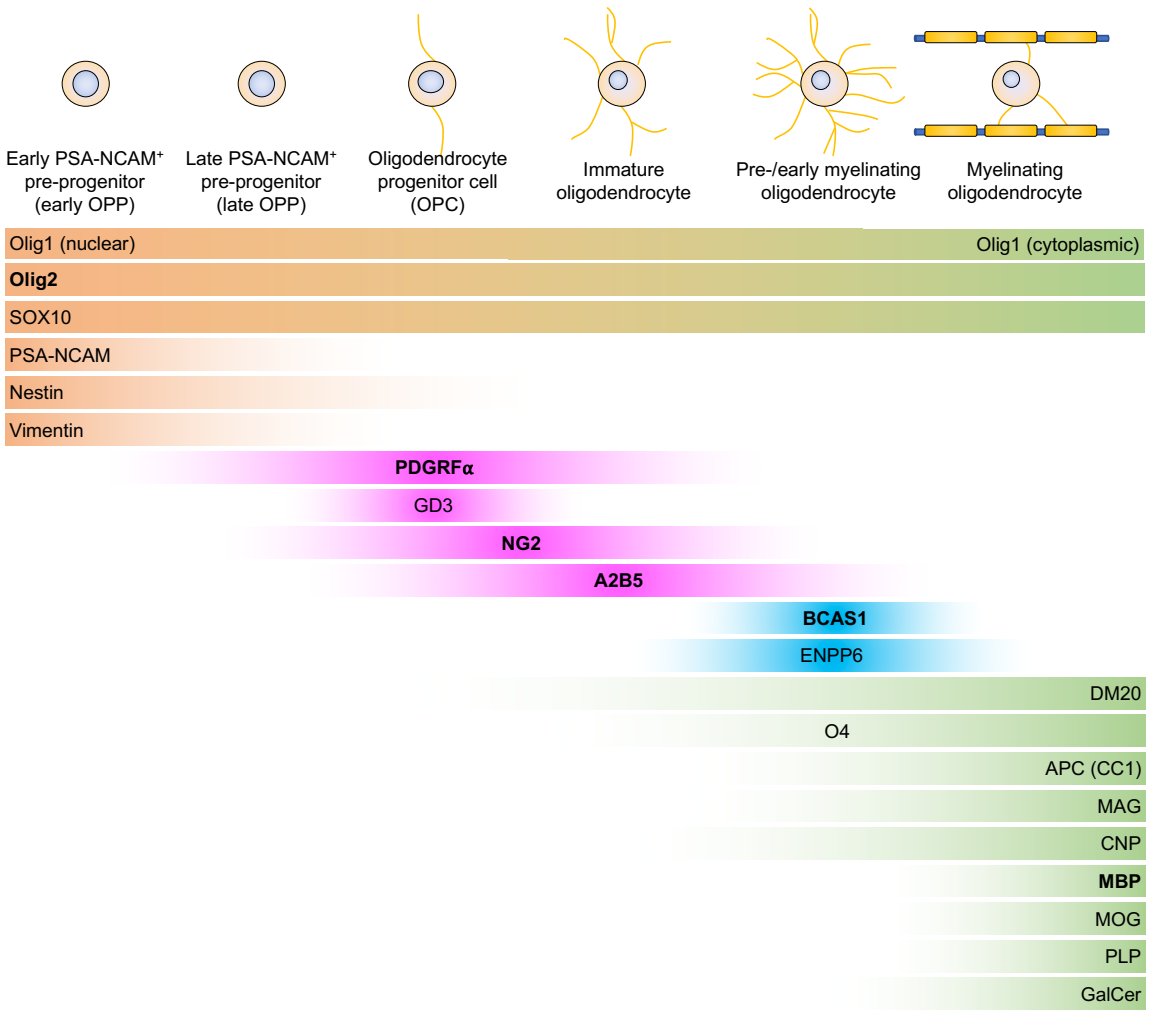

Figure 1.2 | Stages of oligodendroglial maturation and expressed markers. Expression of particular protein markers can be used to determine the developmental stage of oligodendroglia. Bold text signifies a commonly used marker. Figure adapted from Kuhn *et al.* (2019) and supplemented with information from Levine *et al.* (2001), Ghoumari *et al.* (2005), and Fard *et al.* (2017). Abbreviations: A2B5, gangliosides; APC, adenomatous polyposis coli (commonly referred to as CC1); BCAS1, breast carcinoma amplified sequence 1; CNP, 2′-3′-cyclic-nucleotide 3′-phosphodiesterase; DM20, proteolipid protein splice variant; ENPP6, ectonucleotide pyrophosphatase/phosphodiesterase 6; GalC, galactocerebrosidase; GD3, ganglioside; MAG, myelin-associated glycoprotein; MBP, myelin basic protein; MOG, myelin oligodendrocyte glycoprotein; NG2, membrane chondroitin sulfate proteoglycan; O4, sulfatide; Olig1 and 2, oligodendrocyte transcription factor; OPC, oligodendrocyte progenitor cell; OPP, oligodendrocyte pre-progenitor; PDGFRα, platelet-derived growth factor receptor alpha; PLP, proteolipid protein; PSA–NCAM, polysialic acid-neural cell adhesion molecule; SOX10, SRY-box Transcription Factor 10.

during gliogenesis at around E12 in mouse spinal cord or E16 for brain. Like oligodendrocytes, spinal cord and brain astrocytes originate from different areas of the developing CNS (reviewed in Bayraktar *et al.* (2015)). The exact precursor cell population and their expressed markers have not been fully described (Akdemir *et al.*, 2020). Astrocytes are highly proliferative and expand in numbers during early postnatal life to support the growth and expansion of the CNS tissues (Bandeira *et al.*, 2009). Throughout life, astrocytes are one of the main responders to tissue damage, such as trauma or demyelination, by proliferating and taking on a reactive phenotype (reviewed in Escartin *et al.* (2021)).

Astrocytes are the only CNS cells that store glycogen (Waitt *et al.*, 2017), an intracellular glucose store formed by linking glucose residues into branched-chain polymers. Recently, they were shown to accumulate TG-rich lipid droplets in cell culture when provided with a lipid-rich culture medium (Farmer *et al.*, 2019; Smolič *et al.*, 2021) suggesting they have an additional energy reservoir (Lee *et al.*, 2021). Glycogen and lipid metabolism are further discussed in section 1.6.

1.2.5 Microglia

The resident tissue macrophages of the CNS are microglia, which populate the CNS during embryonic development. Currently, the consensus is they are derived from erythromyeloid precursors (macrophage precursors) generated in the yolk sac that migrate into the developing nervous system around E10.5 in mouse (Ginhoux and Guilliams, 2016). Thus, microglial precursors populate the CNS before oligodendrocytes or astrocytes. Microglia in the developing CNS are more mobile and amoeboid in morphology compared to adulthood (Lawson *et al.*, 1990) where they have a ramified morphology. They also have a higher proliferative capacity in early life (Askew *et al.*, 2017; Bennett *et al.*, 2018). It is thought this change in phenotype highlights their involvement in phagocytosis and cellular remodelling during development (reviewed in Matcovitch-Natan *et al.* (2016)). Microglia play a role in neuronal circuit formation by phagocytosing excessive synapses formed during development by “synapse pruning” (reviewed in Wu *et al.* (2015)). Recently, microglia were shown to phagocytose excess myelin produced during myelination and are therefore critical for appropriate myelination (Hughes and Appel, 2020). They also clear myelin debris following

demyelination (Neumann *et al.*, 2009), facilitating remyelination by differentiating OPCs (Kotter *et al.*, 2006).

In the adult brain, microglial somas are typically stationary with their ramified processes surveying their immediate environment by continuously extending and retracting (Nimmerjahn *et al.*, 2005). Microglia become "activated" following exposure to pathogens, inflammatory cytokines, or cell damage. This usually involves them retracting fine cellular processes and secreting pro- or anti-inflammatory factors. Although these functions serve to maintain CNS homeostasis, chronically activated microglia can contribute to disease pathogenesis by causing collateral tissue damage (reviewed in Bachiller *et al.* (2018)).

1.3 Myelin and myelination

The myelin sheath is an extension of the oligodendrocyte cell membrane that is formed into highly organised concentric layers around axons. Myelination increases axon conductance by facilitating saltatory conduction (Tasaki, 1939) and allows myelinated axons to carry electrical signals up to 100-times faster than non-myelinated axons of the same diameter (reviewed in Castelfranco and Hartline (2016)). Additionally, saltatory conduction is very energy efficient as action potentials, and thus ion fluxes, are confined to the node of Ranvier and juxtaparanode rather than along the entire length of the axon (reviewed in Rosenbluth (1999) and Nave and Werner (2014)). In recent years, it has become evident that the oligodendrocyte and its myelin sheath are not simply an axonal insulator: they support and influence axonal function (reviewed in Nave and Werner (2014) and Stassart *et al.* (2018)). Furthermore, myelin is more plastic than previously thought (reviewed in Chorghay *et al.* (2018)) and requires constant turnover throughout life (Meschkat *et al.*, 2020).

1.3.1 Composition of myelin

Myelin is a lipid-rich membrane that consists of approximately 70% lipid and 30% protein by dry weight (Norton and Poduslo, 1973; Norton and Cammer, 1984). In the lipid portion, there are four main classes of lipid: galactosphingolipids (cerebrosides [e.g. hexosylceramides] and sulfatides), sterols such as cholesterol, phospholipids, and plasmalogens (Norton

and Poduslo, 1973). Galactosphingolipids contribute around 27% of myelin lipids and are thought to provide insulating properties and stability (Coetzee *et al.*, 1996). Sterols, such as cholesterol, are vital for the synthesis of all cell membranes and are responsible for their fluid nature (Ikonen, 2008). Cholesterol makes up about 28% of myelin lipids and is synthesised *de novo* in oligodendrocytes (Morell and Jurevics, 1996; Saher *et al.*, 2005). Knockout of squalene synthase required for sterol biosynthesis results in severe hypomyelination in early postnatal life; however, animals that survive this severe phenotype recover normal myelination through the supply of cholesterol from astrocytes (Saher *et al.*, 2005).

In the protein portion, mass spectroscopy analysis by Jahn *et al.* (2009) confirmed that PLP (and its isoform, DM20) and MBP are the most highly expressed. Other major proteins of myelin are myelin-associated oligodendrocytic basic protein (MOBP), myelin oligodendrocyte glycoprotein (MOG), myelin-associated glycoprotein (MAG), and 2′-3′-cyclic-nucleotide 3′-phosphodiesterase (CNP).

1.3.2 Myelination

In humans, myelination of the CNS begins in the final trimester of gestation (Hasegawa *et al.*, 1992) although relatively little myelin is present at birth. Myelination proceeds through postnatal life into adolescence but peaks within the first year: corresponding with the development of motor skills, such as crawling and walking, and cognitive development, including language comprehension (Fields, 2008). In the mouse CNS, myelination begins 1 day before birth in the ventral columns of the cervical spinal cord, specifically in the cuneate fasciculus. Myelination of the spinal cord proceeds in a rostral-to-caudal pattern, reaching a peak at postnatal day (P) 23 (Foran and Peterson, 1992) and is largely complete around P60 (Edgar and Griffiths, 2014). In general, the largest axons are myelinated first with most small-diameter axons acquiring myelin after P20 (Hildebrand *et al.*, 1993).

Myelination is a temporally and spatially controlled process regulated by oligodendrocyte cell-intrinsic and extrinsic factors as well as neuronal activity (Gibson *et al.*, 2014; Hines *et al.*, 2015; Mensch *et al.*, 2015; Mitew *et al.*, 2018). Regional OPC cell density (Rosenberg *et al.*, 2008) and astrocyte secreted factors (Stöckli *et al.*, 1991; Dobrea *et al.*, 1992;

Cellerino *et al.*, 1997; Ishibashi *et al.*, 2009) also influence myelination independently of neuronal activity. At the molecular level, the transcription factor Olig2 is required for OPC development and knockout of *Olig2* results in loss of these cells (Zhou *et al.*, 2001; Lu *et al.*, 2002; Takebayashi *et al.*, 2002). Canonical Wnt/β-catenin signalling that drives OPC proliferation must be downregulated to induce OPC differentiation otherwise hypomyelination occurs (Tawk *et al.*, 2011). Epigenetic regulation by histone deacetylase (HDAC) 1 and 2 influences Wnt/β-catenin activity (Ye *et al.*, 2009) and Olig2 expression (Cunliffe and Casaccia-Bonnefil, 2006), thereby contributing to the regulation of myelination. OPC differentiation into immature oligodendrocytes also requires the transcription factors Olig1, Sox10, Nkx 2.2, and YY1, whose ablation by gene knockout impairs oligodendrocyte generation and myelination (reviewed in Wegner (2008)). Knockout or overexpression of the microRNA processing enzyme, Dicer1, leads to dysmyelination (despite OPC proliferation) or hypermyelination, respectively (Zhao *et al.*, 2010; Lin *et al.*, 2013).

Myelination is initiated by OPCs and newly differentiated oligodendrocytes after contact is established with an axon that can be myelinated (Kirby *et al.*, 2006). Axonally-expressed ligands, such as Jagged (Wang *et al.*, 1998), PSA-NCAM (Charles *et al.*, 2000), and LINGO-1 (Mi *et al.*, 2005), inhibit OPC differentiation and down-regulation/inactivation of these allow myelination to proceed (Fancy *et al.*, 2009; Fu *et al.*, 2009). Other negative regulators such as oligodendrocyte-expressed GPR17 (Chen *et al.*, 2009) and astrocyte-produced hyaluronan (Back *et al.*, 2005) also regulate the onset and progression of myelination. Several astrocyte-secreted factors influence myelination, such as platelet-derived growth factor (PDGF) that inhibits OPC maturation (Raff *et al.*, 1988; Richardson *et al.*, 1988), whereas brain-derived neurotrophic factor (BDNF), ciliary neurotrophic factor (CNTF), and leukaemia inhibitory factor (LIF) promote myelination (Stöckli *et al.*, 1991; Dobrea *et al.*, 1992; Cellerino *et al.*, 1997; Ishibashi *et al.*, 2009).

When contact is established, myelin membrane forms due to growth at the inner tongue leading to new layers forming beneath established ones (Snaidero *et al.*, 2014). Lateral extension of the future myelin internode occurs along the axon towards what will become paranodal regions (Figure 1.3) and is facilitated by an axoglial adhesion complex. The glial proteins contactin-1 (CNTN1) and neurofascin (NFASC; 155 kDa isoform), combined with axonally-expressed contactin-associated protein (CNTNAP1), are critical components

of this complex and are required for node formation and lateral myelinating internode extension (Zonta *et al.*, 2008; Pedraza *et al.*, 2009; Susuki *et al.*, 2013; Çolakoğlu *et al.*, 2014). However, elongation of the inner tongue requires that membrane components are synthesised and transported to the most distal part of the oligodendrocyte myelinating process. Transport is thought to occur through the myelinic channel system, a cytoplasm-filled space within myelin that contains microtubules that provides a route to the inner-most tongue closest to the axon (Ransom *et al.*, 1991). Work by Snaidero *et al.* (2017) showed that CNP promotes the formation and maintenance of myelinic channels, whereas MBP promotes membrane compaction and their shrinkage. Recently, Edgar *et al.* (2021) reported that the myelinic channel system is a dynamic structure, as shown by *in vitro* live imaging.

Myelin membrane is formed in excess (Liu *et al.*, 2013a) and is then pruned by microglia (Hughes and Appel, 2020). Once wrapping is complete, remodelling of mature myelin membranes continues through life (Chorghay *et al.*, 2018) although this slows with ageing (Young *et al.*, 2013; Hill *et al.*, 2018; Hughes *et al.*, 2018). In the adult CNS, experimental demyelination with lysolecithin or ethidium bromide prompts OPC proliferation and differentiation into new myelin-forming oligodendrocytes (Zawadzka *et al.*, 2010).

1.3.3 Myelin maintains myelinated axon function

The myelinic channel system formed during myelination (discussed above) persists in the mature myelin sheath and likely provides a route for the oligodendrocyte to metabolically support “energy-hungry” axons (Nave, 2010a). It is generally accepted based on seminal work by Fünfschilling *et al.* (2012) that the post-myelination oligodendrocyte survives as a glycolytic cell and supplies glycolytic end products to the axon through monocarboxylate transporter (MCT) 1 at the glial-axonal junction (Lee *et al.*, 2012). Indeed, deletion of *Mct1* in oligodendroglia leads to axonal degeneration in aged mice (Philips *et al.*, 2021).

Transgenic models of myelin defects have shown that glial cell function and myelin integrity influence the myelinated axon. For example, in *Plp1* knockout mice, myelin formed by oligodendrocytes lacking PLP/DM20 is minimally abnormal, yet myelinated axons develop swellings (spheroids) reflecting axonal transport deficits (Griffiths *et al.*, 1998; Edgar *et al.*, 2004) and reduced basal axonal ATP levels (Trevisiol *et al.*, 2020). Mice lacking CNP in

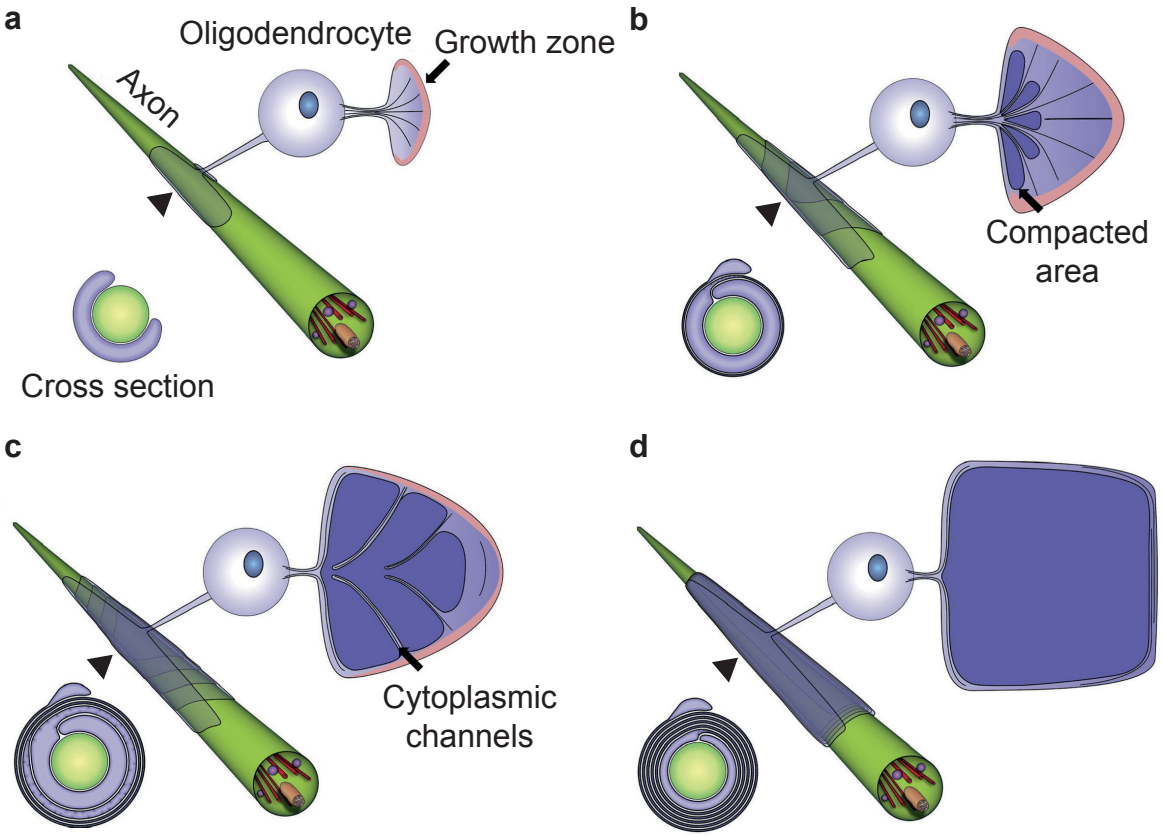

Figure 1.3 | Model of CNS myelination. Illustration of the currently accepted model of myelination. The illustrations on the right of the cell bodies show an unwrapped representation of the cell process. **(a)** Oligodendrocyte process makes contact with the axon and extends membrane (growth zone, pink). **(b)** Membrane grows under consecutive wraps with the growth zone remaining in close contact with the axon. Areas of compacted membrane (dark violet) begin to form. **(c)** Cytoplasmic channels are present through compacted myelin areas during active myelination. **(d)** The post-myelination oligodendrocyte retains cytoplasmic channels around the edge of the myelin wrap. Figure from Snaidero *et al.* (2014). Adapted and reprinted with permission from Elsevier.

Cnp1-null animals share a similar phenotype but axonal pathology is enhanced in *Plp1* and *Cnp1* double knockout mice (Edgar *et al.*, 2009), suggesting different mechanisms are involved. Thus, the glial cell and myelin sheath are critical in maintaining axon function and integrity. The role of the oligodendrocyte in maintaining axonal integrity through metabolic support is discussed in section 1.6.1.

1.4 *In vitro* study of neural cells

Cell culture models are an easily manipulated system to examine the response of cells under controlled conditions. For the study of CNS cells, *in vitro* models are invaluable since they allow experimentation that would be otherwise challenging or impossible *in vivo*. Furthermore, they inform our understanding of the *in vivo* situation and help in the design of *in vivo* experiments.

The earliest reported cultures of CNS cells was conducted over 110 years ago by Harrison *et al.* (1907) and Harrison (1910) who grew neural crest tissue from frogs *in vitro* to study axonal growth. Since then, culture techniques have vastly improved in ease of use, reproducibility, and viability. It is now possible to reliably generate primary cell cultures of every major CNS cell type (Nikolakopoulou *et al.*, 2020). Immortalised cell lines have some use in the study of CNS disease; however, as illustrated for microglia, they cannot always recapitulate key phenotypic features of primary cells (Timmerman *et al.*, 2018).

Culture systems are desirable as they reduce or replace animal use and can often be adapted for high-throughput screening (Bijland *et al.*, 2019; Aldewachi *et al.*, 2021). Cell-type enriched cultures are useful for studying the intrinsic properties of a particular cell type, for example, its energy metabolism (Amaral *et al.*, 2016) or in the case of oligodendrocytes, capacity to wrap inert nanofibers in the absence of neuronal signals (Bechler *et al.*, 2015). The main limitation of cell-type enriched cultures is that the absence of inter-cellular interactions with other glia and neurons likely alters cellular behaviour (Domingues *et al.*, 2016). Mixed co-cultures overcome this limitation and allow complex cellular interactions between neuroglia. The spinal cord myelinating cell co-culture system (Thomson *et al.*, 2006) contains all CNS cell types, produce compact myelin sheaths, are electrically active, and have functional immune responses to insult and injury (as we show in Bijland *et al.*

(2019)). In some cases, when studying glial cell function, metabolism, or response to injury, it can be useful to exclude neurons given they are particularly vulnerable to energy insufficiency and/or oxygen deprivation (Goldberg and Choi, 1993).

Much of the literature on the characteristics of oligodendroglia stems from primary cell cultures obtained from the brain of neonatal rodents according to the original protocols of McCarthy and de Vellis (1980). Whilst this method has been invaluable in expanding our understanding of the oligodendroglial lineage, it has two major limitations. First, oligodendrocytes are differentiated *in vitro* from OPCs, removing the *in vivo* context during this critical window. Second, brain (cortical) and spinal cord oligodendrocytes differ from each other in a number of ways, including in terms of their intrinsic capacity to produce long or short myelin internodes (Bechler *et al.*, 2015).

1.5 An overview of cellular energy production

Cellular energy homeostasis is vital for cell function and viability. Before reviewing the energy metabolism of the CNS later in this chapter, we first provide an overview of basic cellular energy production (summarised in Figure 1.4).

1.5.1 Glycolysis, tricarboxylic acid cycle, and electron transport chain

The primary energy source of most cells is glucose, which is oxidised in glycolysis over a 10-step biochemical pathway to produce NADH, ATP, and pyruvate. Glucose is typically supplied in the bloodstream but some cells store it intracellularly in the form of glycogen.

In the cell cytoplasm, hexokinase phosphorylates glucose to glucose-6-phosphate by consuming one molecule of ATP. An additional ATP molecule is consumed later in the pathway during the conversion of fructose 6-phosphate to fructose 1,6- bisphosphate by phosphofructokinase. Next, glyceraldehyde 3-phosphate and dihydroxyacetone phosphate

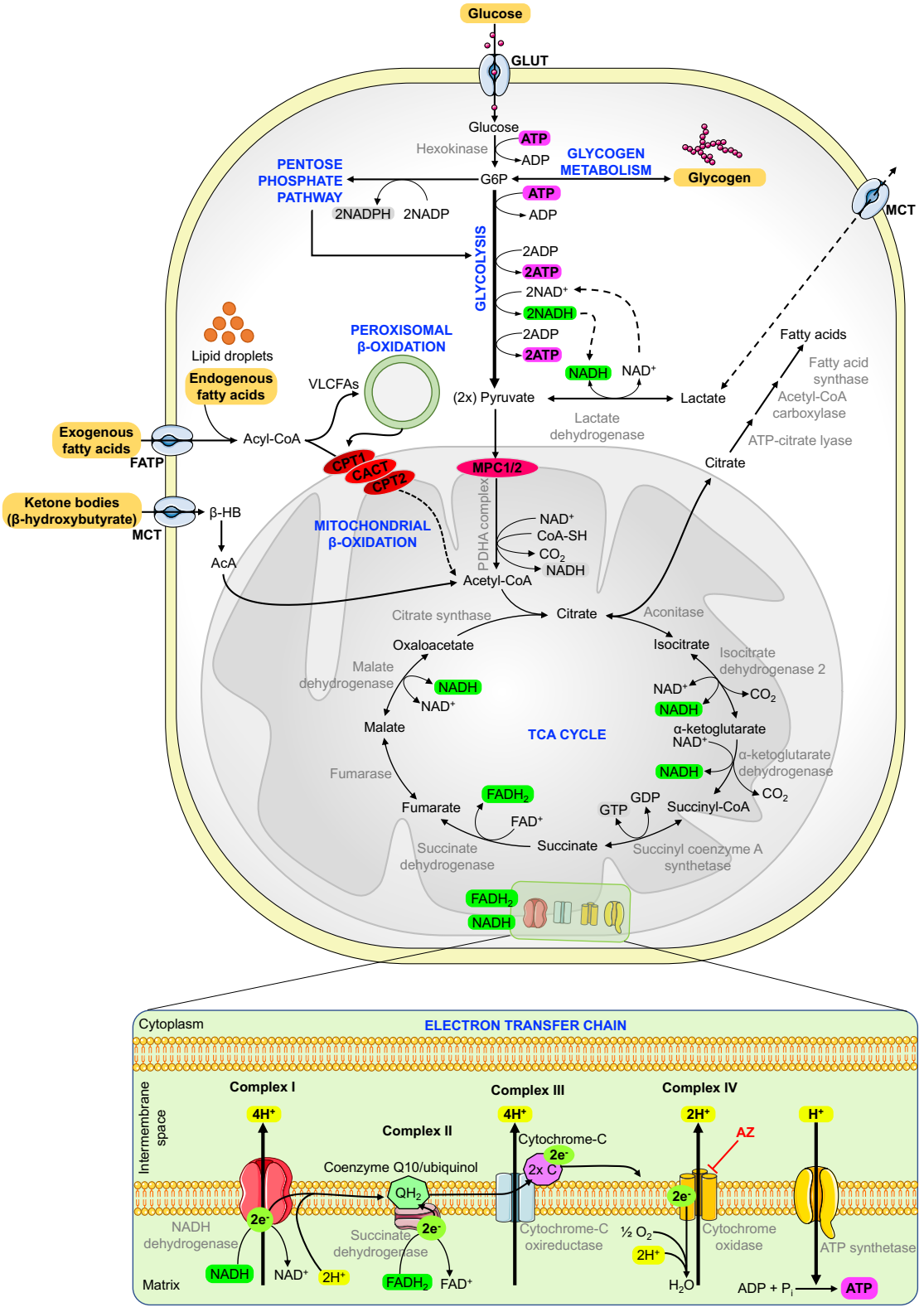

Figure 1.4 | Cellular energy production pathways. *Figure legend continues on the next page.*

Figure 1.4 | *Cont...* Schematic of the major metabolic pathways involved in cellular ATP production. Metabolic pathways are labelled in blue, enzymes in grey, and energy substrates in orange boxes. Glucose is often the primary energy source and enters via glucose transporters (GLUT) or is supplied from limited intracellular glycogen stores. Glycolysis converts glucose to two molecules of pyruvate, producing ATP and NADH. Pyruvate enters mitochondria via porins and mitochondrial pyruvate carriers (MPC) 1 and 2, where it is then converted to acetyl-CoA by the pyruvate dehydrogenase (PDHA) complex. In the absence of glucose, ketone bodies and exogenous/endogenous fatty acids can be metabolised to produce acetyl-CoA. Fatty acids enter the mitochondrial matrix via the carnitine shuttle composed of carnitine palmitoyltransferase 1 (CPT1), carnitine acylcarnitine translocase (CACT), and carnitine palmitoyltransferase 2 (CPT2). The tricarboxylic acid (TCA) cycle produces NADH and $FADH_2$ from acetyl-CoA that can be used as electron donors in the electron transfer chain. Electrons are transferred through complexes I to IV, producing a proton gradient within the mitochondrial intermembrane space. Finally, protons are moved through ATP synthase forming ATP from ADP and inorganic phosphate. Azide (AZ) blocks complex IV of the electron transfer chain and inhibits oxidative phosphorylation. Abbreviations: AcA, acetoacetate; β-HB, β-hydroxybutyrate; FATP, fatty acid transport protein; MCT, monocarboxylate transporter; VLCFA, very-long-chain fatty acid.

are generated and can be interconverted by triose phosphate isomerase. All proceeding reactions in glycolysis occur twice since one molecule of glucose generates two molecules of glyceraldehyde 3-phosphate, which is next converted to 1,3-bisphosphoglycerate by glyceraldehyde 3-phosphate dehydrogenase (GAPDH). This step reduces NAD^+ to NADH. The final steps generate a molecule of ATP and pyruvate (times-two). As two ATP molecules are consumed during glycolysis, the net ATP yield is two (reviewed in Chaudhry and Varacallo (2021)).

Pyruvate is either reduced to lactate, thereby regenerating NAD^+ by oxidation of NADH, or it is oxidised in mitochondria via the tricarboxylic acid (TCA) cycle. If lactate is produced it can be exported and sequestered by another cell as an energy substrate for the TCA cycle, avoiding the need for glucose for energy production. However, glucose must undergo glycolysis to provide carbon substrates for the pentose phosphate pathway, which generates five-carbon sugars for the synthesis of nucleotides and NADPH, the latter being essential for anabolic metabolism and the regeneration of glutathione oxidised in anti-oxidant defence.

Pyruvate crosses the outer mitochondrial membrane through porins (Benz, 1994) and the inner membrane through mitochondrial pyruvate carrier 1 and 2 (Bricker *et al.*, 2012; Herzig *et al.*, 2012). In the matrix, pyruvate is decarboxylated by the pyruvate dehydrogenase complex to acetyl-CoA, reducing NAD^+ to NADH and consuming a molecule of coenzyme-A (CoA). The TCA cycle begins with the condensation of acetyl-CoA and oxaloacetate to citrate by citrate synthase. Following a further 9 biochemical reactions, the TCA cycle produces three molecules of NADH, one GTP (ATP equivalent), and one $FADH_2$ (or one ubiquinol), and regenerates oxaloacetate to begin the next cycle. In this process, two molecules of CO_2 are lost (reviewed in Alabduladhem and Bordoni (2021)). Acetyl-CoA produced from other endogenous or exogenous sources such as ketone bodies and fatty acids (FAs) by β-oxidation is also oxidised via the TCA cycle (reviewed in Dhillon and Gupta (2021)).

The purpose of the TCA cycle is to reduce NAD^+ and FAD to NADH and $FADH_2$, respectively, for use as electron donors in the electron transport chain (ETC). Molecules of NADH produced in glycolysis are also utilised in the ETC. Mitochondrial complexes I to IV transfer protons from NADH across the inner mitochondrial membrane to form an electrochemical

proton gradient between the intermembrane space and matrix. Protons are then driven through ATP synthase, which catalyses the formation of ATP from ADP and inorganic phosphate (Mitchell, 1961). This process is referred to as oxidative phosphorylation (OXPHOS).

The maximum theoretical combined energy yield is ~38 molecules of ATP: 4 from glycolysis and 34 from OXPHOS. However, if glycolysis generates lactate as an end product, the maximal yield is not obtained. The benefit of generating lactate by lactate dehydrogenase (LDH) is that ATP production can continue in the absence of oxygen (short-term; anaerobic glycolysis) or that lactate can be exported to other cells (aerobic glycolysis). Under anaerobic conditions, lactate is produced for this very reason since OXPHOS is inhibited. In all, and after considering energy loss due to proton and electron leakage (Nobes *et al.*, 1990; Kadenbach, 2003; Jastroch *et al.*, 2010), it is estimated that ~30 ATP molecules are generated from a single molecule of glucose (Rich, 2003).

1.5.2 β-oxidation of fatty acids

Acetyl-CoA can be produced from FAs following mitochondrial β-oxidation. FAs include triacylglycerols (triglycerides, TGs), phospholipids, sterol lipids, and sphingolipids. They are formed from carbon chains of various length and saturation. The carbon chain length is used to group FAs: short-chain (less than 7 carbon atoms); medium-chain (7-12 carbon atoms); long-chain (LCFAs, 12-20 carbons); very-long-chain (VLCFAs, $>$ 20 carbon atoms (Kihara, 2012; Schönfeld and Wojtczak, 2016).

Following the release of free FAs from adipocytes, the blood is a common source of FAs, which are imported into cells by one of two known mechanisms. Passive diffusion is energy-independent but is relatively restricted to short- and medium-chain FAs. Alternatively, protein-mediated transport by FA translocase (FAT/CD36) and FA-binding proteins on the cell membrane facilitate the passage of LCFAs into the cell. Intracellular FA-binding proteins 1-9, FA transport proteins 1-6, and caveolin1 play a role in FA transport and metabolism (reviewed extensively in Glatz and van der Vusse (1996) and Glatz *et al.* (2010)). In the CNS, FAs are moved across the BBB in humans and mice by slow diffusion and through FA transport proteins 1 and 4 (Mitchell *et al.*, 2011).

Before being used as an energy substrate, FAs must undergo esterification with CoA to form an "activated" acyl-CoA that can be sequestered by peroxisomes or mitochondria for β-oxidation. This reaction is performed by acyl-CoA synthetase and consumes a molecule of ATP (or high-energy phosphate bond equivalents). Peroxisomes play a specialist role by shortening VLCFAs to LCFAs for transport into mitochondria. Mammalian peroxisomes uniquely express three ATP-binding cassette transporters that allow VLCFAs to enter the peroxisomal lumen where β-oxidation enzymatic machinery shortens the carbon chain length and produces acetyl- and acetoacetyl-CoA (Reddy and Hashimoto, 2001). Upon export from the peroxisome, the shortened FA chains can be transported into mitochondria either by diffusion (for short- and medium-chain FAs) or by the carnitine shuttle (required for LCFAs). The carnitine shuttle consists of 3 enzymes: carnitine palmitoyltransferase 1 (CPT1), carnitine acylcarnitine translocase (CACT), and carnitine palmitoyltransferase 2 (CPT2). The shuttle begins with CPT1 on the outer mitochondrial membrane and converts long-chain acyl-CoA to long-chain acylcarnitine, which can cross the outer mitochondrial membrane passively. Next, the CACT anti-porter located at the inner mitochondrial membrane transfers an acylcarnitine molecule into the matrix and one molecule of carnitine out. Finally, CPT2 on the matrix face of the inner mitochondrial membrane converts acylcarnitine back to acyl-CoA for β-oxidation (Swigonová *et al.*, 2009).

The aim of β-oxidation is to produce acetyl-CoA for the TCA cycle. Essentially, the carbon chains of fatty acyl-CoA molecules are repeatedly cleaved to produce molecules of acetyl-CoA. First, acyl-CoA is dehydrogenated by acyl-CoA dehydrogenases, using FAD as a co-factor. This produces trans-enoyl-CoA (contains a double bond between the α and β carbons) and reduces $FADH_2$ (Swigonová *et al.*, 2009). Second, enoyl-CoA hydratases break the previously formed double bond by adding one molecule of H_2O to form hydroxyenoyl-CoA. Third, 3-hydroxyacyl-CoA dehydrogenases convert the hydroxyl group of hydroxyenoyl-CoA to a keto group, reducing NAD^+ to NADH and forming 3-ketoacyl-CoA. Finally, thiolases cleave 3-ketoacyl-CoA to form a molecule of acetyl-CoA and a shortened acyl-CoA, consuming a molecule of CoA. The process begins again for the shortened acyl-CoA until it is completely oxidised to acetyl-CoA. Carbon chains with an odd number of carbons cannot be fully oxidised and form propionyl-CoA as an end product (3 carbon chain), which is carboxylated to provide succinyl-CoA for the TCA cycle (Mazumder *et al.*,

1961). All $FADH_2$ and NADH produced during β-oxidation contribute to energy production through the ETC (Schönfeld and Wojtczak, 2016).

1.5.3 Lipid droplets

The processing of fatty acyl-CoA molecules in the endoplasmic reticulum can generate lipid droplets, an intracellular store of lipids (Guo *et al.*, 2009; Lee *et al.*, 2021). Lipid droplets predominantly contain neutral lipids such as TGs, cholesterol esters, and diacylglycerols, coated by a monolayer of phospholipids and proteins (Tauchi-Sato *et al.*, 2002; Bartz *et al.*, 2007a; b). One of the major surface protein identifiers of lipid droplets are perilipins (Blanchette-Mackie *et al.*, 1995). The primary role of lipid droplets in adipocytes (and likely in other cells) is to mobilise FAs for mitochondrial β-oxidation in times of increased substrate demand, thereby providing energy substrates for ATP production (Welte and Gould, 2017). FAs are released from lipid droplets by the action of lipases or through lipophagy (Kounakis *et al.*, 2019). Recent interest in CNS lipid droplets stemmed from observations in *Drosophila* brain, where they were observed under physiological conditions and increased in frequency during hypoxic stress *in vivo* (Smolič *et al.*, 2021).

1.5.4 Autophagy

Metabolic stress such as starvation triggers cells to engage autophagy, which degrades and recycles non-critical cellular materials to create energy substrates for ATP production. During starvation, mammalian target of rapamycin complex 1 (mTORC1) translocates to the nucleus and induces expression of several genes that control autophagy and lysosomal biogenesis (reviewed in He and Klionsky (2009)). Macrophagy involves larger cellular components, including organelles, being isolated in a double-membraned autophagosome; microphagy degrades components in lysosomes; chaperone-mediated autophagy involves tagging proteins for trafficking to lysosomes (Glick *et al.*, 2010).

1.6 Energy metabolism in the central nervous system

The brain comprises around 2% of the average human's body mass but accounts for 20% of total energy and oxygen metabolism (Rolfe and Brown, 1997; Magistretti and Allaman, 2015). Neurons are estimated to consumed 80-90% of the energy produced in the CNS (Howarth *et al.*, 2012) with the majority required for membrane repolarisation following action potential propagation (Harris *et al.*, 2012). Energy metabolism in the CNS presents a unique challenge as overall energy consumption is highly dynamic. Nonetheless, constant ATP homeostasis is required to avoid neurological disease as demonstrated in a mouse model of Rett syndrome where impaired ATP homeostasis increases the susceptibility of epileptic seizures (Toloe *et al.*, 2014). We have long understood that periods of increased neuronal activity are supported by an increase in metabolic activity and changes in blood perfusion (Roy and Sherrington, 1890). Metabolism at the cellular level has become clearer in recent years with reports of specialised cell metabolism ascribed to cell function. Glia, such as oligodendrocytes and astrocytes, are considered glycolytic and produce lactate as an end product. Neurons are considered oxidative since this mode of ATP production efficiently supports their high energy demands. In this section, we summarise CNS energy production and the fuel sources utilised.

1.6.1 Glucose, lactate, and neurometabolic coupling

Glucose has long been considered the primary energy source of the CNS with first evidence reported in the 1920s (Himwich and Nahum, 1929) and confirmed in pioneering human studies by Kety and Schmidt (1948) and Sokoloff (1960). Glucose enters the brain from peripheral circulation by crossing through glucose transporters (GLUTs), particularly GLUT1, which is enriched at astrocyte end-feet that contribute to the BBB (Morgello *et al.*, 1995). Glucose reaches neurons through astrocytes or directly through neuron-expressed GLUT3 (Maher *et al.*, 1994). Astrocytes are glycolytic cells that inhibit the degradation of glycolytic regulatory enzymes by the E3 ubiquitin ligase. In particular, high cytosolic levels of phosphofructokinase are maintained compared to neurons (Herrero-Mendez *et al.*, 2009; Bélanger *et al.*, 2011). To sustain glycolysis, LDH regenerates NAD^+ consumed in the glycolytic pathway (Hirrlinger and Dringen, 2010). Post-myelination oligodendrocytes are also

considered glycolytic cells (Fünfschilling *et al.*, 2012; Hirrlinger and Nave, 2014). Neurons rely on OXPHOS to generate ATP but utilise glucose to replenish NADPH consumed by the glutathione antioxidant defence system (Bolaños *et al.*, 2010).

In recent years, lactate has been recognised as a major fuel source of the CNS and is produced *in situ* or enters from the periphery through MCTs expressed on the endothelial cells of the BBB as shown in rodents (Gerhart *et al.*, 1997; Koehler-Stec *et al.*, 1998; Leino *et al.*, 1999) and humans (Froberg *et al.*, 2001; Lauritzen *et al.*, 2015). Lactate was first considered as a fuel source in the ‘90s by Dringen and others who showed cultured rat brain astrocytes release lactate into cell culture media as a product of aerobic glycolysis (Dringen *et al.*, 1993a). They showed subsequently that rat brain neurons consume lactate *in vitro* (Dringen *et al.*, 1993b). *In vivo* evidence from radiotracer experiments has since shown the intact brain consumes lactate with the highest uptake coupled to high neuronal activity (Wyss *et al.*, 2011).

Pellerin and Magistretti (1994) proposed the astrocyte-neuron lactate shuttle (ANLS; Pellerin *et al.*, 1998a and Magistretti and Pellerin, 1999) in which grey matter astrocytes produce lactate as an end product of aerobic glycolysis that is supplied to neurons for metabolic support following axon potential propagation. A similar mechanism was later identified in white matter using *ex vivo* adult mouse optic nerve where axonal firing could be maintained in the absence of glucose so long as glycogen metabolism and lactate shuttling through MCTs was not blocked (Wender *et al.*, 2000; Brown *et al.*, 2003; 2004; Tekkök *et al.*, 2005). These observations highlight the important role of astrocyte glycogen metabolism in maintaining neuronal function in situations of acute energy deprivation. However, glycogen stores are limited and only support compound axon potential propagation at 0.03 Hz for 30 minutes in *ex vivo* optic nerve experiments (Wender *et al.*, 2000).

In mature white matter, myelinated axons are limited in their access to extracellular energy substrates by the myelin sheath. This provides the basis for the proposal that oligodendrocytes also supply lactate to axons as a metabolic end product (Nave, 2010b; Fünfschilling *et al.*, 2012). Appreciation for the role of oligodendrocytes in supplying metabolites to the axon has led to its inclusion in the astrocyte-*oligodendrocyte*-neurone lactate shuttle (Figure 1.5; Philips and Rothstein (2017)). However, the energy metabolism of oligodendroglia

depends on their developmental stage. Whilst OPCs exhibit an oxidative phenotype and therefore consume pyruvate/lactate in the TCA cycle, mature post-myelination cells are considered glycolytic (Rao *et al.*, 2017). The metabolic profile of the intermediate stage EMOL has not been precisely characterised although lactate can replace glucose as a fuel source to support myelination *in vitro* (Sánchez-Abarca *et al.*, 2001) and in *ex vivo* brain slice cultures (Rinholm *et al.*, 2011).

1.6.2 Ketone bodies

At the time of myelination in mammals, the blood contains high levels of ketone bodies produced in the liver from a milk-rich diet (Hawkins *et al.*, 1971; Snell and Walker, 1973; Foster and Bailey, 1976; Gilles, 1976; Kinney *et al.*, 1994). Compared to adults, the CNS of neonates can sequester circulating ketone bodies at a higher rate through the high expression of MCTs on the BBB (Pellerin *et al.*, 1998b). Ketone bodies likely contribute towards the energy requirements of myelination in early life (Nehlig and Pereira de Vasconcelos, 1993) since they are readily metabolised by oligodendrocytes, at least *in vitro* (Edmond *et al.*, 1987). In adults, ketone bodies are used by the CNS as an energy source during starvation when FAs are mobilised from adipose tissue and undergo β-oxidation to produce acetyl-CoA in large quantities in the liver (reviewed in Owen (2005)). There is some evidence that ketogenesis could occur in the brain. For example, rat brain astrocyte cultures produce ketone bodies when supplied with FAs (Auestad *et al.*, 1991) or the amino acid leucine (Bixel and Hamprecht, 1995). Astrocyte ketogenesis has been suggested to play a neuroprotective role by providing energy substrates for neural cells during energy deprivation in hypoxia-ischaemia (Guzmán and Blázquez, 2004). That said, ketone bodies were unable to maintain compound action potential propagation in *ex vivo* optic nerve preparations (Brown *et al.*, 2001) likely because they would not lead to the production of lactate in glia to support axons.

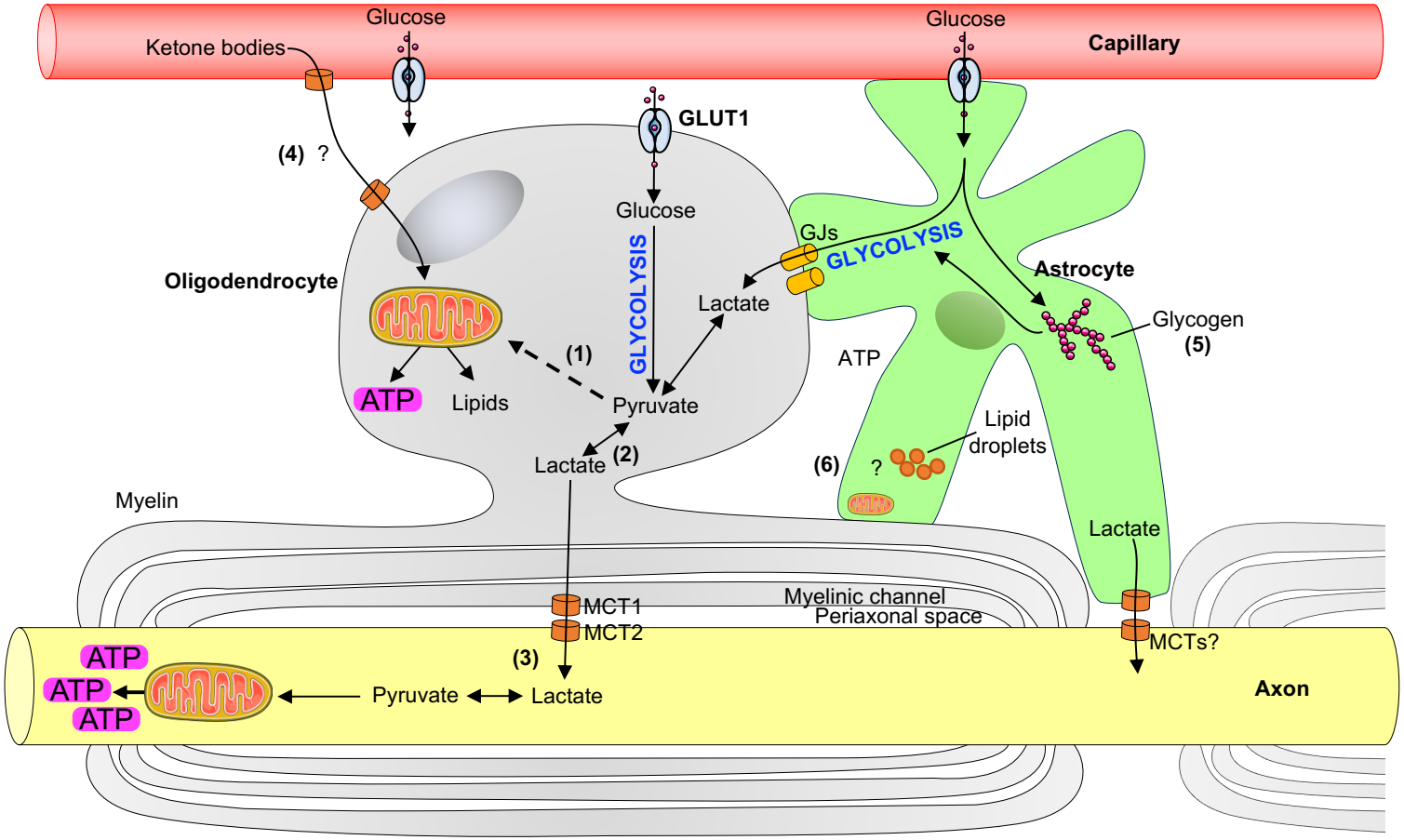

Figure 1.5 | Neurometabolic coupling between the oligodendrocyte, astrocyte, and axon. Glucose enters the CNS from the periphery via GLUT1 transporters highly expressed on astrocyte processes that form the BBB. **(1)** The EMOL utilises glycolytic end products to generate ATP and myelin lipids in mitochondria, whereas **(2)** post-myelination cells shuttle lactate (or pyruvate) to the axonal compartment to **(3)** support axonal energy requirements (Nave, 2010b; Fünfschilling *et al.*, 2012; Hirrlinger and Nave, 2014). **(4)** Ketone bodies are an alternative energy source that are thought to contribute towards the energetic needs of myelination (Nehlig and Pereira de Vasconcelos, 1993). Astrocytes are coupled to oligodendrocytes via gap junctions (GJ) that allow the transfer of energy substrates. **(5)** They contain glycogen stores that can provide a short-term energy reserve **(6)** and recently have been shown to contain lipid droplets although their energetic role is not fully understood. Figure adapted from Fünfschilling *et al.* (2012) and Hirrlinger and Nave (2014). Abbreviations: GLUT, glucose transporter; MCT, monocarboxylate transporter.

1.6.3 Fatty acid metabolism

Lipids contribute up 50% of the brain's dry weight (Vinken *et al.*, 1996), with 40% of that accounted for by myelin (Norton and Poduslo, 1973). Despite being a lipid-rich compartment, the focus remains on glucose energy metabolism in recent reviews (Bélanger *et al.*, 2011; Pellerin and Magistretti, 2012; Falkowska *et al.*, 2015; Magistretti and Allaman, 2015). The topic of β-oxidation in the CNS is highly controversial for the following reasons as summarised by Schönfeld and Reiser (2013): i) β-oxidation requires oxygen, which is somewhat limited in the CNS; ii) lipid oxidation generates reactive oxygen species (ROS) and increases oxidative stress; iii) β-oxidation is a slow way of generating ATP compared to glycolysis. In recent years, the dogma that the CNS does not perform β-oxidation has been challenged, particularly since there is evidence that astrocytes can oxidise lipids *in vivo* (Ebert *et al.*, 2003) and lipid droplet-associated TGs are detected in the murine brain (Etschmaier *et al.*, 2011).

The earliest evidence that the CNS might perform β-oxidation came from *ex vivo* studies that examined the ability of various rat tissue slices, including brain, to oxidise ^{14}C-labelled emulsified TGs (Geyer *et al.*, 1949). However, studies by Quastel and Wheatley (1933) and Weinhouse *et al.* (1950) did not replicate this finding, casting doubt. Volk *et al.* (1952) sought to clarify these contradictory reports but, more importantly, to determine if endogenous FAs can be metabolised. In their experiments, young rats (age not reported) were fed ^{14}C-labelled palmitate, sacrificed, and brain slices maintained in culture where they produced $^{14}CO_2$. These studies were complemented with several *in vitro* experiments that showed brain mitochondria isolates could oxidise FAs (Vignais *et al.*, 1958; Beattie and Basford, 1965). One such study by Warshaw and Terry (1976) reported peak carnitine palmitoyltransferase activity and mitochondrial FA oxidation in P10-15 brain compared to adult, suggesting there is increased β-oxidation in the developing CNS.

Early *in vivo* evidence of CNS β-oxidation was reported by Allweis *et al.* (1966) who showed ^{14}C-labelled palmitic acid was oxidised in cat brain perfused with artificial blood, both in the presence and absence of approximately physiological glucose (~8 mM). The authors provided the first convincing evidence for a normal physiological role for β-oxidation in the CNS. However, the contribution of FA oxidation to CO_2 production was less than 3%,

suggesting it is not a major contributor to brain energy production - at least at the age tested (not reported). In rodents, radiolabelled FAs administered in the diet, or by injection into the tail vein or peritoneum, can enter brain lipid structures, including sphingomyelin (Dhopeshwarkar and Mead, 1970; Dhopeshwarkar *et al.*, 1971). Furthermore, up to 20% of free FAs in the blood can cross the BBB on the first pass (Pardridge and Mietus, 1980) and dietary lipids incorporate into myelin membrane (Camargo *et al.*, 2017). Combined with earlier *ex vivo* and *in vitro* data, these studies demonstrate the brain can oxidise exogenous FAs even when the *preferred* energy source of glucose is provided.

Cellular resolution of β-oxidation was first provided *in vitro* by Edmond *et al.* (1987), reporting that neurons, astrocytes, and oligodendrocytes preferentially oxidised ketone bodies 7-9 times more than glucose. Astrocytes were the only CNS cell found to oxidise FAs and did so at a higher rate than they consumed ketone bodies. These data were later supported with *in vivo* data from adult rats as reported by Ebert *et al.* (2003) in which FA oxidation in the brain was demonstrated by nuclear magnetic resonance spectroscopy following infusion of ^{13}C-labelled octanoate into the bloodstream. Although cellular resolution was not directly possible, astrocytes were determined to be competent in FA oxidation due to the incorporation of ^{13}C into glutamate, a process requiring the astrocyte-specific enzyme glutamine synthetase.

In all, the physiological relevance of FA oxidation in the CNS, rather than the competence of astrocytes, remains highly debated.

1.6.4 The role of gap junctions in glial metabolic coupling

Gap junctions permit rapid bidirectional transfer of cytosolic molecules up to 1-2 kDa between closely apposed cells (Loewenstein, 1981; Neijssen *et al.*, 2005): connecting them electrically and metabolically (Bennett and Zukin, 2004). Gap junction proteins are expressed by all major glial cell types (Wallraff *et al.*, 2004; Garg *et al.*, 2005; Nualart-Marti *et al.*, 2013) and here we summarise gap junction coupling of oligodendrocytes and astrocytes, which is the basis of the pan-glial network described by Rash *et al.* (1997) and Nagy and Rash (2003).

Gap junctions often exist in clusters on the cell membrane and form a cytoplasm-cytoplasm connection through the pairing of two hemichannels on adjacent cells. The channels are composed of six individual connexins (Cx) and form a connexon. Homotypic gap junctions are composed of the same subtype of connexin, whereas heterotypic gap junctions are comprised of different but compatible subtypes (Willecke *et al.*, 2002). Opening of the channel is dynamically regulated by extracellular calcium concentration, phosphorylation, and transmembrane voltage (Gómez-Hernández *et al.*, 2003; Garg *et al.*, 2005; Goodenough and Paul, 2009).

Astrocytes are gap junction-coupled to other astrocytes and oligodendrocytes (Ransom and Kettenmann, 1990; Robinson *et al.*, 1993). Most oligodendrocyte-astrocyte gap junctions are formed by heterotypic pairing of Cx43–Cx47 or Cx30–Cx32 channels and are essential for the maintenance of CNS white matter (reviewed in Basu and Das Sarma (2018)). Gap junctions between oligodendrocytes in brain white matter was recently demonstrated in mouse *ex vivo* slice cultures (Maglione *et al.*, 2010; Wasseff and Scherer, 2011) and are likely formed from Cx47 or Cx32 pairings (reviewed in Papaneophytou *et al.* (2019)).

Gap junctions are essential during neurodevelopment, particularly in white matter areas such as the corpus callosum (reviewed in Sutor and Hagerty (2005)). The function of oligodendrocyte-astrocyte gap junctions is essential for nervous system maintenance and genetic mutation leads to the demyelinating or dysmyelinating phenotypes observed in X-linked Charcot-Marie-Tooth disease (Kleopa and Scherer, 2006), hypomyelinating leukodystrophy type 2 (Uhlenberg *et al.*, 2004; Bugiani *et al.*, 2006; Tress *et al.*, 2011), and Pelizaeus-Merzbacher-like disease (Orthmann-Murphy *et al.*, 2007).

Coupled cells can be revealed by the injection of tracer molecules small enough to diffuse through gap junctions, such as Lucifer yellow or biocytin. This is well established in *ex vivo* preparations (Butt and Ransom, 1989; Vaney, 1991; Peinado *et al.*, 1993; Hampson and Robinson, 1995) with some *in vivo* application (Blivis *et al.*, 2019). Dye-filling a single astrocyte often reveals a vast network of interconnected cells (Ball *et al.*, 2007).

1.6.5 Nanotubes

Nanotubes (also known as tunnelling nanotubes and gliopodia) are long cellular projections that contain an F-actin cytoskeleton and facilitate cell-to-cell communication (Gerdes *et al.*, 2007). They likely allow the intercellular transfer of vesicles and organelles, electrical signals, calcium ions, and pathogens in many diverse cell types (Davis and Sowinski, 2008; Sowinski *et al.*, 2008; Gousset *et al.*, 2009; Abounit and Zurzolo, 2012). Nanotubes have been observed in neuronal cell lines (Rustom, 2004; Gousset *et al.*, 2009) and in primary brain-derived astrocytes and neurons (Wang *et al.*, 2011). These inter-cellular connections couple cells by gap junctions (Wang *et al.*, 2011) or through open-ended cytoplasm-cytoplasm bridges (Gerdes *et al.*, 2007). Thus, nanotubes and similar structures might facilitate trans-cellular energy support; however, the transfer of energy substrates *per se* has not been demonstrated to our knowledge. Cytonemes, which are morphologically similar to nanotubes, have been reported in the CNS during development (Vasenkova *et al.*, 2006; Sanders *et al.*, 2013; Stanganello *et al.*, 2015) where they deliver the morphogen, Sonic Hedgehog, necessary for the formation of the murine neural tube (Hall *et al.*, 2021).

1.7 Vulnerability of white matter to hypoxia

The CNS requires a large proportion of the body's total oxygen to sustain its high energy demands. Oxygen is supplied to the CNS via the vasculature and is estimated to receive 15% of cardiac output (Williams and Leggett, 1989). Cessation of blood flow to the brain results in loss of consciousness within 7 seconds (Kabat and Anderson, 1943) and permanent brain damage after only a few minutes, highlighting the importance of continuous oxygen-rich blood flow. White matter is recognised as particularly vulnerable to hypoxia-ischaemia during development and in adulthood. In this section, we discuss the current understanding of white matter injury as a result of hypoxia-ischaemia during development.

1.7.1 Hypoxic injury

Insufficient oxygen supply to the CNS has severe consequences on cell function with prolonged hypoxic insults leading to neural cell death. As a short-term adaptation, hypoxia-inducible factor 1 (HIF1) activates gene targets involved in vasodilation (Dalkara *et al.*, 1994; Iadecola *et al.*, 1995), angiogenesis (Krupinski *et al.*, 1994), and rewires energy metabolism towards increased glycolysis (reviewed in Sharp and Bernaudin (2004)). In particular, HIF1 activity increases GLUT1 transporters on the cell membrane and upregulates glycolytic enzyme expression to increase ATP production (Semenza *et al.*, 1996; Ratcliffe *et al.*, 1998; Bergeron *et al.*, 1999). Nonetheless, hypoxia in the brain results in an approximately 90% reduction of ATP levels within 5 minutes (Mukandala *et al.*, 2016).

Hypoxia-ischaemia produces a cascade of well-characterised secondary consequences that further compound the initial hypoxic injury. Oxygen deprivation forces anaerobic respiration, which produces lactate as a by-product and leads to extracellular acidification. It has been estimated that under ischaemic conditions, the brain tissue environment can drop to pH 6.6 (Rehncrona, 1985), inducing irreversible cellular changes (Pang *et al.*, 2020). Aside from primary energy failure from the lack of glucose (Shalak and Perlman, 2004), secondary energy failure often follows restored perfusion due to significant cellular stress (Lorek *et al.*, 1994). Brain OPCs and EMOLs are particularly vulnerable to the effects of OGD and reperfusion (Follett *et al.*, 2000; Deng *et al.*, 2003; Follett *et al.*, 2004; Deng *et al.*, 2006). Finally, inflammation ensues as a result of cellular stress, cell death, and pro-inflammatory cytokine secretion (Dawson *et al.*, 1996; Darnall *et al.*, 2017). The resulting weakening of the BBB due to inflammation allows infiltration of peripheral immune cells into the CNS further compounding injury (Palmer *et al.*, 2004).

1.7.2 Developmental white matter injury

The *in utero* environment has a relatively low oxygen tension of 20-25 mmHg (Paller *et al.*, 2002) compared to the adult brain and spinal cord, where the oxygen tension is approximately 35-39 mmHg (Martirosyan *et al.*, 2011). Therefore, the CNS develops in a comparatively low-oxygen environment that is predisposed to hypoxic injury. Pre-term babies are at major risk of hypoxic/ischaemic brain injury since they have underdeveloped

lungs and heart muscle that cannot provide sufficient oxygen and blood to the brain. This often results in white matter injury (WMI), a leading cause of cerebral palsy and life-long cognitive and motor deficits (reviewed in Liu *et al.* (2013b)). In fact, WMI is the most common brain injury associated with pre-term birth (Back and Miller, 2014) with the highest risk window between 24-32 weeks of gestation. At this time, EMOLs are populating the developing brain white matter, which is poorly vascularised and susceptible to hypoxia-ischaemia (Kinney and Back, 1998; Back *et al.*, 2001; Volpe, 2001; 2009). Periventricular leukomalacia (PVL) is the most severe form of pre-term WMI and is characterised by the loss of white matter surrounding the ventricles of the brain.

Multiple factors are proposed to make brain EMOLs particularly vulnerable to hypoxia-ischaemia during development (reviewed in van Tilborg *et al.* (2018)). It has been suggested that dysregulation of the Wnt/β-catenin pathway likely contributes to WMI injury (Fancy *et al.*, 2009; 2011; Lee *et al.*, 2015). Similarly, altered HDAC activity has been shown to inhibit OPC differentiation after hypoxia *in vitro* (Jablonska *et al.*, 2016). Moreover, HIF1 activation in OPCs from hypoxia inhibits differentiation, both *in vitro* and in *ex vivo* brain slice cultures (Yuen *et al.*, 2014; Allan *et al.*, 2021) decreasing the EMOL population.

The pathology of WMI and PVL has been modelled *in vivo* by ligating blood vessels in the brain of P7 rats, which produces a selective vulnerability of white matter. In these models, glutamate excitotoxicity is considered an important pathological factor since WMI is reduced by administering glutamate receptor blockers (Follett *et al.*, 2000; Follett *et al.*, 2004). That said, brain-derived oligodendroglia are vulnerable to OGD without glutamate excitotoxicity *in vitro* (Lyons and Kettenmann, 1998; Deng *et al.*, 2003).

Most of our understanding of EMOL vulnerability to hypoxia-ischaemia comes from experimental evidence examining brain or brain-derived cells. In comparison, the vulnerability of spinal cord EMOLs has not been explored, to our knowledge, within the literature.

1.7.3 Spinal cord white matter susceptibility to hypoxia

The spinal cord vasculature is established in the first 6 months of embryonic development (Gillilan, 1958) and, in comparison to the brain, has 40-60% lower blood perfusion (Martirosyan *et al.*, 2011). Spinal cord white matter has a comparatively sparser capillary

network compared to grey matter (Zhang *et al.*, 1997) and might be more vulnerable to hypoxia-ischaemia (reviewed in Hernandez-Gerez *et al.* (2020)). However, in most cases where pre-term infants or neonates incur brain WMI from hypoxia-ischaemia, there is often no reported involvement of spinal cord white matter. For example, in a questionnaire to paediatricians, Ruggieri and Pike (1999) found that cases of pre-, peri-, and neonatal spinal cord injury was associated with brain haemorrhage rather than a systemic hypoxic event. Based on our review of the literature, it appears the spinal cord is often not involved in developing brain WMI despite it being a poorly vascularised tissue.

Recent work in a mouse model of spinal muscular atrophy (SMA), an often-fatal disease of children, suggests spinal cord EMOLs might be somewhat resistant to hypoxia. SMA is caused by homozygous deletion of the survival of motor neuron (*SMN1*) gene and lower motor neuron cell death (Burghes and Beattie, 2009) but is recognised as a multi-system disorder with extensive tissue damage (Sleigh *et al.*, 2011; Hamilton and Gillingwater, 2013) and vascular deficits (Somers *et al.*, 2012). Work by Somers *et al.* (2016) examined the vasculature of the spinal cord in early postnatal SMNΔ7 transgenic mice, a model of SMA. The authors reported that the spinal cord of SMA mice was significantly less vascularised at P5 compared to control littermates. In subsequent work, Hernandez-Gerez *et al.* (2020) confirmed widespread hypoxia in SMA mouse tissues, including the spinal cord.

O'Meara *et al.* (2017) assessed spinal cord myelination in the same SMNΔ7 transgenic mouse and found it was unaffected at P5 compared to WT littermates as assessed by g-ratio. This is surprising given the vulnerability of brain EMOLs to hypoxia-ischaemia as previously discussed. A similar report was made in mouse pups that were exposed to hypoxia-normoxia (7% oxygen *vs.,* 20%) for 2-minute cycles over 6 hours, daily, until the animals reached P10. Examination of CNS myelination showed mice exposed to this hypoxic protocol had significant hypomyelination in major white matter areas of the brain but not the spinal cord, determined by MBP staining (Cai *et al.*, 2012).

Considering these reports, and given the poorer blood perfusion of the spinal cord compared to the brain, these observations raise the possibility there are divergent susceptibilities of EMOLs to hypoxia-ischaemia based on their anatomical location.

1.8 Thesis aims

The spinal cord EMOL population is poorly characterised in terms of its vulnerability to hypoxia-ischaemia. Our understanding of the oligodendrocyte's metabolic phenotype stems, in large part, from studies examining brain or brain-derived oligodendroglia. However, the oligodendrocytes that populate the spinal cord and brain arise from different compartments in the developing CNS and, as shown recently, cluster differently in RNA sequencing analyses (Floriddia *et al.*, 2020). Furthermore, brain and spinal cord oligodendroglia respond differently in a variety of experimental settings (Chen *et al.*, 2013; Bechler *et al.*, 2015). Based on recent incidental evidence from an SMA mouse model, we hypothesised this could extend to their response to hypoxia-ischaemia.

How spinal cord EMOLs respond to hypoxia-ischaemia is an important question for two principal reasons: i) the spinal cord is exposed to hypoxia-ischaemia in a variety of disease scenarios (reviewed in Hernandez-Gerez *et al.* (2019)) meaning the answer has implications for therapy; ii) it is important to determine if the results of assays done in brain (or using brain oligodendroglia) can be extrapolated to spinal cord and *vice versa*.

Therefore, the overall aim of this thesis was to characterise the response of developing spinal cord EMOLs to the effects of hypoxia-ischaemia using an *in vitro* culture system generated from acutely harvested spinal cord glia. Specific aims were to:

(i) Establish and systematically characterise an *in vitro* model of early myelinating spinal cord mixed glia generated from neonatal mice.

(ii) Use this model to explore how spinal cord EMOLs respond to hypoxia-ischaemia and secondary consequences such as acidosis, energy deprivation, and inflammation.

Unexpectedly, we found spinal cord glia, including EMOLs, survived without exogenous energy substrates for 6 days. Therefore, the aims expanded to:

(i) Explore the putative role of astrocytes in providing metabolic support to the EMOL in the absence of exogenous energy substrates.

(ii) Examine lipid components in the context of glial cell survival when exogenous energy substrates are withdrawn.

Chapter 2

Methods and materials

Product code and manufacturer are in brackets on first mention. Common laboratory chemicals are displayed as formulae (e.g. sodium hydroxide as NaOH). Standard international units are used throughout.

2.1 Commonly used buffers and solutions

Commonly used materials such as buffers and solutions are referenced throughout this chapter. The composition of these are detailed in the following subsections.

2.1.1 Phosphate buffered saline

Phosphate buffered saline (PBS) was made to a final concentration of 137 mM NaCl, 1.8 mM KH_2PO_4, 2.7 mM KCl, and 10 mM Na_2HPO_4, at pH 7.4 in deionised water (diH_2O). Solutions were stored at room temperature. Recipe in Appendix 7.4.1.

2.1.2 Tris-acetate-EDTA buffer

Tris-acetate-EDTA buffer was made to a final concentration of 40 mM Tris, 20 mM acetic acid, 1 mM EDTA in diH_2O. Solutions were stored at room temperature. Recipe in Appendix 7.4.2.

2.1.3 Paraformaldehyde solution

Paraformaldehyde (PFA) powder (P6148, Sigma-Aldrich) was dissolved in PBS (for immunocytochemistry use) or diH_2O (for strong fix) to make an 8% solution and pH was adjusted to 7.4. Solutions were stored at 4 °C. Recipe in Appendix 7.4.3.

2.2 Animals

Wildtype C57BL/6 (WT; Charles River, UK) and "PEOT-*Tg*" transgenic mice (section 2.2.1) on a C57BL/6 background were used for the generation of primary cell cultures. All animals were maintained in the University of Glasgow Biological Services facility and used in accordance with the Animals (Scientific Procedures) Act 1986. Animals were housed under

12-hour light-dark cycle with food and water available *ad libitum*. All experiments were approved by the Ethical Review Committee of the University of Glasgow.

2.2.1 PEOT-*Tg* mice

Compound reporter mice hemizygous for each of three transgenes (Figure 2.1) were used to generate some primary cell cultures. **P**LP-CreER^{T2}::Cnp-m**Eo**s2-PTS1::Ai14(Rosa26-td**T**) or "PEOT-*Tg*" mice are the result of crossing three distinct transgenic lines (Table 2.1) to fluorescently label oligodendrocytes with tdTomato and their peroxisomes with mEos2. Genotyping is described in Appendix 7.2.

Table 2.1 | Transgenic lines crossed to generate the PEOT-*Tg* mouse line.

Transgenic line	Transgene	Function
PLP-CreER^{T2}	CreER^{T2} expression controlled by *Plp1* regulatory region	Cre recombinase expression only in *Plp1* expressing cells (oligodendrocytes) upon exposure to tamoxifen (*in vivo*) or 4-hydroxytamoxifen (*in vitro*)
Ai14(Rosa26-tdT)	tdTomato fluorophore gene in ubiquitously expressed *Rosa26* locus with floxed “stop cassette”	*lox*P-sites flank “stop cassette” that recombines in cells expressing Cre recombinase allowing transcription of tdTomato to fluorescently label the cell of interest
Cnp-mEos2-PTS1	mEos2-encoding gene with a PTS1 tag driven under the *Cnp1* promotor	Expression of mEos2-PTS1 in cells expressing *Cnp1* to fluorescently label peroxisomes

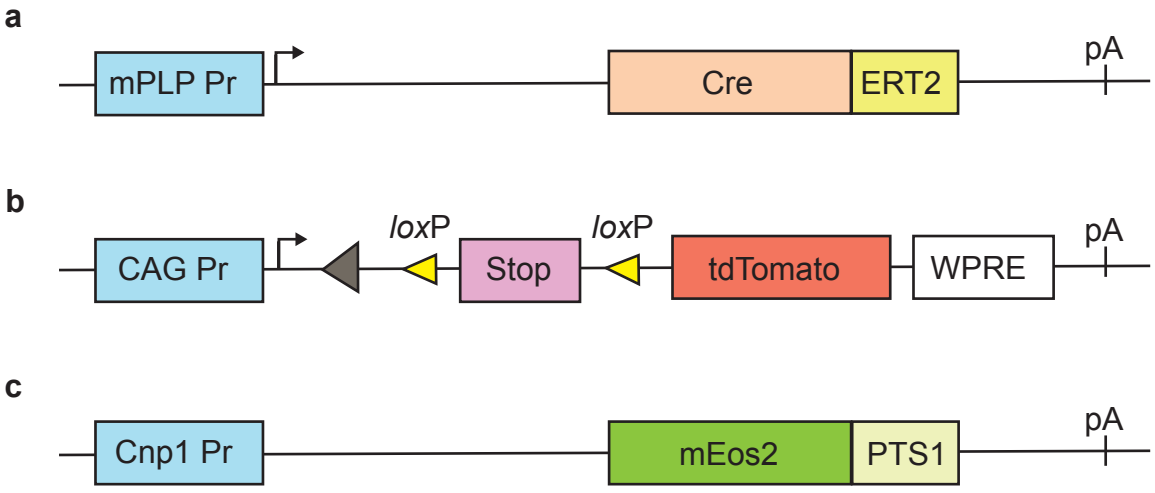

Figure 2.1 | **Transgenes in the PEOT-*Tg* mouse. (a)** PLP-CreER^{T2} transgene from Leone *et al.* (2003). **(b)** *lox*P-flanked "stop cassette" preceding the tdTomato transgene in the *Rosa26* locus (Madisen *et al.*, 2010). Grey triangle indicates FRT site. Yellow triangles indicate *lox*P sites. The transgene contains a woodchuck hepatitis post-translational regulatory element (WPRE) to stabilise the RNA. **(c)** Cnp-mEos2-PTS1 transgene from Richert *et al.* (2014). The transgenes end with a polyA (pA) signal. Information extracted from the cited publications and re-drawn.

2.3 Cell culture

All cultured cells were maintained in an incubator at 37 °C under a humidified 5% CO_2 atmosphere. Aseptic technique was employed throughout and only cell culture grade materials and reagents were used.

2.3.1 Commonly used materials

Commonly used cell culture items are listed below with their catalogue number and manufacturer in brackets:

- 35 mm Petri dish (430165, Corning)
- 140 mm Petri dish (11339283, Thermo Fisher)
- 0.22 µm 500 mL vacuum filter unit (15780319, Fisher Scientific)
- 0.22 µm Sartorius™ Minisart™ syringe filter (10509821, Fisher Scientific)
- BLAUBRAND® Neubauer improved haemocytometer (BR717810-1EA, Merck)
- Glass Pasteur pipettes (11566963, Fisherbrand™)
- Trypan blue, 0.4% solution (T8154, Sigma-Aldrich)
- Cell culture grade PBS (10010023, Gibco™)
- Cell culture grade water (W3500, Sigma-Aldrich)
- Penicillin-streptomycin 100x stock (P0781, Sigma-Aldrich)

2.3.2 Stock solutions and commonly used reagents

2.3.2.1 Boric acid buffer

Boric acid buffer was made to a final concentration of 50 mM H_3BO_3 (boric acid; B0394, Sigma-Aldrich) and 23 mM $Na_2B_4O_7$ (sodium tetraborate; 221732, Sigma-Aldrich) in cell culture grade water (W3500, Sigma-Aldrich). Solutions were filter sterilised and stored at 4°C. Recipe in Appendix 7.4.4.

2.3.2.2 Biotin

D-biotin (B4501, Sigma-Aldrich) diluted to 10 µg/mL in filter sterilised 0.01 M NaOH. Aliquots were stored at -20°C.

2.3.2.3 Deoxyribonuclease

Deoxyribonuclease (DNase) I from bovine pancreas (DN25, Sigma-Aldrich) diluted in Leibovitz's L-15 medium to a final concentration of 0.5 mg/mL. Aliquots were stored at -20°C.

2.3.2.4 Hydrocortisone

Hydrocortisone (H0396, Sigma-Aldrich) dissolved in cell culture grade water to 10 mM (1000x stock) and stored in aliquots at −20 °C. Before use, a working stock was made by diluting 1:1000 in cell culture grade water to 10 µM. Aliquots of the working stock were also stored at -20°C.

2.3.2.5 Insulin

Human recombinant insulin (I2643, Sigma-Aldrich) dissolved in filter sterilised 0.01 M HCl to a final concentration of 2.5 mg/mL. Aliquots were stored at -20°C.

2.3.2.6 Magnetic-activated cell sorting buffer

Magnetic-activated cell sorting (MACS) buffer contained 0.5% bovine serum albumin (A9418, Sigma-Aldrich) dissolved in cell culture grade PBS. The solution was filter sterilised and aliquots were stored at -20°C.

2.3.2.7 N1 supplement

N1 supplement contained 1 mg/mL apo-transferrin (T2252, Sigma-Aldrich), 20 mM putrescine (P5780, Sigma-Aldrich), 4 µM progesterone (P6149, Sigma-Aldrich), 6 µM sodium selenite (S9133, Sigma-Aldrich), made in cell culture grade PBS. Aliquots were stored at -20°C. Recipe in Appendix 7.4.5.

2.3.2.8 Papain

A stock of 333 U/mL papain (P4762, Sigma-Aldrich) was made by dissolving 25 mg in 750 µL of Dulbecco's Modified Eagle Medium (DMEM; 31885-023, Gibco™). The solution was mixed well and incubated at 37°C for 10 minutes. A working stock of 30 U/mL was made by diluting 200 µL of the stock in 3 mL of DMEM (31885-023, Gibco™). A few crystals of L-cysteine (C7352, Sigma-Aldrich) were added before use, producing a slight colour change to orange-yellow.

2.3.2.9 Papain inhibitor solution

Papain inhibitor solution contained 3 mg/mL bovine serum albumin (A9418, Sigma-Aldrich) and 0.04 mg/mL DNase I from bovine pancreas (DN25, Sigma-Aldrich) in cell culture grade PBS. The solution was filter sterilised and aliquots stored at -20°C for a maximum of 6 months.

2.3.2.10 Poly-L-lysine

Poly-L-lysine (P1274, Sigma-Aldrich) dissolved in cell culture grade water to a final concentration of 5 mg/mL. Aliquots were stored at -20°C.

2.3.2.11 1.33% collagenase

Collagenase type I powder (10114532, Gibco™) dissolved in Leibovitz's L-15 media (11415049, Invitrogen™) media to 1.33%. Aliquots were stored at -20°C.

2.3.2.12 30% glucose solution

D-glucose (G7021, Sigma-Aldrich) dissolved in cell culture grade water to 30%, filter sterilised, and stored at 4°C.

2.3.3 Culture media

Cell culture media are based on recipes published by Thomson *et al.*, 2006; 2008.

2.3.3.1 Dissecting media

Hank's balanced salt solution (HBSS) without calcium and magnesium (H9394, Sigma-Aldrich) with 1% penicillin-streptomycin.

2.3.3.2 Plating media

A mixture of 50% DMEM (1 g/L D-glucose plus pyruvate; 31885-023, Gibco™), 25% HBSS with calcium and magnesium (H9269, Sigma-Aldrich), 25% horse serum (26050-088, Gibco™), with 0.75% penicillin-streptomycin.

2.3.3.3 Highly enriched media

DMEM (4.5 g/L D-glucose; 41966-029, Gibco™), 10 ng/mL biotin, 50 nM hydrocortisone, 10 µg/mL insulin, 1% N1 supplement (5 µg/mL apo-transferrin, 16.1 µg/mL putrescine, 20 nM progesterone, 5.19 ng/mL selenium), and 1% penicillin-streptomycin. This is media contained 25 mM glucose, 1 mM pyruvate, and 4 mM glutamine, in addition to amino acids and vitamins described in Table S6.

2.3.4 Poly-L-lysine coated glass coverslips

Primary cell cultures were typically grown on 13 mm borosilicate glass coverslips (631-0150, VWR) coated in poly-L-lysine. A working solution of poly-L-lysine was made by diluting the stock (section 2.3.2.10) in boric acid buffer to 0.1 mg/mL. The working stock was reused a maximum of three times. Autoclaved 13 mm borosilicate glass coverslips were incubated in 50 mL of poly-L-lysine in boric acid buffer for at least 1 hour at 37°C in a 140 mm Petri dish (approximately 200 coverslips per dish). Coverslips were then washed three times in autoclaved diH_2O. Coated coverslips were placed into 35 mm Petri dish (3 per dish) and allowed to air dry for a minimum of 2 hours in a cell culture hood before being stored at 4°C prior to use.

2.3.5 Live-cell imaging dishes

Primary cell cultures used for live-cell imaging were plated on in-house made imaging dishes prepared as described in Bijland *et al.* (2019). Briefly, three equidistant 11 mm diameter holes were drilled into the bottom of Falcon® 35 mm Petri-dishes (353001, Corning) and 25 mm diameter Menzel Gläser glass coverslips (MENZCB00250RAC, Thermo Fisher supplied by VWR) were glued to the base of the dishes using Sylgard® 184 non-toxic silicone adhesive. After curing for 7 days at room temperature, or overnight at 65°C, dishes were cleaned in 70% ethanol and sterilised under ultraviolet light for 30 minutes. The SDS wash step in the published protocol was omitted. Dishes were then coated by pipetting ~2 mL of poly-L-lysine (prepared as described in section 2.3.4) into each imaging dish to coat the entire surface. After 2 hours at 37°C, poly-L-lysine was removed and dishes were rinsed three times with autoclaved diH_2O. After air-drying for a minimum of 2 hours in a cell culture hood, dishes were stored at 4°C.

2.3.6 Primary cell culture

Primary cell cultures were generated from postnatal day (P) 3-5 WT or PEOT-*Tg* mice. Animals used for cell culture were culled using intraperitoneal overdose of pentobarbitone (Euthatal, Vericore, UK) and exsanguination by cutting the femoral artery under Schedule 1 of the Animals (Scientific Procedures) Act 1986. Details of culture media are in section 2.3.3.

2.3.6.1 Mouse primary mixed glial cultures

Euthanised pups were decapitated, sprayed with 70% ethanol (avoiding the exposed spinal cord) to decontaminate the skin, and placed in a Petri dish on ice. Spinal cords were removed using sterile instruments under a dissecting microscope and placed into dissecting media. Meninges and dorsal root ganglia were removed before placing the cords into 1 mL (per 2 cords) dissecting media. The cords were not triturated. The tissue was incubated in 1x trypsin diluted from a 10x stock (T4549, Sigma-Aldrich) in dissecting media at 37°C for 20-25 minutes. Digestion was stopped by adding 1 mL plating media per 2 mL of solution, then DNase was added to a final concentration of 0.04 mg/mL. Tissue was dissociated by triturating with a glass Pasteur pipette, approximately 10 times. The

cell suspension was supplemented with 5 mL plating media then centrifuged at 180 x *g* for 5 minutes. The supernatant was discarded and the cell pellet was resuspended in 1 mL plating media. Cell yield was determined by counting viable cells in 0.2% (final) trypan blue (T8154, Sigma-Aldrich) using a haemocytometer. Cells were plated at 30,000 cells per 13 mm glass coverslip, with three coverslips per 35 mm Petri dish. Cells used for live imaging experiments were handled with some modification as described in section 2.4.8 and plated into 3 wells of live imaging dishes (section 2.3.5). Cells were allowed to adhere for 2 hours at 37°C before an additional 200 µL of plating media and 500 µL of HE media was added to each Petri dish.

2.3.6.2 Mouse primary EMOL-enriched cultures

EMOL-enriched cultures were generated by adapting the protocol of Mayer-Pröschel (1998). A minimum of ten spinal cords were used and dissected as described in section 2.3.6.1. Dissected cords were placed in 3 mL 1.33% collagenase and incubated at 37°C for 30 minutes. The tissue was then centrifuged at 200 x *g* for 5 minutes, then 1,560 x *g* for 1 minute. The cell pellet was resuspended in 3 mL 30 U/mL papain and returned to a 37°C incubator for 30 minutes with gentle mixing every 10 minutes. Digestion was stopped by adding 300 µL papain inhibitor solution. After a 5-minute incubation at room temperature, digested tissue was dissociated by trituration with a glass Pasteur pipette, approximately 10 times. The cells were centrifuged at 200 x *g* for 5 minutes, then 1,560 x *g* for 1 minute, before resuspending the pellet in 2 mL ice-cold MACS buffer. Cell yield was determined by counting viable cells in 0.2% (final) trypan blue (T8154, Sigma-Aldrich) using a haemocytometer. As a quality control measure, only preparations with greater than 4 million cells at this stage were used. The cell suspension was centrifuged again at 200 x *g* for 5 minutes, then 1,560 x *g* for 1 minute, and the cell pellet was resuspended in 180 µL ice-cold MACS buffer. FcR blocking reagent (130-092-575, Miltenyi Biotec) was added to the cell suspension (40 µL per 10 million cells, 40 µL minimum), mixed well, and incubated on ice for 10 minutes. Anti-O4 MicroBeads (130-096-670, Miltenyi Biotec) were added to the cells (20 µL per 10 million cells, 20 µL minimum), mixed well, and incubated on ice for 15 minutes. The cells were washed by adding 2 mL ice-cold MACS buffer, pipetting up and down twice, then centrifuged at 300 x *g* for 5 minutes. The

cell pellet was resuspended in 500 µL ice-cold MACS buffer and passed through an LS column (130-042-401, Miltenyi Biotec) attached to a magnet. The column was flushed three times with 3 mL ice-cold MACS buffer, collecting the unlabelled cells in a 15 mL centrifuge tube. The column was then removed from the magnet and 5 mL ice-cold MACS buffer was gently forced through with a plunger to expel the $O4^+$ MicroBead-labelled cells, which were collected in a centrifuge tube. Cells were centrifuged at 200 x *g* for 5 minutes, then 1,560 x *g* for 1 minute, resuspended in 1 mL plating media, and cell yields determined by counting in the presence of trypan blue as before. Cells were plated at 30,000 cells per 13 mm glass coverslip, three coverslips per 35 mm Petri dish, and allowed to adhere for 2 hours at 37°C. An additional 200 µL plating media and 500 µL HE media was then added to each Petri dish.

2.3.6.3 Mouse myelinating cell cultures

Myelinating cultures were used as experimental controls and prepared according to the protocol in Bijland *et al.* (2019). Briefly, E13.5 mouse embryos were decapitated, spinal cords dissected, and meninges discarded. The tissue was enzymatically digested in 1x trypsin at 37°C for 15 minutes. Digestion was stopped by adding plating media. DNase was added to a final concentration of 0.04 mg/mL and the tissue was triturated with a glass Pasteur pipette. The cells were then treated as described in section 2.3.6.1 but were plated at 150,000 cells per 13 mm glass coverslip. Cultures were fed every 2-3 days with HE media until day *in vitro* (DIV) 12, then the cells received HE media without insulin.

2.4 Cell culture assays

On DIV 1, approximately 18 hours after plating, serum-rich plating media was completely removed and replaced with serum-free HE media containing 1 µM 4-hydroxytamoxifen (4-HT; H7904, Sigma-Aldrich; see Appendix 7.4.7). Cells were incubated with 4-HT for 1 hour at 37°C to induce tdTomato expression in PEOT-*Tg* cells. WT cells were treated identically. After 1 hour, some coverslips were fixed in 4% PFA (as described in section 2.4.14) to represent experimental time zero (t0).

For remaining coverslips, all media was removed, rinsed with 1 mL treatment media (defined as the media used in the assay), and replaced with 1 mL treatment media. All treatment media contained 10 ng/mL biotin, 1% N1 (5 µg /mL apo-transferrin, 16.1 µg/mL putrescine, 20 nM progesterone, 5.19 ng/mL selenium), 50 nM hydrocortisone, and 10 µg/mL insulin. Antibiotic or antifungal agents were not used except in HE media (1% penicillin-streptomycin). All treatment media was pre-warmed to 37°C and equilibrated to 5% CO_2 in a cell culture incubator for 2-3 hours before use. Cells were fed at t3d (t0 plus 3 DIV) by removing 500 µL culture media and replacing with 500 µL fresh treatment media. At time points or the end of experiments, coverslips were fixed as described in section 2.4.14.

2.4.1 DMEM-based and salts-only media

During experimentation, cells were maintained in either DMEM-based media (DM; A1443001, Gibco™; formulation shown in Table S6) containing amino acids and vitamins or in a salts-only (SO) version, containing only the inorganic salts of DMEM (110 mM NaCl, 44 mM $NaHCO_3$, 0.91 mM $NaH_2PO_4 \cdot H_2O$, 5.33 mM KCl, 0.8 mM $MgSO_4$, 1.8 mM $CaCl_2$, 0.2 µM $Fe(NO_3) \cdot 9\,H_2O$). Both media contained the hormones detailed in section 2.4 but lacked glucose, pyruvate, or glutamine unless supplemented. Glucose was added from a 30% D-glucose stock. As a control in some experiments, HE media was used (25 mM glucose, 1 mM pyruvate, 4 mM glutamine) and made as described in section 2.3.3.3.

2.4.2 Metabolic inhibitors

Cells were incubated with azide and/or iodoacetate diluted in DM at 10 mM and 1 mM, respectively. Cells were maintained under these conditions for 5 or 24 hours before fixation. Preparation of the inhibitor stocks is described below in sections 2.4.2.1 and 2.4.2.2.

2.4.2.1 Sodium iodoacetate

Sodium iodoacetate powder (57858-5G-F, Sigma-Aldrich) was thawed and a small amount placed in a bijou and weighed. The required volume of DMEM (A1443001, Gibco™) was added to make a 1 M stock. The solution was then filter sterilised and stored at -20°C.

2.4.2.2 Sodium azide

A small amount of sodium azide powder (S2002, Sigma-Aldrich) was placed in a bijou and weighed. The required volume of DMEM (A1443001, Gibco™) was added to make a 5 M stock. The solution was then filter sterilised and stored at -20°C.

2.4.3 Anoxia and hypoxia

Cells maintained in DM were placed into a hypoxic chamber (27310, Stemcell Technologies) and flushed with 5% CO_2 / 95% N_2 (154906-V-C, BOC, UK) at 20 L/min controlled by a single flow meter (27311, Stemcell Technologies) for 5 minutes. The chamber was sealed under positive pressure and placed in a cell culture incubator. After 24 hours, the chamber was opened and cells were immediately fixed or returned to an incubator for a further 24 hours before fixation.

2.4.4 pH sensitivity

Tolerance of cells to an acidic environment was tested by adjusting the buffering capacity of bicarbonate-free DMEM (D5030, Sigma-Aldrich; same composition shown in Table S6). The powdered media was dissolved to a final volume with 900 mL cell culture grade water at room temperature before filter sterilising. Media was used in 9 mL aliquots and the final pH in 5% CO_2 was adjusted by adding $NaHCO_3^-$ from a 1 M stock (below, section 2.4.4.1). The concentrations of $NaHCO_3^-$ used to achieve the desired pH in 5% CO_2 are shown in Table 2.2, determined by the Henderson-Hasselbalch equation: $\mathrm{pH} = \mathrm{pK_a} + \log(\frac{[\mathrm{A^-}]}{[\mathrm{HA}]})$. Sodium bicarbonate, hormones (section 2.4), and water were added to make the final 10 mL volume. Cells were cultured for 6 days under these conditions before fixation.

2.4.4.1 Sodium bicarbonate solution

Sodium bicarbonate powder (S5761, Sigma-Aldrich) dissolved in cell culture grade water to 1 M then filter sterilised. Solutions were stored at 4°C for up to 1 month.

Table 2.2 | Adjustment of bicarbonate-free cell culture media with sodium bicarbonate to achieve the desired pH in 5% CO_2.

pH in 5% CO_2	$NaHCO_3^-$ (mM)
6.6	4
6.8	6.3
7.0	10
7.2	16
7.4	25
7.6	44

2.4.5 Glucose and nutrient deprivation

To deprive cells of glucose and other exogenous energy substrates (pyruvate and glutamine), treatment media was made in DM (A1443001, Gibco™, formulation shown in Table S6). For nutrient deprivation, cells were grown in SO media lacking the amino acids and vitamins present in DM (section 2.4.1). Cells were cultured in these conditions for 6 days before fixation.

2.4.6 Reintroduction of glucose

Following 5 days of culture in glucose-free DM, a coverslip was fixed at t5d (as a baseline) before all media was replaced with DM containing 5 mM glucose. Cells were returned to the incubator for 24 hours before fixation.

2.4.7 Inflammatory factors

Lyophilized stocks were reconstituted as per the manufacturer's instructions to 100 µg/mL in sterile PBS containing 0.1% bovine serum albumin. The final concentrations in culture were 20 ng/mL IFNγ (485-MI-100, R&D Systems) and 50 ng/mL TNF (410-MT-050, R&D Systems). Cells were cultured in these conditions for 6 days before fixation.

2.4.8 Live-cell imaging

To track cell survival, PEOT-*Tg* spinal cord mixed glia were plated in wells of live-cell imaging dishes as described in section 2.3.6.1 but handled with some modification to that described in section 2.4. Mixed glial cells were plated in plating media containing 1 µM 4-HT. After 2 hours, all media was replaced with 500 µL fresh plating media and 500 µL HE media. On DIV 1, approximately 18 hours after initial plating, media was replaced with fresh serum-free HE media for 1 hour at 37°C. All media was then removed, rinsed once with 1 mL glucose-free DM, and replaced with 1 mL DM containing 5 or 0 mM glucose. Culture dishes were secured in a holder suitable for the microscope (001272, PeCon, Germany) then returned to the incubator for 1 hour. Live-cell imaging was carried out on a Zeiss Z1 Spinning Disk confocal microscope (Carl Zeiss AG, Germany) equipped with a Yokogawa

CSU-X1 filter wheel and spinning disc unit, a Photometrics Evolve 512 delta EM-CCD camera with 568 laser lines, and an 25x/0.8W LCI PlaN objective. During imaging, cells were maintained in the incubator attachment in 5% CO_2 at 37°C. Zen Blue software (Carl Zeiss AG, Germany) was used for control and image acquisition. Fluorescent tdTomato-labelled cells were selected by eye across all 3 wells of an imaging dish. A Z-stack image (max. 10 slices, laser power 5%, and exposure times $<$ 300 ms per slice) was captured and coordinates recorded from the motorised stage. Images were captured daily by returning to the coordinates for each cell until the end of the experiment at t6d.

2.4.9 Dye-filling of EMOLs

Mixed glial cultures were maintained in 5 mM glucose DM until t6d before single EMOLs were dye-filled by whole-cell patch clamp and passive diffusion over 20 minutes at room temperature. EMOLs were identified by phase-contrast. Microelectrodes were pulled from borosilicate glass capillaries (30-0056, Harvard Apparatus) to a resistance of 3-8 MΩ using a Flaming/Brown P-87 micropipette puller (Sutter Instruments, California, USA). Coverslips were placed in an extracellular solution containing: 115 mM NaCl, 5.3 mM KCl, 1.8 mM $CaCl_2$, 0.8 mM $MgCl_2$, 25 mM glucose, 25 mM HEPES, pH 7.4, 292 mOsm/kg. The intracellular solution within the microelectrode contained: 120 mM potassium gluconate, 2 mM $MgCl_2$, 0.5 mM EGTA, 10 mM HEPES, 30 mM KCl, 5% biocytin (B4261, Sigma-Aldrich), 0.5% Lucifer yellow (L0144, Sigma-Aldrich), pH 7.3, 281 mOsm/kg. Dye-filled cells were returned to a cell culture incubator for 1 hour before fixation. Coverslips were then immunostained and the biocytin visualised, as described in sections 2.6 and 2.6.2.

2.4.10 Nanofibers

Mixed glia prepared as described in section 2.3.6.1 were seeded onto inert nanofibers as described by Bechler (2019) with minor modification. Briefly, poly-L-lactic acid electrospun fibres in a scaffold, kindly gifted by Dr Marie Bechler, were coated in poly-L-lysine as described in section 2.3.4 and were stored in autoclaved diH_2O at room temperature until use. Prior to seeding cells, the fibres were incubated for 15 minutes in plating media. All media was removed before seeding 150,000 cells into each well of a 12-well plate

containing the nanofibers. The cells were then treated identically as described previously in sections 2.3.6.1, 2.4 and 2.4.5. At the end of the experiment (t6d), cells on nanofibers were fixed in 4% PFA, washed gently with PBS, and immunostained as described in section 2.6 using 2 mL volumes of primary and secondary antibody solutions. Between incubations, and before mounting, nanofibers were washed in PBS three times on an orbital shaker for 5 minutes. Nanofibers were then mounted on glass slides in Mowiol® 4-88 containing 5 µg/mL DAPI (recipe in Appendix 7.4.6) and left to set for 2 days in the dark before microscopy.

2.4.11 Lactate dehydrogenase release assay

CytoTox 96® non-radioactive cytotoxicity assay (G1780, Promega) was used to detect lactate dehydrogenase (LDH) release, a marker of cell death. Cell culture supernatants were collected at time points (100 µL sample) and the end of experiments. Supernatants were centrifuged at 10,000 x *g* for 1 minute to pellet cell debris, transferred to a new microcentrifuge tube, and used in assay immediately or stored at -20°C. The assay was performed according to the manufacturer's instructions with some modification. Briefly, 25 µL cell supernatant was pipetted in a flat bottom 96 well plate (10695951, Corning™), in triplicate. An LDH positive control in the kit was used in all assays. Fresh culture media was used as a negative control. The colourimetric reaction was started by adding 25 µL substrate mix. After 30-60 minutes at room temperature, 25 µL stop solution was added and the optical density obtained using a Tecan Sunrise™ automated microplate reader (Tecan Group Ltd, Switzerland) with a 492 nm filter and Magellan™ software. The average values for culture media only samples (background) was subtracted from experimental sample.

2.4.12 Propidium iodide labelling

Propidium iodide (PI; P4170, Sigma-Aldrich) was added to live cultures at a final concentration of 5 µg/mL and incubated in a cell culture incubator for 15 minutes. The cells were washed twice with PBS, fixed in 4% PFA, and immediately examined by fluorescence

microscopy. As a positive control for cell death, some cultures were heated in a 50°C water bath for 10 minutes then returned to the incubator for 45 minutes before the addition of PI.

2.4.13 MitoTracker™ labelling

MitoTracker™ Red CMXRos (M7512, Thermo Fisher Scientific) was added to live cultures at a final concentration of 200 nM. After 10 minutes, all media was removed, cultures rinsed three times with 1 mL fresh media, and replaced with 1 mL fresh media. Cells were returned to an incubator for 30 minutes before fixation in 4% PFA.

2.4.14 Fixation

Cells were fixed by: i) placing coverslips into a solution of 37°C 4% PFA, or ii) adding an equal volume of 37°C 8% PFA to the cell culture media already in the dish (4% final). Fixation time was 10 minutes at room temperature. Cells were then washed three times with PBS and stored in PBS at 4°C.

2.5 Cryosectioning

Spinal cords were dissected from P3 and P60 mice. For P3 tissues, the whole animal was immersion fixed in 4% PFA for 15 minutes then cords were dissected. For P60 tissues, animals were transcardially perfused with physiological saline (0.89% NaCl) then 4% PFA. All tissues were post-fixed in 4% PFA for a further 2 hours before being transferred into 30% sucrose solution in PBS (cryopreservative) until they sank ($\sim$2 days). Small blocks of cervical and lumbar cord were positioned in Tissue-Tek® O.C.T. Compound (4583, Sakura) and frozen by immersion in 2-methylbutane chilled in liquid nitrogen. The frozen blocks were wrapped in Parafilm® (P7793, Sigma-Aldrich) and stored at -20°C until processing.

Tissues were sectioned using an “OTF” cryostat (Bright Instruments, UK) at 10 µm thickness. Transverse sections were cut of cervical spinal cord at C1 – C4 level and lumbar spinal cord at L1 – L4 level. Tissue sections were mounted on Thermo Scientific™ SuperFrost Plus™ Adhesion slides (10149870, Fisher Scientific) and allowed to air dry for 2 hours at room temperature before storing at -20°C until staining.

2.6 Immunocytochemistry and staining of cell cultures

Solutions were pipetted onto a Parafilm® (P7793, Sigma-Aldrich) lined tray and coverslips placed on top. Cells were permeabilized with 0.5% Triton™ X-100 (X100, Sigma-Aldrich) in PBS for 10 minutes at room temperature. The coverslips were then washed three times in PBS and blocked in blocking buffer (10% normal goat serum [G9023, Sigma-Aldrich] in PBS) for 1 hour at room temperature. Coverslips were then transferred onto primary antibodies (see Table 2.3) diluted in blocking buffer and incubated overnight at 4°C in a humidified environment. Coverslips were washed thoroughly before application of secondary antibodies (see Table 2.4) diluted 1:1000 in blocking buffer for 1 hour at room temperature. All secondary antibodies were purchased from Invitrogen™ and used Alexa Fluor™ fluorophores. Coverslips were washed three times in PBS and once in diH_2O before mounting on glass slides (12362098, Thermo Scientific) with Mowiol® 4-88 mounting medium containing 5 µg/mL DAPI (recipe in Appendix 7.4.6). The mounting medium was allowed to set before microscopy.

2.6.1 Phalloidin staining

To visualise F-actin, Alexa Fluor™ 488 phalloidin stain (A12379, Invitrogen™; reconstituted in methanol) was applied to coverslips after the application of secondary antibodies (1:40 in blocking buffer) for 1 hour at room temperature.

2.6.2 Streptavidin labelling of biocytin

Biocytin-filled EMOLs were labelled with streptavidin Texas Red® (SA-5006-1, Vector Laboratories) at 1:200 applied with secondary antibodies as described in section 2.6.

2.6.3 Lipid stains

Neutral lipids were identified in cells at t0 using LipidTOX™ Green (H34475, Invitrogen™) applied to fixed cells at 1:1000 in 0.89% saline for 30 minutes. Excess liquid was blotted off with lint-free tissue and coverslips were placed on glass slides (without mounting medium) before imaging by fluorescence microscopy. At t6d, neutral lipids were labelled with Nile Red

(ab228553, Abcam) according to the manufacturer's instructions following immunostaining. Briefly, solutions were applied at 1:500 for 15 minutes at room temperature in the dark. Coverslips were then washed three times in PBS, once in diH_2O, and mounted on glass slides with Mowiol® 4-88 mounting medium as described in section 2.6.

Table 2.3 | Primary antibodies used for immunofluorescence microscopy.

Antigen	Host	Isotype	Dilution	Manufacturer	Product code
β-tubulin IV	Mouse	IgG_1	1:200	Abcam	ab11315
BCAS1	Rabbit	IgG	1:1000	Synaptic Systems	445 003
CC1[1]	Mouse	IgG_{2b}	1:200	Novus Biologicals	NB600-1021
CD45	Rat	IgG	1:400	Bio-Rad	MCA1388
Cleaved caspase-3	Rabbit	IgG	1:1000	Abcam	ab49822
CNP	Mouse	IgG_1	1:1000	Abcam	ab6319
GFAP	Rabbit	IgG	1:1000	Agilent	Z0334
MBP	Rat	IgG	1:400	Bio-Rad	MCA409S
NeuN	Rabbit	IgG	1:500	Sigma-Aldrich	ABN78
NG2	Rabbit	IgG	1:200	Sigma-Aldrich	AB5320
Olig2	Mouse	IgG_{2a}	1:200	Merck	MABN50
PLP[2]	Rabbit	IgG	1:1000	NA	NA
SMI31	Mouse	IgG_1	1:1000	BioLegend	801601

[1] Product discontinued. [2] Gifted from Prof. N. Groom to Dr I. R. Griffiths, then Prof. J. M. Edgar.

Table 2.4 | Alexa Fluor™ secondary antibodies used for immunofluorescence microscopy.

Antibody	Product code		
	Alexa Fluor™ 488	Alexa Fluor™ 568	Alexa Fluor™ 647
Goat anti-mouse IgG_1	A21121	A21124	A21240
Goat anti-mouse IgG_{2a}	-	A21134	A21241
Goat anti-mouse IgG_{2b}	-	A21144	-
Goat anti-Rabbit IgG	A11008	A11036	A21244
Goat anti-Rat IgG	A11006	A11077	A21247

2.7 Immunohistochemistry on tissue sections

Tissues were washed in PBS for 10 minutes on an orbital shaker before permeabilization and blocking using 0.5% Triton™ X-100 in blocking buffer (section 2.6) for 1 hour. Primary antibodies (Table 2.3) were applied in the same buffer overnight at 4°C. After washing three times in PBS, secondary antibodies (1:1000; Table 2.3) were applied for 1 hour at room temperature in blocking buffer. Sections were washed three times in PBS, once in diH_2O, then mounted with CitiFLUOR (Electron Microscopy Science, USA) containing 5 µg/mL DAPI. Coverslips were sealed with nail enamel.

2.8 Fluorescence microscopy

2.8.1 Illustrative images

Illustrative images were captured using a Zeiss Axio Imager M2 fluorescent microscope and Zen Blue software (Carl Zeiss AG, Germany) or a Leica DMi8 microscope with Hamamatsu ORCA flash 4 V3 sCMOS camera and Leica Imaging Software (Leica, Germany).

2.8.2 Qualitative assessments

Qualitative assessments of immunostained cultures were made for some experiments by an independent researcher who was blinded to the experimental conditions. Qualitative statements were made in comparison to control cultures.

2.8.3 Quantitative imaging

Images for quantification were captured using a Zeiss Axio Imager M2 fluorescent microscope and Zen Blue software. Data acquisition was carried out blinded. To avoid bias, 10 images were captured across the coverslip in approximately the same position between coverslips (shown in Figure 2.2) using a 20x air objective. The DAPI channel was used to set focus for the image before capturing all other appropriate channels. Files were saved and analysed in `.CZI` format before converting to `.TIFF` format for space-efficient storage.

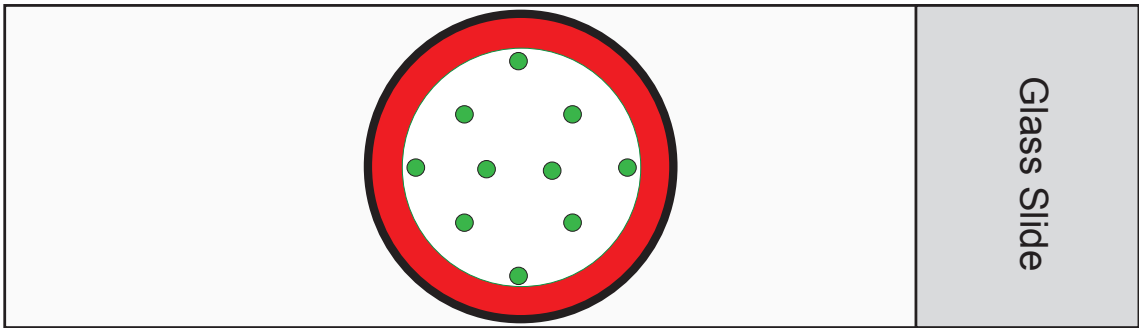

Figure 2.2 | Locations where images were captured for quantification across cell culture coverslips. Images were captured in 10 locations (green dots) across the coverslip (bold black circle) at least 3 mm from the edge since cultures were sparser in these areas (red area).

2.9 Quantification from microscopy

Quantification was carried out manually using FiJi image analysis software (Schindelin *et al.*, 2012) using images captured for quantification as described in section 2.8.3. Image files were opened in `.CZI` format using the "Bio-Formats" plugin by Besson *et al.* (2019).

2.9.1 Cell density

Cell density quantification was carried out by placing a region of interest (ROI) 127,840 μm^2 centrally on an image and counting all healthy-appearing DAPI-labelled nuclei (described in section 2.9.1.1) within the ROI or overlapping the east or south border. The "cell counter" plugin within FiJi was used to record counts. Cells labelled with a cell-type marker (e.g. CD45, CNP, GFAP) were quantified when coinciding with a previously counted healthy-appearing DAPI-labelled nucleus. The cell counts for each experimental condition and time point were totalled across 10 images (or 20 where a technical duplicate was available), divided by the total area analysed and multiplied by one million to obtain the number of cell/mm^2. Any t0 coverslip from mixed glial cultures that had $<$ 190 cells/mm^2 were excluded. Cell densities were then expressed as a percentage of the t0 density for each biological replicate.

2.9.1.1 Healthy-appearing DAPI-labelled nuclei

Healthy-appearing DAPI-labelled nuclei were assessed visually based on nuclear morphology as described by Cummings and Schnellmann (2004). Healthy nuclei have a diffuse pale background with visible puncta of condensed chromatin. These are visually distinct from dying or dead cell nuclei, which appear bright and small due to nuclear condensation (pyknotic) or fragmented due to nuclear fragmentation (karyorrhectic).

2.9.2 EMOL cell size

EMOL cell size was quantified by measuring the area occupied by the cell as delineated by CNP staining. Images were converted to 8-bit and a threshold of 12-15 (min) and 225 (max) was applied. To ensure consistent measurements, all images were adjusted in the

same way within an experiment. Overlapping EMOLs were separated using the line tool to erase an area of staining where the cells touched. An ROI was then drawn around the entire cell and measured, expressing the area as mm^2 (illustrated in Figure 2.3). For mouse primary mixed glial cultures, at least 30 cells were included in the final data after ROUT analysis (maximum false discovery rate of 5%) per condition, across two technical replicates. For EMOL-enriched cultures, at least 19 cells were included in the final data after ROUT analysis.

2.9.3 EMOL nanotube-like structures

Quantification of EMOL nanotube-like structures was carried out manually using CNP staining to delineate them. The number of processes on a single EMOL were counted using the "cell counter" plugin if: i) the process width was $<$ 2 µm, and ii) extended greater than 5 µm from the cell body. CNP^+ EMOLs were selected at random to be analysed and only cells in areas where the structures could be clearly identified were included in the analysis. For mouse primary mixed glial cultures, at least 18 cells per condition were assessed across two technical replicates. At least 14 cells were included in the final data after ROUT analysis (maximum false discovery rate of 5%) per condition, across two technical replicates. In mouse primary EMOL-enriched cultures, 10 cells per condition were assessed.

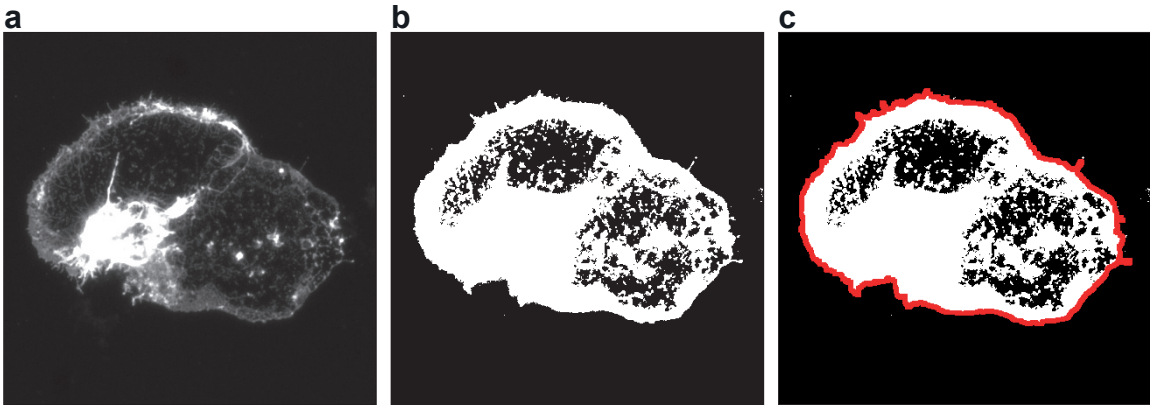

Figure 2.3 | Quantification of EMOL cell size as measured by the outline of CNP staining. **(a)** An image of a CNP^+ EMOL. **(b)** A threshold is applied to the image to create a solid outline of the cell. **(c)** The area occupied by the cell is measured (red outline) and the area in mm^2 is obtained.

2.10 Electron microscopy

Preparation of spinal cord for electron microscopy was carried out as described in Edgar *et al.* (2020) with some modification.

2.10.1 Tissue processing

Briefly, spinal cords from P3 mice were collected as described in section 2.5. For P60 cord, animals were transcardially perfused with physiological saline then strong fixative (5% glutaraldehyde, 4% paraformaldehyde, 0.009 M $CaCl_2$, 0.08 M sodium cacodylate, pH 7.4). All tissues were post-fixed in strong fixative for more than 2 weeks before processing. Tissue samples were washed in isotonic sodium cacodylate buffer (0.07 M sodium cacodylate, 0.07 M NaCl, 0.0005 M $CaCl_2$, 0.001 M $MgCl_2$, pH 7.2–7.4) before incubation in 1% osmium tetroxide in sodium cacodylate buffer for 2 hours. Samples were washed again in isotonic sodium cacodylate buffer for 10 minutes then progressively dehydrated in ethanol before washing in propylene oxide. The tissues were impregnated with a 1:1 mixture of propylene oxide:araldite resin overnight, followed by a 1:3 mixture overnight, and finally 100% araldite overnight. Processed tissues were then embedded in silicone moulds using fresh araldite and cured in an oven at 65°C for 48 hours.

2.10.2 Transmission electron microscopy

Transmission electron microscopy was carried out on 70 nm ultrathin sections cut using a Leica Ultramicrotome EM UC7 (Leica Biosystems) and mounted on a copper grid. Mounted thin sections were stained with 2% uranyl acetate in 50% ethanol for 10 minutes in the dark, washed, then stained with Reynold's lead citrate for 10 minutes in the dark. Illustrative images were captured on a JEOL 1200EX transmission electron microscope (TEM) running at 80 kV using a 2Kx2K digital camera (Cantega) and Olympus iTEM software.

2.11 Molecular biology

Prior to RNA extraction, pipettes and work areas were cleaned using RNaseZap™ RNase Decontamination Solution (AM9780, Invitrogen™). Before RT-qPCR, pipettes and work areas were cleaned with 70% ethanol. Plastics and microcentrifuge tubes were autoclaved prior to use (unless provided as part of a kit) and certified nuclease and DNA-free.

2.11.1 RNA extraction

The guanidinium thiocyanate–phenol–chloroform method (Chomczynski and Sacchi, 1987) was used to extract RNA-containing cell lysates from mixed glial cell cultures. Briefly, all culture media was removed from the culture dish and replaced with 500 µL TRIzol™ Reagent (15596018, Invitrogen™) to lyse cells. After 10 minutes, the lysate was pipetted over each 13 mm glass coverslip in the dish three times to dislodge any remaining cells. The total cell lysate was then transferred to a microcentrifuge tube. Between 3 and 6 cell culture dishes were used and pooled, per experimental condition, to obtain enough RNA for downstream use. The cell lysate was either processed immediately or stored at −80 °C.

2.11.2 RNA purification

To isolate RNA, 200 µL chloroform was added to each sample per 500 µL cell lysate, vortexed vigorously, and allowed to incubate for 2 minutes at room temperature. Samples were then centrifuged at 12,000 x *g* at 4 °C for 15 minutes. The clear aqueous phase containing the RNA was transferred to a new microcentrifuge tube (200 µL aqueous phase per 500 µL of original lysate) containing an equal volume of 70% ethanol and vortexed. The RNA was purified using the PureLink™ RNA Mini Kit (12183018, Invitrogen™) according to the manufacturer's instructions. Briefly, samples were loaded onto a spin column and centrifuged at 12,000 x *g* for 15 seconds. The flow-through was discarded and the spin column was washed with wash buffer 1 before being treated with DNase (79254, Qiagen) for 15 minutes at room temperature. The spin column was washed again with wash buffer 1, then wash buffer 2, before drying by centrifugation at 12,000 x *g* for 2 minutes. The purified RNA was eluted into a recovery tube (provided with the kit) by pipetting 15 µL

nuclease-free water (nfH_2O) onto the spin column membrane, incubating for 2 minutes, then centrifuging at 16,000 x *g* for 2 minutes. The RNA yield was determined using a DeNovix DS-11+ spectrophotometer (DeNovix, Washington, USA).

2.11.3 cDNA synthesis

SuperScript™ IV Reverse Transcriptase (Invitrogen™, 18090010) was used to synthesise cDNA from 150 ng of purified RNA. Reaction mixtures were prepared in advance and added in two steps.

Reaction mix one:

11 µL	RNA (150 ng) in nfH_2O
1 µL	dNTPs (N0447S, New England Biolabs)
1 µL	Random hexamers (N8080127, Invitrogen™)

Reaction mix two:

4 µL	SuperScript™ IV buffer
1 µL	SuperScript™ IV reverse transcriptase
1 µL	DTT
1 µL	RNaseOUT™ (10777019, Invitrogen™)

Reaction mix one was heated to 65 °C for 5 minutes then placed on ice. Reaction mixed two was added to reaction mix one, mixed by pipetting, and heated to 23 °C, 55 °C, and 80 °C, for 10 minutes each. SuperScript™ IV reverse transcriptase was replaced with nfH_2O in no reverse-transcriptase (NRT) controls. Samples were then diluted 1:10 with nfH_2O and stored at −80 °C.

2.11.4 Primer design

Primers were designed using Primer-BLAST (Ye *et al.*, 2012) for use in mouse (*Mus musculus*, taxid: 10090) and purchased from Integrated DNA Technologies (Leuven, Belgium). Primer design parameters were kept constant where possible and are summarised in Table 2.5. Outer primers were designed to start/end at least 40 bp from the inner primer

sequence. Primers were reconstituted in nfH_2O to 100 µM and stored at −20 °C. All primers were validated by end-point PCR as described in Appendix 7.3.

2.11.5 RT-qPCR with standard curves

A panel of genes that encode key regulatory enzymes in metabolism (Table 2.6) were examined by standard curve RT-qPCR described by McKimmie and Fazakerley (2005). This method allows for the semi-quantitative comparison of relative copies (R.C) of a gene of interest (GOI) between experimental conditions.

2.11.5.1 Generation of standard curves

Standard curves were made by serial dilution of PCR products generated using the outer primers. Mixed glial cultures maintained in HE media for 6 days were used to obtained template cDNA since they expressed all GOI we tested. The PCR products were generated using the following reaction mix:

45.0 µL	JumpStart™ REDTaq® ReadyMix™ (P0982, Sigma-Aldrich)
0.50 µL	Forward primer at 100 µM
0.50 µL	Reverse primer at 100 µM
3.00 µL	nfH_2O
1.00 µL	cDNA

The PCR cycling parameters were:

1. 95 °C for 2 minutes
2. 95 °C for 15 seconds
3. 60 °C for 60 seconds
4. 72 °C for 30 seconds $\rightarrow$ # 2 for 40x cycles
5. 72 °C for 10 minutes
6. 4 °C and pause

The PCR products were purified using the PureLink™ PCR Purification Kit (K310001, Invitrogen™) according to the manufacturer's instructions. Briefly, 200 µL binding buffer B2 was mixed with 50 µL PCR reaction mix containing the PCR product. The sample was added to a spin column and centrifuged at 10,000 x *g* for 1 minute. The spin column

Table 2.5 | Primer design parameters for inner and outer primers.

Parameter	Inner primers	Outer primers
Primer size (bp)	20-23	
Primer GC content (%)	40-65	
Primer T_m	Desired 59.5°C, min. 56°C	
Max self-complementarity	Any = 2, 3' = 1	
Max pair complementarity	Any = 3	
Intron inclusion	Yes, min. 200 bp	
PCR product size (bp)	Desired 50-150, max. 200	Desired 700, max. 1,000

Table 2.6 | Primer sequences used in RT-qPCR experiments.

Target NCBI ref.	Inner primers (5′-3′)		Outer primers (5′-3′)	
	Forward	Reverse	Forward	Reverse
Acaca NM_133360.2	TGGCTTCTCCA GCAGAATTT [1]	AGATCGCATG CATTTCACTG [1]	GCTAAACCAG CACTCCCGAT	ATCCCTTTCC CTCCTCCTCC
Acly NM_001199296.1	GGTGACTCCCG ACACAGACT [1]	AAGCTTTCCT CGACGTTTGA [1]	CTTACGGACA GAGAGCCACAC	CCACATCCA CACCCCCTTC
Atg5 NM_053069.6	AGTCTGTCC TTCCGCAGT	CCTGGCTCCT CTTCTCTCCA	ATGAAGGCAC ACCCCTGAAA	GCGAGGAGG ACACACTCTTT
Becn1 NM_019584.4	CCTCTGAAAC TGGACACGAG	CCTGGGCTGT GGTAAGTAATG	AGGGGTCTAA GGCGTCCAG	GCTGCTCACT GTCATCCTCA
Cpt1a NM_013495.2	TGACTATGCG CTACTCGCTG	CGACCCGAGA AGACCTTGAC	CCCTGGGCAT GATTGCAAAG	GGGTTGGGGT GATGTAGAGC
Fasn NM_007988.3	AGTTGCCCGA GTCAGAGAA [1]	CGTCGAACTTG GAGAGATCC [1]	TCCAGAGCCC AGACAGAGAA	CACTCACACC CACCCAGAC
Hk1 NM_001146100.1	TGCCATGCGG CTCTCTGATG [2]	CTTGACGGAGG CCGTTGGGTT [2]	CTTGTAGCCA ATGGGGACTGA	CCATGCTGAC GTTCTGACTCT
Ldha NM_001136069.2	CATTGTCAAGTAC AGTCCACACT [3]	TTCCAATTACTC GGTTTTTGGGA [3]	CGCCCTCTGCT CTTGATTTTTG	ACATTCACACC ACTCCACACAG
Pdha1 NM_008810.3	AGATGCTTGC CGCTGTATCC	GCCCTCTTCT AGCCGATGAA	ACCACTCCTT TTGAGTGCCT	AGCTGATCCG CCTTTAGCTC
Pfkl NM_001358793.1	GGGTCATGTA CAGCGAGGA [4]	GGCCTCCATA CCCATCTTG [4]	GGATGCCTCC AGAACCACAGA	GTAGCCTCACA GACTGGTTCC
Pik3c3 NM_181414.6	GGCAGAACAA GCAGCACACT	CCAGCCAATC CACTTTCACCA	AACCGTGTC GCTCTTTGGA	ACTCCTTGTCA TCGCACTTGA
Pkm NM_001253883.1	GCCGCCTGG ACATTGACTC [5]	CCATGAGAGAA ATTCAGCCGAG [5]	TGATTGGAAG TGCCCGATGC	GTCAAAGGCTG ATGGTGTCCC
Pygl NM_133198.2	TAGATGATGTG GCTGCTTTGGA	AGGTCTGGCT GATTGGGAGA	TGTGGCAGAA GTGGTGAACAA	ATTGCTGGACT CGTTGGATAGG
Tbp NM_013684.3	ACCGTGAATCT TGGCTGTAAACT	CAGTTGTCCG TGGCTCTCTT	ACCCCACAACTCT TCCATTCTC	GTTCTTCACTC TTGGCTCCTGT

Published sequences: [1] Young *et al.* (2017), [2] Moon *et al.* (2015), [3] Liu *et al.* (2016), [4] Miyazawa *et al.* (2017), [5] Shi *et al.* (2011).

membrane was then washed with 650 µL wash buffer and centrifuged at 10,000 x *g* for 1 minute. The membrane was dried by centrifuging at 16,000 x *g* for 3 minutes. Purified PCR product was eluted in 50 µL nfH_2O into a recovery tube (provided with the kit) by centrifugation at 16,000 x *g* for 2 minutes. The yield of purified PCR product was quantified using a DeNovix DS-11+ spectrophotometer (DeNovix, Washington, USA) and $>$ 10 ng/µL was required to proceed. The purified products were run on an agarose gel (as described in Appendix 7.3) to confirm they were of the expected molecular weight. Neat purified products and 1:100 (10^{-2}) dilutions in nfH_2O were stored at −20 °C until use. The 10^{-2} dilution was used to make 1:10 serial dilutions (up to 8 standards) for each GOI.

2.11.5.2 RT-qPCR

Primer and master mixes for each GOI were made to cover:

8	standards (10^{-4}–10^{-11})
χ	number of samples
χ	number of controls (no RT and nfH_2O only)

Multiplied by 3 (all ran in triplicate), plus an additional 20 to allow for pipetting error.

The RT-qPCR master mix contained the following:

7.50 µL	*Power* SYBR™ Green Master Mix (4367659, Applied Biosystems™)
0.30 µL	Primer mix (50 pM/µL forward and reverse primer)
5.20 µL	nfH_2O

MicroAmp™ 96-well reaction plates (4346907, Applied Biosystems™) were chilled on StarChill PCR 96-well Chiller Racks (E2396, StarLab) and 13 µL RT-qPCR master mix was added to each well as required. Two µL of standard, sample cDNA, or control sample (NRT or nfH_2O) was pipetted onto the side of the appropriate well. Reaction plates were sealed with a MicroAmp™ Optical Adhesive Film (4311971, Applied Biosystems™) and centrifuged at 400 x *g* for 1 minute. RT-qPCR was then performed on an Applied Biosystems Fast Real-Time PCR System (ABI 7500, Applied Biosystems™) using the following PCR cycling programme:

1. 95 °C for 10 minutes
2. 95 °C for 15 seconds
3. 60 °C for 1 minute → # 2 for 40x cycles

Expression of each GOI was normalised to TATA-box binding protein (*Tbp*) and quantitative analysis based on the standard copy number method was performed.

2.12 Lipidomics

Mixed glia or EMOL-enriched cultures were used for lipidomics analysis after culturing as described in sections 2.4 and 2.4.5 with some modification. Rather than fixing cells, coverslips at t0 and t6d were washed once in room temperature PBS, the excess liquid removed with a piece of tissue paper, then frozen in a 12-well plate placed on dry ice. Each condition had 3 or 4 technical repeats. Coverslips were stored at -80°C until shipping on dry ice to the Hornemann lab (University of Zurich), who kindly performed lipid extraction and liquid chromatography-mass spectroscopy.

2.12.1 Lipid extraction and liquid chromatography-mass spectroscopy

The protocols below was provided by Dr Gergely Karsai and is based on previous work (Karsai *et al.*, 2019) with some modifications. Briefly, coverslips with adhered cells were crushed and placed in a reaction tube with 1 mL methanol:methyl *tertiary*-butyl ether:chloroform (referred to as MMC; 4:3:3 [v/v/v]). The MMC mix contained butylated hydroxytoluene (100 mg/L) and was fortified with 100 pmoles/mL of internal standards (Avanti Polar Lipids): d5-deoxymethylsphinganine (m17:0), dihydroceramide (d18:0:12:0), 1-deoxydihydroceramide (m18:0/12:0), ceramide (d18:1/12:0), 1-deoxyceramide (m18:1/12:0), glucosylceramide (d18:1/8:0), sphingomyelin (18:1/12:0), 50 pmoles/mL d7-sphingosine-1-phosphate, and 2.5 µL/mL SPLASH® LIPIDOMIX® mass spec standard. After vortexing, the samples were continuously mixed in a Thermomixer (Eppendorf) at 37 °C, 1,400 rpm, for 60 minutes. Protein precipitates were pelleted by centrifugation at 16,000 x *g* for 5 minutes. Single-phase

supernatants were collected, dried under N_2 and stored at −20 °C until further use. Before analysis, dried lipids were dissolved in 100 µL methanol.

Liquid chromatography was performed using a C30 Accucore LC column (Thermo Fisher Scientific, 150 mm x 2.1 mm x 2.6 µm) with the following mobile phases (0.26 mL/min): a) acetonitrile:water (6:4) with 10 mM ammonium acetate and 0.1% formic acid; b) isopropanol:acetonitrile (9:1) with 10 mM ammonium acetate and 0.1% formic acid. The following gradient was applied:

1. 0.0 - 2.0 minutes (ramp 90-80% a, 10-20% b)
2. 2.0 - 3.0 minutes (ramp 80-70% a, 20-30% b)
3. 0 - 7.0 minutes (ramp 70-40% a, 30-60% b)
4. 7.0 - 18.0 minutes (ramp 40-10% a, 60-90% b)
5. 18.0 - 24.0 minutes (ramp 10-0% a, 90-100% b)
6. 24.0 - 28.0 minutes (isocratic 0% a, 100% b)
7. 28.0 - 28.1 minute (ramp 0-90% a, 100-10% b)
8. 28.1 - 30.0 minutes (isocratic 90% a, 10% b)

Liquid chromatography was coupled to a Q Exactive™ Hybrid Quadrupole-Orbitrap™ Mass Spectrometer (Thermo Scientific™). Samples were analysed in positive and negative mode using a heated electrospray ionization interface. The following parameters were used: spray voltage 3.5 kV; auxiliary gas heater temperature 300 °C; sheath gas flow rate 40 AU; auxiliary gas 10 AU; capillary temperature of 300 °C. The detector was set to an MS2 method using a data-dependent acquisition with a “top10” approach and stepped collision energy set between 25 and 30. A 70,000 resolution was used for the full spectrum and a 17,500 for MS2. A dynamic exclusion filter was applied, which excludes fragmentation of the same ions for 20 seconds to prevent duplication. Identification and quantification was achieved with the following criteria: resolution accuracy of 5 ppm from the predicted mass at a resolving power of 70,000 at 200 m/z; isotopic pattern fitting to expected isotopic distribution; matching retention time on synthetic standards (if available) and specific fragmentation patterns. Quality control was performed using TraceFinder 4.1 (Thermo Fisher Scientific) for peak picking and matching to an in-house lipid database.

2.12.2 Data normalisation and analysis

Data were normalised to the number of coverslips used and the average total cell density per coverslip, per experimental condition, obtained previously from cell density quantification. The data used are shown in Figures S3 and S8.

Analyses were performed by using the average lipid quantity (per lipid species) of 3-4 technical repeats, per condition, and compared using a Student's *t*-test (two-tailed, paired). Fold changes were calculated using the $\log_2$ function on the average of 3 biological repeats, per lipid species, per condition. Lipid species with a fold change of more than 1 and a *p* value < 0.05 were considered significantly changed.

2.13 Statistical analyses and presentation of data

Statistical analyses and most presentation of data were performed using GraphPad Prism 9 software (GraphPad Software, California USA). Volcano plots were generated using VolcaNoseR (Goedhart and Luijsterburg, 2020). Bar and scatter graphs show error bars representing the standard error of the mean (SEM). Some data are presented on SuperPlots (Lord *et al.*, 2020) showing mean values from independent biological replicates ($\pm$ SEM) overlaid on the raw data, which are colour-coded per experiment.

Data sets were assumed normally distributed. A *p* value < 0.05 was used to denote statistical significance. Where stated, ROUT analysis was applied to remove outliers in datasets at a maximum false discovery rate of 5%. Statistical tests applied and the number of biological replicates obtained are stated in figure legends.

A biological replicate is defined as an independent cell culture generated by pooling animals from one or more litters. In some cases, three biological replicates were obtained from the culture of single spinal cords taken from pups born in two independent litters.

Chapter 3

An *in vitro* model of early myelinating spinal cord white matter glia

3.1 Introduction

In the developing brain, EMOLs are particularly vulnerable to hypoxia-ischaemia as observed in PVL and associated disease models (Follett *et al.*, 2000; Follett *et al.*, 2004). Conversely, in a murine model of SMA, myelination of the spinal cord proceeds normally (O'Meara *et al.*, 2017) despite widespread tissue hypoxia - including in the spinal cord (Somers *et al.*, 2016; Hernandez-Gerez *et al.*, 2020). This raises the possibility that spinal cord EMOLs are more resistant to hypoxia than those in the brain. Certainly, there is increasing recognition that brain and spinal cord oligodendroglia have distinct transcriptional and phenotypic properties (Chen *et al.*, 2013; Bechler *et al.*, 2015; Floriddia *et al.*, 2020).

The recently identified EMOL-specific marker, BCAS1, reported in murine and human brain, permits the selective study of this population (Fard *et al.*, 2017); however, it has not, to our knowledge, been characterised in spinal cord. After confirming it labels EMOLs in the early postnatal spinal cord, we generated cell cultures from this tissue and characterised them as a model of early myelinating spinal cord white matter glia. This cell culture system lacks neuronal soma to: (i) mimic spinal cord white matter, which contains few neuronal soma; (ii) preclude the confounding effects of neuronal death, an inevitable outcome of the energy deprivation conditions we aimed to test.

Neonatal (P3-5) mouse spinal cord has been used previously to establish mixed glial cultures (Thomson *et al.*, 2008; Goebbels *et al.*, 2017) but the cellular composition has not been characterized. Therefore, the overall aim of this chapter was to characterise this mixed glial culture system for use as a model to study the susceptibility of spinal cord EMOLs to components of the hypoxic environment. The specific aims were to:

(i) Determine if BCAS1 is expressed by EMOLs in the neonatal mouse spinal cord and confirm this population can be retained in primary cell culture.

(ii) Systematically characterise the cellular composition of neonatal mouse spinal cord mixed glial cell cultures at plating and after 6 days.

(iii) Determine the metabolic pathways that can be used for energy production (assessed in terms of cell survival) by spinal cord mixed glia.

(iv) Examine the response of spinal cord EMOLs to transient oxygen deprivation.

Much of the data presented in this chapter are qualitative as its purpose was to determine parameters for systematic evaluation in subsequent chapters.

3.2 BCAS1$^+$ EMOLs are present in mouse neonatal spinal cord

Myelination in mouse begins approximately 1 day before birth in the ventral columns of the cervical spinal cord and peaks around P23 (Foran and Peterson, 1992). We confirmed BCAS1$^+$ EMOLs were present in cervical and lumbar spinal cord of P3 mice using immunostaining (Figure 3.1). BCAS1$^+$ soma were present in “white matter” areas and BCAS1$^+$ myelin sheaths frequently colocalised with CNP (Figure 3.1 b, c). In contrast, BCAS1$^+$ cells were infrequent in P60 spinal cord, which unlike P3 cord, was heavily stained with anti-MBP (Figure 3.1 a-c). Some BCAS1$^+$ cell soma in P3 cord were also positive for CC1: a marker of early myelinating and mature oligodendrocytes (Figure 3.1 c).

By electron microscopy of P3 spinal cord “white matter”, we identified cells with a dark cytoplasm wrapping small numbers of adjacent axons with thin compact myelin. The cytoplasm of these cells was rich in mitochondria (Figure 3.2). We concluded these are likely the BCAS1$^+$ EMOLs seen by immunohistochemistry.

In summary, our observations confirmed that BCAS1 is a marker of EMOLs in neonatal mouse spinal cord, as in brain.

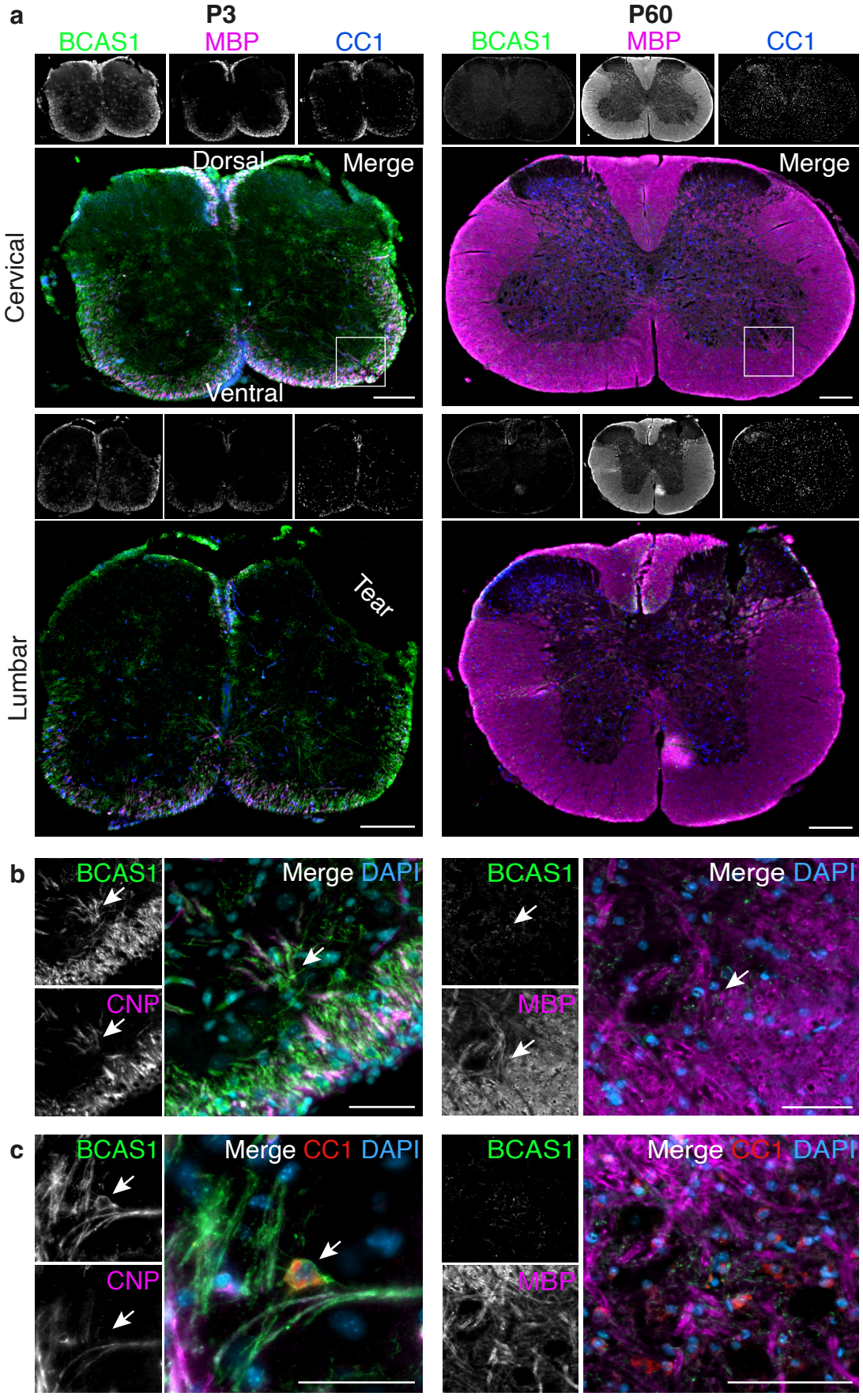

Figure 3.1 | Postnatal day 3 mouse spinal cord contains BCAS1$^+$ oligodendroglia in future white matter areas. *Figure legend continues on the next page.*

Figure 3.1 | *Cont...* Illustrative images of spinal cord sections taken from P3 and P60 C57BL/6 mice. **(a)** Mouse cervical and lumbar spinal cord at P3 contains BCAS1$^+$ EMOLs (green) as myelination proceeds (MBP, magenta). Most CC1 positive oligodendrocytes (blue) are observed in white matter regions. P60 mouse spinal cord has very few BCAS1$^+$ cells but is abundant in MBP. Mature oligodendrocytes (CC1$^+$) appear equally distributed across the section. Scale bars = 200 µm. Squares denote high magnification areas (ventral horns) shown in **(b)** and **(c)** where some overlap of BCAS1 and CNP is observed in P3 cord. Few BCAS1$^+$ cells are observed in P60 cord. All tissues were immunostained at the same time and digitally enhanced identically. Images from the observation of one animal of each age. Scale bar = 50 µm.

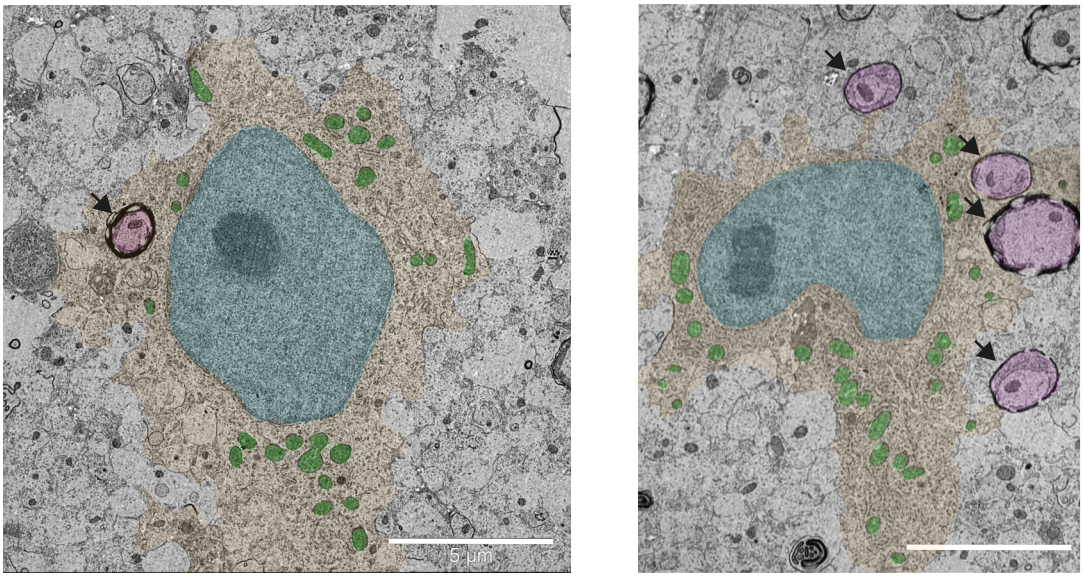

Figure 3.2 | Postnatal day 3 mouse spinal cord contains EMOLs rich in mitochondria. Electron micrographs with pseudocolour overlay showing EMOL cytoplasm (orange) rich in mitochondria (green) in cervical spinal cord. Some nearby axons (purple) are surrounded by thin compact myelin (arrows). Cell nuclei in blue. Scale bar = 5 µm.

3.3 Cell culture of spinal cord BCAS1$^+$ EMOLs and glia

Next, we determined the composition of mixed glial cell cultures generated from P3-5 mouse spinal cord. Cultures were established in serum-rich media for approximately 18 hours then maintained for 6 days in DMEM-based serum-free media (DM; without pyruvate or glutamine) supplemented with 5 mM glucose.

At time-zero (t0) and plus 6 days (t6d) cultures contained, in decreasing proportions: oligodendroglia (Olig2$^+$) including OPCs (NG2$^+$), astrocytes (GFAP$^+$), and microglia (CD45$^+$; Figure 3.3 a-d) but were largely devoid of neuronal cell bodies (NeuN$^+$; Figure 3.3 e and Figure 3.4 a-d). Notably, myelin debris was present at both t0 and t6d, appearing to have adhered to the coverslips at the time of plating (Figure S1).

Within the Olig2$^+$ population at t0, 80% were NG2$^+$, 40% were BCAS1$^+$, and 25% were CNP$^+$. At t6d, these values were 44%, 40%, and 20%, respectively (Figure 3.4 e-g). At both time points, almost all CNP$^+$ cells were BCAS1$^+$ (Figure 3.3 f, g; Figure 3.4 h). CNP$^+$ cells were rich in mitochondria (Figure 3.3 h), increased in size over time, and expressed the major myelin proteins, PLP and MBP at both time points (Figure 3.5).

Expression of CNP in BCAS1$^+$ oligodendrocytes is a confirmatory marker of myelination. Given that almost all CNP$^+$ oligodendrocytes were also BCAS1$^+$, we instead used CNP as a marker of EMOLs in subsequent experiments.

In summary, P3-5 mouse spinal cord cultures are enriched in BCAS1$^+$ EMOLs, contain all other major neuroglia but almost completely lack neurons making them a useful tool to study early myelinating spinal cord glia.

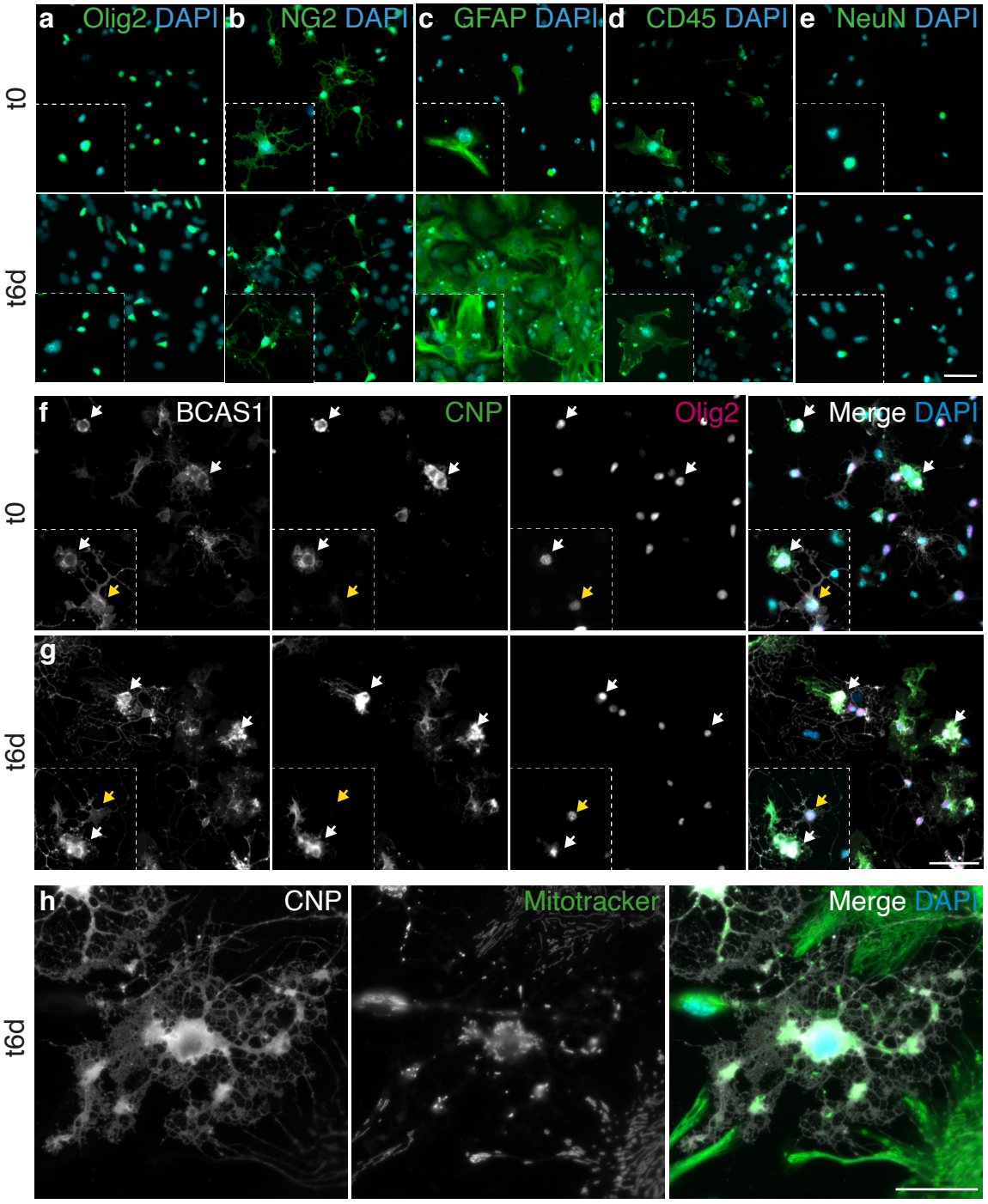

Figure 3.3 | Mouse spinal cord mixed glial cultures contain BCAS1$^+$ CNP$^+$ EMOLs. Illustrative immunofluorescence images of mixed glial cultures grown at t0 and after 6 days in DM supplemented with 5 mM glucose (t6d). Cultures contained **(a)** oligodendroglia (Olig2$^+$) including **(b)** NG2$^+$ OPCs, **(c)** astrocytes (GFAP$^+$), **(d)** and microglia (CD45$^+$) **(e)** but very few neuronal cell bodies (NeuN$^+$). Insets show higher magnification views. Scale bar = 100 µm. **(f, g)** Nearly all CNP$^+$ cells were BCAS1$^+$ Olig2$^+$ (white arrows). Insets illustrate that cultures contained BCAS1$^+$ (yellow arrows) and BCAS1$^+$ CNP$^+$ oligodendroglia (white arrows). Scale bar = 50 µm. **(h)** BCAS1$^+$ CNP$^+$ EMOLs contained many mitochondria that appeared round or elongated. Scale bar = 25 µm. Observations representative of 3 biological repeats. Abbreviations: DM, DMEM-based media.

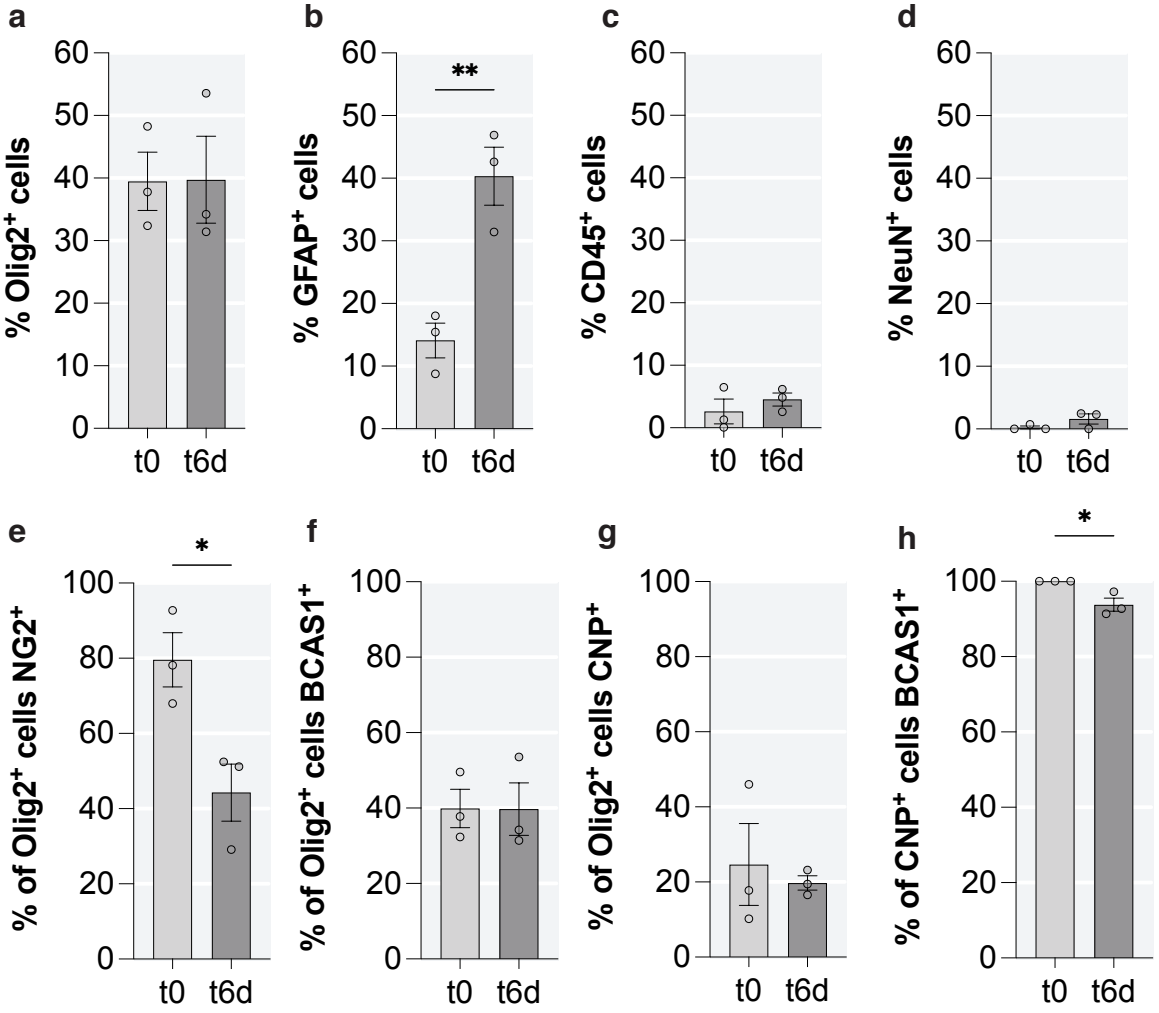

Figure 3.4 | **Mouse spinal cord mixed glial cultures are particularly enriched in oligodendroglia, including BCAS1$^+$ CNP$^+$ EMOLs.** Quantification of cell types present in cultures grown at t0 and after 6 days (t6d) in DM supplemented with 5 mM glucose. Data are expressed as a percentage of all DAPI$^+$ cells. **(a)** Olig2$^+$ oligodendroglia, **(b)** GFAP$^+$ astrocytes, **(c)** CD45$^+$ microglia, and **(d)** NeuN$^+$ neurons. Within the Olig2$^+$ population, there were **(e)** NG2$^+$ OPCs, as well as **(f)** BCAS1$^+$ and **(g)** CNP$^+$ cells. **(h)** Almost all CNP$^+$ oligodendrocytes were BCAS1$^+$. Time points were compared using an unpaired two-way Student's *t*-test. * = $p < 0.05$, ** = $p < 0.01$. Data were obtained from 3 biological repeats. Abbreviations: DM, DMEM-based media.

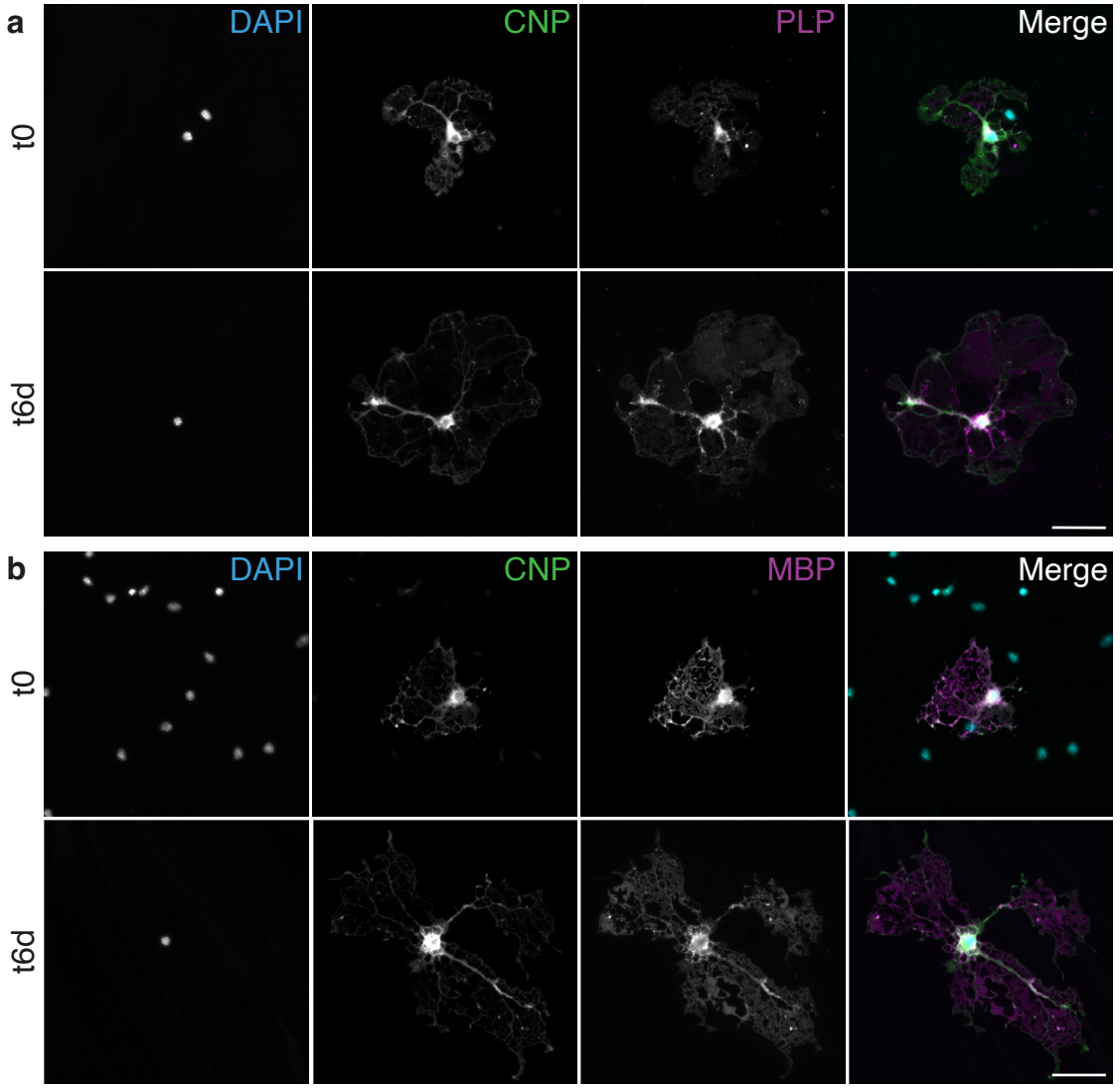

Figure 3.5 | **Spinal cord EMOLs grow over 6 DIV and express myelin proteins.** Illustrative immunofluorescence images of EMOLs in mixed glial cultures at t0 and after 6 days in DM supplemented with 5 mM glucose (t6d). Cell nuclei are labelled with DAPI (blue). EMOLs in culture increase in size and express major myelin proteins such as CNP (green), **(a)** PLP, and **(b)** MBP (purple). Representative images from a single experiment. Scale bar = 50 µm. Abbreviations: DM, DMEM-based media.

3.4 Spinal cord EMOLs are not acutely sensitive to OXPHOS inhibition

Oligodendroglial metabolism changes with maturation: OPCs are considered oxidative and post-myelination cells glycolytic. The metabolic characteristics of spinal cord EMOLs have not been described. To determine the metabolic pathways available for energy production, mixed glia were maintained in DM supplemented with 5 mM glucose and cell survival was assessed following pharmacological manipulation with iodoacetate (IA), which inhibits glycolysis at the level of GAPDH (Sabri and Ochs, 1971), or azide (AZ), which blocks OXPHOS at cytochrome oxidase (oxygen-requiring step) and induces “chemical hypoxia” (Swanson, 1992). As a non-pharmacological inhibitor of glycolysis, some cells were cultured in unsupplemented DM (0 mM glucose; also lacking pyruvate and glutamine).

Five hours after culture in unsupplemented DM, EMOLs (CNP^+) and astrocytes ($GFAP^+$) appeared unaffected compared to controls grown in 5 mM glucose-supplemented DM (Figure 3.6 a). However, in cultures treated for 5 hours with 1 mM IA, there appeared to be a reduction in $DAPI^+$ cells overall. Astrocytes appeared particularly sensitive, having abnormal morphology and pyknotic nuclei (Figure 3.6 b). In contrast, EMOLs appeared normal. In cultures treated with 10 mM AZ for 5 hours, neither EMOLs nor astrocytes appeared altered compared to controls and overall cell densities appeared unaffected (Figure 3.6 c). When both glycolysis and OXPHOS were inhibited pharmacologically, $DAPI^+$ cell densities appeared reduced and both EMOLs and astrocytes appeared morphologically abnormal with pyknotic nuclei (Figure 3.6 d).

Surprisingly, 24 hours after culturing cells in unsupplemented DM, EMOLs and astrocytes still appeared unaffected (Figure 3.7 a). However, 24 hours inhibition of glycolysis by IA, or OXPHOS by AZ, resulted in a reduction of $DAPI^+$ nuclei overall and the loss of EMOLs and astrocytes (Figure 3.7 b, c). Pharmacological inhibition of both pathways resulted in the loss of all cells and disintegration of nuclei (Figure 3.7 d).

LDH release assay at 24 hours after each of the three pharmacological treatments indicated an absence of the enzyme at this time point. This result can be interpreted in two ways: (i) all cells are viable, or (ii) all cells are already dead and previously released all available

LDH that has since degraded. Clearly, given the morphological signs, the latter is true in this case. In contrast, the assay detected release of LDH in both control (5 mM glucose) and 0 mM glucose treatments, presumably from cell turnover (Figure 3.8).

Given the apparent survival of cells following 24 hours in unsupplemented DM, we increased the culture time to 48 hours. To our surprise, this did not appear to adversely affect $DAPI^+$, EMOL, or astrocyte densities compared to those in 5 mM glucose DM (Figure 3.7 e).

These data suggest that spinal cord EMOLs can alternatively utilise glycolysis or OXPHOS for energy production, at least for 5 hours. Additionally, both EMOLs and astrocytes appeared resistant to short-term (5 hours) chemical hypoxia by AZ treatment. Survival of both cell types in the absence of glucose for 48 hours was unexpected.

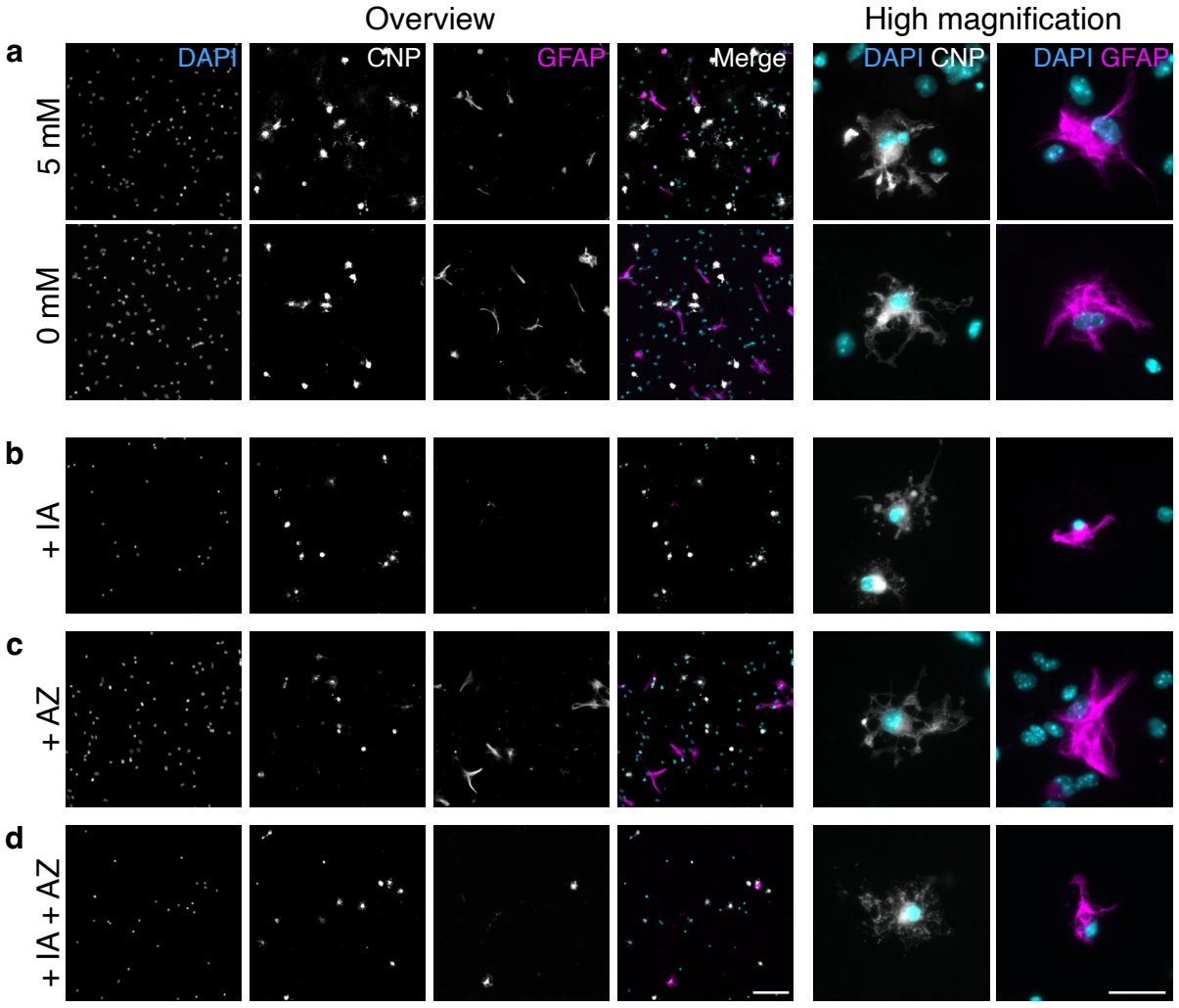

Figure 3.6 | Pharmacological inhibition of glycolysis for 5 hours does not appear to affect EMOLs but is detrimental to astrocytes, whereas both appear resistant to 5 hours oxidative phosphorylation inhibition. Illustrative immunofluorescence images of mixed glial cultures 5 hours after treatment. **(a)** Withdrawal of glucose did not result in cell loss. **(b)** Astrocytes (magenta, $GFAP^+$) were vulnerable to glycolysis inhibition with 1 mM sodium iodoacetate (+ IA). **(c)** EMOLs (white, CNP^+) and astrocytes were resistant to oxidative phosphorylation inhibition by 10 mM sodium azide (+ AZ). **(d)** Both cell types were vulnerable to inhibition of glycolysis and oxidative phosphorylation as shown by pyknotic nuclei (blue, $DAPI^+$). Observations representative of 3 biological repeats. Scale bar = 100 µm for overview images and 25 µm for high magnification images.

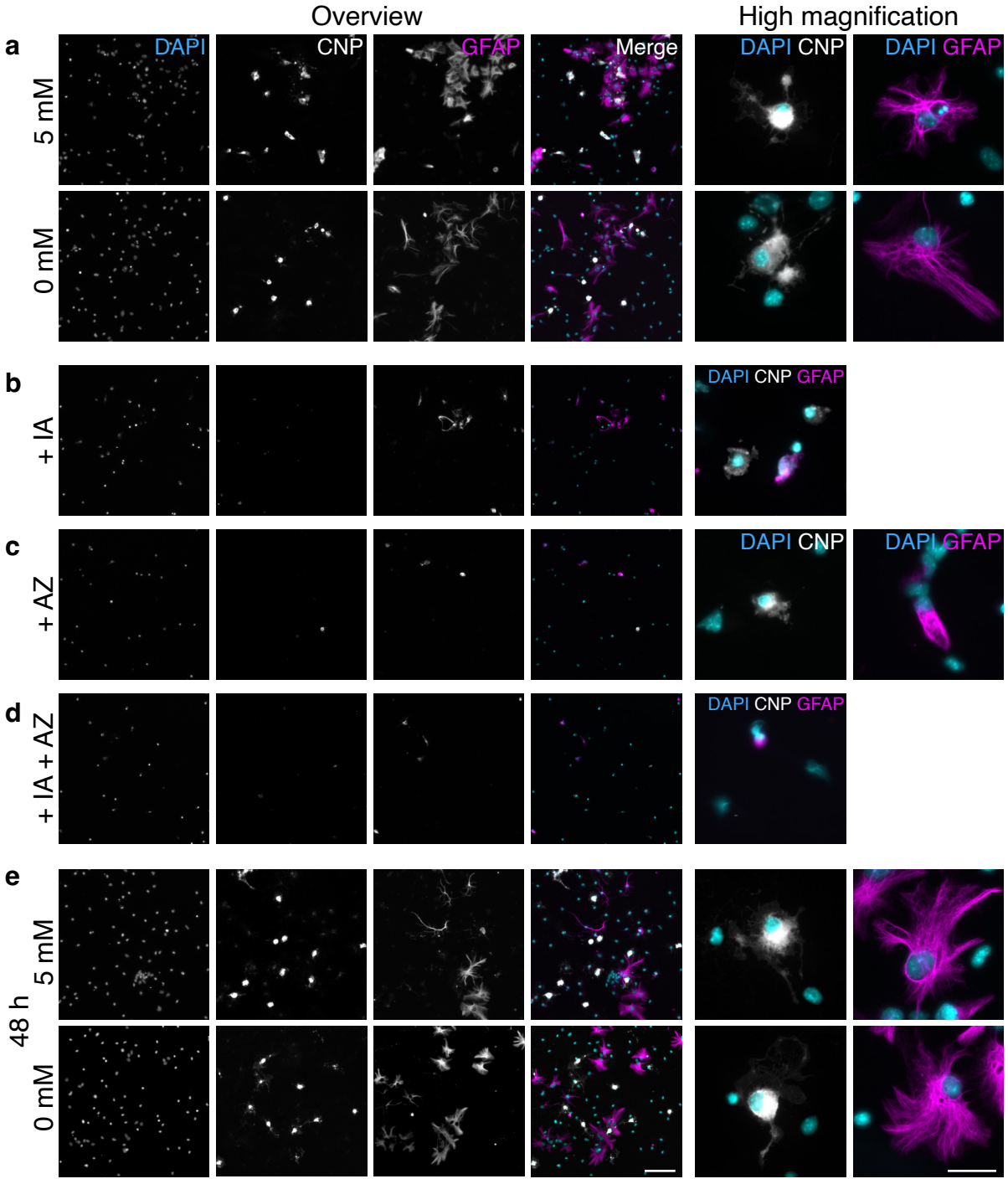

Figure 3.7 | Pharmacological inhibition of glycolysis and/or oxidative phosphorylation for 24 hours, but not withdrawal of glucose for 48 hours, impacts EMOLs and astrocytes. Illustrative immunofluorescence images of mixed glial cultures 24 hours after treatment. **(a)** Withdrawal of glucose did not result in cell loss. **(b)** EMOLs (white, CNP^+) and astrocytes (magenta, $GFAP^+$) were vulnerable to inhibition of glycolysis with 1 mM sodium iodoacetate (+ IA), **(c)** oxidative phosphorylation with 10 mM sodium azide (+ AZ), **(d)** or both. **(e)** Extending glucose deprivation to 48 hours did not appear to affect the cultures compared to 5 mM glucose. Observations representative of 3 biological repeats. Scale bar = 100 µm for overview images and 25 µm for high magnification images.

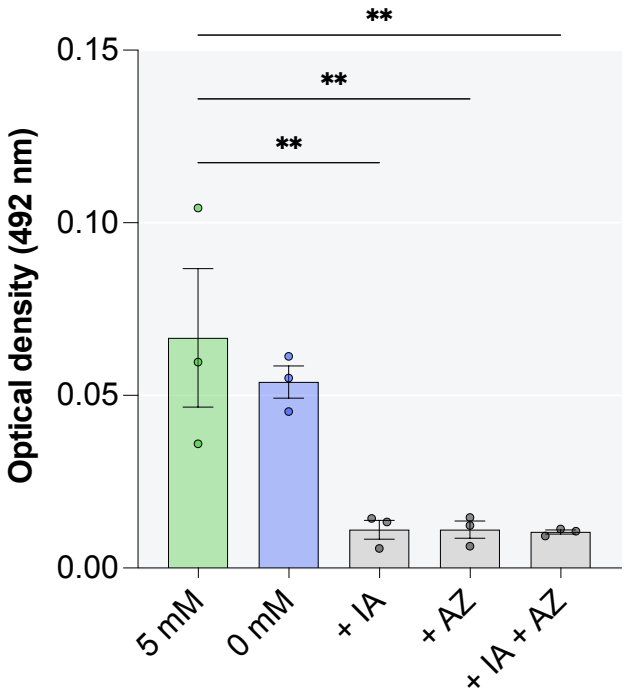

Figure 3.8 | Absence of LHD activity following 24 hours pharmacological inhibition of glycolysis and/or oxidative phosphorylation. LDH release assay performed on supernatants from mixed glial cultures. The optical density values were similar for cells grown for 24 hours in 0 mM glucose compared to 5 mM glucose. Addition for 24 hours of 1 mM sodium iodoacetate (inhibitor of glycolysis, + IA), 10 mM sodium azide (inhibitor of oxidative phosphorylation, + AZ), or both, resulted in virtually no detected LDH (values near background levels). Media-only values were subtracted from sample readings. Data were compared to the 5 mM untreated control using an unpaired one-way ANOVA with Dunnett's multiple comparison test. ** = $p < 0.01$. Data were obtained from 3 biological repeats.

3.5 EMOLs and astrocytes are not sensitive to hypoxia *per se*

The results described in the previous section suggest that spinal cord glia are not susceptible to 5 hours of "chemical hypoxia" but are vulnerable at 24 hours. However, pharmacological inhibitors can cause cytotoxicity by indirect mechanisms, such as the accumulation of upstream metabolic substrates. To further explore whether spinal cord EMOLs are vulnerable to oxygen deprivation, we maintained cells in a 95% N_2/5% CO_2 (0% oxygen) atmosphere for 24 hours in 5 mM glucose DM. Some cells were subjected to oxygen-glucose deprivation (OGD) to mimic ischaemia and some were subsequently returned to atmospheric oxygen for 24 hours to mimic reperfusion.

First, we examined whether 24 hours experimental hypoxia led to acidification by observing the colour of phenol red-supplemented media. Media in which cell-dense "*myelinating cultures*" were maintained turned yellow indicating acidification and serving as a positive control for oxygen deprivation. However, media containing low density mixed glia remained salmon-pink indicating physiological pH (Figure 3.9). Importantly, these observations demonstrate that the protocol models hypoxia *per se*, independent of lactic acidosis, which we explore further in Chapter 4.

Compared to cells maintained under normoxia (Figure 3.10 a), EMOLs and astrocytes subjected to 24 hours oxygen deprivation or OGD, with or without 24 hours reperfusion, appeared similar to controls in terms of cell density and morphology (Figure 3.10 b, c). Despite the normal appearance of EMOLs and astrocytes following these manipulations, LDH release was significantly higher in all cultures exposed to oxygen deprivation compared to controls (Figure 3.11). This suggests a delay in the appearance of morphological changes following cytotoxicity and/or that other cell types contribute to LDH release.

In summary, following 24 hours of oxygen deprivation, with or without 24 hours reperfusion, EMOL and astrocyte cell densities and morphology did not appear markedly altered. These data suggest that spinal cord EMOLs are not vulnerable to hypoxia *per se* and provide evidence they readily use glycolysis for survival. Unexpectedly, cells also appeared resistant to 24 hours combined OGD. This surprising finding is discussed below.

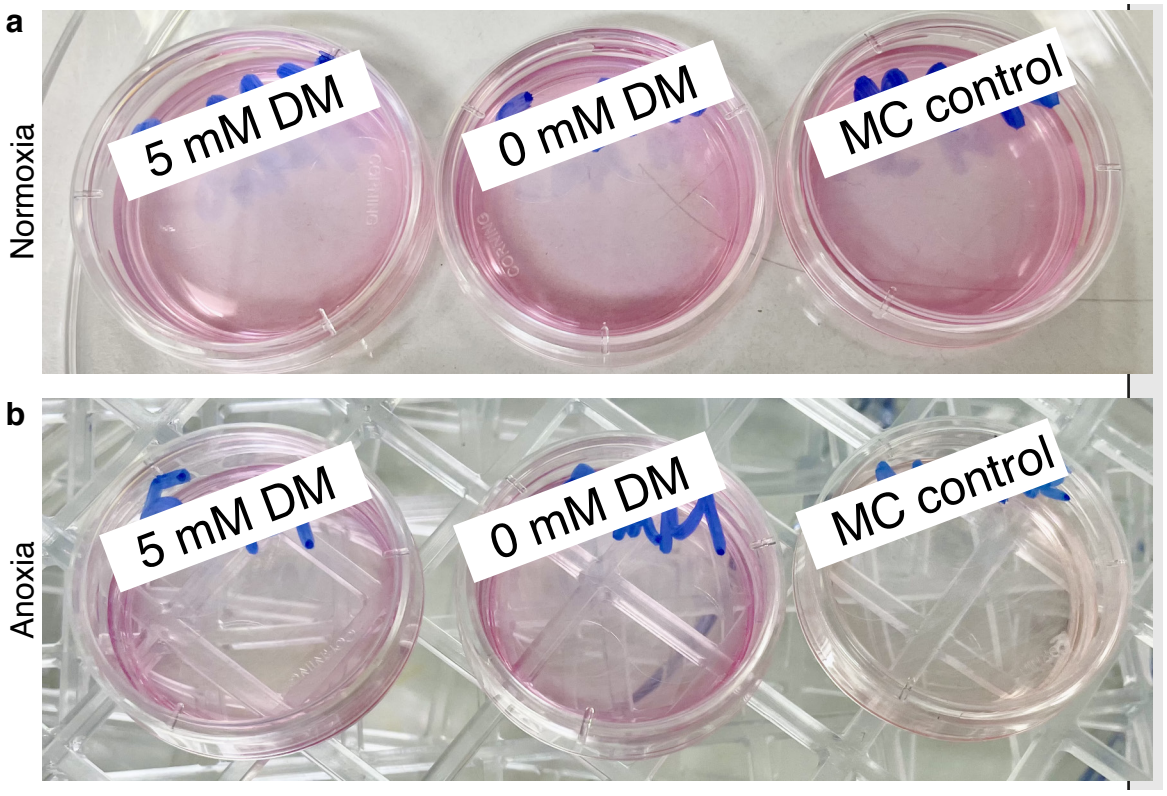

Figure 3.9 | Mixed glial culture media does not acidify after 24 hours in an oxygen-depleted atmosphere. (a) In normoxic conditions at 24 hours, cell culture media remains salmon-pink indicating the pH is within physiological parameters. **(b)** After 24 hours in an oxygen-deprived atmosphere, there was no acidification of the mixed glial culture media, either with or without glucose. The cell culture media in which myelinating cultures (DIV 15, positive control) were maintained appeared yellow indicating acidification. Observations representative of 3 biological repeats.

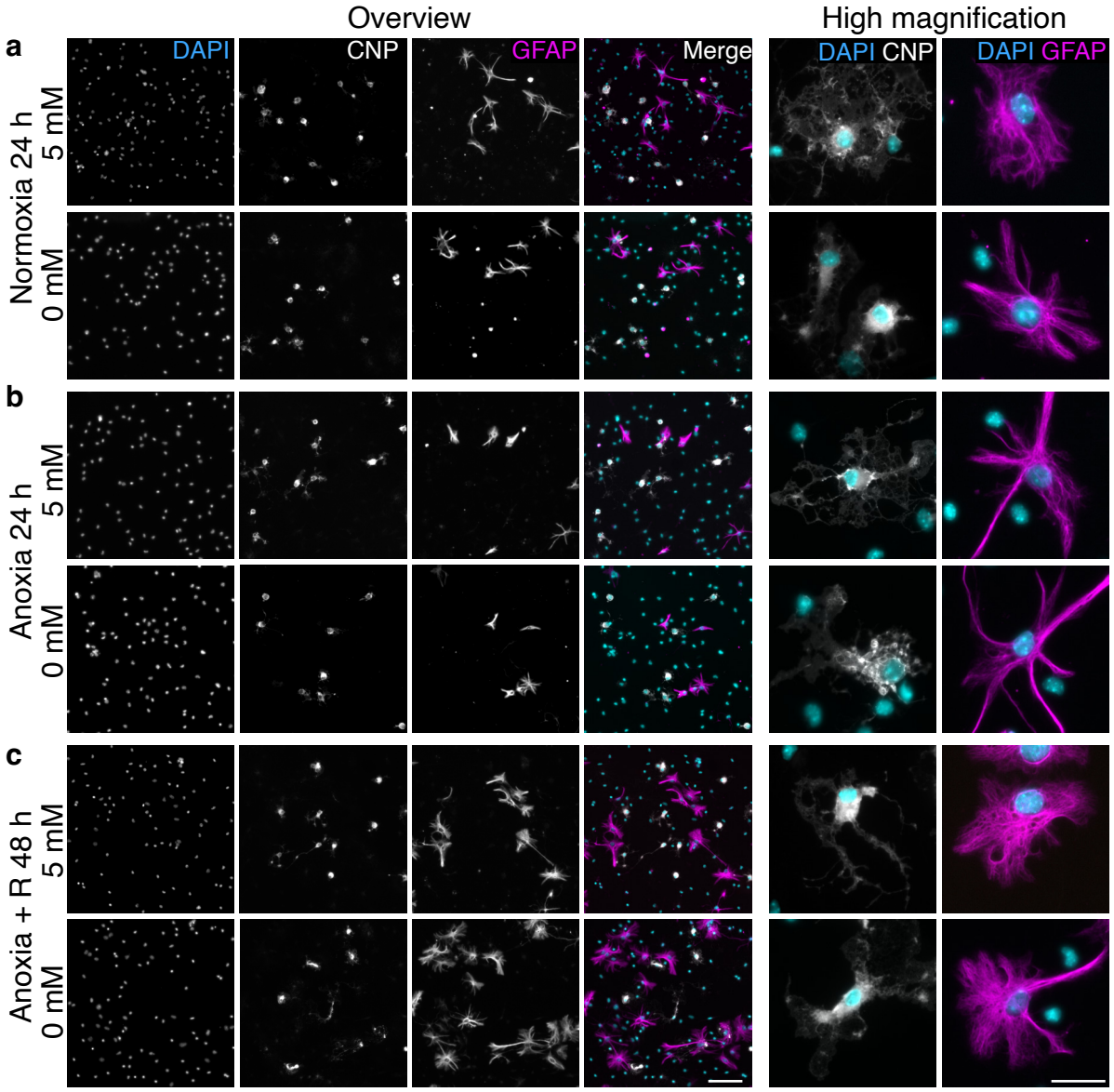

Figure 3.10 | Acute oxygen deprivation and subsequent reperfusion does not appear to impact EMOLs and astrocytes. Illustrative immunofluorescence images of mixed glial cultures. Compared to control cultures **(a)**, cells maintained in a 0% oxygen atmosphere (anoxia) did not appear markedly altered at 24 hours. **(b)** EMOLs (white, CNP^+) and astrocytes (magenta, $GFAP^+$) did not show signs of nuclear pyknosis (blue, DAPI). **(c)** Cells cultured in anoxia for 24 hours then returned to atmospheric oxygen for 24 hours (reperfusion) did not appear markedly altered and had no signs of increased nuclear pyknosis compared to normoxia (**fig a**). Observations representative of 3 biological repeats. Scale bar = 100 µm for overview images and 25 µm for high magnification images.

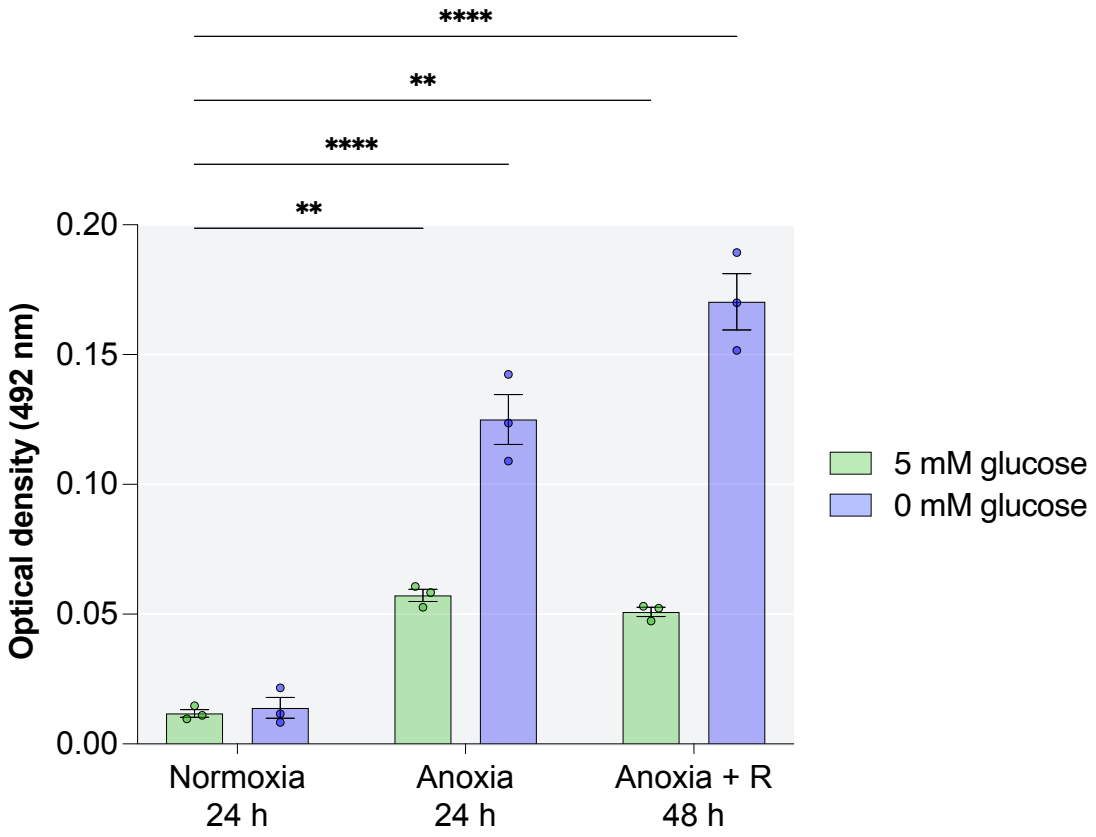

Figure 3.11 | Anoxia-induced cytotoxicity in mixed glial cultures is enhanced by glucose deprivation. LDH release assay performed on supernatants from mixed glial cultures. Cultures subjected to 24 hours anoxia, with (+R) or without reperfusion, had significantly more LDH release compared to cultures maintained in normoxia. Media-only values were subtracted from sample readings. Data were compared to 5 mM glucose normoxia 24 hours using a two-way ANOVA with Dunnett's multiple comparison test. ** = $p < 0.01$, **** = $p < 0.0001$. Data were obtained from 3 biological repeats.

3.6 Discussion

In this chapter, we showed that mouse neonatal spinal cord is rich in BCAS1$^+$ cells (a novel marker of EMOLs) and that this population can be cultured alongside astrocytes and microglia as a model of spinal cord white matter glia. In the absence of neurons, which are particularly vulnerable to hypoxia-ischaemia, our model allows us to examine the intrinsic responses of glial cells akin to the situation in white matter, which lacks neuronal cell bodies. Using this model, we provided evidence that EMOLs can alternatively use glycolysis or OXPHOS, with one pathway able to sustain survival for 5 hours when the other is blocked. Furthermore, EMOLs appeared to tolerate 24 hours of hypoxia *per se*, confirming that glycolysis alone can support survival. Unexpectedly, EMOLs appeared tolerant also to 24 hours OGD. At face value, the last of these observations suggests the cell survival assay is insufficiently sensitive to detect cell death; however, we discuss further below the likelihood that oxygen deprivation was incomplete.

The recent observation of BCAS1 expression in brain EMOLs (during development and remyelination) permits the specific visual identification of early, actively myelinating oligodendrocytes (Fard *et al.*, 2017). Previously, only OPCs and mature oligodendrocytes could be unequivocally distinguished using maturation-specific markers. We observed several features of spinal cord BCAS1$^+$ cells shared with those in the neonatal brain. First, P3-5 mouse spinal cord is rich in BCAS1$^+$ oligodendroglia in future white matter areas and that these cells decreased with age and MBP expression. Second, some CC1$^+$ BCAS1$^+$ cells formed early internodes. Thus, BCAS1 is also a transient marker of EMOLs during myelination in the mouse spinal cord. These findings provide an opening for further research examining the specific vulnerabilities of EMOLs *in vivo* using BCAS1 as a marker, for example, in models of SMA, spinal cord injury, and remyelination in demyelinating disease.

Oligodendrocyte cultures are commonly established from neonatal rat cortex OPCs using the shake-off method (McCarthy and de Vellis, 1980; Barres *et al.*, 1992; Avellana-Adalid *et al.*, 1996). Here, serum-rich media is required to grow and maintain the cortical cells before OPCs are shaken off and differentiated into oligodendrocytes in serum-free media. However, when addressing questions relating to spinal cord EMOLs, brain-derived cells have limitations as these two organs contain diverse sub-classes of oligodendroglia (Bradl

and Lassmann, 2010; Floriddia *et al.*, 2020). To study spinal cord EMOLs, we established mixed glial cultures from P3-5 mouse spinal cord in serum-free media after initial plating in serum-containing media. These cultures contained all major CNS glia but were enriched for oligodendroglia including BCAS1$^+$ CNP$^+$ EMOLs. Compared to other spinal cord cultures, such as the myelinating cell cultures (Thomson *et al.*, 2006; 2008), our model was largely devoid of neurons and can be regarded as a model of spinal cord white matter with the grey matter neuronal component removed. We acknowledge the limitations introduced by excluding the neuronal population given that the function of EMOLs is to ensheath axons. However, unlike monocultures, our mixed glial model allows inter-glia interactions as occurs *in vivo* (Domingues *et al.*, 2016). Moreover, it contains astrocytes that are essential for EMOL function since they supply lactate and lipid for myelinogenesis (Sánchez-Abarca *et al.*, 2001; Rinholm *et al.*, 2011; Saher and Stumpf, 2015; Camargo *et al.*, 2017), the perturbation of which leads to abnormal myelin formation *in vivo* (Liedtke *et al.*, 1996).

We observed that EMOLs were rich in mitochondria as previously observed, for example, in P3 rat cortex (Luse, 1956), mouse neonatal spinal cord white matter (Schultz *et al.*, 2021), and during remyelination in adult cat spinal cord (Duncan *et al.*, 2018). This suggests a high density of mitochondria is a hallmark of actively myelinating cells. Kirischuk *et al.* (1995) noted that immature oligodendrocytes in culture had many mitochondria localised to the tips of processes where they are assumed to provide ATP at the site of myelin wrapping (Meyer and Rinholm, 2021). In contrast to EMOLs, mature oligodendrocytes appear to have fewer mitochondria (Rinholm *et al.*, 2016).

The metabolic profiles of OPCs and mature oligodendrocytes differ, with the former being primarily oxidative and the latter glycolytic (Rao *et al.*, 2017). However, little is known about the energy metabolism of spinal cord EMOLs. We probed the metabolic pathways used in EMOLs by treating mixed glial cultures with pharmacological inhibitors of glycolysis or OXPHOS. We found that 5 hours inhibition of either pathway did not result in EMOL cell death; however, simultaneous inhibition of both pathways was detrimental. The effects of pharmacologically inhibiting glycolysis in oligodendrocytes have not been previously reported to our knowledge. However, IA, which is an inhibitor of GAPDH, effectively inhibited glycolysis *in vitro* in mature oligodendrocytes as shown using an intracellular FRET glucose

sensor (Saab *et al.*, 2016). Thus, we show that spinal cord EMOLs are indeed tolerant to short-term glycolysis inhibition.

In contrast, we found that astrocytes were susceptible to pharmacological inhibition of glycolysis, an observation previously reported in brain-derived astrocyte cultures. Ogata *et al.* (1995) and Schmidt and Dringen (2009) demonstrated that 1 mM IA caused astrocyte death after 1 hour - a result we replicated at 5 hours. However, the authors identified off-target effects on glutathione metabolism, an important pathway for protection against oxidative stress in the CNS (Dringen *et al.*, 2000). In contrast to OPCs, both astrocytes and oligodendrocytes withstand glutathione depletion (Back, 2006; Waak and Dringen, 2006). Therefore, if IA has the same off-target effect in EMOLs, we can extrapolate that they too are likely tolerant to glutathione depletion. Others have shown that 100 µM IA can cause ATP depletion by 3 hours in cultured brain astrocytes and neurons (Nodin *et al.*, 2005; Hernández-Fonseca *et al.*, 2008); therefore, a lower concentration of IA could be used in future studies to mitigate off-target effects.

In the current study, short-term pharmacological inhibition of OXPHOS (5 hours) did not cause observable changes in the viability of EMOLs or astrocytes. Cultured brain astrocytes have been shown previously to withstand inhibition of OXPHOS (Ogata *et al.*, 1995; Swanson *et al.*, 1997) and are generally regarded as glycolytic cells (Supplie *et al.*, 2017). However, the effects of inhibiting OXPHOS on oligodendrocytes are less clear due to conflicting reports. For example, Ziabreva *et al.* (2010) showed that *in vitro* differentiated mature MBP^+ oligodendrocytes are vulnerable after 3 hours exposure to 100 µM AZ. However, seminal work by Fünfschilling *et al.* (2012) demonstrated that post-myelination oligodendrocytes in mice can survive as glycolytic cells and thus do not require OXPHOS. Clarity was provided by Rao *et al.* (2017) who showed adult isolated mature oligodendrocytes from rat brain were glycolytic compared to neonatal *in vitro* differentiated oligodendrocytes, which were oxidative. The latter result is likely explained by the absence of the metabolic switch proposed by Fünfschilling *et al.* (2012) that directs post-myelination oligodendrocytes to become glycolytic to support the axons they have myelinated. This highlights a critical issue to consider when characterising cells *in vitro*: that in the absence of relevant physiological cues, cells can behave differently compared to their *in vivo* counterparts. Our spinal cord mixed glial cultures likely reflect the *in vivo* situation more

closely than systems that require *in vitro* differentiation. Thus, we conclude that spinal cord EMOLs can utilise either glycolysis or OXPHOS for survival.

Although EMOL survival was not compromised following AZ-mediated inhibition of OXPHOS for 5 hours, the effects of mitochondrial disruption on lipid synthesis should be considered. In EMOLs, mitochondrial function is required for acetyl-CoA production, cholesterol synthesis, lipogenesis, and myelinogenesis. Sub-lethal mitochondrial complex I inhibition *in vitro* inhibits oligodendroglial maturation and highlights the importance of mitochondrial function distinct from energy production (Schoenfeld *et al.*, 2010). Moreover, mitochondria perform numerous physiological roles such as calcium buffering, regulation of cell growth, cell cycle, cell differentiation, autophagy, and apoptosis (Osellame *et al.*, 2012). Therefore, when considering the cause of EMOL death at 24 hours in our study, it is challenging to conclude whether this was the result of chemical hypoxia and energy crisis, mitochondrial dysfunction and oxidative stress, or both.

We subjected mixed glia to 24 hours of oxygen deprivation or OGD and neither EMOLs nor astrocytes appeared vulnerable, even after reperfusion, in the time scales examined. Others have typically examined cell types in isolation. Lyons and Kettenmann (1998) subjected cell-type enriched cultures of rat brain glia to hypoxia or OGD and found oligodendrocytes to be most vulnerable, compared to astrocytes or microglia. Similarly, Deng *et al.* (2006) reported immature brain oligodendrocytes were vulnerable to OGD. Conversely, astrocytes are resistant to transient (6 hours) hypoxia or OGD (Lyons and Kettenmann, 1998) although aged cells *in vitro* are susceptible (Juurlink *et al.*, 1992; Danilov and Fiskum, 2008). In the above studies, the oligodendrocyte population was likely EMOLs since they were described as beyond precursor cells but still immature. In a more physiologically relevant *ex vivo* study using rat hippocampal slices, Ziemka-Nalecz *et al.* (2018) found OPCs to be most vulnerable to OGD. It has long been known that OPCs are sensitive to oxidative stress (Back *et al.*, 1998; Baud *et al.*, 2004; French *et al.*, 2009) and the death of OPCs likely accounts for increased LDH release following oxygen deprivation or OGD in our experiments.

As a non-pharmacological inhibitor of glycolysis, we maintained spinal cord mixed glia in glucose-free media (also lacking pyruvate and glutamine) for up to 48 hours and found no

obvious detrimental effect on EMOLs or astrocytes. In contrast, pharmacological inhibition of glycolysis was detrimental to astrocytes. This apparent dichotomy can be explained by the fact that astrocytes store glycogen, which can sustain cellular metabolism via glycolysis in the absence of exogenous energy substrates, in the short term. Indeed, others observed a similar result in *ex vivo* rat hippocampal slices where despite 24 hours of glucose deprivation, astrocytes remained viable (Cater *et al.*, 2001). Conversely, inhibition of glycolysis with 2-deoxyglucose led to marked astrocyte death since glycogen could not be metabolised (Cater *et al.*, 2001). Subsequent studies using *ex vivo* optic nerve demonstrated that astrocytes support neurons with glycogen-derived lactate during glucose deprivation (Wender *et al.*, 2000; Brown *et al.*, 2005; Tekkök *et al.*, 2005). However, astrocyte glycogen stores are limited and became depleted after 30 minutes of action potential generation at 0.03 Hz in *ex vivo* optic nerve (Wender *et al.*, 2000). In the absence of energy-hungry axons in our model system, astrocyte glycogen is likely not depleted rapidly. The oligodendrocyte is now considered part of the ANLS, forming a tripartite structure for the support of neuronal function (Amaral *et al.*, 2013; Philips and Rothstein, 2017). Therefore, EMOLs might also be metabolically sustained by astrocyte glycogen-derived lactate when exogenous energy substrates are not available in our model system.

Unexpectedly, EMOLs and mixed glia appeared resistant to OGD. Although we placed cells in an anoxic chamber, all oxygen was most certainly not eliminated and we therefore describe these experiments as oxygen-deprived. We conclude this based on the fact EMOLs would require oxygen to metabolise astrocyte glycogen-derived lactate to maintain cell viability in the absence of exogenous glucose. Indeed, others who gassed culture media with 95% N2/5% CO_2 for 1 hour found that 3% of the starting oxygen tension remained at the end (Lyons and Kettenmann, 1998).

In this chapter, we showed that neonatal mouse spinal cord is rich in $BCAS1^+$ oligodendroglia, as reported for the brain, and that the EMOL population can be maintained *in vitro*. Spinal cord EMOLs in culture retained a high density of mitochondria but were not sensitive to short-term inhibition of OXPHOS. EMOLs were not vulnerable to acute glycolysis inhibition and, to our surprise, were also resistant to 48 hours of glucose deprivation. In all, we provide a characterised *in vitro* model of spinal cord white matter glia to allow for subsequent study of EMOL susceptibility to components of the hypoxic environment.

Chapter 4

Assessing the susceptibility of spinal cord early myelinating oligodendrocytes to secondary components of the hypoxic environment

4.1 Introduction

Hypoxia-ischaemia produces well-characterised secondary consequences, such as acidosis, energy crisis, and inflammation (Obrenovitch, 1995; Minhas *et al.*, 2017). In the previous chapter, we found a population of spinal cord EMOLs were tolerant to short-term oxygen depletion or chemical hypoxia, possibly because these secondary consequences were absent. An early consequence of hypoxia is extracellular acidosis through the accumulation of lactic acid from anaerobic glycolysis, which further compounds hypoxic insult as shown in the brains of neonatal humans and animals (Lorek *et al.*, 1994; Hanrahan *et al.*, 1996; Pang *et al.*, 2020). The interruption in glucose delivery from the blood in hypoxia-ischaemia results in cellular energy crisis to which brain OPCs and EMOLs are particularly vulnerable (Deng *et al.*, 2003; Follett *et al.*, 2004; Deng *et al.*, 2006). However, other important factors are supplied via the blood, such as amino acids and vitamins, which, to our knowledge, are rarely considered within the literature but are essential for cellular metabolism and growth. Finally, the resulting cell stress and cell death triggers the release of inflammatory factors primarily from microglia (Block *et al.*, 2007; Deng *et al.*, 2008). Interferon-gamma (IFNγ) and tumour necrosis factor (TNF) are two cytotoxic inflammatory factors found in the neuroinflammatory environment that directly induce apoptosis in brain-derived EMOLs *in vitro* (Selmaj and Raine, 1988; Vartanian *et al.*, 1995; Hisahara *et al.*, 1997; Jurewicz *et al.*, 2005). In summary, the literature reports that brain EMOLs are particularly susceptible to the hypoxic/ischaemic environment.

This leads us to question how spinal cord myelination proceeds normally in a murine model of SMA despite tissue hypoxia (Somers *et al.*, 2016; O'Meara *et al.*, 2017; Hernandez-Gerez *et al.*, 2020). The healthy spinal cord is poorly perfused compared to brain, having up to 60% lower blood supply (Martirosyan *et al.*, 2011). Based on these two observations, we hypothesised that spinal cord EMOLs might be more resistant to components of the hypoxic environment than those in the brain.

Therefore, the specific aim of this chapter was to examine the response of spinal cord EMOLs to the individual secondary components of the hypoxic environment: extracellular acidosis, energy substrate deprivation, and inflammatory insult. To do this, we used the *in vitro* model of spinal cord white matter glia introduced in Chapter 3.

4.2 EMOLs and astrocytes are susceptible to an acidic environment

To test if spinal cord EMOLs are vulnerable to extracellular acidosis, we assessed cell survival after culturing mixed glia across a range of pH values, with or without 5 mM glucose in DM, the latter to replicate failure of glucose delivery in ischaemia. Given the resilience of EMOLs and astrocytes to 48 hours of exogenous energy deprivation in Chapter 3, we selected a 6-day endpoint (t6d) for these experiments. Raw data are displayed in Figure S2.

Following maintenance for 6 days, within the physiological pH range (7.6-7.0) cultures appeared dense ($DAPI^+$ nuclei) with many EMOLs (CNP^+), astrocytes ($GFAP^+$), and some microglia ($CD45^+$; Figure 4.1 a; Figure 4.2 a-d). However, in an acidic environment (pH 6.6-6.8), total cell and EMOL densities, as a percentage of the starting densities, were significantly reduced compared to control (Figure 4.1 b, c; significance levels are indicated in Figure 4.2 a, b). Surprisingly, at a physiological pH, the complete withdrawal of glucose for 6 days did not markedly alter total, EMOL, astrocyte, or microglial cell densities compared to cells grown in DM supplemented with 5 mM glucose (Figure 4.1 a, upper *vs.,* lower panel; Figure 4.2 a-d, green *vs.,* blue bars).

Astrocyte densities increased markedly at physiological pH, reaching up to 400% of t0 values. However, final densities tended to decrease at pH < 7.0 such that end-point values were closer to starting values. This was true whether or not glucose was present. However, due to intra-experiment variability, these changes did not reach significance (Figure 4.2 c). Conversely, microglial densities were greater in pH 6.6 media compared to controls, reaching significance when glucose was absent (Figure 4.1 c, Figure 4.2 d).

These data demonstrate that EMOLs are vulnerable to an acidic extracellular milieu, the effect of which is not compounded by glucose deprivation. Astrocytes appeared susceptible although starting values were retained under acidic conditions. Microglial densities increased in an acidic milieu, particularly when glucose was absent.

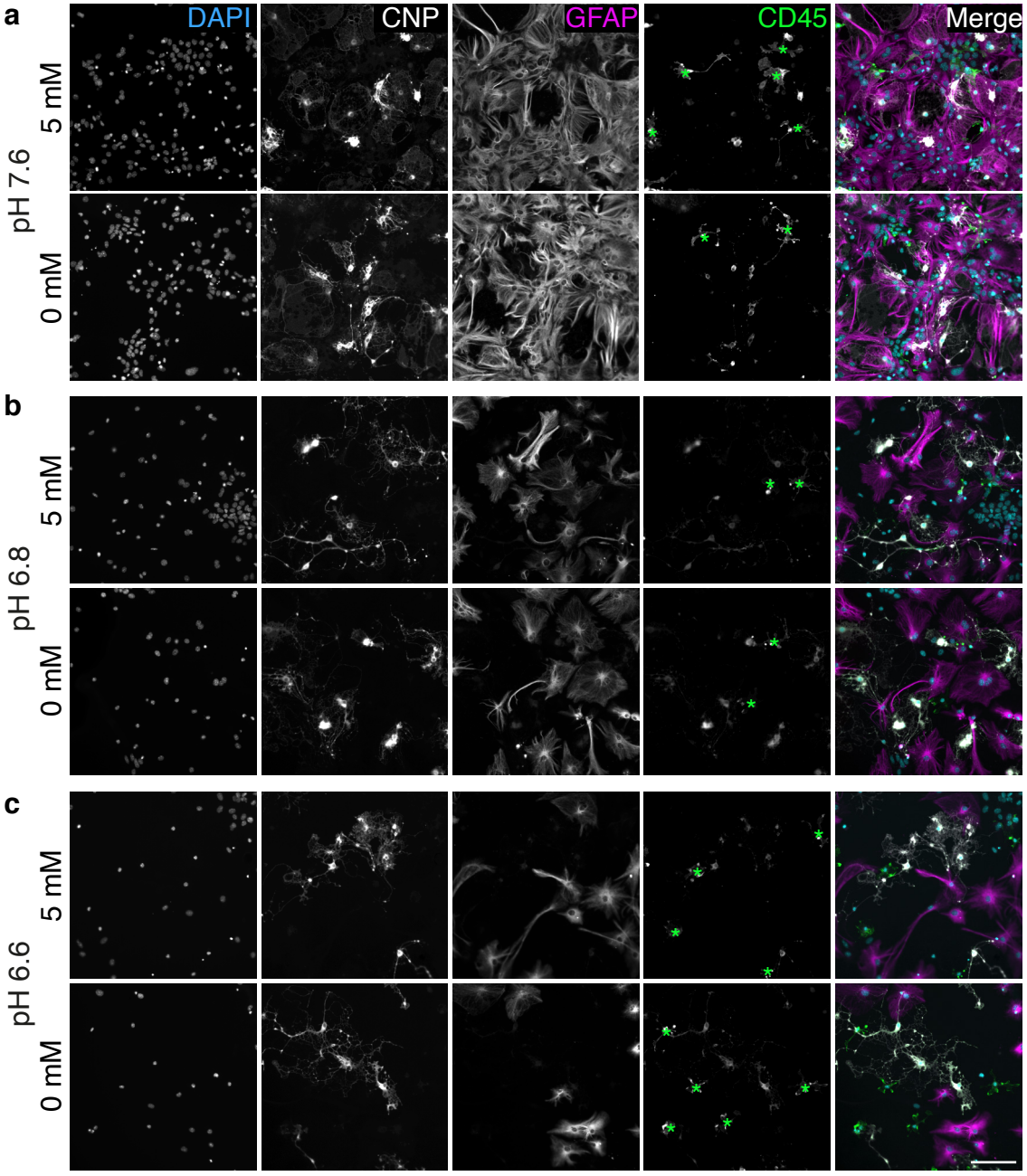

Figure 4.1 | **An acidic milieu impacts EMOLs and astrocytes but glucose deprivation does not compound the effect.** Representative images of mixed glia cultured for 6 days in DM at various pHs, with and without 5 mM glucose. **(a)** Mixed glia cultured at physiological pH (cell nuclei; blue, $DAPI^+$) were abundant in EMOLs (white, CNP^+), astrocytes (magenta, $GFAP^+$), and microglia (green, $CD45^+$). The cells did not appear affected by 6 days of glucose deprivation (lower panel compared to upper panel). **(b)** EMOLs and astrocytes appeared vulnerable at pH 6.8 and **(c)** 6.6; however, $CD45^+$ microglia densities appeared maintained in the latter condition in the absence of glucose. Green asterisks mark $CD45^+$ microglia due to bleed-through from other fluorophores. Scale bar = 100 µm. Abbreviations: DM, DMEM-based media.

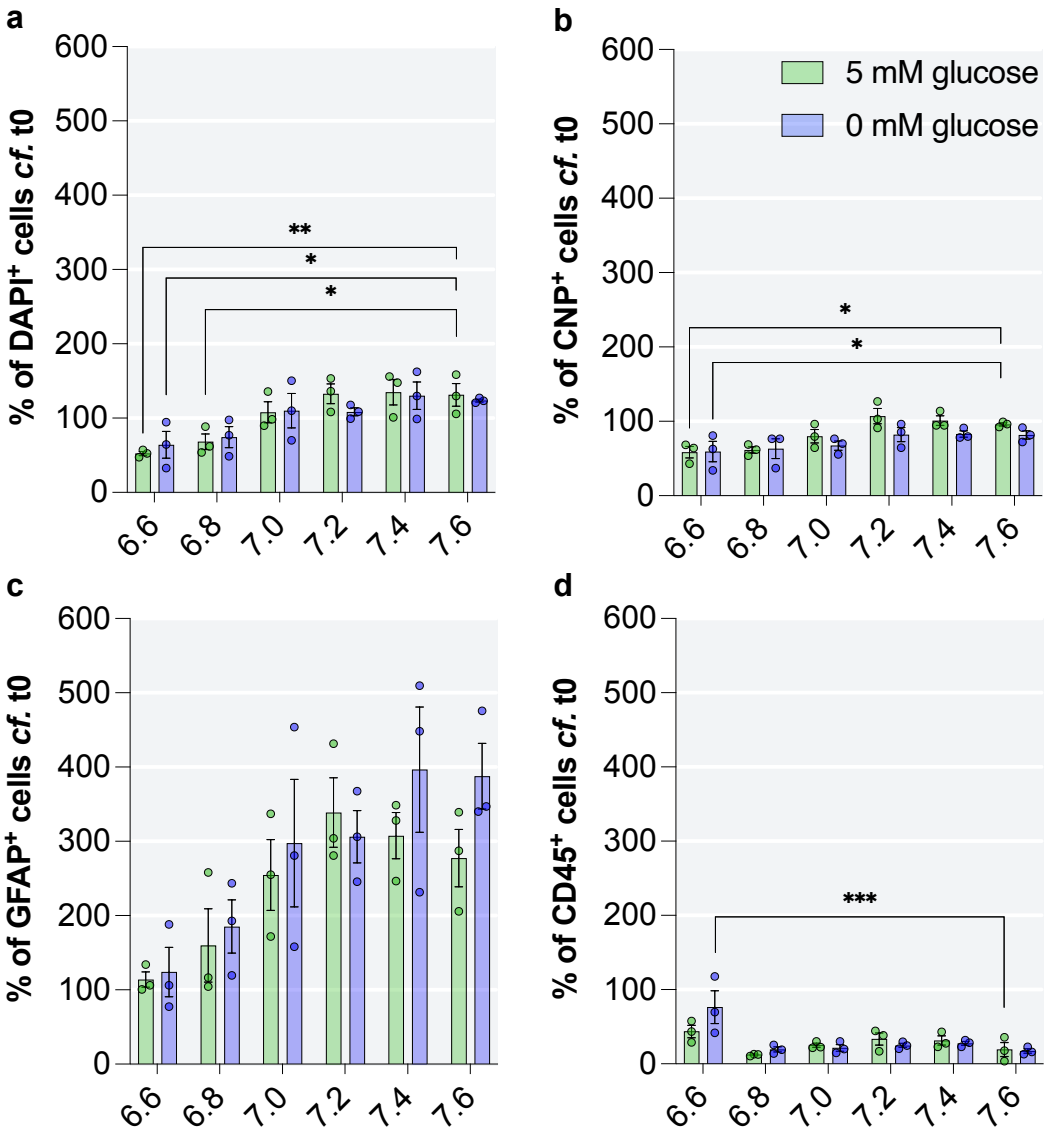

Figure 4.2 | An acidic milieu impacts cell densities in mixed glial cultures but the effect is not compounded by glucose deprivation. Graphs of cell densities at t6d as a percentage of the t0 value. Cultures were maintained in DM across a range of pH values containing 5 mM glucose (green) or 0 mM glucose (blue). **(a)** Compared to controls, total cell ($DAPI^+$) and **(b)** EMOL (CNP^+) cell densities were significantly reduced at acidic pH regardless of glucose supplementation. **(c)** Astrocyte ($GFAP^+$) densities, which increased markedly at physiological pH, tended towards t0 values at acidic pH. **(d)** Microglial ($CD45^+$) densities tended to increase at pH 6.6 compared to controls. Data were compared to pH 7.6 with 5 mM glucose using a two-way ANOVA with Dunnett's multiple comparison test. * = $p < 0.05$, ** = $p < 0.01$, *** = $p < 0.001$. Data were obtained from 3 biological repeats. Abbreviations: DM, DMEM-based media.

4.3 Withdrawal of amino acids and/or vitamins impacts densities of EMOLs more than glucose deprivation

In Chapter 3, we described the remarkable resilience of EMOLs to 48 hours of exogenous energy deprivation in glucose-free media (also lacking pyruvate and glutamine). In the previous section (section 4.2), we unexpectedly found that cells survived 6 days of exogenous energy substrate deprivation. To explore this further, we cultured mixed glia for 6 days in DMEM-based media (DM) or in a matched salts-only (SO) media lacking amino acids and vitamins, the latter to replicate the deprivation of essential factors as might occur in ischaemia. Both DM and SO media were either supplemented with 5 mM glucose only or left unsupplemented (0 mM glucose). To test if 5 mM glucose was limiting for cell survival, we also cultured cells in highly enriched (HE) DM containing 25 mM glucose, 1 mM pyruvate, and 4 mM glutamine. Raw data are shown in Figure S3.

Remarkably, after 6 days in DM with 0 mM glucose, neither total ($DAPI^+$), EMOL, astrocyte, or microglial cell densities were significantly altered compared to controls (5 mM glucose DM; Figure 4.3 a; Figure 4.4 a-d). However, EMOL densities were significantly reduced in both SO conditions and total cell densities were reduced in SO media without glucose (Figure 4.3 b; Figure 4.4 a, b). Astrocyte and microglial densities were not significantly altered in either SO media compared to control although there was a downward trend in both cases (Figure 4.3 b; Figure 4.4 c, d).

In HE media, total cell densities were significantly increased compared to control but densities of EMOLs and astrocytes were similar to those grown in 5 mM glucose supplemented DM (Figure 4.3 c; Figure 4.4 a-c). Microglial cell densities appeared to increase but these were not quantified (Figure 4.3 c).

Qualitatively, all CNP^+ cells at t6d in 5 or 0 mM glucose DM co-expressed MBP, a marker of myelin formation (n = 1; Figure 4.3 d).

These data demonstrate that spinal cord EMOLs are remarkably resistant to glucose deprivation when the amino acids and vitamins present in DM are available. Unsurprisingly, glucose alone did not support survival in the absence of amino acids and vitamins.

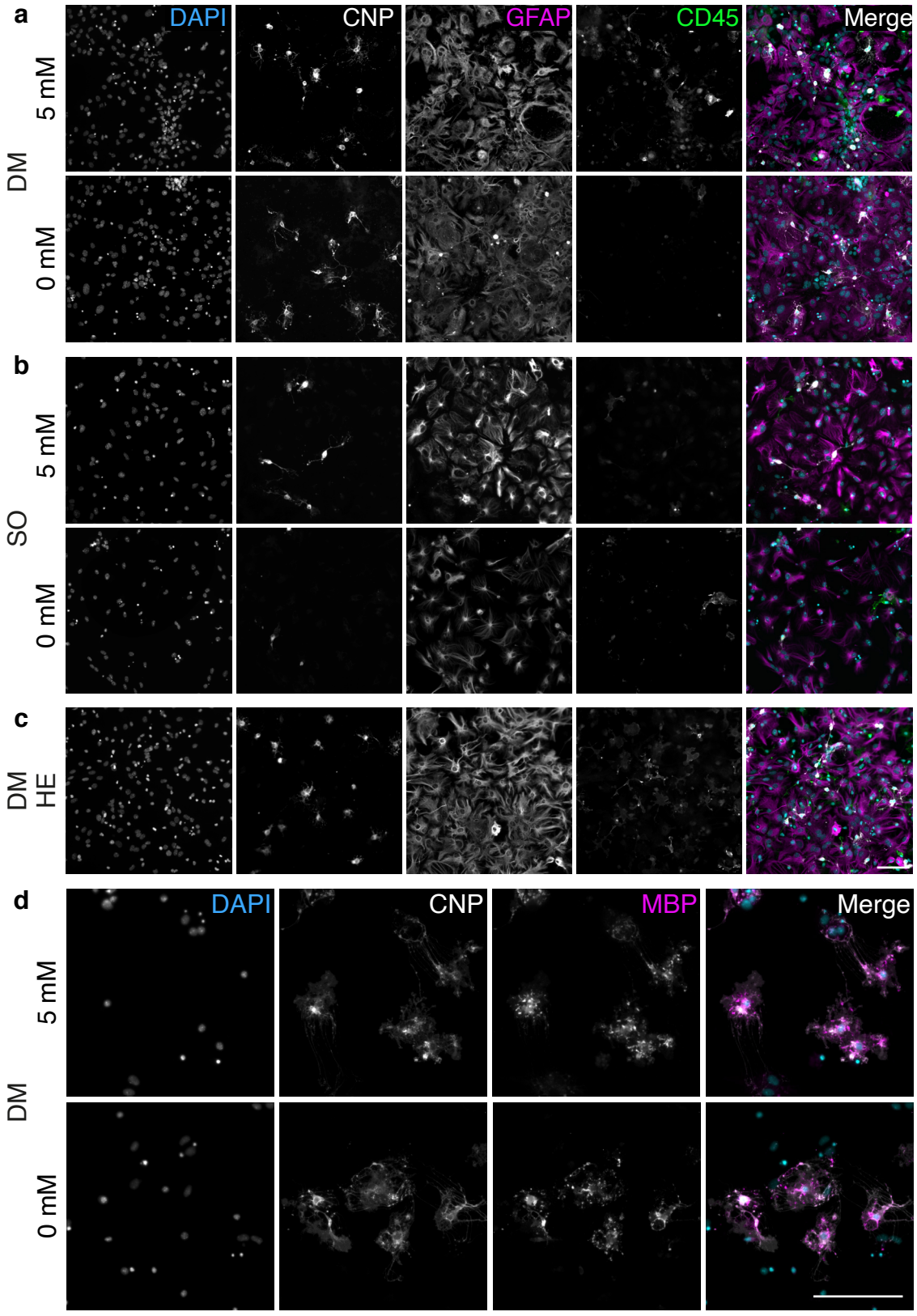

Figure 4.3 | Withdrawal of amino acids and/or vitamins impacts EMOLs more than glucose deprivation in mixed glial cultures. *Figure legend continues on the next page.*

Figure 4.3 | *Cont...* Illustrative images of mixed glial cultures grown for 6 days in DM containing amino acids and vitamins or a SO equivalent, with or without 5 mM glucose. **(a)** Total cell (blue, $DAPI^+$), EMOL (white, CNP^+), and astrocyte (magenta, $GFAP^+$) cell densities appeared similar in 0 mM glucose DM compared to 5 mM glucose DM. Microglia (green, $CD45^+$) appeared less dense in the absence of glucose. **(b)** In SO media, EMOL and astrocytes cell densities appeared most reduced in the 0 mM glucose condition. **(c)** Cultures maintained in HE media for 6 days appeared similar to those in 5 mM glucose though more microglia were observed. **(d)** EMOLs were MBP^+ (magenta) at t6d even in the absence of glucose. Scale bar = 100 µm. Abbreviations: DM, DMEM-based media; SO, salts-only; HE, DMEM-based media highly enriched in energy substrates.

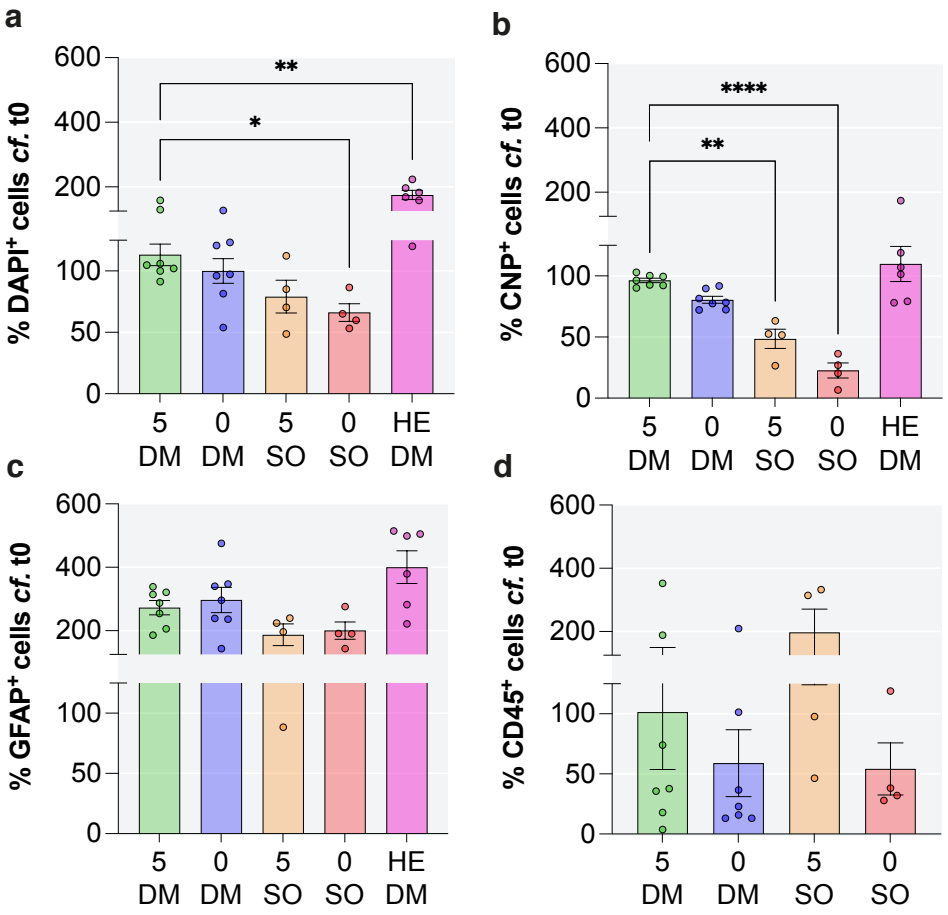

Figure 4.4 | Withdrawal of amino acids and/or vitamins impacts EMOL cell densities more than glucose deprivation in mixed glial cultures. Graphs of cell densities at t6d as a percentage of t0 values. **(a)** Total cell ($DAPI^+$) densities tended to decrease with increasing deprivation but reached significance only in the most deprived condition (red bar). In contrast, densities were significantly increased in HE media. **(b)** EMOL densities were unchanged in DM in the absence of glucose and were not increased in HE media. **(c)** Astrocyte ($GFAP^+$) densities were variable and unchanged across all conditions though they increased markedly from the t0 density. **(d)** Microglia ($CD45^+$) densities were variable across experiments. Data were compared to 5 mM glucose DM using a one-way ANOVA with Dunnett's multiple comparison test. * = $p < 0.05$, ** = $p < 0.01$, **** = $p < 0.0001$. Data were obtained from up to 7 biological replicates (see data points). Abbreviations: DM, DMEM-based media; SO, salts-only; HE, DMEM-based media highly enriched in energy substrates.

4.3.1 EMOL growth requires amino acids and/or vitamins but appears not to be dependent on glucose

Oligodendrocytes are highly biosynthetic cells that produce enormous volumes of cell membrane rich in lipids and protein. Under stress, cells can recycle cellular and membrane components using autophagy, which reduces cell size as a consequence (Lum *et al.*, 2005; Hosokawa *et al.*, 2006). Therefore, we determined if EMOL cell densities were maintained at the expense of their cell size in deprived media by measuring the area of individual cells delineated by CNP staining at t0 and t6d (Figure 4.5 a, b).

The mean EMOL size at t0 was 610 μm^2. At t6d, EMOLs were significantly larger in 5 mM glucose DM (control), compared to t0, with an average size of 1623 μm^2. EMOLs maintained in 0 mM glucose DM reached a similar size of 1964 μm^2. In SO media, with or without glucose, EMOLs were significantly smaller compared to controls. EMOLs in HE media attained a similar size to those in control media (Figure 4.5 c).

These data demonstrate that EMOL survival in DM without glucose does not occur at the expense of cell size. However, withdrawal of amino acids and/or vitamins limited growth even when glucose was provided.

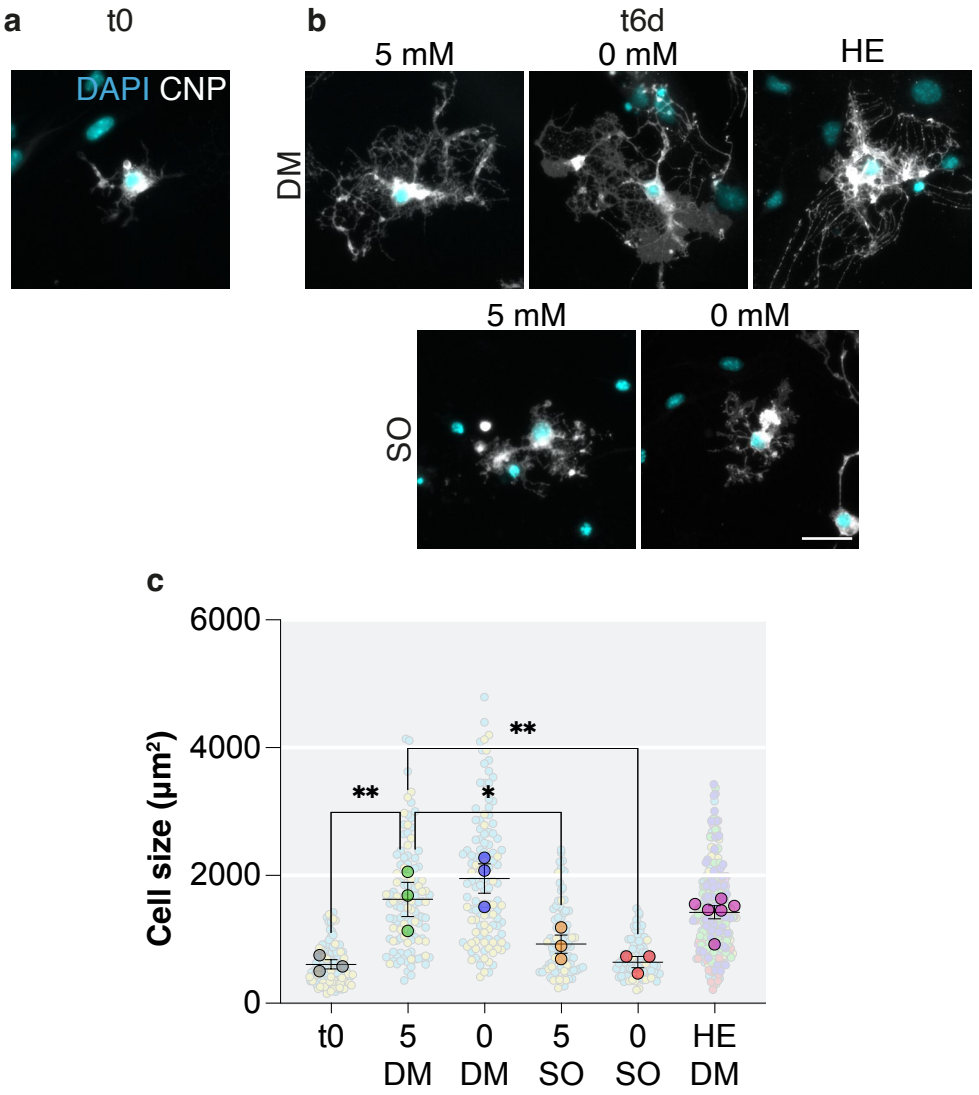

Figure 4.5 | Growth of EMOLs requires amino acids and/or vitamins but is not influenced by glucose availability in mixed glial cultures. Representative images of EMOLs (white, CNP^+) and their cell nuclei (blue, $DAPI^+$) in mixed glial cultures at **(a)** t0 and **(b)** t6d. **(c)** EMOL cell size measured by the area of CNP staining and displayed on a SuperPlot. At least 30 cells were included after ROUT analysis per biological replicate. Data were compared to 5 mM glucose DM using a one-way ANOVA with Dunnett's multiple comparison test performed on average values. * = $p < 0.05$, ** = $p < 0.01$. Data were obtained from 3 or 6 biological repeats (see data points). Scale bar = 25 µm. Abbreviations: DM, DMEM-based media; SO, salts-only; HE, DMEM-based media highly enriched in energy substrates.

4.3.2 Most EMOLs at t6d in glucose-deprived media persist from t0

Oligodendrocyte cell death stimulates OPC differentiation into new myelinating cells that can restore cell densities (Hesp *et al.*, 2015; Ziemka-Nalecz *et al.*, 2018). Therefore, it was important to determine if EMOL densities were being maintained in DM following 6 days of glucose deprivation by: i) survival of cells present at the beginning of experimentation; ii) differentiation of OPCs into new EMOLs, or iii) both. To address this, we generated mixed glial cultures containing tdTomato-labelled EMOLs and imaged cells at t0 and daily thereafter using live-cell imaging (Figure 4.6 a, b).

The highest rate of EMOL loss was observed after the first 24 hours with 3 of 14 cells lost in the 5 mM glucose condition and 7 of 15 cells lost in 0 mM glucose media. An additional cell was lost by t2d in the 5 mM glucose condition. The number of cells remained constant until t6d, where 71% and 53% of EMOLs selected at t0 survived in 5 mM or 0 mM glucose supplemented media, respectively (Figure 4.6 c).

Due to limited biological repeats, we tentatively conclude that a majority of EMOLs survive for 6 days under glucose deprivation in DM. However, we cannot rule out the possibility that OPC differentiation into EMOLs also contributes to the maintenance of EMOL cell densities.

4.3.3 Reintroducing glucose does not induce cell death in mixed glia maintained in energy substrate deprived media

To determine if EMOLs persisted in culture because they could not execute apoptosis due to energy insufficiency, mixed glia were maintained in 0 mM glucose DM until t5d then supplemented with 5 mM glucose for 24 hours. Cells were then fixed (at t6d) and immunostained for cell type-specific markers and cleaved caspase-3 (CC3), a marker of apoptosis.

At t5d, densities of $CC3^+$ $DAPI^+$ nuclei appeared similar in 5 or 0 mM glucose DM. Where present, CC3 always colocalised with pyknotic nuclei (Figure 4.7 a). Twenty four hours after introducing 5 mM glucose, $CC3^+$ cells did not appear to increase in frequency compared to control cultures maintained in 5 mM glucose throughout. Healthy-appearing $DAPI^+$ EMOL

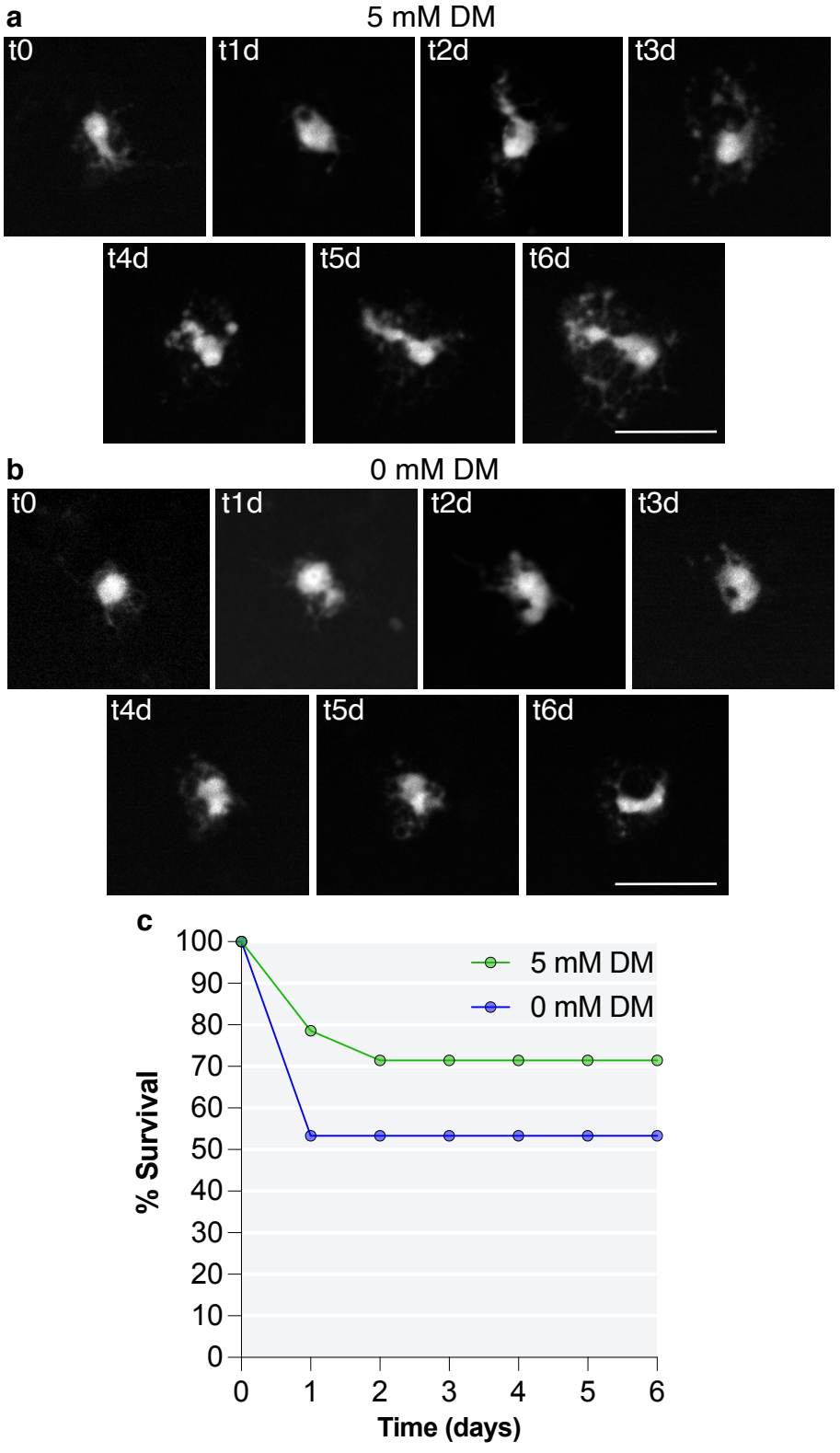

Figure 4.6 | A majority of EMOLs persist from t0 in DMEM-based media without glucose. Maximum intensity projection confocal images of single EMOLs (white, TdTomato-expressing) taken daily by live-cell imaging using a spinning disc confocal microscope during culture in **(a)** 5 or **(b)** 0 mM glucose supplemented DM. Scale bar = 50 µm. **(c)** Graph of percentage of cells selected at t0 that were alive at increasing days in culture, based on imaging a minimum of 14 cells. Data were obtained from 1 biological repeat. Abbreviations: DM, DMEM-based media.

cell nuclei appeared pale with areas of condensed chromatin and were negative for CC3 (Figure 4.7 b).

To confirm that cells persisting in glucose-free DM were not necrotic, we treated mixed glia with propidium iodide (PI). As positive controls for necrosis, mixed glia were heat-treated or cultured in SO media for 6 days. Cultures maintained in 5 or 0 mM glucose DM, or SO media with 5 mM glucose, had very few PI^+ nuclei at t6d. In comparison, positive control cultures had many more PI^+ nuclei (Figure 4.7 c). Healthy-appearing $DAPI^+$ nuclei did not co-label with PI^+ cells under any condition.

Next, we performed an LDH assay on cell supernatants from mixed glia at t6d. Similar levels of LDH release were found in the 5 mM glucose DM (control) compared to 0 mM DM. Significantly more LDH release, compared to control, was detected in the SO media conditions, particularly when glucose was absent (Figure S4 a). Additionally, total $DAPI^+$ cell density averages (reported in Figure 4.4 a) and LDH release assay optical density averages displayed a strong Pearson correlation (r_p = -0.9907; Figure S4 b).

Finally, we tested the possibility that the 0 mM glucose DM was erroneously contaminated with an energy substrate by incubating an “energy-hungry” cell population in it. Myelinating cultures at DIV 25 contain neurons, astrocytes, OPCs, microglia and myelinating oligodendrocytes. These were switched from HE media to DM with 5 or 0 mM glucose for 24 hours. Axons ($SMI31^+$) and myelinating cells (PLP^+) were maintained in 5 mM glucose; however, both were absent in 0 mM glucose media and overall cell densities appeared reduced (Figure S5).

These findings validate our cell density quantifications and help confirm the composition of the glucose-free media. In all, these data support our finding that a majority of EMOLs can survive in culture in the absence of exogenous energy sources such as glucose (but also pyruvate and glutamine) for an extended time if provided with the amino acids and/or vitamins present in DM.

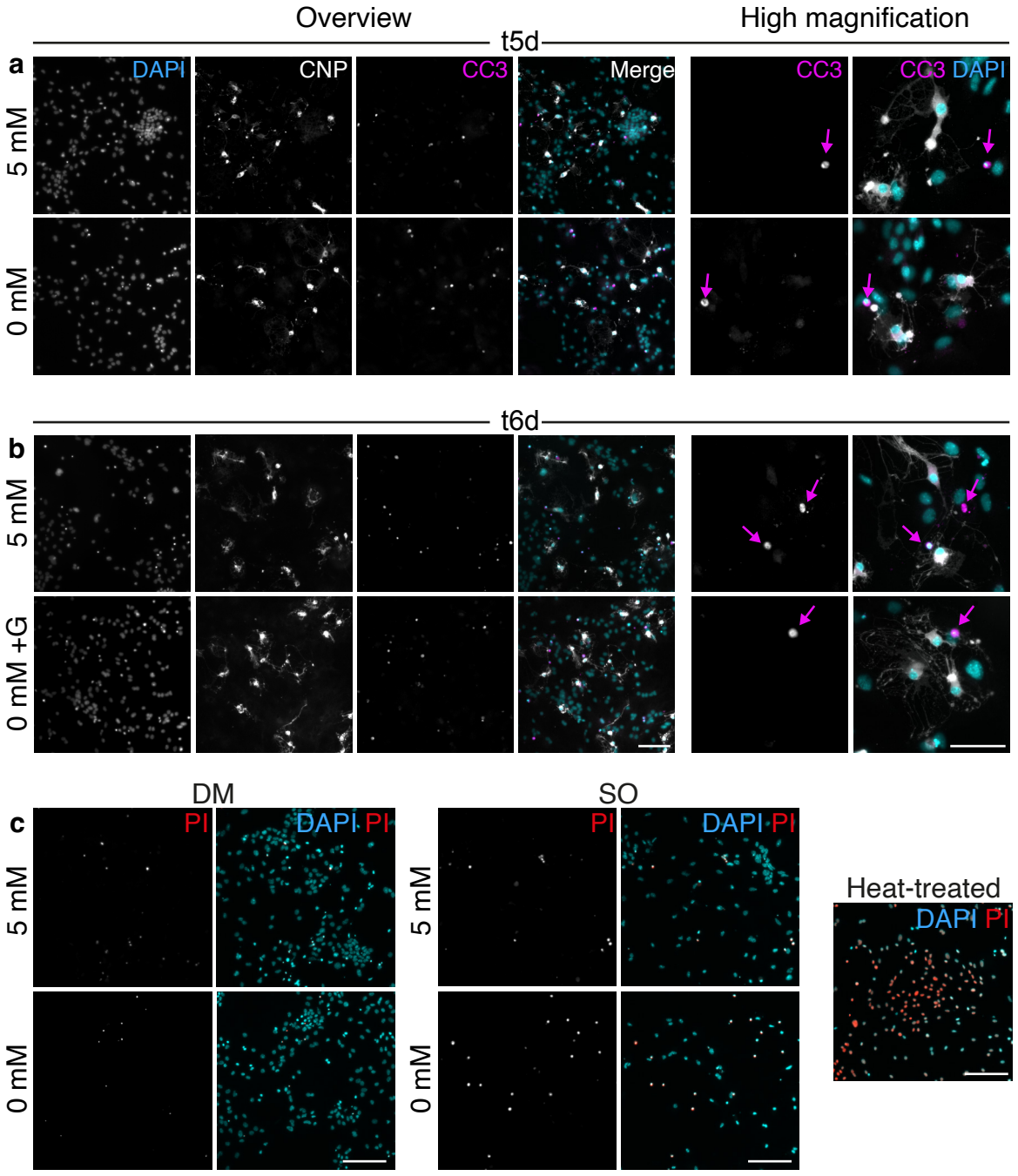

Figure 4.7 | Markers of cell death are not noticeably increased in mixed glial cultures after 6 days in glucose-free medium or following glucose reintroduction. Illustrative immunofluorescence images of mixed glial cultures. **(a)** Cultures grown in DM with 5 or 0 mM glucose at t5d had few cleaved caspase-3$^+$ cells (CC3; magenta, arrows) **(b)** and no increase in CC3 staining was observed in EMOLs (white, CNP$^+$) 24 hours after the addition of 5 mM glucose to deprived cultures (+ G). Scale bar = 100 µm for overview images and 25 µm for high magnification images. **(c)** Propidium iodide (PI; red) labelling of cultures grown in DM or SO media, with and without 5 mM glucose. Healthy-appearing nuclei (blue, DAPI$^+$) did not co-label with PI. Heat-treated cultures served as a positive control for PI stain. Scale bar = 100 µm. Representative images from a single experiment. Abbreviations: DM, DMEM-based media; SO, salts-only.

4.4 EMOLs are tolerant to IFNγ and TNF compared to astrocytes

To test the susceptibility of spinal cord EMOLs to inflammatory factors present in the hypoxic/ischaemic environment, mixed glial cultures were grown in 5 mM glucose DM with 20 ng/mL IFNγ and 50 ng/mL TNF for 6 days. As an additional stressor, some cells were grown in unsupplemented DM (0 mM glucose). Heat inactivated (HI) cytokines were used in control cultures and all were assessed qualitatively by immunofluorescence.

Compared to control cultures (5 mM glucose with HI cytokines; Figure 4.8 a), treatment with IFNγ and TNF resulted in a reduction of DAPI$^+$ cells overall with a particular loss of astrocytes. EMOLs were not as vulnerable and appeared similar to control (Figure 4.8 b). Compared to these, cytokine-treated cultures grown in 0 mM glucose appeared similar, suggesting the lack of glucose did not compound the effect of inflammatory factors.

These data suggest that EMOLs are less susceptible than astrocytes to the inflammatory factors, IFNγ and TNF.

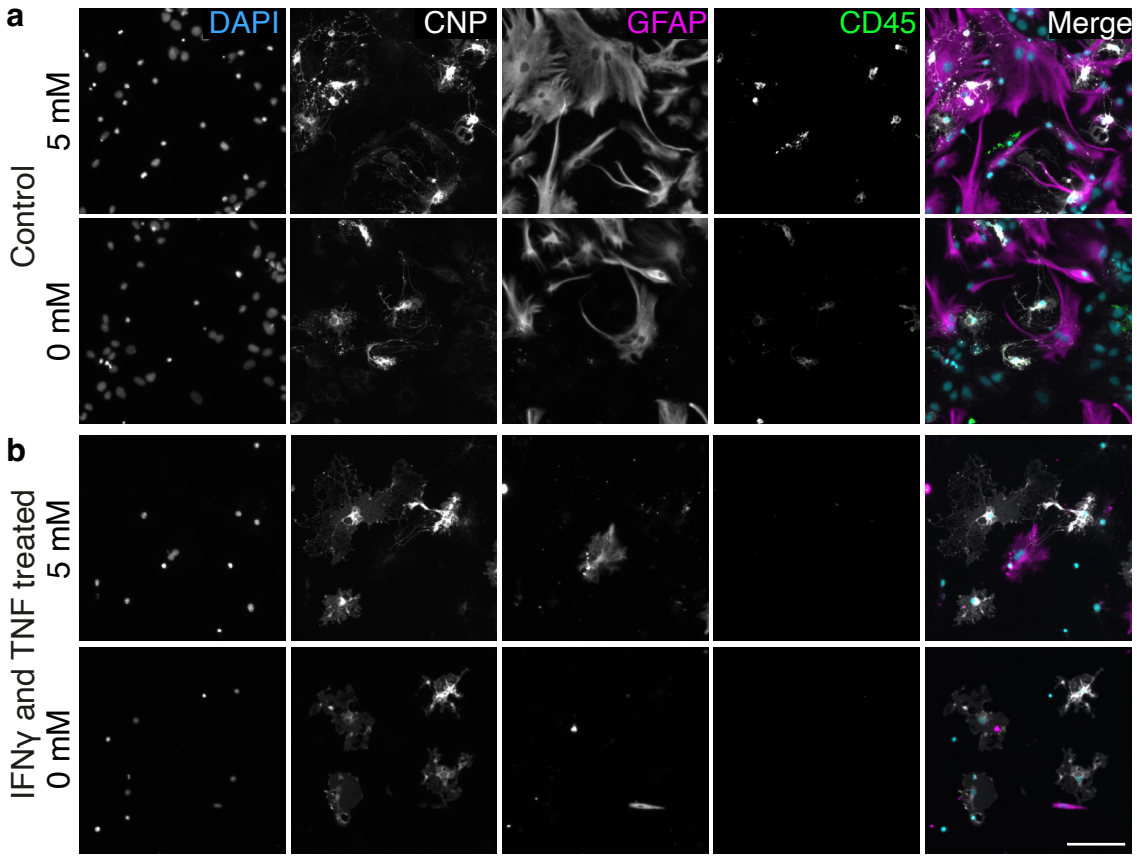

Figure 4.8 | Inflammatory factors do not appear to impact EMOLs, whereas astrocytes appear vulnerable after 6 DIV. Illustrative images of mixed glial cultures after 6 days of treatment with IFNγ and TNF in DM with and without 5 mM glucose. **(a)** Control cultures were treated with heat-inactivated (HI) inflammatory factors. **(b)** Treatment with TNF and IFNγ resulted in loss of astrocytes (magenta, GFAP$^+$) and reduced cell densities overall (blue, DAPI$^+$). EMOLs (white, CNP$^+$) did not appear vulnerable at 6 days. Glucose deprivation did not appear to compound the effects of inflammatory factor exposure. Observations representative of 3 biological repeats from 2 independent litters. Scale bar = 100 µm. Abbreviations: DM, DMEM-based media.

4.5 Discussion

In this chapter, we used our model of spinal cord white matter glia characterised in Chapter 3 to examine the intrinsic responses of spinal cord EMOLs and other glia to individual secondary components of the hypoxic environment. Using this model, which lacks the confounding effects of neuronal cell death, we found that spinal cord EMOLs were vulnerable when cultured for 6 days in an environment mimicking lactic acidosis or when cultured in the absence of amino acids and vitamins. In contrast, EMOLs were relatively resistant to inflammatory insult compared to astrocytes and, most surprisingly, to 6 days of culture in the absence of exogenous energy substrates. To understand these results, we discuss below the robustness of our assay and the possible contribution of alternative energy sources to maintain glial cell viability.

Acidosis is a consequence of oxygen deprivation, which forces cells to use anaerobic respiration and causes the accumulation of extracellular lactic acid. We showed that following 6 days incubation, spinal cord EMOLs were vulnerable to an acidic extracellular milieu. These data are compatible with prior reports. The effects of acidosis *per se* were shown to severely impair neural tissue recovery after lactate clearance *in vivo* (Rehncrona *et al.*, 1981) and is a significant pathological factor in neonatal brain hypoxic injury (Pang *et al.*, 2020). Furthermore, Jagielska *et al.* (2013) found that whilst rat brain-derived OPCs migrate towards an acidic environment (pH of 6.0), survival, proliferation, and maturation into myelinating cells is compromised compared to pH 7.0. Therefore, we extend the current understanding of oligodendroglial vulnerability to acidosis by showing spinal cord EMOLs are also susceptible.

In contrast to EMOLs, at pH 6.6 astrocyte densities were maintained compared to t0. Conversely, at physiological pH, astrocyte densities increased $\sim$4-fold compared to starting values. This suggests that astrocyte proliferation or differentiation from precursors is adversely impacted by acidosis but survival is not. Norenberg *et al.* (1987) and Swanson *et al.* (1997) showed that neonatal rat brain astrocytes *in vitro* were susceptible to death within 3 hours of extracellular acidosis at pH < 6, whereas cells remained viable for at least 7 hours at pH 6.6. These acute data agree with our observations and suggest astrocytes are only vulnerable to extreme acidosis.

In general, the lack of exogenous energy substrates did not compound the effects of acidosis on EMOLs or astrocytes. Microglia densities however were significantly greater than controls following combined acidosis and glucose deprivation. This is likely due to microglial activation and proliferation, an effect seen in an inflammatory microenvironment (Sato *et al.*, 2020; Ritzel *et al.*, 2021). The activation of microglia as a contributor to injury in the hypoxic environment should not be overlooked as pro-inflammatory cytokines secreted by them can generate a self-sustaining positive-feedback loop that is cytotoxic to other glia (Kuno *et al.*, 2005).

The lack of glucose delivery to the CNS during hypoxia-ischaemia results in cellular energy failure and cell death (reviewed in Shalak and Perlman (2004)). In contrast, and to our surprise, we found that depriving mixed glia of glucose (pyruvate and glutamine) did not significantly reduce EMOL cell densities after 6 days *in vitro*. As mentioned in Chapter 3, others have reported that *ex vivo* rat hippocampal slices are maintained under glucose deprivation for at least 24 hours, likely due to astrocyte glycogen-derived lactate (Cater *et al.*, 2001). The EMOL likely receives glycogen-derived lactate under glucose deprivation in our model system; however, it seems unlikely that astrocyte glycogen alone could sustain mixed glia for 6 days in the absence of exogenous energy substrates.

Dringen and others showed that glycogen stores in brain-derived astrocytes are depleted under glucose deprivation after only 1 to 2 hours *in vitro*. The authors maintained rat or mouse astrocytes in 5 mM glucose with 10% foetal calf serum until DIV 15-21 then found subsequent glucose deprivation depleted glycogen stores in ~60 minutes (Dringen *et al.*, 1993a) or ~120 minutes (Dringen and Hamprecht, 1993), respectively. In these experiments, cells were maintained at 5-times the density used in our cultures and it is not clear if the 10% foetal calf serum was removed during their glycogen assays. Notably, astrocyte survival was not assessed after glycogen stores were depleted; therefore, it is not known for how long they remained viable after glycogen was exhausted in glucose-free media. These studies, nonetheless, highlight species-dependent differences in brain glycogen metabolism. In both studies, *in vitro* matured cells were used, which might have an altered cellular metabolism compared to the acutely obtained cells used in our experiments.

Experimental reports on the effects of extended glucose deprivation in primary astrocyte cultures are limited. In one study, surviving astrocytes obtained from mouse brain were reduced by over 60% at 72 hours following glucose deprivation (Li *et al.*, 2021). In Li's study, astrocytes were maintained in Minimal Essential Medium, which contains about a quarter of the concentration of amino acids and vitamins present in DMEM. Additionally, in contrast to us, the authors did not include N1 hormone supplement (insulin, progesterone, apo-transferrin, sodium selenite) or biotin in any condition. Moreover, the plating density was not reported. A study conducted by Kogel *et al.* (2021) where rat brain astrocytes were cultured for up to 15 days in DMEM containing 25 mM, 2 mM or 0 mM glucose is more comparable to ours. However, the authors used LDH release as an output of cell death so we cannot directly compare their data with ours. Nonetheless, their data suggest that 30% of astrocytes were lost in glucose-free media at 6 DIV although pyruvate was present at an unreported concentration. Complicating the interpretation is the fact that LDH has a half-life of 9 hours and cannot be used as a cumulative indicator of cell loss. In both studies described above, *in vitro* differentiated astrocytes were used, which as mentioned previously might exhibit different metabolic vulnerabilities compared to cells harvested acutely from tissue. In all, data on astrocyte vulnerability to glucose (as well as glutamine and pyruvate) deprivation is lacking though our data demonstrate densities are not affected by exogenous energy substrate deprivation, or amino acid and vitamin withdrawal, for 6 days at least.

OPCs in the spinal cord can proliferate and replace lost oligodendrocytes as shown in spinal cord injury (Blakemore, 1978) and demyelinating disease (reviewed in Franklin and ffrench-Constant (2017)). In fact, direct injury to EMOLs in the spinal cord at P4-6 resulted in only temporary hypomyelination that largely resolved after 2 weeks due to the proliferation of OPCs (Caprariello *et al.*, 2015). Might OPC proliferation and differentiation maintain EMOL densities also in our model system? We showed using live-cell imaging that a majority of spinal cord EMOLs present at the start of our experiments remained at the end. Moreover, our total cell densities did not change between t0 and t6d in 5 or 0 mM glucose DM making it unlikely that cells proliferated in response to glucose deprivation. However, proliferation matched to the rate of cell death should not be discounted. Thus, we tentatively conclude that cell densities were unlikely maintained by OPC proliferation

and differentiation over the course of 6 days in glucose-free DM.

We sought to ensure cell densities were not artefactually maintained in 0 mM glucose DM due to slow cell death by necrosis. We did not observe differences in PI^+ or $CC3^+$ cell numbers at t6d between 5 or 0 mM glucose, which suggested cells in the latter condition were indeed viable. Therefore, we concluded that mixed glia in 0 mM glucose DM must have access to an endogenous energy source to maintain cellular integrity in the absence of glucose (as well as glutamine and pyruvate). The possibility that astrocyte glycogen supports EMOLs has already been discussed here and in Chapter 3.

Oligodendroglia require autophagy for cell survival and maturation (Smith *et al.*, 2013; Bankston *et al.*, 2019; Stone *et al.*, 2020) and express high levels of autophagy-related proteins (Bankston *et al.*, 2019). We hypothesised EMOL autophagy might provide an alternative source of energy substrates and contribute to EMOL maintenance under exogenous energy substrate deprivation. Active autophagy in starved cells reduces cell size as observed in immortalised cell lines (Lum *et al.*, 2005; Hosokawa *et al.*, 2006); however, we excluded autophagy as a major means to maintain EMOLs upon finding cell growth was not sacrificed.

Although oligodendrocytes do not store glycogen, they are lipid-rich cells that could, in theory, use their membrane lipids as a fuel source. However, the function of EMOLs is to synthesise enormous quantities of myelin lipid and it is therefore believed that myelinating glia do not favour lipids as a fuel source (Schönfeld and Reiser, 2013; Poitelon *et al.*, 2020). Moreover, the subject of CNS β-oxidation is highly debated and astrocytes are the only neural cell considered likely to do so *in vivo* (Ebert *et al.*, 2003). The possible use of endogenous lipids as an energy substrate in our mixed glial culture system is an important question and is explored in Chapter 5.

To our knowledge, few groups have examined the effects of amino acid and vitamin deprivation on neural cells for an extended time. Rone *et al.* (2016) examined the effect of withdrawing hormones (N1; insulin, apo-transferrin, sodium selenite, putrescine, and progesterone) from DMEM on human oligodendrocyte cultures and found 30% of cells remained viable after 6 days in 25 mM glucose. However, their control condition (with N1), where little cell death occurred, was made using DMEM-F12 (contains pyruvate, linoleic

acid, and lipoic acid) making it hard to conclude whether hormones and/or additional DMEM-F12 components kept their human oligodendrocyte alive. These additional factors were not required to maintain mouse spinal cord glia *in vitro* and we show that removal of amino acids and vitamins alone is detrimental to EMOL survival. Considering all these data, interruption in the supply of amino acids, vitamins, and hormones in the context of hypoxia-ischaemia is likely a contributing pathological factor since these nutrients are supplied by the bloodstream.

High extracellular levels of TNF and IFNγ induce apoptosis in brain-derived oligodendrocytes by acting on membrane-expressed receptors (Probert *et al.*, 1995; Vartanian *et al.*, 1995; Dopp *et al.*, 1997; Agresti *et al.*, 1998; Akassoglou *et al.*, 1998; Pouly *et al.*, 2000; Bohatschek *et al.*, 2004). In particular, TNF-receptor 1 expressed by oligodendrocytes and astrocytes contains an intracellular death domain that triggers caspase-dependent apoptosis when activated (Nakazawa *et al.*, 2006). Further, TNF enhances the injurious effect of IFNγ (Andrews *et al.*, 1998) and both cytokines are released following hypoxic injury *in vivo* (Dawson *et al.*, 1996; Darnall *et al.*, 2017). Previously, mouse brain-derived EMOLs were reported vulnerable to TNF after 3 DIV (Hisahara *et al.*, 1997) and under similar conditions in a mixed glial culture system (Ye and D'Ercole, 1999) but using twice the concentration we used. In our study, spinal cord EMOLs did not appear vulnerable to treatment with these cytokines. Astrocytes however were susceptible as previously reported *in vitro* (Kralingen *et al.*, 2013). Depriving mixed glia of glucose during exposure to IFNγ and TNF did not appear to compound the effects of these inflammatory factors. Therefore, our data suggest that a population of spinal cord EMOLs are somewhat resistant to inflammatory insult although the true levels of cytokines *in vivo* are not known.

In this chapter, we examined the response of spinal cord EMOLs to individual secondary components of the hypoxic environment since tolerance to these could account for why they appear resistant to hypoxia *in vivo*. We showed that spinal cord EMOLs are vulnerable to extracellular acidosis and deprivation of amino acids and vitamins but are resistant to deprivation of exogenous energy substrates and exposure to inflammatory factors. Our data demonstrating that spinal cord EMOLs and glia can survive 6 days of glucose deprivation are remarkable. Therefore, we explore potential metabolic adaptations and fuel sources that might allow survival under exogenous energy substrate deprivation next in Chapter 5.

Chapter 5

Spinal cord early myelinating oligodendrocytes and astrocytes might utilise alternative fuel sources to survive glucose deprivation

5.1 Introduction

Oligodendrocytes and astrocytes are highly interconnected by gap junctions that allow the transfer of low molecular weight molecules, including energy substrates and glycolytic end products (Orthmann-Murphy *et al.*, 2008; Hertz *et al.*, 2014; Hirrlinger and Nave, 2014). In Chapter 4, we found spinal cord EMOLs were remarkably resistant to exogenous energy substrate deprivation in our mixed glial culture system and hypothesised astrocytes, which store glycogen, might be maintaining the cells as observed in *ex vivo* optic nerve preparations (Wender *et al.*, 2000; Tekkök *et al.*, 2005). However, glycogen stores are limited and we must therefore consider alternative energy sources. Recently, lipid droplets were reported within glia in the *Drosophila* brain under homeostatic conditions (Smolič *et al.*, 2021) and it is known that the CNS can sequester FAs from serum in circulation, as shown in adult rats and early postnatal mice (Pardridge and Mietus, 1980; Camargo *et al.*, 2017). Cultured astrocytes accumulate small, TG-rich organelles called lipid droplets when grown in serum-rich medium, which can provide an intracellular lipid store for β-oxidation under subsequent glucose deprivation (Farmer *et al.*, 2019). Indeed, metabolism of lipid droplets has been shown to maintain cell viability under exogenous energy deprivation in non-CNS cell types (Cabodevilla *et al.*, 2013) and could, in theory, support astrocytes and other glia in the absence of exogenous energy supplies. Therefore, in this chapter, we explored how EMOLs might obtain energy substrates to sustain cellular energy metabolism in the absence of exogenous glucose, pyruvate, and glutamine.

The specific aims were to:

(i) Determine if trans-cellular transport of gap junction permeable dyes (a surrogate for energy substrates) occurs between EMOLs and astrocytes in our mixed glial model.

(ii) Explore the metabolic adaptations of mixed glia at the level of mRNA expression that might explain their survival under exogenous energy substrate deprivation.

(iii) Assess changes in lipid abundance in mixed glia and EMOLs following 6 days of exogenous energy substrate deprivation as an indicator of whether lipids might be used as an energy source.

(iv) Determine if EMOL function (myelination) is maintained after 6 days of exogenous energy substrate deprivation.

5.2 EMOLs extend nanotube-like structures towards astrocytes that allow the exchange of materials

After culturing mixed glia for 6 days, we observed that EMOLs extended long, narrow, nanotube-like structures (subsequently referred to as *nanotubes*) towards astrocytes and hypothesised these could provide a bridge for the transfer of metabolic substrates under exogenous energy substrate deprivation. Nanotubes were CNP^+, suggesting they were cytoplasm-filled (Figure 5.1 a), and positive for β-tubulin IV and F-actin (Figure 5.1 b, c). By generating cultures from mice expressing Cnp-mEos2-PTS1, we observed $mEos2^+$ oligodendroglial peroxisomes within nanotubes (Figure 5.1 a, b). These were motile even in the absence of all exogenous energy sources (Figure S7).

These observations suggest nanotubes might provide a sequestration route for EMOLs to receive metabolic support from astrocytes, possibly involving breakdown products of glycogen and/or FAs.

5.2.1 EMOL nanotubes allow dye-coupling with astrocytes

To determine if EMOL nanotubes allow the exchange of materials with astrocytes, single EMOLs were dye-filled with gap junction-permeable compounds. Following growth for 6 days in 5 mM glucose DM, EMOLs were identified by phase-contrast and filled with biocytin and Lucifer yellow, the latter facilitated visualisation of the cell during filling. In three of three experiments, we successfully filled EMOLs and in one of these, biocytin from a single filled EMOL was observed in two adjacent $GFAP^+$ astrocytes (Figure 5.2).

As the only visible physical connection between the cell types was EMOL nanotubes, we conclude these provide a transfer route for gap junction-permeable materials between EMOLs and astrocytes.

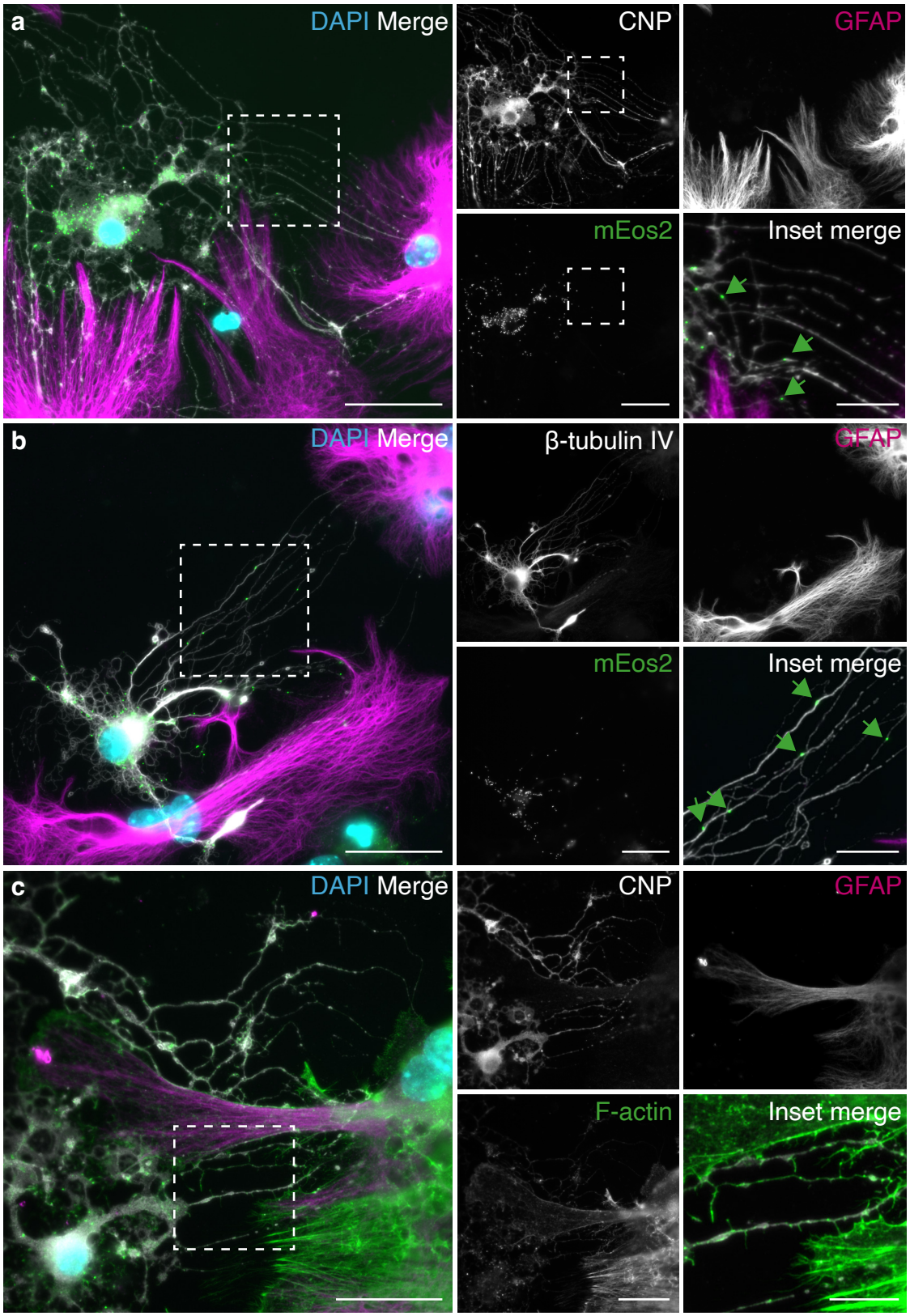

Figure 5.1 | **Nanotube-like structures containing peroxisomes are extended by EMOLs towards astrocytes *in vitro*.** Illustrative images of mixed glia grown for 6 days in highly enriched media. **(a)** Cytoplasm-filled nanotube-like structures from EMOLs (white, CNP^+) containing peroxisomes (green, mEos2-labelled) extend towards astrocytes (magenta, $GFAP^+$). These structures also contain **(b)** β-tubulin IV (white), and **(c)** F-actin (green). Scale bar = 25 µm for overview images and 10 µm for inset images.

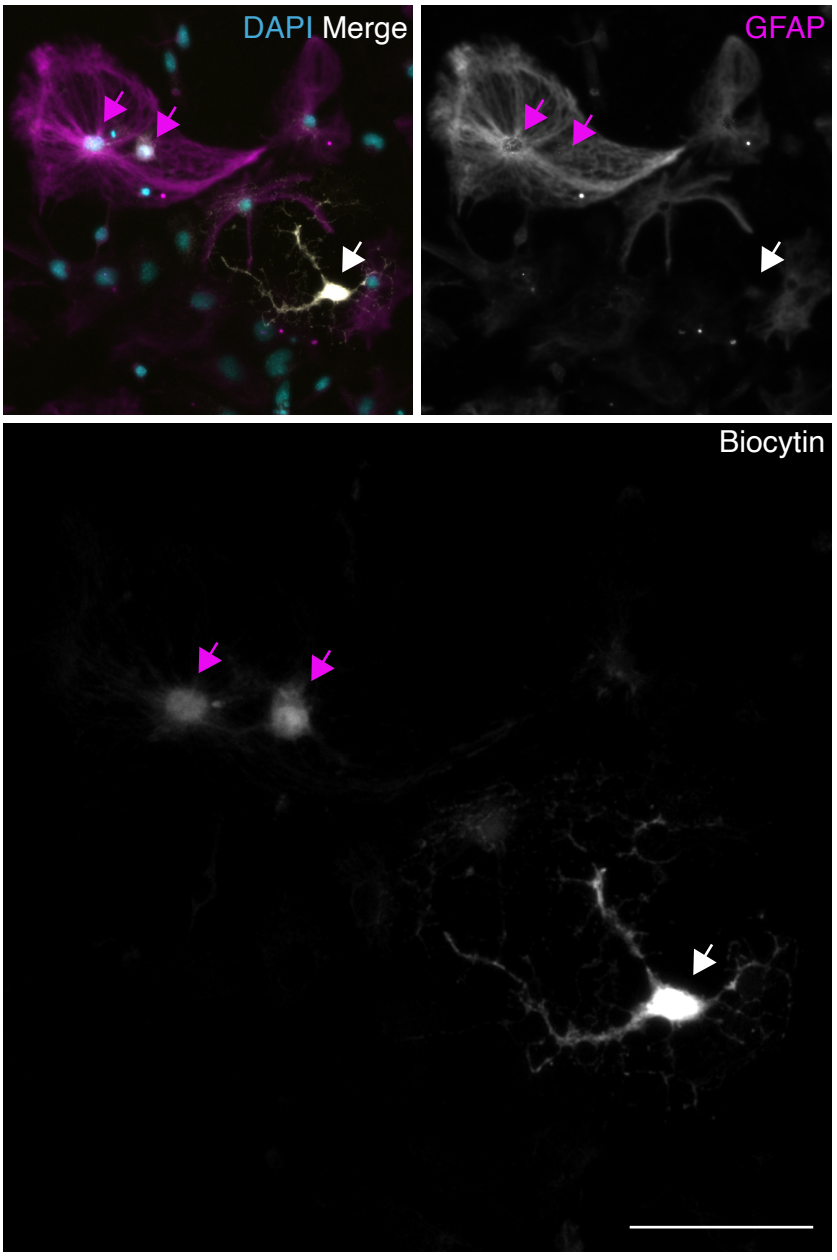

Figure 5.2 | Gap junction-permeable biocytin can transfer from EMOLs to astrocytes. Representative immunofluorescence images from an experiment where the transfer of gap junction-permeable biocytin was observed from a single dye-filled EMOL (white arrow) to nearby astrocytes (magenta arrows; $GFAP^+$) in a mixed glial culture. One hour after filling, cells were fixed and immunostained. Scale bar = 50 µm.

5.2.2 Exogenous energy substrate deprivation does not increase the frequency of EMOL nanotubes

To explore whether EMOL nanotubes might act as a route for the transfer of metabolites to the energy starved EMOL, we quantified the percentage of EMOLs with nanotubes and the number of nanotubes per cell after 6 days of culture in 5 or 0 mM glucose DM, or HE media.

At t0, few EMOLs had nanotubes and those that did had very few (Figure 5.3 a, c, d). At t6d, a significantly higher percentage of EMOLs had nanotubes compared to t0. However, the proportion of cells with nanotubes was similar across all conditions (Figure 5.3 b, c) as was the average number of nanotubes per EMOL (Figure 5.3 d).

These data suggest that the function of EMOL nanotubes is unrelated to trans-cellular energy provision, at least in response to exogenous energy substrate deprivation.

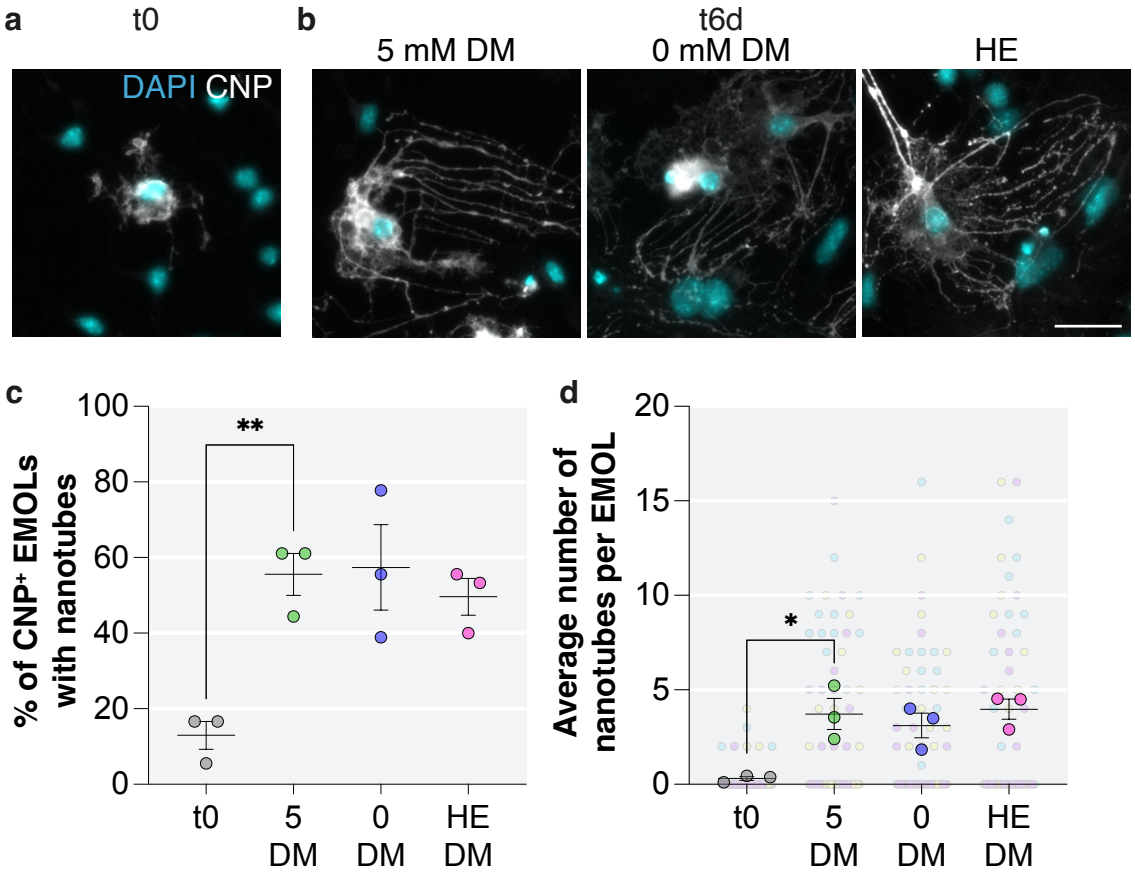

Figure 5.3 | Nanotubes are extended by EMOLs regardless of energy substrate availability. Representative images of EMOLs (blue, DAPI$^+$ nuclei; white, CNP$^+$) at **(a)** t0 and **(b)** after 6 days culture in 5 or 0 mM glucose DM, or HE media. Scale bar = 25 µm. **(c)** Graph showing the average number of EMOLs that had nanotubes. **(d)** The average number of nanotubes per EMOL displayed on a SuperPlot. In each condition, 18 EMOLs were randomly assessed for the presence of nanotubes. Data were compared to 5 mM glucose DM (green dots) using a one-way ANOVA with Dunnett's multiple comparison test performed on average values. Outliers were removed from the average number of nanotubes per cell data by ROUT analysis. * = $p < 0.05$, ** = $p < 0.01$. Data were obtained from 3 biological repeats. Abbreviations: DM, DMEM-based media; HE, DMEM-based media highly enriched in energy substrates.

5.3 RT-qPCR analysis of metabolic enzyme gene expression suggests fatty acid metabolism is altered as a result of energy substrate deprivation

Flux through metabolic pathways is regulated at the level of specific regulatory enzymes. Their activity can be modulated in a variety of ways, including at the level of mRNA expression. To understand what fuel sources might be used to sustain EMOLs and mixed glia under 6 days of exogenous energy deprivation, we used RT-qPCR to probe the expression of genes that encode key enzymes that regulate metabolic flux through a variety of pathways. As a quality control measure, we estimated the amount of RNA per cell in each condition and found it to be similar (Figure S6).

5.3.1 Expression of glycogen phosphorylase is not altered except in the most deprived condition

Glycogen phosphorylase (*Pygl*) encodes the enzyme required for glycogen breakdown in astrocytes. Transcript levels were unaltered compared to control (5 mM glucose DM) except in the 0 mM SO condition, where levels were significantly reduced (Figure 5.4 a).

5.3.2 Expression of genes encoding enzymes that regulate glycolytic flux are not markedly altered in energy-deprived conditions

Next, transcripts encoding enzymes that regulate glycolytic flux were examined. Compared to control (5 mM glucose DM), no differences in hexokinase (*Hk1*) expression were found (Figure 5.4 b). Transcript levels of phosphofructokinase (*Pfkl*) tended towards an increase in all deprived conditions but differences did not reach significance due to intra-experimental variability in the dataset (Figure 5.4 c). Expression levels of pyruvate kinase (*Pkm*; Figure 5.4 d) and lactate dehydrogenase (*Ldha*) were unchanged compared to control except in the 5 mM glucose SO condition, where *Ldha* levels were significantly increased (Figure 5.4 e).

5.3.3 Expression of carnitine palmitoyltransferase 1a is reduced in the absence of glucose

Entry of glycolytic end products into the TCA cycle is regulated by pyruvate dehydrogenase, a large enzyme comprising 3 subunits. None of the deprivation conditions led to changes in the expression levels of pyruvate dehydrogenase (*Pdha*) compared to control (Figure 5.5 a). Besides glycolysis, carbons can also enter the TCA cycle following import of FAs through the carnitine shuttle and β-oxidation. In comparison to control, we observed significantly reduced transcripts of carnitine palmitoyltransferase 1a (*Cpt1a*) in both DM and SO media lacking glucose and other exogenous energy substrates (Figure 5.5 b).

5.3.4 Fatty acid biosynthesis is not altered at the level of gene expression in energy-deprived conditions

Given that glucose is also required for biosynthesis, we hypothesised that fatty acid biosynthesis will be downregulated under conditions of exogenous energy substrate deprivation. Compared to control, expression of ATP citrate lyase (*Acly*) was unchanged except in 0 mM glucose SO where it was significantly reduced (Figure 5.6 a). Transcripts of acetyl-CoA carboxylase alpha (*Acaca*) and fatty acid synthase (*Fasn*) were not significantly changed in any condition but trended towards a decrease in both SO media (Figure 5.6 b, c).

5.3.5 Autophagy-related gene expression is largely unchanged in energy-deprived conditions

Finally, we hypothesised that autophagy will be upregulated to support survival under conditions of exogenous energy substrate starvation. We therefore examined the expression of three autophagy-related genes. Expression of phosphoinositide-3-kinase (*Pik3c3*) trended towards an increase in the 0 mM glucose DM and both SO conditions compared to control. However, significantly increased expression was observed in the HE media control suggesting the trend above is unrelated to energy substrate deprivation (Figure 5.7 a). No differences in expression were observed for beclin 1 (*Becn1*) or autophagy-related 5 (*Atg5*; Figure 5.7 b, c).

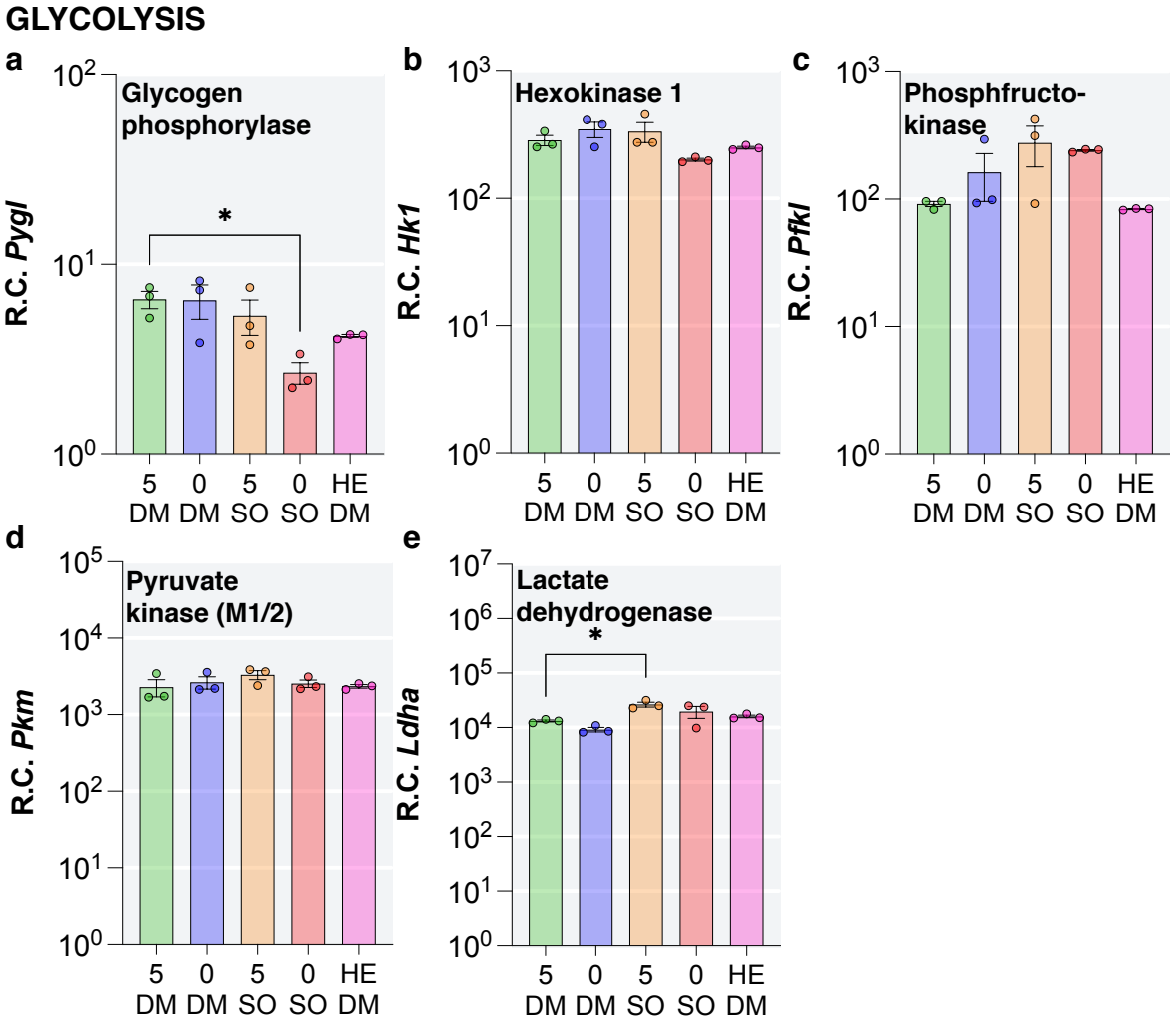

Figure 5.4 | Glycolytic flux in mixed glia appears largely unaltered as a result of glucose deprivation at the level of mRNA expression. RT-qPCR analysis of genes involved in the regulation of metabolic flux through glycolysis **(a-e)**. Mixed glia were maintained in DM or SO media, with or without 5 mM glucose, or in HE media. Relative copies (R.C) of genes are normalised to relative copies of TATA-box binding protein (*Tbp*). Data were compared to 5 mM glucose DM using a one-way ANOVA with Dunnett's multiple comparison test. * = $p < 0.05$. Data were obtained from 3 biological repeats. Abbreviations: DM, DMEM-based; SO, salts-only; HE, DMEM-based media highly enriched in energy substrates.

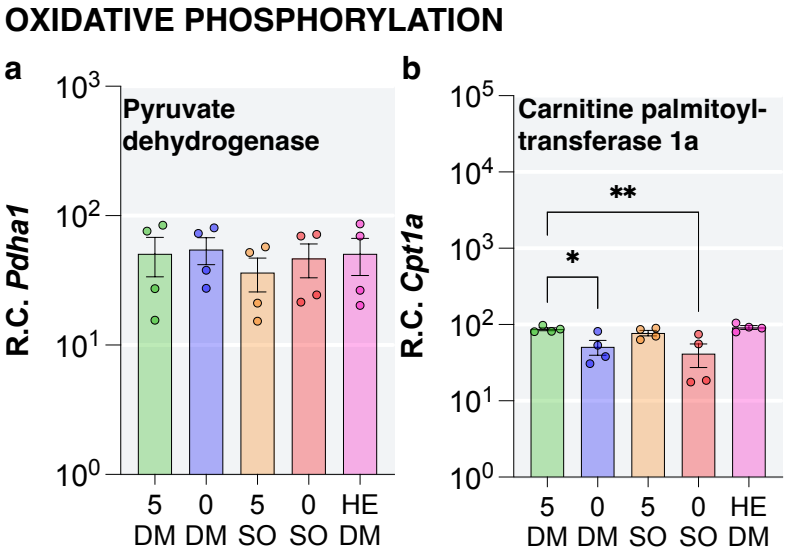

Figure 5.5 | Fatty acid import into mitochondria might be altered in mixed glia as a result of glucose deprivation indicated at the level of *Cpt1a* mRNA expression. RT-qPCR analysis of genes involved in the regulation of metabolic flux through oxidative pathways **(a, b)**. Mixed glia were maintained in DM or SO media, with or without 5 mM glucose, or in HE media. Relative copies (R.C) of genes are normalised to relative copies of TATA-box binding protein (*Tbp*). Data were compared to 5 mM glucose DM using a one-way ANOVA with Dunnett's multiple comparison test. * = $p < 0.05$, ** = $p < 0.01$. Data were obtained from 4 biological repeats. Abbreviations: DM, DMEM-based; SO, salts-only; HE, DMEM-based media highly enriched in energy substrates.

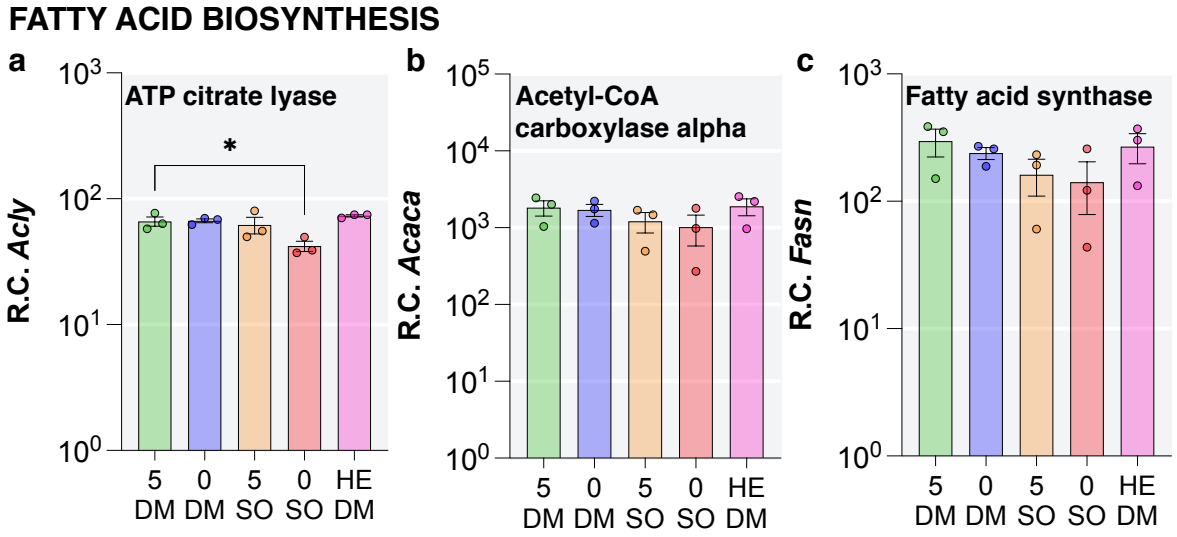

Figure 5.6 | Expression of fatty acid biosynthesis genes in mixed glia is largely unchanged after 6 days of energy substrate deprivation. RT-qPCR analysis of genes involved in the regulation of fatty acid biosynthesis **(a-c)**. Mixed glia were maintained in DM or SO media, with or without 5 mM glucose, or in HE media. Relative copies (R.C) of genes are normalised to relative copies of TATA-box binding protein (*Tbp*). Data were compared to 5 mM glucose DM using a one-way ANOVA with Dunnett's multiple comparison test. * = $p < 0.05$. Data were obtained from 3 biological repeats. Abbreviations: DM, DMEM-based; SO, salts-only; HE, DMEM-based media highly enriched in energy substrates.

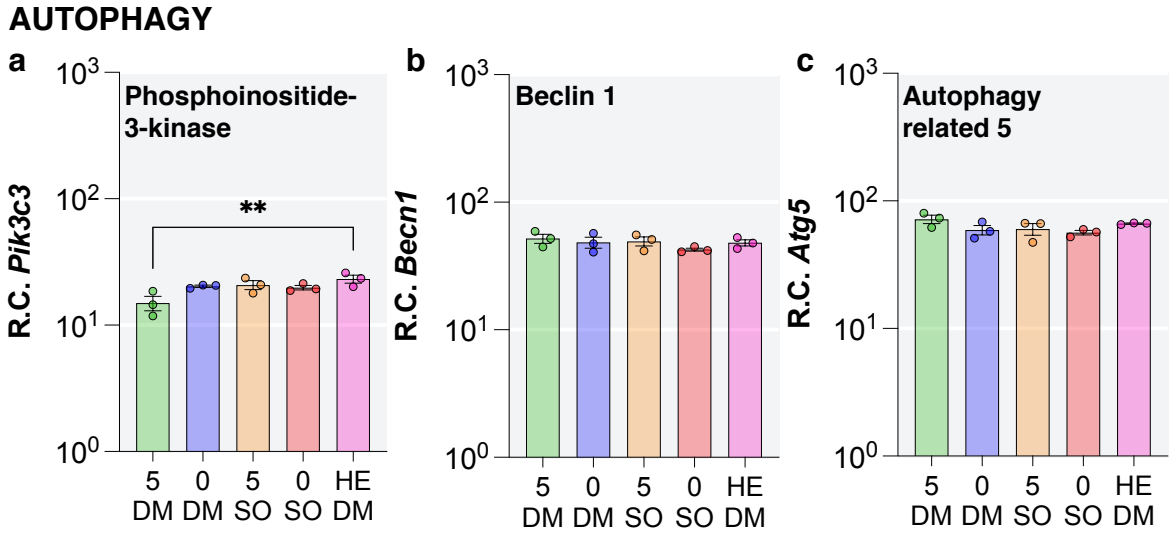

Figure 5.7 | Expression of autophagy-related genes in mixed glia is largely unchanged after 6 days of energy substrate deprivation. RT-qPCR analysis of genes involved in the regulation of autophagy **(a-c)**. Mixed glia were maintained in DM or SO media, with or without 5 mM glucose, or in HE media. Relative copies (R.C) of genes are normalised to relative copies of TATA-box binding protein (*Tbp*). Data were compared to 5 mM glucose DM using a one-way ANOVA with Dunnett's multiple comparison test. ** = $p < 0.01$. Data were obtained from 3 biological repeats. Abbreviations: DM, DMEM-based; SO, salts-only; HE, DMEM-based media highly enriched in energy substrates.

In all, these data show few consistent changes in the expression of genes involved in glucose metabolism, fatty acid synthesis, or autophagy. However, the differential expression of *Cpt1a* under conditions of glucose (pyruvate and glutamine) deprivation suggests an adaptation of glia involving changes in fatty acid import into mitochondria.

5.4 Lipid droplets are present in mixed glia and might provide a fuel source in the absence of exogenous energy substrates

In the presence of exogenous lipids naturally found in serum, cultured astrocyte cell lines can generate lipid droplets that provide a reservoir for β-oxidation during subsequent glucose deprivation (Farmer *et al.*, 2019). To determine if astrocytes or other glia accumulate lipid droplets in our culture conditions, we applied lipophilic stains to mixed glial cultures. Subsequently, we used lipidomic analysis to explore whether there were changes in levels of lipid droplet-associated lipids following 6 days of glucose deprivation.

5.4.1 Lipid droplets are abundant in astrocytes but rare in EMOLs

First, we examined mixed glia at t0 (after approximately 18 hours in serum-rich plating media) to determine if lipid droplets are present at the start of experimentation. LipidTOX™-labelled lipid droplets (green puncta) were observed throughout the culture by fluorescence microscopy (Figure 5.8 a). Cell types could not be assessed because LipidTOX™ is not compatible with immunohistochemistry and cell morphologies are similar across all cell types at this time.

Next, cells maintained in 5 mM glucose DM for 6 days were stained with Nile Red (max emissions at 585 nm for neutral TGs and 638 nm for polar phospholipids) and cell types were determined based on morphology. When excited at 450-490 nm and imaged at 515-565 nm emission, very few lipid droplets were observed in EMOLs (Figure 5.8 b); many were observed in astrocytes (Figure 5.8 c); cells assumed to be microglia contained few (Figure 5.8 d). Whilst lipid droplets were rare in the soma of EMOLs, some were

observed in EMOL nanotubes (Figure 5.8 e). In all cells, the lipid droplet puncta were faint or absent when excited at 540-552 nm and imaged at 575-640 nm emission, which suggests they are composed mainly of neutral lipids such as TGs. Due to time constraints, we did not examine lipid droplets in cultures deprived of exogenous energy substrates and this represents an essential future step in this study.

In all, these data show that EMOLs, astrocytes and microglia can store lipid droplets; however, astrocytes appeared to have many more lipid droplets than the other cell types, at least at t6d.

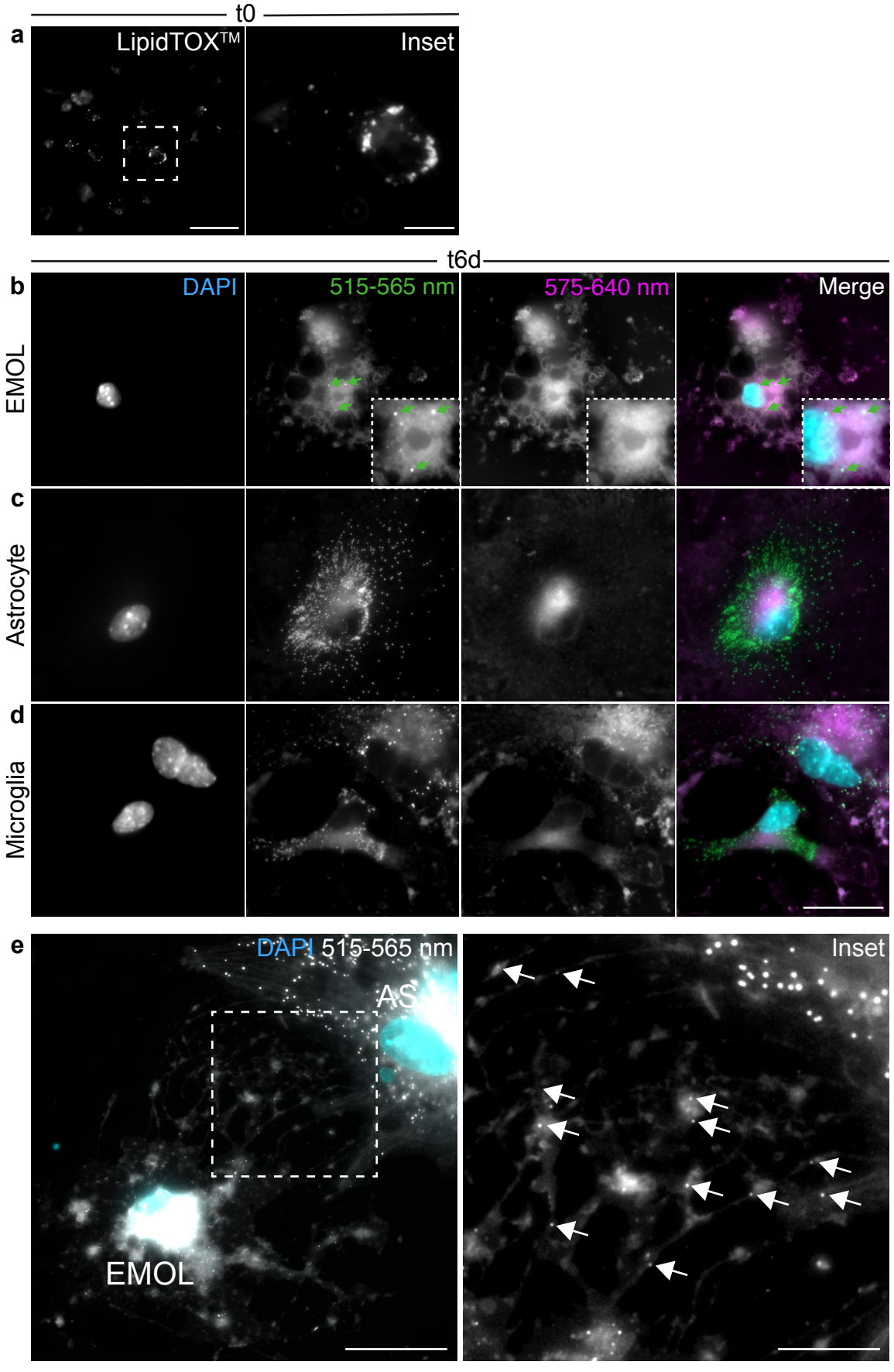

Figure 5.8 | Mixed glia contain lipid droplets that are particularly abundant in astrocytes. *Figure legend continues on the next page.*

Figure 5.8 | *Cont...* Representative immunofluorescence images of mixed glia labelled with lipid stains. **(a)** LipidTOX™-labelled lipid droplets (white puncta) in cells at t0 immediately after 18 hours in serum-rich plating medium. Scale bar = 50 µm for overview image and 10 µm for inset. After 6 days in 5 mM glucose DM, Nile Red was used to visualise lipid droplets. Cell nuclei (blue) were labelled with DAPI and images were captured at 450-490 nm excitation/515-565 nm emission (green) and 540-552 nm excitation/575-640 nm emission (magenta). Green puncta were observed in all major glial cells: **(b)** EMOLs, **(c)** astrocytes, **(d)** and microglia, as assessed by cell morphology. Lipid droplets appeared most abundant in astrocytes and were rare in EMOLs (**fig b,** arrows). The bright puncta in the green channel indicate neutral lipids such as triglycerides. Scale bar = 25 µm. **(e)** Lipid droplets were also visible outside of the perinuclear area (arrows in inset), presumably in nanotubes between EMOLs and astrocytes (AS). Scale bar = 25 µm for overview image and 10 µm for inset. Representative images from a single experiment. Abbreviations: DM, DMEM-based media.

5.4.2 Levels of triglycerides decrease with time in culture, especially in the absence of exogenous energy substrates

To explore whether lipids might be used as a fuel source in the absence of exogenous energy substrates, we conducted lipidomic analysis in collaboration with Professor Thorsten Hornemann and Dr Gergely Karsai (University of Zurich) on mixed glia at t0 and after 6 days of culture in 5 or 0 mM glucose DM, or HE media.

First, we compared mixed glia cultured for 6 days to cells collected at t0. Our primary focus were changes in species of triglyceride (TG) and diacylglycerol (DAG) as they are major components of lipid droplets, or fatty acid (FA) and acylcarnitine (AcCa), which are products of fatty acid metabolism. These species are not abundant in myelin membranes or cellular debris present in the cultures, particularly at t0 (Figure S1). After 6 days, TG species were significantly reduced in all conditions compared to t0 although the highest fold changes were observed in the 0 mM glucose DM condition (Figure 5.9 a-c). Notably, in both 5 and 0 mM glucose, AcCa (a component of the carnitine shuttle involved in transporting LCFAs into mitochondria) was significantly decreased compared to t0 but was unchanged in the HE media, compared to t0.

Next, we compared across conditions at t6d. As expected, mixed glia cultured in 0 mM glucose DM had significantly decreased TG species compared to cells in 5 mM glucose DM, with all top 10 hits comprising this class of lipid (Figure 5.10 a). Unexpectedly, in 5 mM glucose DM compared to HE media, species of TG were significantly increased (Figure 5.10 b). Surprisingly, comparison of 0 mM glucose DM to HE media did not reveal changes in TG species (Figure 5.10 c).

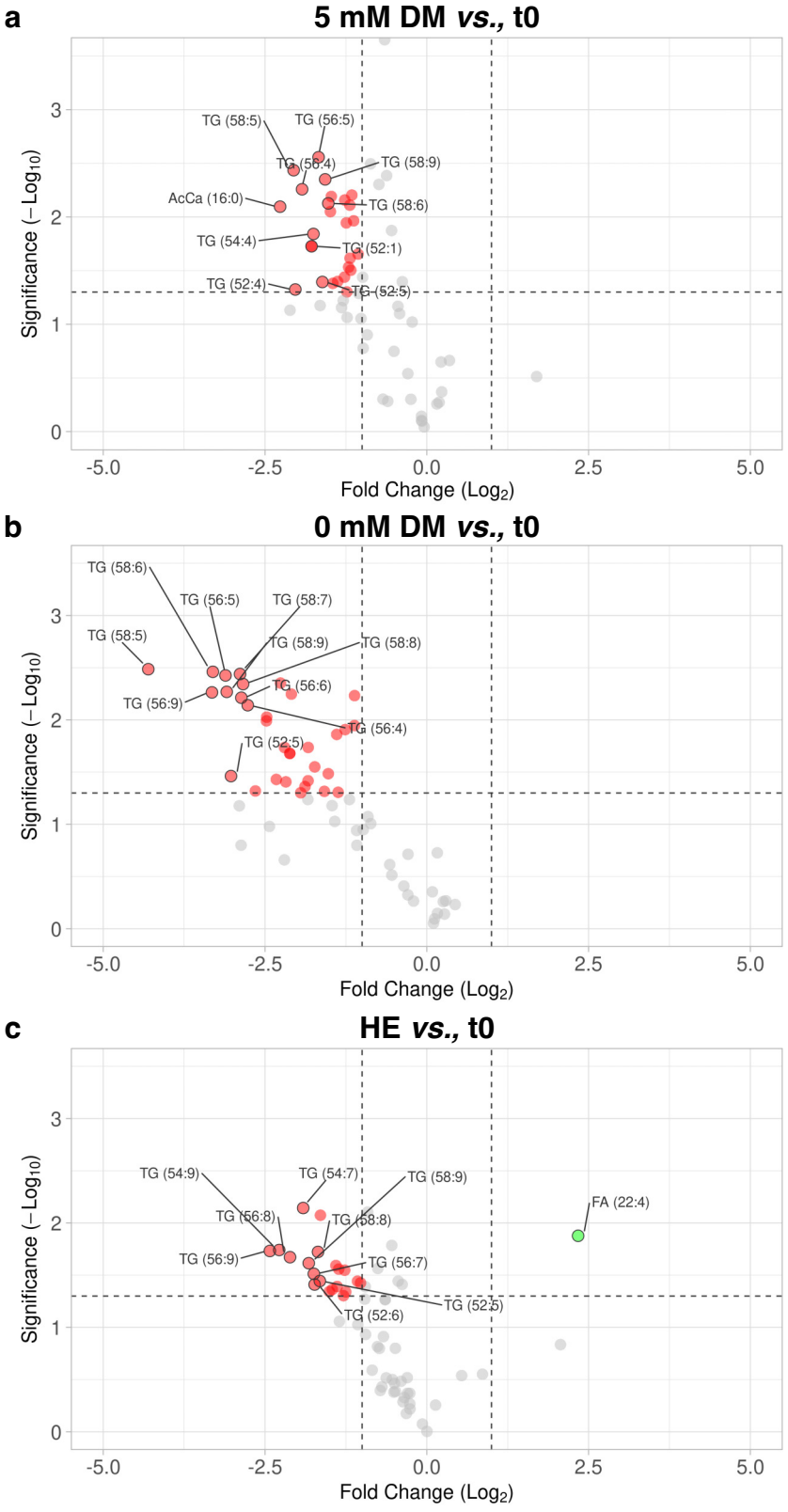

Figure 5.9 | Mixed glia contain less triglyceride after 6 days of culture regardless of energy substrate supplementation. *Figure legend continues on the next page.*

Figure 5.9 | *Cont...* Volcano plots of lipidomic analysis performed on mixed glial cultures. The top 10 most changed lipid species are labelled. Comparisons were made between cultures sampled at t0 and after 6 days in **(a)** 5 mM glucose DM, **(b)** 0 mM glucose DM, **(c)** or HE media. Myelin lipids were excluded due to contamination with myelin debris in the culture. Only triglyceride (TG), diacylglycerol (DAG), fatty acid (FA) and acylcarnitine (AcCa) species are plotted. Data were normalised to cell counts obtained previously then plotted as $\log_2$ fold change *vs.,* -$\log_{10}$ adjusted P-value, compared using a Student's *t*-test (two-tailed, paired). Data were obtained from 3 biological repeats using the average value from 4 technical repeats per condition, per experiment. Abbreviations: DM, DMEM-based media; HE, DMEM-based media highly enriched in energy substrates.

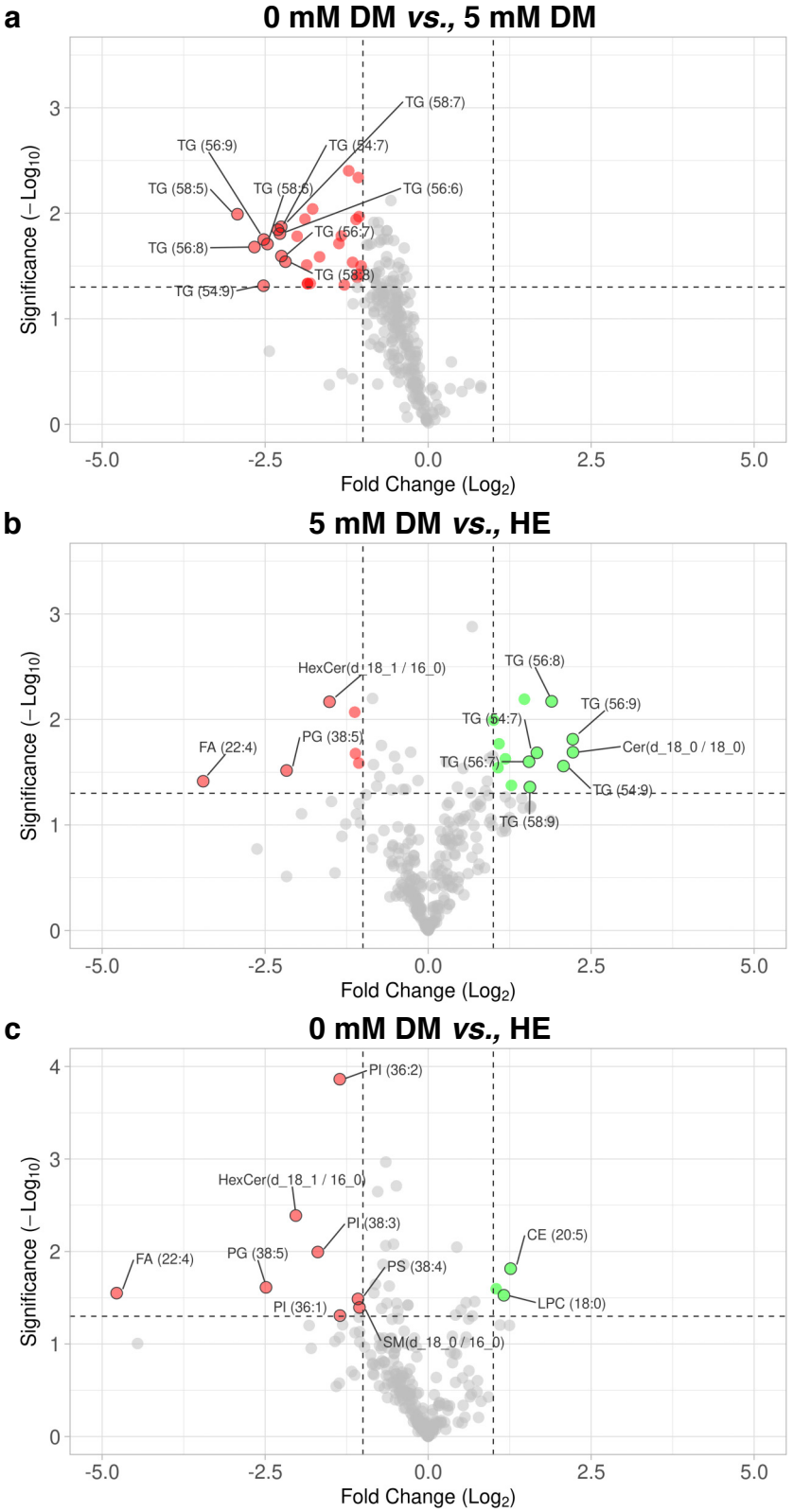

Figure 5.10 | Mixed glia contain less triglyceride after 6 days of culture in energy substrate-deprived media compared to those cultured with 5 mM glucose. *Figure legend continues on the next page.*

Figure 5.10 | *Cont...* Volcano plots of lipidomic analysis performed on mixed glial cultures. The top 10 most changed lipid species are labelled. Samples were taken after 6 days in DM with different levels of energy substrate supplementation and comparisons were made between **(a)** 0 mM glucose DM *vs.,* 5 mM glucose DM; **(b)** 5 mM glucose DM *vs.,* HE; **(c)** 0 mM glucose DM *vs.,* HE. Data were normalised to cell counts obtained previously then plotted as $\log_2$ fold change *vs.,* -$\log_{10}$ adjusted P-value, compared using a Student's *t*-test (two-tailed, paired). Data were obtained from 3 biological repeats using the average value from 4 technical repeats per condition, per experiment. Abbreviations: DM, DMEM-based media; HE, DMEM-based media highly enriched in energy substrates.

Together, these data suggest mixed glia accumulate lipid droplets during initial culture in serum-rich, energy-rich media and consume lipid droplet-stored TGs during 6 days in culture regardless of energy substrate availability. These data provide evidence that the presumed consumption of TGs is highest when glucose and other exogenous energy substrates are absent.

5.5 Astrocytes are not required for EMOL survival or growth during 6 days of exogenous energy substrate deprivation

As astrocytes store glycogen and appeared to have more lipid droplets than EMOLs, we hypothesised they were required for the survival of EMOLs under conditions of exogenous energy deprivation. To test this, we generated EMOL-enriched ($O4^+$) cultures depleted of astrocytes. In these cultures at t0, $43 \pm 0.66\%$ of $DAPI^+$cells were CNP^+ and less than 1% of cells were $GFAP^+$ or $CD45^+$. At t6d, $< 4\%$ of all $DAPI^+$ cells were $GFAP^+$ astrocytes (raw data in Figure S8). Cultures were grown in 5 or 0 mM glucose in DM or SO media, or in HE media for 6 days as for mixed glia.

5.5.1 EMOLs do not require astrocyte-derived energy sources to survive exogenous energy substrate deprivation

First, we examined total cell densities ($DAPI^+$) at t6d. Compared to control (5 mM glucose DM), there was a general trend towards a reduction with increasing deprivation but this reached significance only in 0 mM glucose SO (Figure 5.11 a, b, d). Next, we examined EMOL densities at t6d. Surprisingly, compared to control, densities were maintained in 0 mM glucose DM although they trended towards a reduction in SO media and reached significance in the most deprived condition (Figure 5.11 a, b, e). Cultures maintained in HE media (Figure 5.11 c) had significantly increased total cell densities compared to control (Figure 5.11 d) but EMOL cell densities were unchanged (Figure 5.11 e).

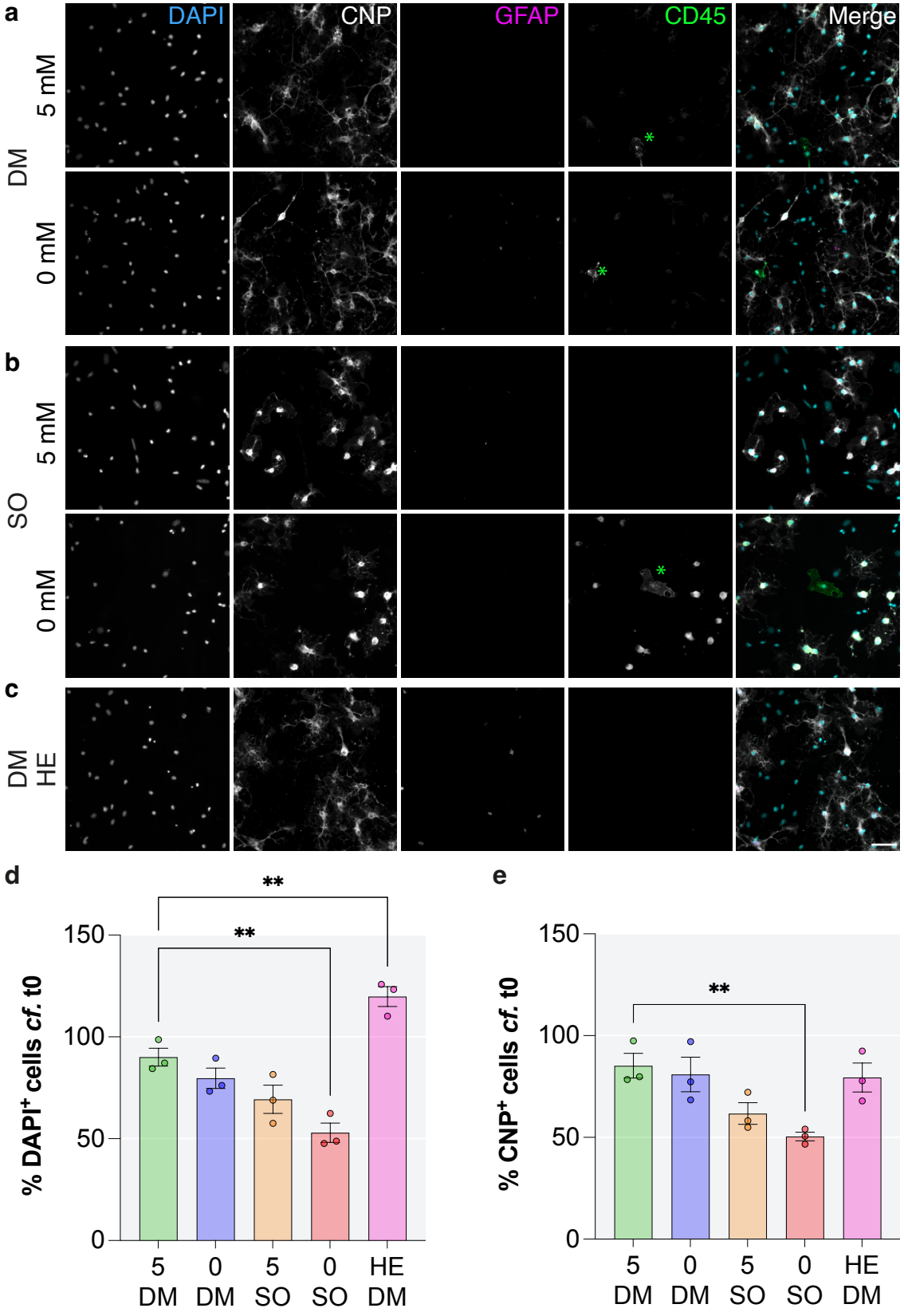

Figure 5.11 | Withdrawal of amino acids and/or vitamins impacts EMOL densities more than deprivation of exogenous energy substrates in EMOL-enriched cultures.

Figure legend continues on the next page.

Figure 5.11 | *Cont...* Illustrative images of EMOL-enriched ($O4^+$) cultures grown for 6 days in DM containing amino acids and vitamins, or a SO media, with or without glucose supplementation. **(a)** Total cell (blue, $DAPI^+$) and EMOL (white, CNP^+) densities appeared similar in 0 mM glucose DM compared to 5 mM glucose DM. **(b)** EMOL cell densities appeared most reduced in the 0 mM glucose SO condition. **(c)** Cultures maintained in HE media did not appear remarkably different to cultures provided 5 mM glucose DM (**fig a**). These cultures were largely devoid of astrocytes (magenta, $GFAP^+$) and microglia (green, $CD45^+$). Scale bar = 50 µm. Graphs of **(d)** total cell and **(e)** EMOL densities at t6d as a percentage of t0 values. Densities were compared to controls (5 mM glucose DM) using a one-way ANOVA with Dunnett's multiple comparison test. ** = $p < 0.01$. Data were obtained from 3 biological repeats. Abbreviations: DM, DMEM-based media; SO, salts-only; HE, DMEM-based media highly enriched in energy substrates.

These data demonstrate that EMOLs do not require astrocyte-derived energy sources to survive glucose (pyruvate and glutamine) deprivation for 6 days *in vitro* when in culture media containing amino acids and vitamins.

5.5.2 EMOL growth is independent of astrocytes and glucose but is inhibited by the withdrawal of amino acids and/or vitamins

We next asked if cell densities in EMOL-enriched cultures were maintained at the expense of cell size after 6 days of exogenous energy substrate deprivation. Size was determined by the area of CNP staining per EMOL at t0 and t6d (Figure 5.12 a, b).

The mean EMOL cell size at t0 was 498 μm^2 (Figure 5.12 c), which was similar to that in mixed glial cultures reported in section 4.3.1 (n.s, unpaired Student's *t*-test). EMOL size increased significantly in 5 mM glucose DM (control) at t6d compared to t0. EMOLs cultured for 6 days in 0 mM glucose DM increased in size to a similar extent. In SO media, EMOLs were significantly smaller compared to controls. Culturing EMOLs in HE media resulted in them attaining a significantly larger size compared to those in control media.

These data demonstrate that EMOL survival in the absence of exogenous energy sources and in the absence of astrocytes does not occur at the expense of growth. However, withdrawal of amino acids and/or vitamins limited growth even when glucose was provided.

5.5.3 Nanotubes are not produced by EMOLs in the absence of astrocytes

In EMOL-enriched cultures, nanotubes were not observed under any growth condition (n = 3; illustrated in Figure 5.12 a, b). This observation suggests astrocytes mediate the formation of EMOL nanotubes *in vitro*.

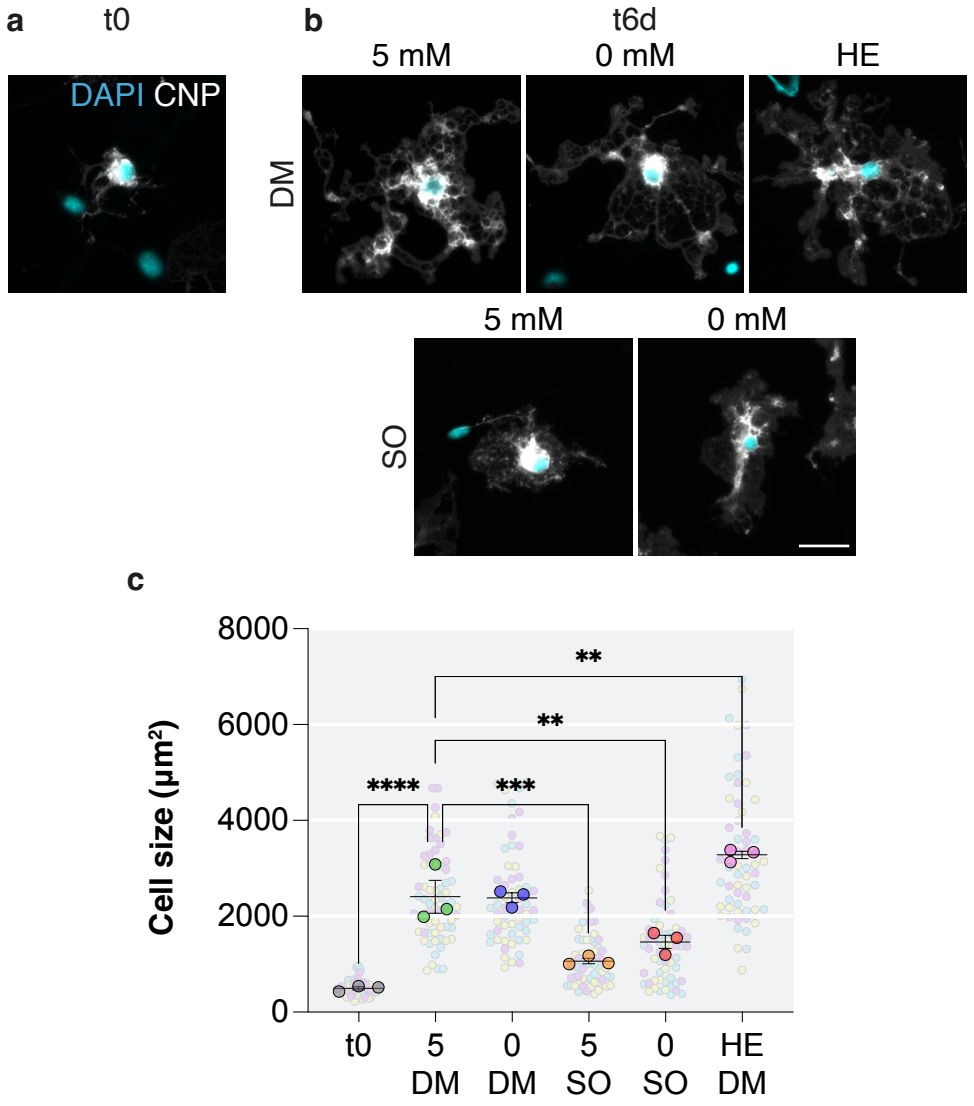

Figure 5.12 | Growth of EMOLs in the absence of astrocytes requires amino acids and/or vitamins but is not influenced by glucose availability. Representative images of EMOLs (white, CNP^+) and their cell nuclei (blue, $DAPI^+$) in EMOL-enriched cultures at **(a)** t0 and **(b)** t6d. Scale bar = 25 µm. **(c)** EMOL cell size was measured by the area of CNP staining and displayed on a SuperPlot. At least 19 cells were included after ROUT analysis per biological replicate. Data were compared to 5 mM glucose DM using a one-way ANOVA with Dunnett's multiple comparison test performed on average cell size values. ** = $p < 0.01$, *** = $p < 0.001$, **** = $p < 0.0001$. Data were obtained from 3 biological repeats. Abbreviations: DM, DMEM-based media; SO, salts-only; HE, DMEM-based media highly enriched in energy substrates.

5.6 EMOLs in isolation do not sacrifice lipids after 6 days of exogenous energy substrate deprivation

To determine if levels of lipids are altered in EMOL-enriched cultures in the absence of glucose (glutamine and pyruvate), we performed lipidomic analysis on cells obtained at t0 and after 6 days in 5 or 0 mM glucose DM as described in section 5.4.2.

At t6d, lipid levels were almost unchanged in either growth condition compared to t0: one diacylglycerol (DAG) species was significantly decreased in 5 mM glucose DM (Figure 5.13 a); two TG species and DAG were significantly decreased in 0 mM glucose DM (Figure 5.13 b). At t6d, in 5 *vs.,* 0 mM glucose, there was a significant increase in one TG species and a decrease in another (Figure 5.13 c).

These data suggest EMOLs do not accumulate or degrade lipids as a fuel source during 6 days of exogenous energy substrate deprivation.

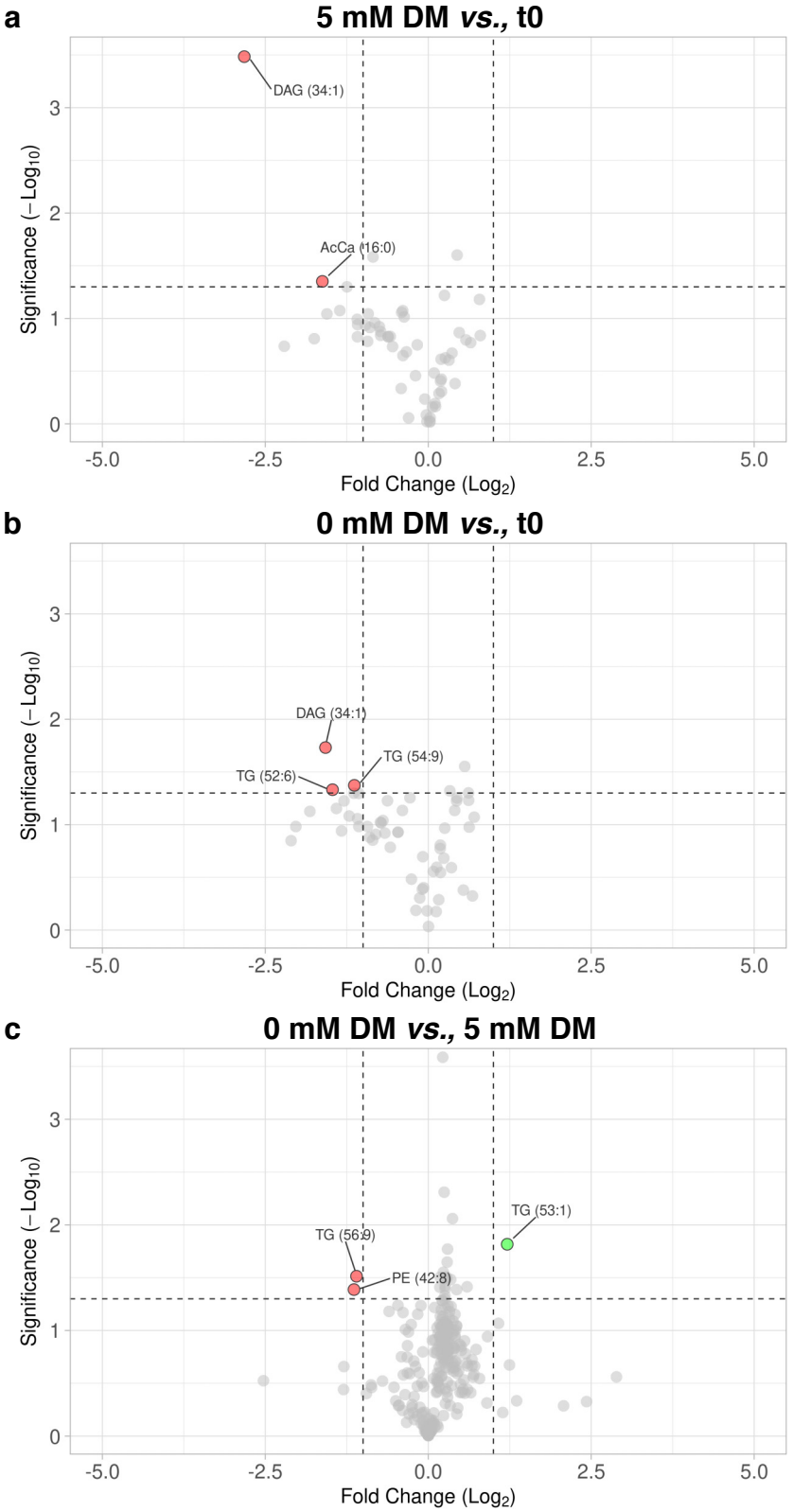

Figure 5.13 | Lipid abundance is largely unchanged in EMOL-enriched cultures following 6 days of exogenous energy substrate deprivation. *Figure legend continues on the next page.*

Figure 5.13 | *Cont...* Volcano plots of lipidomic analysis performed on EMOL-enriched cultures. The top 10 most changed lipid species are labelled. Comparisons were made between cultures sampled at t0 and after 6 days in **(a)** 5 mM glucose DM or **(b)** 0 mM glucose DM. Only triglyceride (TG), diacylglycerol (DAG), fatty acid (FA) and acylcarnitine (AcCa) species are plotted. **(c)** At t6d, 0 mM glucose DM was compared to 5 mM glucose DM and all detectable lipid species are plotted. Data were normalised to cell counts obtained previously, then plotted as $\log_2$ fold change *vs.,* $-\log_{10}$ adjusted P-value, compared using a Student's *t*-test (two-tailed, paired). Data were obtained from 3 biological repeats using the average value from 4 technical repeats per condition, per experiment. Abbreviations: DM, DMEM-based media; HE, DMEM-based media highly enriched in energy substrates.

5.7 EMOLs are unable to wrap nanofibers in the absence of exogenous energy substrates

We have demonstrated that EMOLs can survive and grow *in vitro* in the absence of glucose (and other exogenous energy substrates) whether cultured alone or with astrocytes and microglia. As there was evidence for cell growth but little evidence of lipid synthesis, we next asked if EMOLs are capable of synthesising myelin sheaths. Mixed glia were seeded onto inert nanofibers, cultured for 6 days, then qualitatively assessed.

After 6 days in 5 mM glucose DM, we observed MBP^+ ensheathment of nanofibers and EMOLs had healthy-appearing $DAPI^+$ nuclei (Figure 5.14 a). In contrast, EMOLs in 0 mM glucose DM had punctate MBP staining and abnormal or pyknotic nuclei (Figure 5.14 b). In both cases, cell densities appeared much lower than on glass coverslips, likely due to the 3D architecture of the nanofibers. Together, these observations led us to speculate that cell-to-cell contact might be important for survival in the absence of exogenous energy substrates (see Discussion).

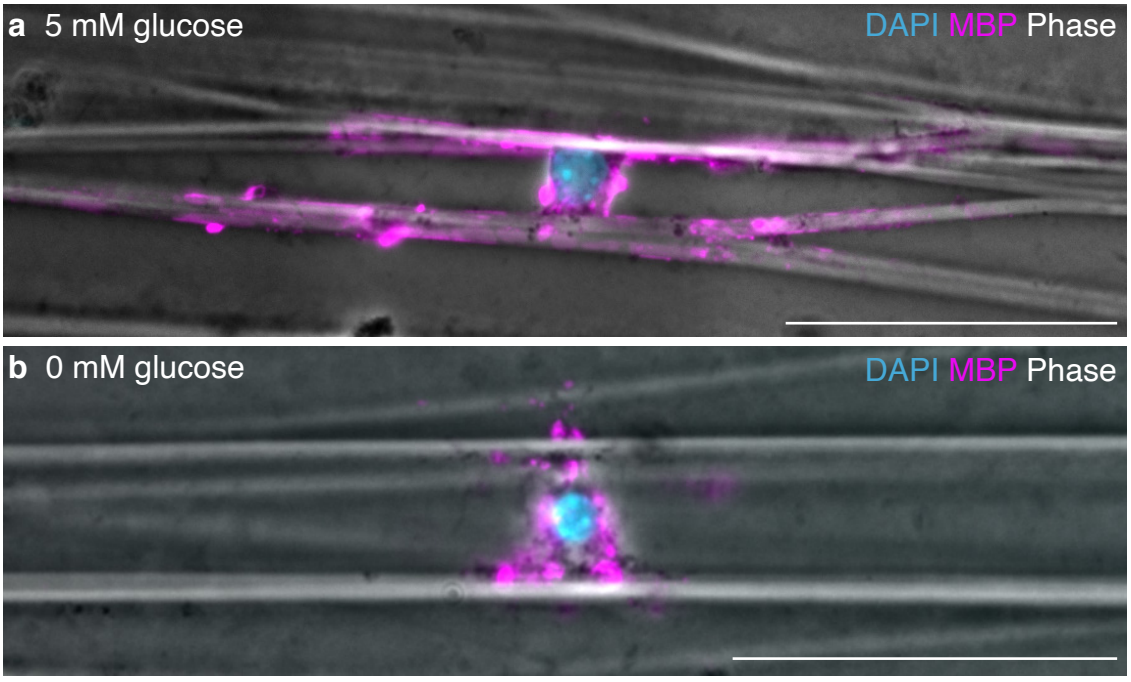

Figure 5.14 | Myelin wraps on nanofibers are not produced and/or maintained by EMOLs during 6 days of exogenous energy substrate deprivation. Illustrative immunofluorescence images of spinal cord EMOLs in a mixed glia preparation seeded onto nanofibers and maintained in 5 or 0 mM glucose DM for 6 days. **(a)** In 5 mM glucose DM, EMOLs formed MBP^+ wraps (magenta, ensheathment). These wraps were associated with healthy-appearing nuclei (blue, $DAPI^+$). **(b)** In 0 mM glucose DM at 6 days, EMOLs showed no evidence of wrapping nanofibers and had condensed nuclei. The orientation of the nanofibers is visible by phase contrast. Representative images from a single experiment. Scale bar = 50 µm. Abbreviations: DM, DMEM-based media.

5.8 Discussion

In this chapter, we explored the metabolic adaptations and fuel sources that EMOLs and other glia use when glucose and other exogenous energy substrates are absent. We found that EMOLs extend cytoplasm-filled nanotubes towards astrocytes that can act as a transport route for gap junction-permeable substances; however, EMOL nanotubes were not influenced by media composition and we conclude they are unlikely to play a role in trans-cellular exchange of energy metabolites. Using RT-qPCR and lipidomic analysis of mixed glia, we provide tentative evidence that lipids are used as a fuel source in the absence of exogenous energy substrates. Combined with observing lipid droplets, particularly in astrocytes, we conclude lipid droplets provide an energy reservoir for the survival of cells under exogenous energy substrate deprivation. Nonetheless, EMOLs cultured alone maintained their densities in the absence of exogenous energy substrates despite that lipidomic analysis suggested lipids were not consumed. Together, these data suggest that in the absence of glucose (pyruvate and glutamine), EMOLs can use sources other than lipid droplets from which to obtain energy for survival and growth. Finally, when EMOLs (in mixed glial cultures) were challenged to 'wrap' inert nanofibers in the absence of glucose, not only did wrapping fail but in contrast to 2D culture, survival was prevented.

Glucose is considered the obligate energy source in the CNS. Therefore, we were surprised to observe in Chapter 4 that depriving spinal cord mixed glia of glucose (in addition to pyruvate and glutamine) for 6 days did not reduce EMOL or astrocyte densities. Therefore, in this chapter, we used RT-qPCR to probe for metabolic adaptations that might explain this observation. In doing so, we found differential expression of *Cpt1a* in cultures lacking glucose and other energy substrates. In brain, the CPT1a isoform of CPT1 is the rate-limiting enzyme in mitochondrial β-oxidation of LCFAs. Astrocytes but not oligodendrocytes, microglia, nor neurons express CPT1a (Jernberg *et al.*, 2017), at least in rat brain. However, metabolic regulation does not occur primarily at the level of gene expression. Allosteric regulation mediates metabolic enzyme activity and CPT1a is inhibited by malonyl-CoA generated from fatty acid biosynthesis (McGarry *et al.*, 1977; Fadó *et al.*, 2021). Therefore, the changes in *Cpt1a* transcripts we observed in the current study point to adaptations

in FA metabolism in astrocytes, which we hypothesise maintains cells under exogenous energy substrate deprivation.

Lipid metabolism in the CNS has long been debated but recent reports of lipid droplet storage in astrocytes *in vitro* and in *Drosophila* brain glia *in vivo* has re-ignited discussion (reviews by Lee *et al.* (2021) and Ralhan *et al.* (2021)). In our culture conditions, astrocytes appeared to have many more lipids droplets than other glial cell types and we hypothesise they could provide a fuel source during 6 days of exogenous energy substrate deprivation. Farmer *et al.* (2019) examined lipid droplet accumulation *in vitro* using mouse brain astrocyte cell lines expressing variants of apolipoprotein E (*ApoE*), some of which are associated with increased risk of Alzheimer's disease. The authors found that when astrocytes are provided with oleate (a LCFA), lipid droplets accumulate. The same observations have been made in rat hippocampal slice astrocytes (Smolič *et al.*, 2021). Moreover, Farmer *et al.* (2019) provide some evidence that subsequent glucose deprivation mobilised stored lipids (shown using ^{14}C-oleate and $^{14}CO_2$ release), which was inhibited using the CPT1a inhibitor, etomoxir. These data suggest that the lipid droplets observed in our study were derived from serum lipids present in the plating medium. However, it remains to be determined if they could derive also from myelin debris in the cultures or from biosynthesis following incubation in glucose-rich media at the start of the culture. These data are consistent with our lipidomic analysis showing higher lipid droplet-associated TG species at t0 compared to t6d, under all growth conditions, suggesting that following plating in serum- and glucose-rich media, astrocytes accumulate lipid droplets. Our observations add to existing evidence that astrocytes can accumulate and store lipids. Further work is required to unequivocally determine the source of the lipid droplets in our system.

Recently, Smolič *et al.* (2021) found that 24 hours of glucose deprivation increased the number and size of lipid droplets in rat cultured and *ex vivo* hippocampal slice astrocytes. In *Drosophila* brain *in vivo*, lipid droplets were observed under healthy conditions and subjecting the flies to hypoxia and starvation increased the number of lipid droplets. The authors report lipid droplets were present in astrocyte-like glia but did not provide evidence that their reporter (*repo-Gal4 > UAS-L10a-EGFP*) is cell-type specific. Nonetheless, the

authors provide evidence that lipid droplets might have a role in brain cell responses to acute cellular stress, such as hypoxia.

When considering these data with ours, the enhanced reduction we observed in TGs after 6 days of energy substrate deprivation in mixed glial cultures suggests lipid droplet contents are consumed after energy deprivation-induced cellular stress. Therefore, we add to the accumulating knowledge that astrocyte lipid droplets might act as an energy reserve. Our data suggest lipid droplets can sustain cellular metabolism beyond what is possible with glycogen but this remains to be confirmed. Preliminary experiments using 4-bromochrotonic acid to block β-oxidation led to cell death in mixed glial cultures maintained in glucose-free DM, whilst cells survived when glucose was present.

Our mixed glial cultures (but not the EMOL-enriched cultures) contained myelin debris, a lipid-rich substance that could, in theory, supply lipids to astrocytes after serum is withdrawn from the medium. Astrocytes within multiple sclerosis (MS) demyelinating lesions contain myelin debris (Lee *et al.*, 1990; Morcos *et al.*, 2003; Ponath *et al.*, 2017) suggesting they are phagocytic cells. Moreover, it has recently been shown that cultured rat brain astrocytes can phagocytose spinal cord myelin debris within 45 minutes of addition (Ponath *et al.*, 2017). The processing of myelin lipids via the endoplasmic reticulum likely leads to the synthesis of lipid droplets (Lee *et al.*, 2021), as shown in microglia (Marschallinger *et al.*, 2020). Therefore, it will be important to determine if myelin debris in our cell culture system provides an alternative fuel source for lipid droplet synthesis and β-oxidation.

Unlike astrocytes, oligodendrocytes do not express CPT1a (Jernberg *et al.*, 2017) and are not known to be competent in β-oxidation (Edmond *et al.*, 1987). We rarely observed lipid droplets in EMOLs in mixed glial cultures. Surprisingly, in the absence of astrocytes, a majority of EMOLs survived 6 days of exogenous energy substrate deprivation demonstrating astrocyte β-oxidation is not essential for the survival of EMOLs under these conditions. Compared to other glia, oligodendrocytes are lipid-rich cells that could, in theory, utilise their membrane lipids as a fuel source. However, it is believed that myelinating glia do not favour lipids as a fuel source to prevent the catabolism of myelin lipids (Poitelon *et al.*, 2020). This suggestion is supported by our lipidomic analysis of EMOL-enriched cultures that showed little change in lipid levels between t0 and t6d in the presence or absence of glucose.

However, there is not enough evidence to conclude EMOLs do not perform β-oxidation since current understanding comes only from *in vitro* differentiated cells (Edmond *et al.*, 1987). In all, it is unlikely that EMOLs utilise lipid droplets as an energy source but this requires confirmation.

DMEM, the basis for DM in our study, contains vitamins and low levels of all essential amino acids, some conditionally essential amino acids, and the non-essential amino acids glycine, L-serine, and L-tyrosine: equating to 6.68 mM when combined. Amino acids can be oxidised to generate ATP but their contribution to energy production in neural cells is not known. Oligodendrocytes, like all cells, detect amino acid availability via individual intracellular sensor proteins that convey changes to mTORC1, a transcription factor that regulates anabolic and catabolic processes. In oligodendrocytes, mTORC1 is required for normal myelination (Lebrun-Julien *et al.*, 2014) and likely orchestrates myelin biogenesis since it involves substantial lipid and protein synthesis, thus consuming large amounts of amino acids. That said, the precise mechanisms that regulate intracellular amino acids concentrations are not fully understood (Gauthier-Coles *et al.*, 2021).

Amino acids can be converted to energy substrates in cells by oxidative deamination or transamination, which generates intermediates of glycolysis and the TCA cycle, and ketone bodies for acetyl CoA production. Cell culture DMEM contains amino acids that competent cells can convert to acetyl-CoA, α-ketoglutarate, succinyl-CoA, fumarate, and pyruvate. Moreover, oligodendrocytes are reportedly capable of pyruvate carboxylation meaning they can generate oxaloacetate from pyruvate to sustain the TCA cycle (Amaral *et al.*, 2016). Therefore, in theory, amino acids alone could sustain EMOL energy metabolism. Had time allowed, we would have cultured mixed glia or EMOLs in amino acid-free DMEM and returned individual amino acids to assess if they enhanced survival or growth.

The question is, do oligodendroglia contain the enzymatic machinery required to utilise amino acids for energy production? To our knowledge, this question has not been addressed within the literature although the possibility has been considered. For example, Rinholm *et al.* (2011) examined the effects of glucose and lactate on OPC maturation and myelination in rat *ex vivo* slice cultures. However, the authors made their low glucose treatments (1.4 and 2.9 mM) in DMEM containing more amino acids than their high glucose treatments

(5.5, 10, 41.5 mM) and acknowledged that the additional amino acids in the low glucose conditions could, in theory, be used for ATP production. However, the authors found that glucose had the dominant effect with oligodendroglial survival and maturation proportional to glucose availability. Therefore, the contribution of amino acids to energy production is likely negligible in comparison to glucose, at least in *ex vivo* models.

There is currently no evidence that oligodendrocytes perform gluconeogenesis (Tepavčević, 2021); therefore, amino acids would not provide carbons for the pentose phosphate pathway to generate NADPH, which oligodendrocytes require to support lipid biosynthesis (Amaral *et al.*, 2016). Lack of pentose phosphate pathway activity would also limit nucleotide production for RNA synthesis although we found no differences in RNA content per cell (estimated from cell counts and RNA yield) in the glucose deprived conditions. Moreover, amino acids are required for biosynthetic processes including the synthesis of metabolic enzymes for cellular metabolism and energy production. We acknowledge that in our SO media there was also a lack of B vitamins required in some metabolic pathways (Baj and Sieniawska, 2017). Therefore, it is not clear whether withdrawal of amino acids and vitamins affect EMOLs by depriving them of energy sources, removal of building blocks, lack of co-factors for cell metabolism, or all of the above.

We found that EMOLs in enriched cultures were similar in size whether grown in 5 and 0 mM glucose DM but were larger in HE media. This suggests 5 mM glucose is limiting for growth. As discussed in Chapter 4, autophagy is utilised by cells under stress to provide energy substrates (Lum *et al.*, 2005; Hosokawa *et al.*, 2006) and myelinating oligodendrocytes express high levels of autophagy-related proteins (Banks, 2016). Therefore, the activity of autophagy in EMOL-enriched cultures should be assessed in future experiments as a candidate for supporting survival in the absence of exogenous energy substrates.

When mixed glia were plated onto nanofibers, EMOLs formed myelin wraps when provided with glucose but not in conditions lacking major energy substrates. This is unsurprising as others have reported that glucose deprivation inhibits myelination. Yan and Rivkees (2006) and Rinholm *et al.* (2011) found in rat or mouse brain slice cultures, respectively, that < 3 mM glucose inhibited myelination and reduced the number of MBP^+ cell counts. In both studies, DMEM-based culture media was used and therefore amino acids in the absence

of glucose did not provide sufficient energy to support myelination. In our nanofibers experiment, we observed a low cell density and cannot rule out the effects of disrupted inter-glia support, particularly since astrocytes supply lipids for myelination (Camargo *et al.*, 2017). Others have reported myelination of nanofibers by primary oligodendrocytes, in the absence of astrocytes, when energy substrates were provided (Lee *et al.*, 2012; 2013; Li *et al.*, 2014; Bechler *et al.*, 2015; Bechler, 2019).

Oligodendrocytes and astrocytes are highly interconnected by gap junctions *in vivo* (reviewed by Orthmann-Murphy *et al.* (2008) and Papaneophytou *et al.* (2019)): likely less so in 2D cultures, helping explain why EMOL-astrocyte dye coupling was observed only rarely. Presumably, gap junctions occur at the termini of EMOL nanotube-like structures on astrocytes. We are, to our knowledge, the first to report that EMOLs extent nanotube-like structures toward astrocytes. However, we found that nanotubes were present to the same extent regardless of exogenous energy substrate availability, suggesting their function is likely independent of trans-cellular energy provision under these experimental conditions.

The formation of nanotubes in glia is poorly understood. Using fluorescent protein-expressing cells *in vitro*, Wang *et al.* (2011) reported that astrocyte-astrocyte or astrocyte-neuron nanotubes formed as a result of cellular stress. Specifically, they showed that astrocytes deprived of serum for 7 days then returned to co-culture with non-stressed cells extended nanotubes towards these neighbouring cells. We found that EMOLs only extended nanotubes when astrocytes were present regardless of energy substrate availability, suggesting they are induced by astrocytes or astrocyte-derived factors. EMOL nanotubes are likely an exaggeration of inter-glial connections *in vivo* that are enhanced due to increased cellular spacing *in vitro*.

Astrocytes secrete a plethora of proteins that function in neurogenesis, axon guidance, extracellular matrix organisation, and homeostasis (Jha *et al.*, 2018). Moreover, the astrocyte secretome includes key proteins that are known to regulate oligodendrocyte maturation and myelination (section 1.3.2). EMOL-astrocyte nanotubes represent an area for further investigation and provide preliminary evidence that the EMOL might actively seek to connect with astrocytes.

EMOL nanotubes contained peroxisomes, which are small organelles involved in the breakdown of VLCFAs (for mitochondrial β-oxidation) and are transported along microtubules (Schrader *et al.*, 1996; Wiemer *et al.*, 1997) by molecular motors such as dyneins and kinesins (Hirokawa *et al.*, 2009; Kardon and Vale, 2009). In the post-myelination oligodendrocyte *in vivo*, peroxisomes are found in paranodal loops (Kassmann *et al.*, 2011) but their definitive function remains to be understood. Kassmann (2014) hypothesised that myelin peroxisomes perform β-oxidation of VLCFA to LCFAs for trans-cellular exchange to supply lipid to the axonal compartment. Our data suggest they might instead sequester VLCFAs from astrocytes to support myelination.

In this chapter, we aimed to understand the mechanisms that allow spinal cord EMOLs and other glia to survive 6 days of exogenous energy substrate deprivation. We showed that EMOLs extend nanotubes towards astrocytes but these likely do not contribute to trans-cellular energy provision. Therefore, we probed the metabolic adaptations of mixed glial cultures and found evidence for changes in lipid metabolism. Examining mixed glial cultures for lipid droplets revealed that astrocytes contain many and, as suggested by lipidomic analysis, are likely consumed as an energy source during 6 days of glucose (glutamine and pyruvate) deprivation. Astrocyte lipid droplets however are unlikely to support EMOL cell metabolism and an alternative fuel source must sustain them in the absence of major energy substrates, which we speculate could be amino acids or products of autophagy. As a final test of cell function, exogenous energy substrate-deprived EMOLs did not myelinate nanofibers and we speculate that the absence inter-glial contact could contribute to this deficit.

Chapter 6

Discussion

6.1 Summary of main findings

During development, brain EMOLs are particularly susceptible to injury from hypoxia-ischaemia. Based on differences in regions of origin and transcriptional profiles of brain *vs.,* spinal cord EMOLs (Floriddia *et al.*, 2020) as well as in blood vessel densities of the two CNS compartments (O'Meara *et al.*, 2017; Hernandez-Gerez *et al.*, 2020), the overarching aim of this thesis was to characterise the response of spinal cord EMOLs to hypoxia. This was done to help understand their response in disease paradigms of development such as SMA but also of adulthood where EMOLs remyelinate demyelinated axons following pathology. The unexpected finding that cells survived for 6 days in the absence of glucose and other major energy sources led us to expand the aims of this thesis to explore the role of endogenous energy substrate storage and utilisation.

6.1.1 Limitations of the study

The current study has several limitations that should be considered when extrapolating the data to the *in vivo* situation. First, as with all *in vitro* studies, the *in vivo* context is missing. This includes not only CNS components in their entirety but also connection to the endocrine and immune systems as well as the gut microbiome. Nonetheless, *in vitro* models can be useful when one is interested in understanding cell-intrinsic properties removed from external influences or where the question cannot be easily addressed *in vivo*, for example, due to the suffering it would cause. An essential component of the white matter *in vivo* is neuronal axons. Our *in vitro* model excluded neuronal cell bodies (which are rare in white matter) and inevitably, their axons. Nonetheless, this conferred an advantage as it allowed us to study the response of EMOLs to hypoxia and its secondary effects in the absence of neuronal cell death, which is likely to confound interpretation of glia-specific responses.

In Chapter 3, we maintained cell cultures in an anoxic chamber, which likely did not result in full oxygen depletion due to oxygen present in the media at the start of experimentation despite the oxygen-depleted atmosphere. We did however demonstrate that EMOLs were resistant to acute chemical hypoxia (a surrogate for oxygen deprivation). Our experiments

subjecting mixed glia to oxygen deprivation should be repeated with additional zero-oxygen gas flushes of the anoxic chamber.

In Chapter 4, we studied the response of spinal cord EMOLs and other glia to the individual secondary components of hypoxia. Whilst acknowledging that hypoxic/ischaemic injury in the CNS combines hypoxia and/or glucose deprivation with all these secondary consequences, the approach we took allowed us to identify individual factors that contribute to injury, most particularly an acidic extracellular milieu.

With respect to the total withdrawal of exogenous glucose, this is likely a rare event *in vivo* since it is the metabolism of glucose to pyruvate then lactate that is responsible for the lactic acidosis in hypoxia-ischaemia. However, *in vitro* modelling often requires increased severity and duration of insult to induce cellular injury comparable to the *in vivo* situation. Consequently, the complete withdrawal of glucose (in addition to pyruvate and glutamine) was anticipated to provide a positive control for cell death in Chapter 3. The unexpected finding that cells were resistant to exogenous energy substrate deprivation became the focus of Chapter 5.

In Chapter 5, we examined mRNA levels as a marker of the expression levels of key regulatory metabolic enzymes. This approach has two limitations: first mRNA levels do not necessarily reflect protein levels; second, modulation of enzymatic activity occurs at multiple levels with mRNA expression being only one of them.

Finally, although we were interested in understanding the susceptibility of brain *vs.,* spinal cord EMOLs to hypoxia, this would have required two sets of animals at different ages to simultaneously capture and cultivate cells at similar developmental time points. This proved too difficult to achieve within the time frame but does not detract from our observations.

6.1.2 Metabolic characteristics of spinal cord EMOLs

Despite the acknowledged limitations of the study, we found in Chapter 3 that neonatal murine spinal cord was rich in BCAS1$^+$ EMOLs from which we subsequently generated mixed glial cultures to use as an *in vitro* model of early myelinating spinal cord glia. Using pharmacological inhibitors of glycolysis and OXPHOS, we found that spinal cord EMOLs

were resistant to chemical hypoxia in the short term. Unexpectedly, EMOLs and other glia were resistant to 48 hours of glucose deprivation. These data alone contrast with published literature for brain EMOLs and suggest there is limited scope for studies carried out in the brain (or their cells) to be extrapolated to the spinal cord. Notwithstanding, we found no other study that completely depleted glucose and other exogenous energy substrates for an extended period of time as was done in the current study. Therefore, comparable growth conditions are required to allow a full comparison. Nonetheless, our data are in line with the *in vivo* work of O'Meara *et al.* (2017) who reported spinal cord myelination, and therefore EMOL viability, is unperturbed by tissue hypoxia in a mouse SMA model.

In Chapter 4, we examined the response of spinal cord EMOLs to secondary components of the hypoxic environment to understand what factors might confer increased tolerance to hypoxia. We found that EMOLs were vulnerable to extracellular acidosis or the complete withdrawal of amino acids and vitamins but were remarkably tolerant to treatment with TNF and IFNγ for 6 days. Recent *in vivo* evidence from Ando *et al.* (2020) using the same SMA mouse model as O'Meara *et al.* (2017) showed increased markers of microglial oxidative stress and astrogliosis in the spinal cord indicative of inflammation. Therefore, our data are compatible with the resilience to inflammation observed *in vivo* in SMA models where developmental myelination proceeds normally, at least until the study endpoint (P5). Most surprisingly, our spinal cord glia survived 6 days in the absence of glucose (pyruvate and glutamine). This suggests they must use substrates that eventually undergo OXPHOS to generate ATP. Obviously, this would not be possible in a hypoxic environment and these observations took the work in a different direction; one in which we examined endogenous energy substrate storage and use.

Despite their survival on glass coverslips, spinal cord EMOLs failed to myelinate nanofibers in the absence of exogenous energy substrates and cells failed to survive. We concluded cell density might be important in survival since cell-to-cell contact, which was lacking in the nanofiber experiments, would facilitate metabolic support between glia. It is unsurprising given the energy requirements of myelination that it failed in these circumstances. In the work of O'Meara *et al.* (2017), where no deficit in myelination was observed despite hypoperfusion of the spinal cord, cell-to-cell contact and the provision of minimal quantities of energy substrates and nutrients were likely able to support myelination.

In summary, spinal cord EMOLs *in vitro* are relatively resistant to hypoxia and withdrawal of exogenous energy substrates so long as minimal quantities of essential factors (amino acids and vitamins) can reach cells.

6.1.3 Astrocytes likely store and utilise lipids regardless of energy substrate availability

The survival of spinal cord EMOLs and glia following 6 days of exogenous glucose deprivation (and other exogenous energy substrates) led us to investigate the metabolic adaptations that might explain this in Chapter 5. In addition to storing limited reserves of glycogen, very recent reports demonstrate that astrocytes can store lipids in lipid droplets (Farmer *et al.*, 2019; Smolič *et al.*, 2021) and mobilise them in the absence of exogenous glucose, which the authors speculate supports energy metabolism (Farmer *et al.*, 2019). Our lipidomic analysis showed that lipid-droplet associated TG species were reduced after 6 days of culture with the highest reduction in glucose-free DM. Thus, we demonstrate for the first time that following the withdrawal of glucose (pyruvate and glutamine), changes in lipid droplet-associated lipids correspond with maintenance of cell densities and survival. This suggests that lipids stored at the outset of the experiment from the serum-rich media, myelin debris, or that are synthesised from glucose, are utilised to some degree regardless of energy substrate availability. This finding raises the intriguing possibility that glucose might not be the obligate energy source for spinal cord glia.

Is this simply an *in vitro* phenomenon? Can astrocytes or CNS cells in general access lipids from the periphery *in vivo*? Serum present in media during initial culture plating is akin to circulating lipids in the periphery, which as discussed in section 1.6.3 can cross the BBB and be metabolised *in vivo* (Allweis *et al.*, 1966; Ebert *et al.*, 2003; Camargo *et al.*, 2017). Early postnatal mammals have a milk-rich diet and a relatively high level of circulating lipids, which is postulated to support myelination following ketogenesis in the liver (Nehlig and Pereira de Vasconcelos, 1993). Storage of lipids from the periphery in astrocytes would, in principle, allow *in situ* ketogenesis to support neural cells with ketone bodies as proposed by Guzmán and Blázquez (2004). Although lipids can cross the BBB at all ages, lipid droplet storage might be a specific feature of “young” cells in the spinal cord and brain

to support the particularly high energy and biosynthetic demands of the developing CNS. This could be easily examined using antibodies to lipid droplet-associated proteins such as perilipin2 (Farmer *et al.*, 2019; Smolič *et al.*, 2021). Whether or not spinal cord astrocytes and glia metabolise or store lipids differently from those in the brain is unknown – this is a developing field. In addition to the above, I speculate that the relatively poor vascularisation of the spinal cord might necessitate the storage of lipids at all developmental stages to act as an energy reserve in times of decreased energy supply.

Oligodendrocytes are not known to be competent in β-oxidation (Edmond *et al.*, 1987). In fact, the mature post-myelination oligodendrocyte is considered incapable to avoid the breakdown of myelin lipids (Poitelon *et al.*, 2020). To our knowledge, there are no reports of β-oxidation in oligodendroglia. That said, adult rat brain oligodendrocytes can sequester lipids *in vitro* and *in vivo* as shown by fluorescent detection of alkyne FA analogues following administration into the periphery (Hofmann *et al.*, 2017). The fate of tracer lipids in the above study could not be determined. If EMOLs sequester lipids from serum present during initial culture plating as we propose for astrocytes, they appear to have limited storage capacity since they only occasionally contained Nile Red^{+} lipid droplets. Alternatively, myelin lipids could function as a lipid reservoir. Myelin as an energy store for the oligodendrocyte has been proposed by the Nave lab. They found that oligodendrocytes perform β-oxidation of myelin lipids to survive in glucose-free *ex vivo* optic nerve preparations after the death of astrocytes by energy exhaustion (Asadollahi et al., submitted for publication).

Ultimately, the ability of glia to perform β-oxidation of lipids provided from the circulation would not provide any resistance to hypoxia since lipid oxidation produces energy substrates for the TCA cycle and subsequently requires oxygen for OXPHOS. Nonetheless, we highlight the possible contribution of serum-derived lipids and/or myelin debris to energy metabolism and its potentially confounding influence in metabolic studies *in vitro*, which has not been considered, to our knowledge, by others. These alternative energy sources present in model systems such as ours likely sustain glia for some time in the absence of all other exogenous energy sources. It is likely these energy sources, if present, also contribute to energy generation *in vivo*.

6.2 Future work

The results obtained in this thesis raise many questions. Whether spinal cord EMOLs are more resistant to hypoxia than brain EMOLs, as we speculated at the outset, remains unanswered. In future studies, a direct comparison between spinal cord and brain EMOLs is necessary although this will require matching of brain and spinal cord cells for developmental stage. Therefore, two experimental cohorts will be needed for any *in vitro* or *in vivo* studies: the latter involving, for example, housing animals in low oxygen conditions.

Whether or not CNS glia perform β-oxidation has long been debated and dogma states that glucose is the primary energy source. However, recent reports that astrocytes can store lipid droplets and therefore have an active lipid metabolism has reignited this debate (Lee *et al.*, 2021; Ralhan *et al.*, 2021). Further quantitative studies are required to confirm our preliminary observation that astrocytes are rich in lipid droplets and that lipid droplet-associated TGs decrease over 6 days of culture, more so in glucose-free media.

In vitro studies facilitate the use of Seahorse assays, which measure oxygen consumption and extracellular acidification as outputs of mitochondrial function and glycolytic flux, respectively. Furthermore, *in vitro* systems permit the use of pharmacological inhibitors of mitochondrial β-oxidation to study the consequences of inhibiting FA metabolism. However, caution is required as highlighted by the recently reported effects of such compounds, which generate cytotoxic quantities of ROS species (O'Connor *et al.*, 2018) to which oligodendrocytes are particularly vulnerable (Juurlink *et al.*, 1998).

Ultimately, the ability of spinal cord glia to perform β-oxidation *in vivo* requires verification. This might be achieved using cell type-specific ablation of machinery involved in FA oxidation. White *et al.* (2020) knocked out *Cpt2* in all neural cells and thus CNS oxidation of medium and long-chain FAs. Although neurodevelopment and behaviour were largely unaltered, the authors reported the accumulation of long-chain acylcarnitines: incomplete import of LCFAs into mitochondria. Their data confirmed CNS β-oxidation *in vivo* but did not shed light on its physiological role. Potentially, challenging the animals with complex behavioural tasks or inducing disease/injury could reveal a role for CNS β-oxidation.

As most oligodendrocytes in mixed cultures appeared to not contain lipid droplets, we speculated that amino acids provide an energy source when cultured in the absence of astrocytes. A murine RNA sequencing database (Zhang *et al.*, 2014) confirms oligodendroglia express mRNA for the enzymes necessary to convert amino acids to pyruvate for ATP production. Although we consider amino acids an unlikely fuel source, we acknowledge their key role as building blocks of metabolic enzymes amongst other cellular machinery and await the results of metabolomic analyses aimed at examining how their quantities change over time in EMOL-enriched cultures.

6.3 Wider implications

Our model system and data are relevant to the study of other neuroinflammatory conditions. BCAS1$^+$ EMOLs are also present in the brain during re-myelination (Fard *et al.*, 2017). Presumably, this is also true for the spinal cord. The presence of myelin debris in our cultures make it a disease-relevant model for studying the response of glia in demyelinating diseases such as MS. Given that the spinal cord is a common site of demyelination in MS (Moccia *et al.*, 2019), a model system to study spinal cord oligodendrocytes in the context of demyelinating disease is a useful tool considering subsets of spinal cord and brain oligodendrocytes cluster differently in RNA sequencing analyses (Floriddia *et al.*, 2020) and, as our data suggest, might respond differently to cellular stress and disease.

The neuroinflammatory lesion in MS is speculated to create “virtual hypoxia” (Trapp and Stys, 2009; Desai *et al.*, 2016; Desai and Smith, 2017); therefore, our model system can also be utilised to study the vulnerability of adult re-myelinating EMOLs in this context.

Our observations, combined with those of Jagielska *et al.* (2013) who showed that OPCs migrate towards an acidic environment, suggest that in MS lesions OPCs might reach the demyelinated lesion but upon differentiation into BCAS1$^+$ remyelinating oligodendrocytes fail to survive in the acidic milieu. Our data present an area for therapeutic approach. Indeed, there is empirical evidence that some patients with MS find beneficial effects of hyperbaric oxygen (Bennett and Heard, 2010; Rae-Grant *et al.*, 2014). Our data support the possibility this is due to improved efficiency of remyelination through reducing acidosis and fuelling oxidation of lipids.

Uncovering differences at the molecular level that confer increased resistance of spinal cord EMOLs to the hypoxic environment, in comparison to brain, is potentially of interest where neural stem cell (NSC) transplantation could be used as a therapeutic. For example, a recent study by Kim *et al.* (2018) showed that modified NSCs (F3.olig2 OPCs) transplanted into the brains of rats after induction of neonatal PVL restored motor and cognitive performance. A similar success was demonstrated by the transplantation of NSCs into a mouse model of Pelizaeus-Merzbacher disease where myelination was restored (Gruenenfelder *et al.*, 2020). If spinal cord EMOLs are more resilient to WMI then factors driving NSCs to take on this phenotype might improve therapeutic results.

Finally, we provide a well-characterised model that is complementary to existing *in vitro* systems of spinal cord white matter, for example, myelinating cultures (Bijland *et al.*, 2019) and the recently developed human iPSC myelinoids (James *et al.*, 2021). Specifically, we provide an additional tool for the further study of BCAS1$^+$ EMOLs in health and disease.

6.4 Concluding remarks

To summarise, we have developed and characterised an *in vitro* model to study spinal cord glial metabolism and vulnerability to hypoxia-ischaemia. Using this model, we have shown that spinal cord EMOLs are resistant to short-term oxygen deprivation but are vulnerable to acidosis and a lack of amino acids and vitamins. We also demonstrate the surprising resilience of spinal cord EMOLs and glia to 6 days of exogenous energy substrate deprivation and provide evidence to a growing field supporting astrocytes as CNS lipid-storing and oxidising cells. Our data might also indicate that serum lipids and myelin debris can sustain glial cell metabolism for 6 days in the absence of all other exogenous energy sources. This platform provides a useful tool for future studies where all the consequences of hypoxia can be combined to examine the response of spinal cord glia. Moreover, this model system can be expanded to examine other diseases involving WMI.

Chapter 7

Appendices

7.1 Supplementary figures

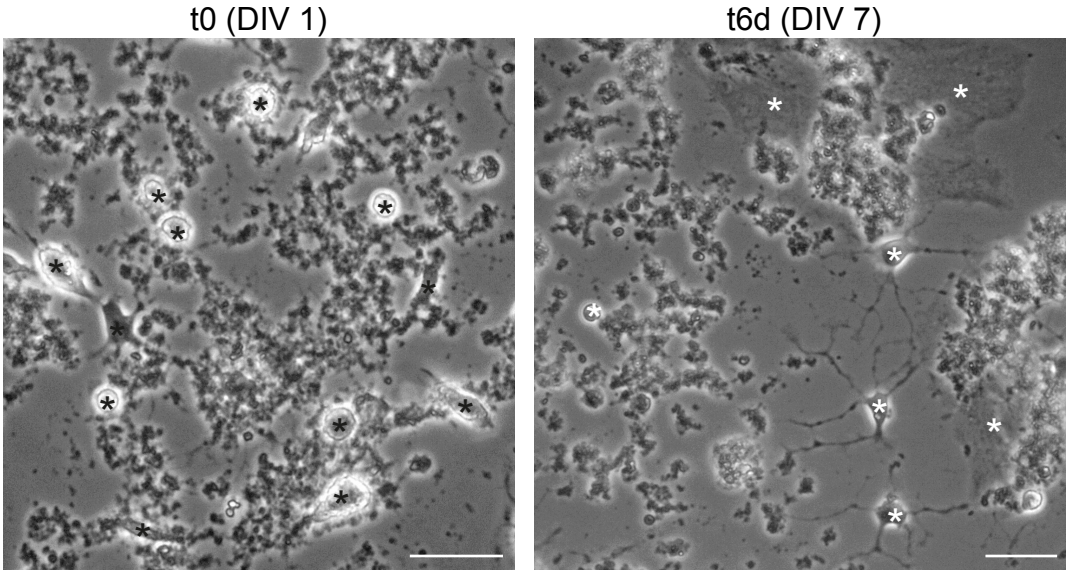

Figure S1 | **Postnatal mouse spinal cord mixed glial cultures contain myelin debris.** Phase-contrast images of cultures at t0 and t6d showing the presence of myelin debris from the culture preparation. Asterisks label cell bodies. Scale bar = 25 µm.

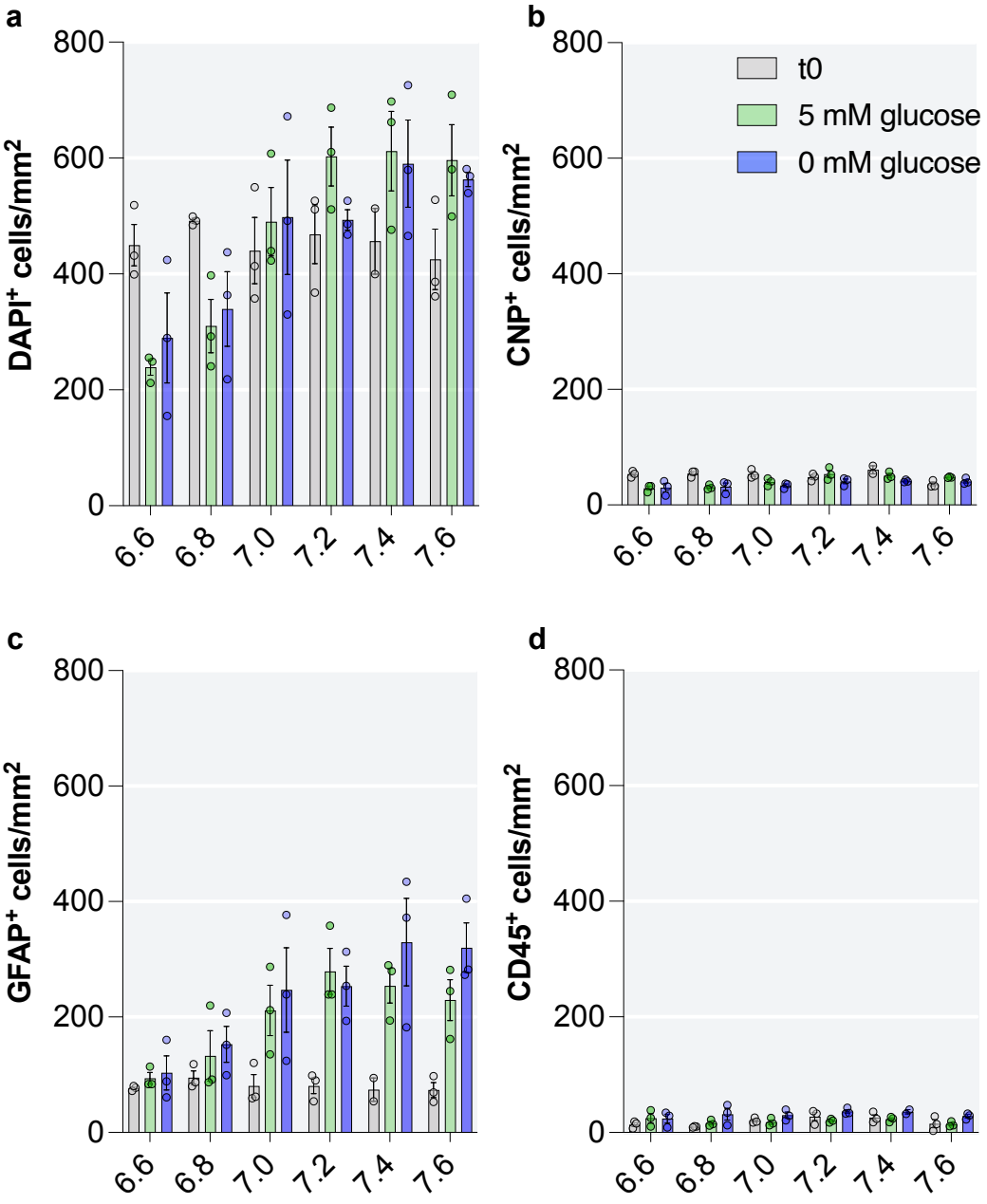

Figure S2 | **An acidic milieu impacts cell densities at t6d in mixed glial cultures but the effect is not compounded by glucose deprivation.** Graphs of raw data from cell density quantification at t0 (grey) and t6d (green and blue). Cultures were maintained in DM across a range of pH values containing 5 mM glucose (green) or 0 mM glucose (blue). Cell densities are shown for **(a)** all DAPI$^+$ cells, **(b)** EMOLs (CNP$^+$), **(c)** astrocytes (GFAP$^+$), and **(d)** microglia (CD45$^+$). Data were obtained from 3 biological repeats. Abbreviations: DM, DMEM-based media.

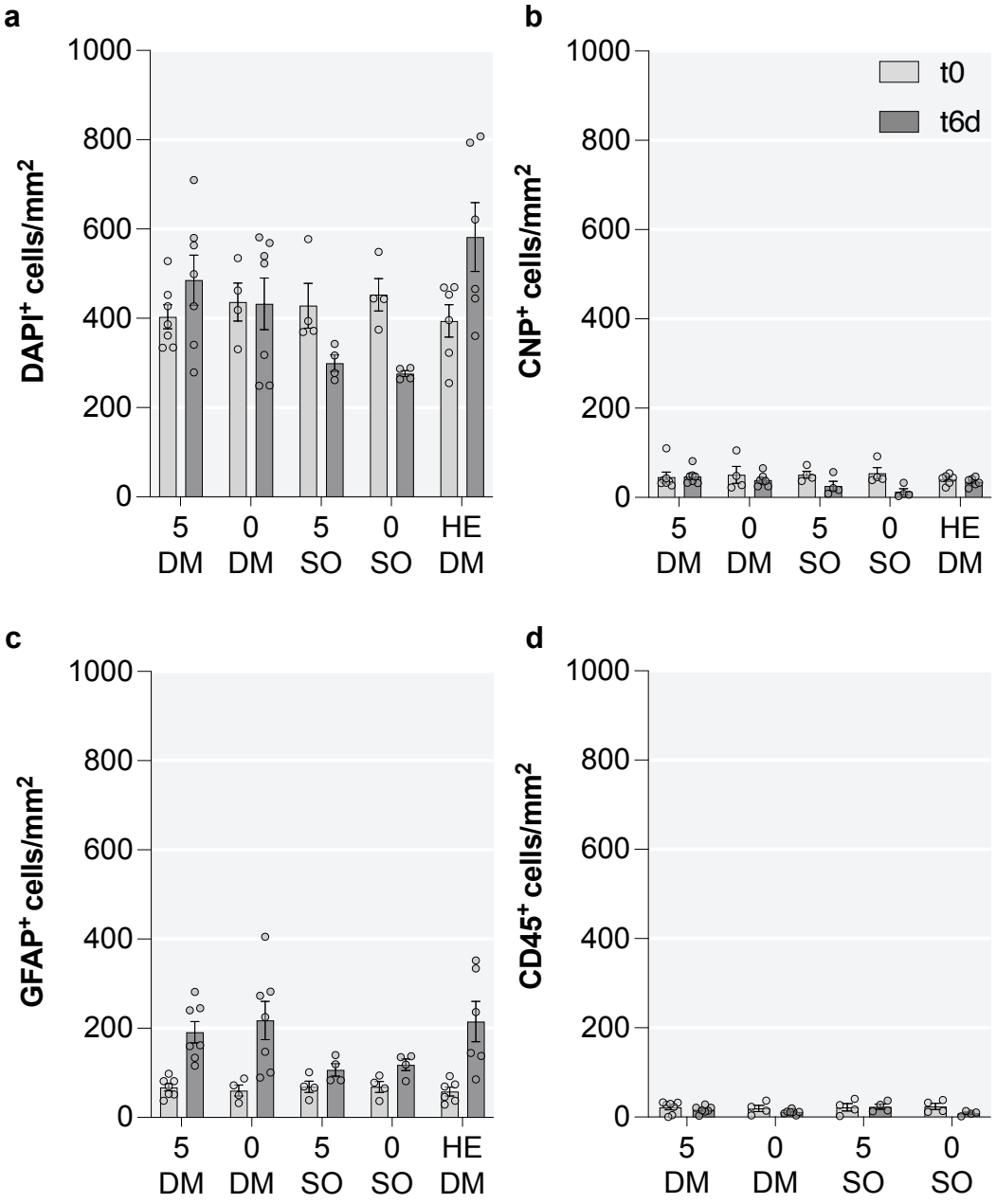

Figure S3 | Withdrawal of amino acids and vitamins impacts total cell and EMOL cell densities after 6 days in culture. Graphs of raw data from cell density quantification at t0 and after 6 days of culture in DM or SO media, with or without 5 mM glucose, or in HE media. Cell densities of **(a)** all DAPI$^+$ cells, **(b)** EMOLs (CNP$^+$), **(c)** astrocytes (GFAP$^+$), and **(d)** microglia (CD45$^+$). Data were obtained from 4 or 7 biological repeats. Abbreviations: DM, DMEM-based media; SO, salts-only; HE, DMEM-based media highly enriched in energy substrates.

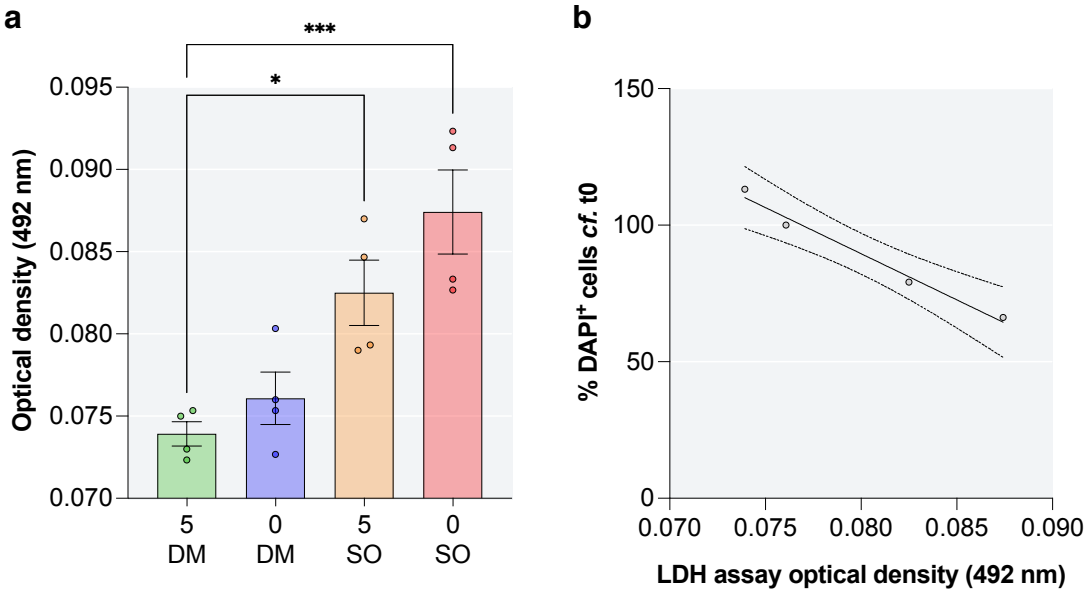

Figure S4 | Release of LDH is compounded by the absence of amino acids and vitamins after 6 days and correlates with total cell densities. **(a)** LDH release assay performed on cell supernatants from mixed glial cultures grown in DM or SO media, with and without 5 mM glucose. Media-only values were subtracted from sample readings. Data were compared to 5 mM glucose DM using a one-way ANOVA with Dunnett's multiple comparison test. * = $p < 0.05$, *** = $p < 0.001$. Data were obtained from 4 biological repeats. **(b)** Pearson correlation carried out on total DAPI$^+$ cell density averages per condition (reported in Figure 4.4 a) and LDH release assay optical density averages (**fig a**; r_p = -0.9907). Abbreviations: DM, DMEM-based media; SO, salts-only.

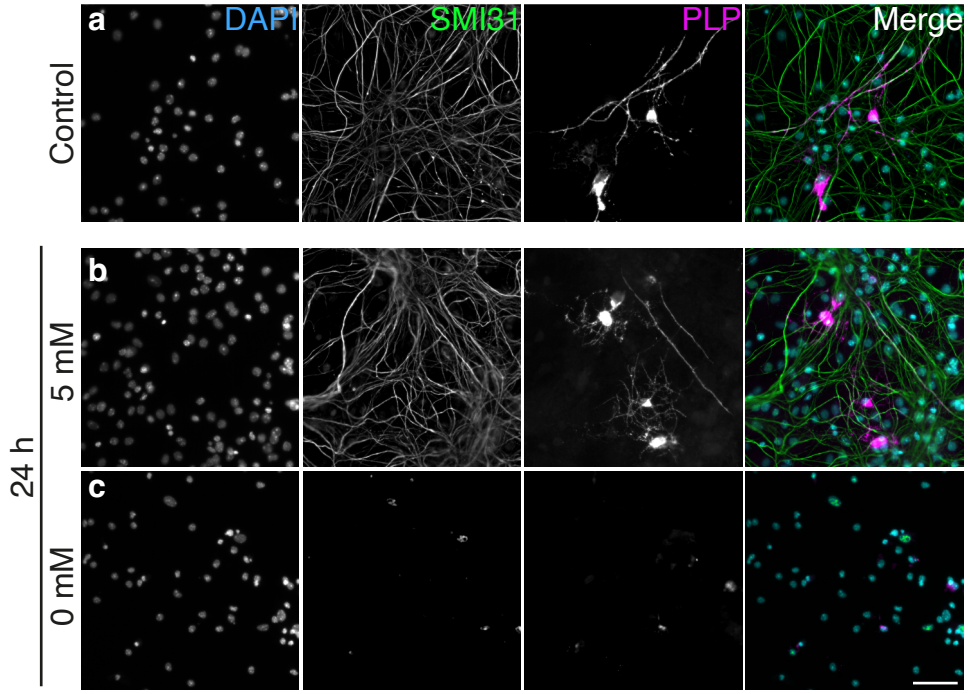

Figure S5 | **Myelinating cultures degenerate rapidly under exogenous energy substrate deprivation.** Illustrative immunofluorescence images of E13.5 mouse spinal cord myelinating cultures at DIV 25. **(a)** Cultures in HE control media (25 mM glucose, 1 mM pyruvate, 4 mM glutamine) where axons (green, SMI31^{+}) are myelinated (magenta, PLP^{+}). **(b)** After 24 hours in 5 mM glucose DM, axons and myelin sheaths remain **(b)** but are lost in 0 mM glucose DM. Observations representative of 2 biological repeats. Scale bar = 50 µm. Abbreviations: DM, DMEM-based media; HE, DMEM-based media highly enriched in energy substrates.

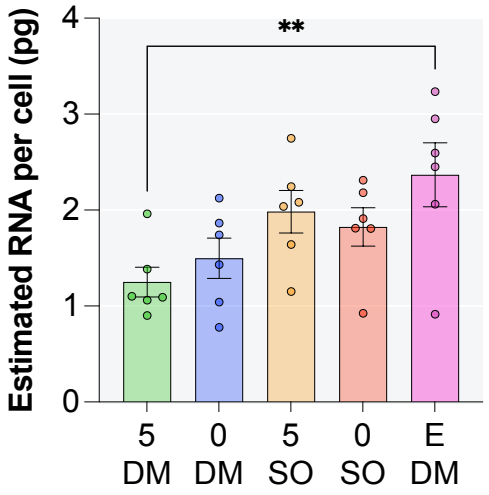

Figure S6 | Estimated RNA per cell is unchanged in mixed glia after 6 days of exogenous energy substrate deprivation. RNA per cell was estimated using the yield obtained after RNA purification for cDNA synthesis and RT-qPCR. The yield was divided by the total number of cells harvested calculated from the average t6d cell density (reported in Figure S3) and multiplied by the total area of 13 mm coverslips used. Data were compared to 5 mM glucose DM using a one-way ANOVA with Dunnett's multiple comparison test. ** = $p < 0.01$. Data were obtained from 6 biological repeats.

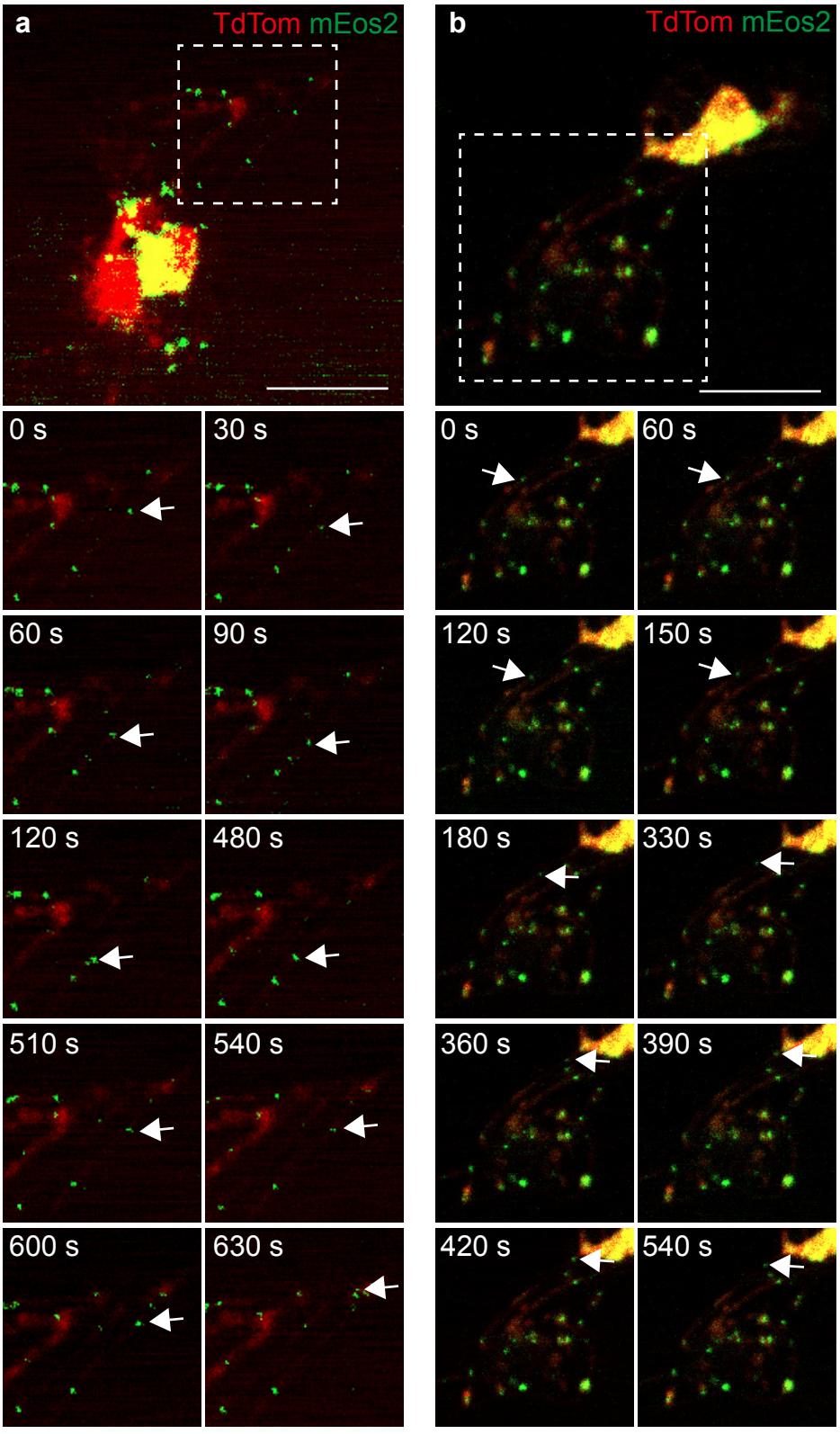

Figure S7 | Peroxisomes in EMOL nanotubes are motile even in the absence of exogenous glucose. Illustrative images of a TdTomato-labelled (red) EMOL with mEos2-labelled peroxisomes (green). A time series (inset) was captured using spinning disk confocal live-cell imaging. Motile peroxisomes are observed (arrows) in EMOL nanotubes in 0 mM glucose SO media at **(a)** t3d and **(b)** t6d. Scale bar = 25 µm. Abbreviations: SO, salts-only; s, seconds.

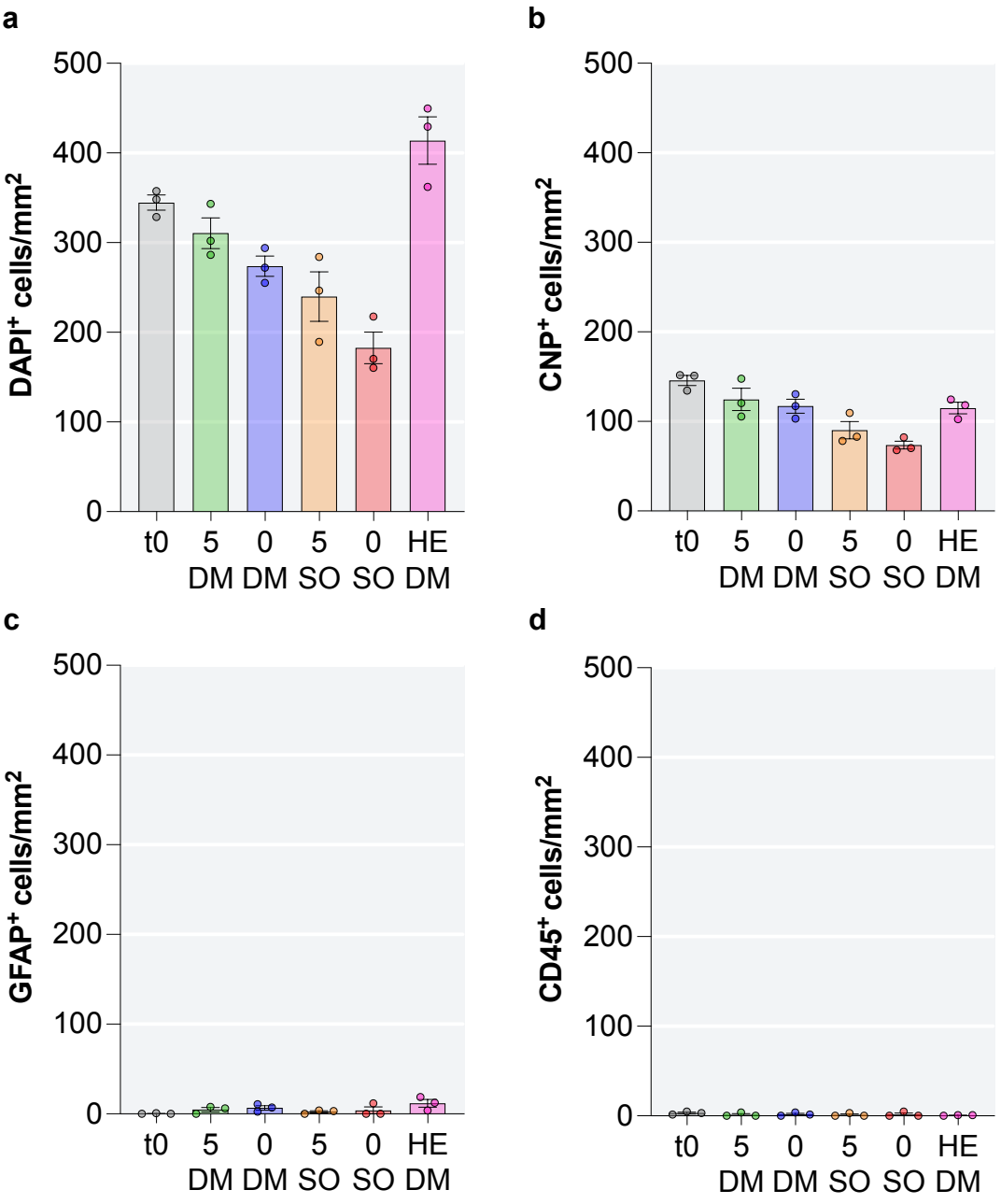

Figure S8 | Withdrawal of amino acids and vitamins impacts EMOL cell densities in EMOL-enriched cultures after 6 days. Graphs of raw data from cell density quantification at t0 and after 6 days of culture in DM or SO media, with or without 5 mM glucose, or HE media. Cell densities of **(a)** all DAPI$^+$ cells and **(b)** EMOLs (CNP$^+$). These cultures were largely devoid of **(c)** astrocytes (GFAP$^+$) **(d)** and microglia (CD45$^+$). Data were obtained from 3 biological repeats. Abbreviations: DM, DMEM-based media; SO, salts-only; HE, DMEM-based media highly enriched in energy substrates.

7.2 PEOT-*Tg* genotyping

Genotyping was performed using gDNA obtained from ear samples according to the "HotSHOT" method described by Truett *et al.* (2000) with some modifications. Briefly, small ear notch samples were heated in 100 µL 50 mM NaOH to 95 °C for 1 hour 30 mins. The samples were vortexed, neutralised with 10 µL 1 M Tris-HCl at pH 5, diluted 1 in 5 in autoclaved diH_2O and stored at −20 °C until use. Primers, expected product size, and PCR reaction mixtures are shown in Tables S1 and S2.

PCR cycling parameters for each transgene are detailed below:

PLP-CreERT^{T2}

1. 95 °C for 3 minutes
2. 95 °C for 15 seconds
3. 60 °C for 15 seconds
4. 72 °C for 40 seconds $\rightarrow$ # 2 for 30x cycles
5. 72 °C for 10 minutes
6. 4 °C and pause

Ai14

1. 94 °C for 2 minutes
2. 94 °C for 30 seconds
3. 58 °C for 30 seconds
4. 72 °C for 1 minute 20 seconds $\rightarrow$ # 2 for 30x cycles
5. 72 °C for 2 minutes
6. 4 °C and pause

Cnp-mEos2-PTS1

1. 95 °C for 3 minutes
2. 60 °C for 30 seconds

3. 72 °C for 1 minute 30 seconds
4. 95 °C for 30 seconds → # 2 for 35x cycles
5. 60 °C for 1 minute
6. 72 °C for 10 minutes
7. 4 °C and pause

PCR products were run on a 2% agarose gel (16500500, Invitrogen™) containing 0.5 µg/mL ethidium bromide (E1385, Sigma-Aldrich) made in Tris-acetate-EDTA buffer. A 100 bp interval DNA ladder (G2101, Promega) was used for reference. The gel was imaged under ultraviolet illumination.

Table S1 | Primers used for genotyping PEOT-*Tg* mice and expected product size.

Transgene	Forward primer (5′-3′)	Reverse primer (5′-3′)	Product size
PLP-CreER^{T2}	TGGACAGCTGGGACAA AGTAAGC	CGTTGCATCGACCGGT AATGCAGGC	Reporter ~250bp
Ai14	TACGGCATGGACGAGC TGTACAAGTAA	CAGGCGAGCAGCCAAG GAAA	WT ~330bp, Reporter ~250bp
Cnp-mEos2-PTS1	CTTCTTACACAGGCCAC CATGAGTGCG	GGATCCTTACTTAGTTA AGCTTGGATCGT	Reporter ~800bp

Table S2 | Reaction mixture for PCR genotyping of PEOT-*Tg* mice.

Component	PLP-CreER^{T2}	Ai14	Cnp-mEos2-PTS1
REDTaq™[1]	0.8 µL	0.8 µL	0.75 µL
10x Buffer[1]	2 µL	2 µL	2 µL
dNTPs[2]	2 µL	2 µL	2 µL
Forward primer (100 µM)	0.5 µL	0.5 µL	0.4 µL
Reverse primer (100 µM)	0.5 µL	0.5 µL	0.4 µL
Nuclease-free water	13.2 µL	13.2 µL	14.45 µL
cDNA	1 µL	1 µL	1 µL
Total	**20 µL**	**20 µL**	**21 µL**

[1]R2523, Sigma-Aldrich, [2]N0447S, New England Biolabs.

7.3 RT-qPCR primer validation

All primers were validated by end-point PCR using cDNA obtained from mixed glial cultures grown in HE media for 6 days. The PCR reaction mix contained:

6.25 µL	JumpStart™ REDTaq® ReadyMix™ (P0982, Sigma-Aldrich)
0.25 µL	Forward primer at 100 µM
0.25 µL	Reverse primer at 100 µM
2.75 µL	nfH_2O
3.00 µL	cDNA

The PCR cycling parameters were:

1. 95 °C for 1 minute
2. 95 °C for 1 minute
3. 56 °C for 2 minutes
4. 72 °C for 2 minutes 30 seconds $\rightarrow$ # 2 for 30x cycles
5. 72 °C for 10 minutes
6. 4 °C and pause

The PCR products were run on a 1.5% agarose gel (UltraPure™ agarose, 16500500, Invitrogen™) made in Tris-acetate-EDTA buffer containing 0.5x GelRed® nucleic acid stain (SCT123, Merck). A 100 bp interval DNA ladder (G2101, Promega) was used for size determination. Gels were imaged under ultraviolet illumination and are shown in Figure S9. Inner primers were considered specific if a single band of the expected size was observed. Inner primers were also validated with melt curve analysis and are shown in Figure S10. Primer efficiencies are shown in Table S3.

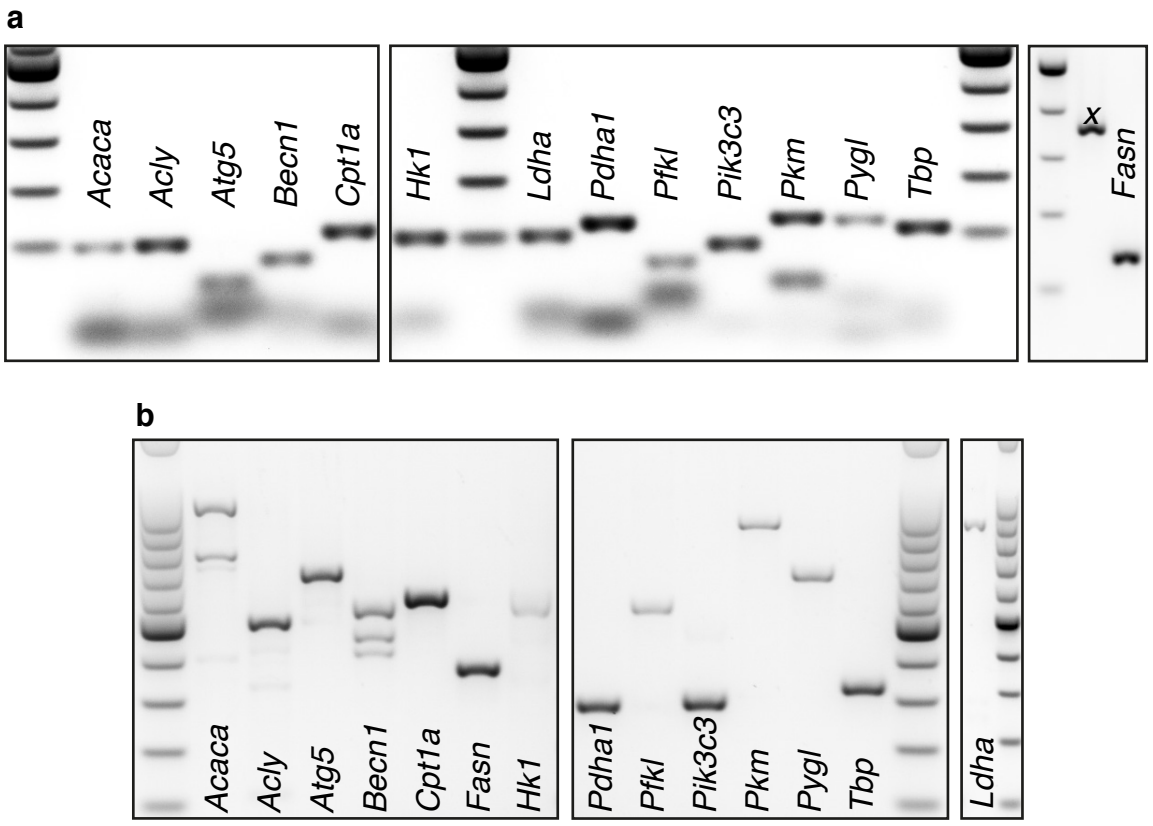

Figure S9 | **Gel validation of primers used in RT-qPCR.** Images of PCR products run on an agarose gel and imaged under UV illumination. **(a)** Products from inner primer pairs and approximate size from left to right: *Acaca* 104 bp, *Acly* 109 bp, *Atg5* 50 bp, *Becn1* 85 bp, *Cpt1a* 121 bp, *Hk1* 106 bp, *Ldha* 113 bp, *Pdha1* 140 bp, *Pfkl* 73 bp, *Pik3c3* 100 bp, *Pkm* 145 bp, *Pygl* 127 bp, *Tbp* 121 bp, *Fasn* 150 bp. Ladder bottom to top is 100 - 500 bp (bold band). **(b)** Products from outer primer pairs and approximate size from left to right: *Acaca* 924 bp, *Acly* 489 bp, *Atg5* 633 bp, *Becn1* 528 bp, *Cpt1a* 588 bp, *Fasn* 362 bp, *Hk1* 556 bp, *Pdha1* 298 bp, *Pfkl* 546 bp, *Pik3c3* 317 bp, *Pkm* 848 bp, *Pygl* 652 bp, *Tbp* 334 bp, *Ldha* 848 bp. Ladder from bottom to top is 100 - 1500 bp with 500 bp in bold.

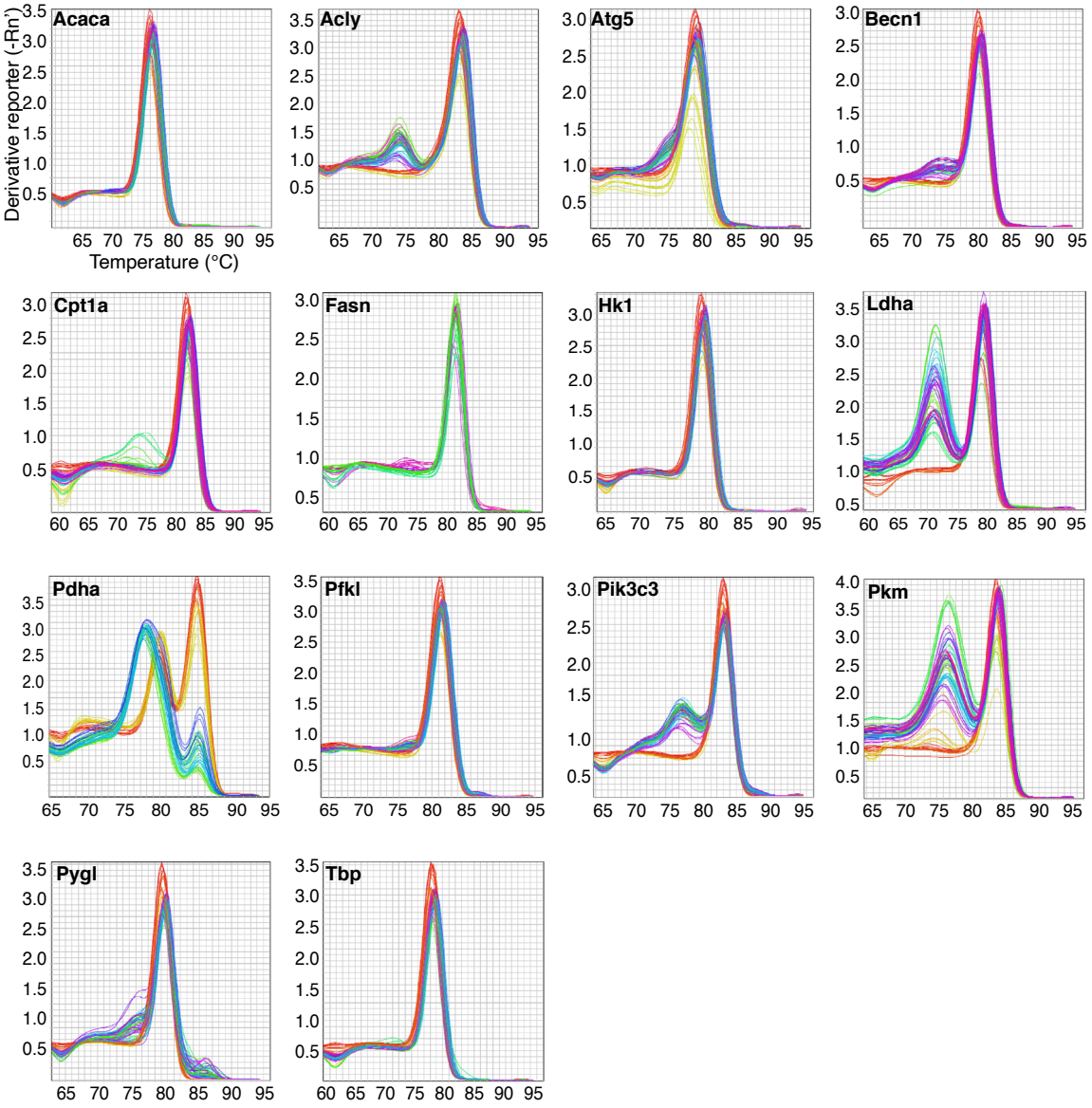

Figure S10 | **Inner primer melt curves from RT-qPCR.** Red and yellow lines were generated from standards. All other colours were generated from experimental samples.

Table S3 | Inner primer efficiencies from RT-qPCR.

Primer	Standard curve R^2	Efficiency
Acaca	0.997	91.98%
Acly	0.997	97.70%
Atg5	0.998	99.59%
Becn1	0.998	99.52%
Cpt1a	0.999	97.9%
Fasn	0.988	88.18%
Hk1	0.996	95.39%
Ldha	0.999	96.89%
Pdha1	0.998	99.05%
Pfkl	0.998	95.76%
Pik3c3	0.999	100.69%
Pkm	0.981	98.46%
Pygl	0.999	101.23%
Tbp	0.999	100.06%

7.4 Recipes

7.4.1 Phosphate buffered saline

A 10x stock was prepared in 800 mL diH_2O by dissolving the following salts:

80 g	NaCl
14.4 g	Na_2HPO_4
2.4 g	KH_2PO_4
2 g	KCl

The pH was adjusted to 7.4 with HCl and the volume made up to 1 L with diH_2O. A 1x solution was made by diluting 100 mL of 10x stock with 900 mL diH_2O. All solutions were stored at room temperature.

7.4.2 Tris-acetate-EDTA buffer

A 50x stock was prepared in 700 mL diH_2O by combining the following:

242 g	Tris-base
57.1 mL	100% Glacial acetic acid
100 mL	0.5 M EDTA pH 8.0

The volume was then adjusted to 1 L at which point the pH should be 8.5 (no adjustment). A 1x solution was made by diluting 20 mL of 50x stock with 980 mL diH_2O. All solutions were stored at room temperature.

7.4.3 8% paraformaldehyde

Dissolve 40 g of paraformaldehyde (P6148, Sigma-Aldrich) in 400 mL of PBS or water (as required), heat to 65 °C, and mix with a magnetic stirrer. Add a few drops of 1 M NaOH until the solution clears. Cool solution to room temperature then filter through filter paper. Adjust pH to 7.4 with HCl and make up the volume to 500 mL with PBS or water, as required. Store at 4 °C.

7.4.4 Boric acid buffer

Dissolve 1.24 g of boric acid (B6768, Sigma-Aldrich) and 1.9 g of sodium tetraborate (221732, Sigma-Aldrich) in 350 mL of cell culture grade water (W3500, Sigma-Aldrich) by heating to 80 °C with stirring. Cool solution and adjust pH to 8.5. Make up to 400 mL with cell culture grade water then sterilise through a 0.22 µm filter. Store at 4 °C.

7.4.5 N1 supplement

This recipe is from Thomson *et al.*, 2006 and Thomson *et al.*, 2008. Stock solutions were prepared as shown in Table S4 using cell culture grade materials obtained from Sigma-Aldrich. Reagents were then combined as described in Table S5 to give the final N1 mixture composition. Filter sterilise and store at −20 °C in 500 µL aliquots.

7.4.6 Mowiol® 4-88 mounting medium

To make 50 mL, combine 4.8 g of Mowiol® 4-88 (81381, Sigma-Aldrich) with 12 g of glycerol (10795711, Fisher Scientific) and shake vigorously. Top up with 12 mL of diH_2O then stir continuously for 2 hours with a stir bar at room temperature. Heat the mixture to 50 °C and add 24 mL of 0.2 M Tris base (pH 8.5), continuing to stir for 30 minutes before clarifying by centrifugation at 4,000 x *g* for 30 minutes. Stored in 2 mL aliquots at −20 °C. Before use, thaw and add 4′,6-diamidino-2-phenylindole (DAPI; D1306, Invitrogen™; diluted in PBS) to a final concentration of 5 µg/mL. Store at 4 °C.

7.4.7 4-Hydroxytamoxifen

4-hydroxytamoxifen (H7904, Sigma-Aldrich) stock solution was made by reconstituting in molecular grade methanol (M/4056/17, Fisher Scientific) to 10 mg/mL (25 mM). Aliquots were stored in small volumes at −20 °C. Working solutions were made by further diluting the stock to 1 mM in DMEM (41966-029, Gibco™) containing 1% penicillin-streptomycin. Working solutions were stored at 4 °C.

Table S4 | Stock solutions and components of N1 mix.

Stock solution	Weight	Dissolve in	Working dilutions
Apo-transferrin (T2252)	25 mg	5 mL PBS = 5 mg/mL	N/A
Putrescine (P7505)	80.55 mg	5 mL PBS = 100 mM	N/A
Progesterone (P6149)	1 mg	1.59 mL 90% ethanol = 2 mM (store at -20°C)	50 µL to 10 mL PBS = 10 µM
Selenium as sodium selenite (S9133)	5.19 mg	100 mL PBS = 300 µM (store at -20°C)	500 µL to 4.5 mL PBS = 30 µM

Table S5 | Composition of N1 mix.

Component	Volume	N1 mix conc.	Final conc. in medium
Apo-transferrin (5 mg/mL)	5 mL	1 mg/mL	5 µg/mL
Putrescine (100 mM)	5 mL	20 mM	100 µM
Progesterone (10 µM)	10 mL	4 µM	20 nM
Selenium (30 uM)	5 mL	6 µM	30 nM

7.5 Composition of DMEM A14430

Table S6 | Concentrations of amino acids and vitamins in DMEM (A14430, Gibco™). This media lacks glucose, pyruvate, and glutamine unless supplemented.

Component	Concentration (mM)
Amino acids	
Glycine	0.4
L-Arginine hydrochloride	0.39810428
L-Cystine 2HCl	0.20127796
L-Histidine hydrochloride-H_2O	0.2
L-Isoleucine	0.8015267
L-Leucine	0.8015267
L-Lysine hydrochloride	0.7978142
L-Methionine	0.20134228
L-Phenylalanine	0.4
L-Serine	0.4
L-Threonine	0.79831934
L-Tryptophan	0.078431375
L-Tyrosine disodium salt dihydrate	0.39846742
L-Valine	0.8034188
Vitamins	
Choline chloride	0.028571429
D-Calcium pantothenate	0.008385744
Folic acid	0.009070295
Niacinamide	0.032786883
Pyridoxine hydrochloride	0.019607844
Riboflavin	0.0010638298
Thiamine hydrochloride	0.011869436
i-Inositol	0.04

Formulation obtained from manufacturer's website on 22nd March 2019.

Chapter 8

References

Abbott, N. J., Rönnbäck, L. and Hansson, E. (2006). “Astrocyte–endothelial interactions at the blood–brain barrier”. *Nature Reviews Neuroscience*, 7, pp. 41–53. doi: 10.1038/nrn1824.

Abounit, S. and Zurzolo, C. (2012). “Wiring through tunneling nanotubes – from electrical signals to organelle transfer”. *Journal of Cell Science*, 125, pp. 1089–1098. doi: 10.1242/jcs.083279.

Agresti, C., …, and Coccia, E. M. (1998). “Synergistic stimulation of MHC class I and IRF-1 gene expression by IFN-gamma and TNF-alpha in oligodendrocytes”. *The European Journal of Neuroscience*, 10, pp. 2975–2983. doi: 10.1111/j.1460-9568.1998.00313.x.

Akassoglou, K., …, and Probert, L. (1998). “Oligodendrocyte apoptosis and primary demyelination induced by local TNF/p55TNF receptor signaling in the central nervous system of transgenic mice: models for multiple sclerosis with primary oligodendrogliopathy”. *The American Journal of Pathology*, 153, pp. 801–813. doi: 10.1016/S0002-9440(10)65622-2.

Akdemir, E. S., Huang, A. Y.-S. and Deneen, B. (2020). “Astrocytogenesis: where, when, and how”. *F1000Research*, 9, F1000 Faculty Rev–233. doi: 10.12688/f1000research.22405.1.

Alabduladhem, T. O. and Bordoni, B. (2021). “Physiology, Krebs Cycle”. *StatPearls*. Treasure Island (FL): StatPearls Publishing. url: http://www.ncbi.nlm.nih.gov/books/NBK556032/.

Aldewachi, H., …, and Salman, M. M. (2021). “High-throughput screening platforms in the discovery of novel drugs for neurodegenerative diseases”. *Bioengineering*, 8, p. 30. doi: 10.3390/bioengineering8020030.

Allan, K. C., …, and Tesar, P. J. (2021). “Non-canonical targets of HIF1a impair oligodendrocyte progenitor cell function”. *Cell Stem Cell*, 28, 257–272.e11. doi: 10.1016/j.stem.2020.09.019.

Allweis, C., …, and Magnes, J. (1966). “The oxidation of uniformly labelled albumin-bound palmitic acid to CO2 by the perfused cat brain”. *Journal of Neurochemistry*, 13, pp. 795–804. doi: 10.1111/j.1471-4159.1966.tb05874.x.

Amaral, A. I., …, and Sonnewald, U. (2013). “Metabolic aspects of neuron-oligodendrocyte-astrocyte interactions”. *Frontiers in Endocrinology*, 4. doi: 10.3389/fendo.2013.00054.

Amaral, A. I., …, and Sonnewald, U. (2016). “Characterization of glucose-related metabolic pathways in differentiated rat oligodendrocyte lineage cells”. *Glia*, 64, pp. 21–34. doi: 10.1002/glia.22900.

Ando, S., …, and Hara, H. (2020). “Survival motor neuron protein regulates oxidative stress and inflammatory response in microglia of the spinal cord in spinal muscular atrophy”. *Journal of Pharmacological Sciences*, 144, pp. 204–211. doi: 10.1016/j.jphs.2020.09.001.

Andrews, T., Zhang, P. and Bhat, N. R. (1998). “TNFalpha potentiates IFNgamma-induced cell death in oligodendrocyte progenitors”. *Journal of Neuroscience Research*, 54, pp. 574–583. doi: 10.1002/(SICI)1097-4547(19981201)54:5<574::AID-JNR2>3.0.CO;2-0.

Askew, K., …, and Gomez-Nicola, D. (2017). “Coupled proliferation and apoptosis maintain the rapid turnover of microglia in the adult brain”. *Cell Reports*, 18, pp. 391–405. doi: 10.1016/j.celrep.2016.12.041.

Auestad, N., …, and Edmond, J. (1991). “Fatty acid oxidation and ketogenesis by astrocytes in primary culture”. *Journal of Neurochemistry*, 56, pp. 1376–1386. doi: 10.1111/j.1471-4159.1991.tb11435.x.

Avellana-Adalid, V., …, and Baron-Van Evercooren, A. (1996). “Expansion of rat oligodendrocyte progenitors into proliferative oligospheres that retain differentiation potential”. *Journal of Neuroscience Research*, 45, pp. 558–570. doi: 10.1002/(SICI)1097-4547(19960901)45:5<558::AID-JNR6>3.0.CO;2-B.

Azevedo, F. A. C., …, and Herculano-Houzel, S. (2009). “Equal numbers of neuronal and nonneuronal cells make the human brain an isometrically scaled-up primate brain”. *The Journal of Comparative Neurology*, 513, pp. 532–541. doi: 10.1002/cne.21974.

Bachiller, S., …, and Boza-Serrano, A. (2018). “Microglia in neurological diseases: A road map to brain-disease dependent-inflammatory response”. *Frontiers in Cellular Neuroscience*, 12, p. 488. doi: 10.3389/fncel.2018.00488.

Back, S. A., …, and Volpe, J. J. (1998). “Maturation-dependent vulnerability of oligodendrocytes to oxidative stress-induced death caused by glutathione depletion”. *Journal of Neuroscience*, 18, pp. 6241–6253. doi: 10.1523/jneurosci.18-16-06241.1998.

Back, S. A., …, and Kinney, H. C. (2001). “Late oligodendrocyte progenitors coincide with the developmental window of vulnerability for human perinatal white matter injury”. *The Journal of Neuroscience*, 21, pp. 1302–1312. doi: 10.1523/jneurosci.21-04-01302.2001.

Back, S. A., …, and Sherman, L. S. (2005). “Hyaluronan accumulates in demyelinated lesions and inhibits oligodendrocyte progenitor maturation”. *Nature Medicine*, 11, pp. 966–972. doi: 10.1038/nm1279.

Back, S. A. (2006). “Perinatal white matter injury: the changing spectrum of pathology and emerging insights into pathogenetic mechanisms”. *Mental Retardation and Developmental Disabilities Research Reviews*, 12, pp. 129–140. doi: 10.1002/mrdd.20107.

Back, S. A. and Miller, S. P. (2014). “Brain injury in premature neonates: A primary cerebral dysmaturation disorder?” *Annals of Neurology*, 75, pp. 469–486. doi: 10.1002/ana.24132.

Baj, T. and Sieniawska, E. (2017). “Chapter 13 - Vitamins”. *Pharmacognosy*. Boston: Academic Press, pp. 281–292. isbn: 978-0-12-802104-0. doi: 10.1016/B978-0-12-802104-0.00013-5.

Ball, K. K., …, and Dienel, G. A. (2007). “Astrocytic connexin distributions and rapid, extensive dye transfer via gap junctions in the inferior colliculus: Implications for [14C]glucose metabolite trafficking”. *Journal of Neuroscience Research*, 85, pp. 3267–3283. doi: 10.1002/jnr.21376.

Bandeira, F., Lent, R. and Herculano-Houzel, S. (2009). “Changing numbers of neuronal and non-neuronal cells underlie postnatal brain growth in the rat”. *Proceedings of the National Academy of Sciences*, 106, pp. 14108–14113. doi: 10.1073/pnas.0804650106.

Banks, W. A. (2016). “From blood–brain barrier to blood–brain interface: new opportunities for CNS drug delivery”. *Nature Reviews Drug Discovery*, 15, pp. 275–292. doi: 10.1038/nrd.2015.21.

Bankston, A. N., …, and Whittemore, S. R. (2019). “Autophagy is essential for oligodendrocyte differentiation, survival, and proper myelination”. *Glia*, 67, pp. 1745–1759. doi: 10.1002/glia.23646.

Barres, B. A., …, and Raff, M. C. (1992). “Cell death and control of cell survival in the oligodendrocyte lineage”. *Cell*, 70, pp. 31–46. doi: 10.1016/0092-8674(92)90531-g.

Barres, B. A. (2008). “The mystery and magic of glia: a perspective on their roles in health and disease”. *Neuron*, 60, pp. 430–440. doi: 10.1016/j.neuron.2008.10.013.

Bartz, R., …, and Liu, P. (2007a). “Dynamic activity of lipid droplets: protein phosphorylation and GTP-mediated protein translocation”. *Journal of Proteome Research*, 6, pp. 3256–3265. doi: 10.1021/pr070158j.

Bartz, R., …, and Chapman, K. D. (2007b). “Lipidomics reveals that adiposomes store ether lipids and mediate phospholipid traffic”. *Journal of Lipid Research*, 48, pp. 837–847. doi: 10.1194/jlr.M600413-JLR200.

Basu, R. and Das Sarma, J. (2018). “Connexin 43/47 channels are important for astrocyte/oligodendrocyte cross-talk in myelination and demyelination”. *Journal of Biosciences*, 43, pp. 1055–1068. doi: 10.1007/s12038-018-9811-0.

Baud, O., …, and Rosenberg, P. A. (2004). “Developmental up-regulation of MnSOD in rat oligodendrocytes confers protection against oxidative injury”. *The European Journal of Neuroscience*, 20, pp. 29–40. doi: 10.1111/j.0953-816X.2004.03451.x.

Bayraktar, O. A., …, and Rowitch, D. H. (2015). “Astrocyte development and heterogeneity”. *Cold Spring Harbor Perspectives in Biology*, 7, a020362. doi: 10.1101/cshperspect.a020362.

Beattie, D. S. and Basford, R. E. (1965). “Brain mitochondria—III: fatty acid oxidation by bovine brain mitochondria”. *Journal of Neurochemistry*, 12, pp. 103–111. doi: 10.1111/j.1471-4159.1965.tb11945.x.

Bechler, M. E., Byrne, L. and ffrench-Constant, C. (2015). “CNS myelin sheath lengths are an intrinsic property of oligodendrocytes”. *Current Biology*, 25, pp. 2411–2416. doi: 10.1016/j.cub.2015.07.056.

Bechler, M. E. (2019). “A neuron-free microfiber assay to assess myelin sheath formation”. *Oligodendrocytes: Methods and Protocols*. New York, NY: Springer, pp. 97–110. isbn: 978-1-4939-9072-6. doi: 10.1007/978-1-4939-9072-6_6.

Bélanger, M., Allaman, I. and Magistretti, P. J. (2011). “Brain energy metabolism: focus on astrocyte-neuron metabolic cooperation”. *Cell Metabolism*, 14, pp. 724–738. doi: 10.1016/j.cmet.2011.08.016.

Bennett, F. C., …, and Barres, B. A. (2018). “A combination of ontogeny and CNS environment establishes microglial identity”. *Neuron*, 98, 1170–1183.e8. doi: 10.1016/j.neuron.2018.05.014.

Bennett, M. and Heard, R. (2010). “Hyperbaric oxygen therapy for multiple sclerosis”. *CNS Neuroscience & Therapeutics*, 16, pp. 115–124. doi: 10.1111/j.1755-5949.2009.00129.x.

Bennett, M. V. L. and Zukin, R. S. (2004). “Electrical coupling and neuronal synchronization in the mammalian brain”. *Neuron*, 41, pp. 495–511. doi: 10.1016/S0896-6273(04)00043-1.

Benz, R. (1994). “Permeation of hydrophilic solutes through mitochondrial outer membranes: review on mitochondrial porins”. *Biochimica et Biophysica Acta (BBA) - Reviews on Biomembranes*, 1197, pp. 167–196. doi: 10.1016/0304-4157(94)90004-3.

Bergeron, M., …, and Sharp, F. R. (1999). “Induction of hypoxia-inducible factor-1 (HIF-1) and its target genes following focal ischaemia in rat brain”. *The European Journal of Neuroscience*, 11, pp. 4159–4170. doi: 10.1046/j.1460-9568.1999.00845.x.

Besson, S., …, and Swedlow, J. R. (2019). “Bringing open data to whole slide imaging”. *Digital Pathology*. Cham: Springer International Publishing, pp. 3–10. isbn: 978-3-030-23937-4. doi: 10.1007/978-3-030-23937-4_1.

Bijland, S., …, and Edgar, J. M. (2019). “An in vitro model for studying CNS white matter: functional properties and experimental approaches”. *F1000Research*, 8, p. 117. doi: 10.12688/f1000research.16802.1.

Bin, J. M., Harris, S. N. and Kennedy, T. E. (2016). “The oligodendrocyte-specific antibody ’CC1’ binds quaking 7”. *Journal of Neurochemistry*, 139, pp. 181–186. doi: 10.1111/jnc.13745.

Bixel, M. G. and Hamprecht, B. (1995). “Generation of ketone bodies from leucine by cultured astroglial cells”. *Journal of Neurochemistry*, 65, pp. 2450–2461. doi: 10.1046/j.1471-4159.1995.65062450.x.

Blakemore, W. F. (1978). “Observations on remyelination in the rabbit spinal cord following demyelination induced by lysolecithin”. *Neuropathology and Applied Neurobiology*, 4, pp. 47–59. doi: 10.1111/j.1365-2990.1978.tb00528.x.

Blanchette-Mackie, E. J., …, and Londos, C. (1995). “Perilipin is located on the surface layer of intracellular lipid droplets in adipocytes.” *Journal of Lipid Research*, 36, pp. 1211–1226. doi: 10.1016/S0022-2275(20)41129-0.

Blivis, D., Falgairolle, M. and O’Donovan, M. J. (2019). “Dye-coupling between neonatal spinal motoneurons and interneurons revealed by prolonged back-filling of a ventral root with a low molecular weight tracer in the mouse”. *Scientific Reports*, 9, p. 3201. doi: 10.1038/s41598-019-39881-0.

Block, M. L., Zecca, L. and Hong, J.-S. (2007). “Microglia-mediated neurotoxicity: uncovering the molecular mechanisms”. *Nature Reviews Neuroscience*, 8, pp. 57–69. doi: 10.1038/nrn2038.

Bohatschek, M., …, and Raivich, G. (2004). “Microglial major histocompatibility complex glycoprotein-1 in the axotomized facial motor nucleus: regulation and role of tumor necrosis factor receptors 1 and 2”. *The Journal of Comparative Neurology*, 470, pp. 382–399. doi: 10.1002/cne.20017.

Bolaños, J. P., Almeida, A. and Moncada, S. (2010). “Glycolysis: a bioenergetic or a survival pathway?” *Trends in Biochemical Sciences*, 35, pp. 145–149. doi: 10.1016/j.tibs.2009.10.006.

Bradl, M. and Lassmann, H. (2010). “Oligodendrocytes: biology and pathology”. *Acta Neuropathologica*, 119, pp. 37–53. doi: 10.1007/s00401-009-0601-5.

Bricker, D. K., …, and Rutter, J. (2012). “A mitochondrial pyruvate carrier required for pyruvate uptake in yeast, drosophila, and humans”. *Science*, 337, pp. 96–100. doi: 10.1126/science.1218099.

Brown, A. M., Wender, R. and Ransom, B. R. (2001). “Metabolic substrates other than glucose support axon function in central white matter”. *Journal of Neuroscience Research*, 66, pp. 839–843. doi: 10.1002/jnr.10081.

Brown, A. M., Tekkök, S. B. and Ransom, B. R. (2003). “Glycogen regulation and functional role in mouse white matter”. *The Journal of Physiology*, 549, pp. 501–512. doi: 10.1113/jphysiol.2003.042416.

Brown, A. M., Baltan Tekkök, S. and Ransom, B. R. (2004). “Energy transfer from astrocytes to axons: the role of CNS glycogen”. *Neurochemistry International*, 45, pp. 529–536. doi: 10.1016/j.neuint.2003.11.005.

Brown, A. M., …, and Ransom, B. R. (2005). “Astrocyte glycogen metabolism is required for neural activity during aglycemia or intense stimulation in mouse white matter”. *Journal of Neuroscience Research*, 79, pp. 74–80. doi: 10.1002/jnr.20335.

Bugiani, M., …, and Zeviani, M. (2006). “GJA12 mutations in children with recessive hypomyelinating leukoencephalopathy”. *Neurology*, 67, pp. 273–279. doi: 10.1212/01.wnl.0000223832.66286.e4.

Bullock, T. H., Moore, J. K. and Fields, R. D. (1984). “Evolution of myelin sheaths: both lamprey and hagfish lack myelin”. *Neuroscience Letters*, 48, pp. 145–148. doi: 10.1016/0304-3940(84)90010-7.

Bullock, T. H. (2004). “The natural history of neuroglia: an agenda for comparative studies”. *Neuron Glia Biology*, 1, pp. 97–100. doi: 10.1017/s1740925x04000250.

Burghes, A. H. M. and Beattie, C. E. (2009). “Spinal muscular atrophy: why do low levels of survival motor neuron protein make motor neurons sick?” *Nature Reviews. Neuroscience*, 10, pp. 597–609. doi: 10.1038/nrn2670.

Butt, A. M. and Ransom, B. R. (1989). “Visualization of oligodendrocytes and astrocytes in the intact rat optic nerve by intracellular injection of lucifer yellow and horseradish peroxidase”. *Glia*, 2, pp. 470–475. doi: 10.1002/glia.440020609.

Cabodevilla, A. G., …, and Claro, E. (2013). “Cell survival during complete nutrient deprivation depends on lipid droplet-fueled β-oxidation of fatty acids”. *Journal of Biological Chemistry*, 288, pp. 27777–27788. doi: 10.1074/jbc.M113.466656.

Cai, J., …, and Gozal, D. (2012). “Mouse intermittent hypoxia mimicking apnoea of prematurity: effects on myelinogenesis and axonal maturation”. *The Journal of Pathology*, 226, pp. 495–508. doi: 10.1002/path.2980.

Camargo, N., …, and Verheijen, M. H. G. (2017). “Oligodendroglial myelination requires astrocyte-derived lipids”. *PLOS Biology*, 15, e1002605. doi: 10.1371/journal.pbio.1002605.

Caprariello, A. V., …, and Miller, R. H. (2015). “Apoptosis of oligodendrocytes during early development delays myelination and impairs subsequent responses to demyelination”. *The Journal of Neuroscience*, 35, pp. 14031–14041. doi: 10.1523/JNEUROSCI.1706-15.2015.

Castelfranco, A. M. and Hartline, D. K. (2016). “Evolution of rapid nerve conduction”. *Brain Research*, 1641 (Pt A), pp. 11–33. doi: 10.1016/j.brainres.2016.02.015.

Cater, H. L., Benham, C. D. and Sundstrom, L. E. (2001). “Neuroprotective role of monocarboxylate transport during glucose deprivation in slice cultures of rat hippocampus”. *The Journal of Physiology*, 531 (Pt 2), pp. 459–466. doi: 10.1111/j.1469-7793.2001.0459i.x.

Cellerino, A., …, and Barde, Y.-A. (1997). “Reduced size of retinal ganglion cell axons and hypomyelination in mice lacking brain-derived neurotrophic factor”. *Molecular and Cellular Neuroscience*, 9, pp. 397–408. doi: 10.1006/mcne.1997.0641.

Charles, P., …, and Lubetzki, C. (2000). “Negative regulation of central nervous system myelination by polysialylated-neural cell adhesion molecule”. *Proceedings of the National Academy of Sciences*, 97, pp. 7585–7590. doi: 10.1073/pnas.100076197.

Chaudhry, R. and Varacallo, M. (2021). “Biochemistry, Glycolysis”. *StatPearls*. Treasure Island (FL): StatPearls Publishing. url: http://www.ncbi.nlm.nih.gov/books/NBK482303/.

Chen, C.-D., …, and Abraham, C. R. (2013). “The antiaging protein klotho enhances oligodendrocyte maturation and myelination of the CNS”. *Journal of Neuroscience*, 33, pp. 1927–1939. doi: 10.1523/JNEUROSCI.2080-12.2013.

Chen, Y., …, and Lu, Q. R. (2009). “The oligodendrocyte-specific G protein-coupled receptor GPR17 is a cell-intrinsic timer of myelination”. *Nature Neuroscience*, 12, pp. 1398–1406. doi: 10.1038/nn.2410.

Chomczynski, P. and Sacchi, N. (1987). “Single-step method of RNA isolation by acid guanidinium thiocyanate-phenol-chloroform extraction”. *Analytical Biochemistry*, 162. doi: 10.1006/abio.1987.9999.

Chong, S. Y. C., …, and Chan, J. R. (2012). “Neurite outgrowth inhibitor Nogo-A establishes spatial segregation and extent of oligodendrocyte myelination”. *Proceedings of the National Academy of Sciences*, 109, pp. 1299–1304. doi: 10.1073/pnas.1113540109.

Chorghay, Z., Káradóttir, R. T. and Ruthazer, E. S. (2018). “White matter plasticity keeps the brain in tune: axons conduct while glia wrap”. *Frontiers in Cellular Neuroscience*, 12, p. 428. doi: 10.3389/fncel.2018.00428.

Coetzee, T., …, and Popko, B. (1996). “Myelination in the absence of galactocerebroside and sulfatide: normal structure with abnormal function and regional instability”. *Cell*, 86, pp. 209–219. doi: 10.1016/s0092-8674(00)80093-8.

Çolakoğlu, G., …, and Ranscht, B. (2014). “Contactin-1 regulates myelination and nodal/-paranodal domain organization in the central nervous system”. *Proceedings of the National Academy of Sciences*, 111, E394–E403. doi: 10.1073/pnas.1313769110.

Cummings, B. S. and Schnellmann, R. G. (2004). “Measurement of cell death in mammalian cells”. *Current Protocols in Pharmacology*, 25, pp. 12.8.1–12.8.22. doi: 10.1002/0471141755.ph1208s25.

Cunliffe, V. T. and Casaccia-Bonnefil, P. (2006). “Histone deacetylase 1 is essential for oligodendrocyte specification in the zebrafish CNS”. *Mechanisms of Development*, 123, pp. 24–30. doi: 10.1016/j.mod.2005.10.005.

Dalkara, T., …, and Moskowitz, M. A. (1994). “Dual role of nitric oxide in focal cerebral ischemia”. *Neuropharmacology*, 33, pp. 1447–1452. doi: 10.1016/0028-3908(94)90048-5.

Danilov, C. A. and Fiskum, G. (2008). “Hyperoxia promotes astrocyte cell death after oxygen and glucose deprivation”. *Glia*, 56, pp. 801–808. doi: 10.1002/glia.20655.

Darnall, R. A., …, and Hunt, C. E. (2017). “Early postnatal exposure to intermittent hypoxia in rodents is proinflammatory, impairs white matter integrity, and alters brain metabolism”. *Pediatric Research*, 82, pp. 164–172. doi: 10.1038/pr.2017.102.

Davis, D. M. and Sowinski, S. (2008). “Membrane nanotubes: dynamic long-distance connections between animal cells”. *Nature Reviews Molecular Cell Biology*, 9, pp. 431–436. doi: 10.1038/nrm2399.

Dawson, D. A., Martin, D. and Hallenbeck, J. M. (1996). “Inhibition of tumor necrosis factor-alpha reduces focal cerebral ischemic injury in the spontaneously hypertensive rat”. *Neuroscience Letters*, 218, pp. 41–44. doi: 10.1016/0304-3940(96)13116-5.

Del Río-Hortega, P. (1921). “La glía de escasa radiaciones (oligodendroglia)[Glia with many processes (oligodendroglia)]”. *Trab Lab Histol Patol*, 1, pp. 1–43.

Deng, W., …, and Jensen, F. E. (2003). “Calcium-permeable AMPA/kainate receptors mediate toxicity and preconditioning by oxygen-glucose deprivation in oligodendrocyte precursors”. *Proceedings of the National Academy of Sciences*, 100, pp. 6801–6806. doi: 10.1073/pnas.1136624100.

Deng, W., …, and Jensen, F. E. (2006). “Oligodendrocyte excitotoxicity determined by local glutamate accumulation and mitochondrial function”. *Journal of Neurochemistry*, 98, pp. 213–222. doi: 10.1111/j.1471-4159.2006.03861.x.

Deng, Y., …, and Kaur, C. (2008). “Amoeboid microglia in the periventricular white matter induce oligodendrocyte damage through expression of proinflammatory cytokines via MAP kinase signaling pathway in hypoxic neonatal rats”. *Brain Pathology*, 18, pp. 387–400. doi: 10.1111/j.1750-3639.2008.00138.x.

Desai, R. A., …, and Smith, K. J. (2016). “Cause and prevention of demyelination in a model multiple sclerosis lesion”. *Annals of Neurology*, 79, pp. 591–604. doi: 10.1002/ana.24607.

Desai, R. A. and Smith, K. J. (2017). “Experimental autoimmune encephalomyelitis from a tissue energy perspective”. *F1000Research*, 6, p. 1973. doi: 10.12688/f1000research.11839.1.

Dhillon, K. K. and Gupta, S. (2021). “Biochemistry, Ketogenesis”. *StatPearls*. Treasure Island (FL): StatPearls Publishing. url: http://www.ncbi.nlm.nih.gov/books/NBK493179/.

Dhopeshwarkar, G. A. and Mead, J. F. (1970). “Fatty acid uptake by the brain: III. Incorporation of [l-14C]oleic acid into the adult ratbrain”. *Biochimica et Biophysica Acta (BBA) - Lipids and Lipid Metabolism*, 210, pp. 250–256. doi: 10.1016/0005-2760(70)90169-4.

Dhopeshwarkar, G. A., Subramanian, C. and Mead, J. F. (1971). “Fatty acid uptake by the brain V. Incorporation of [1-14C]linolenic acid into adult rat brain”. *Biochimica et Biophysica Acta (BBA) - Lipids and Lipid Metabolism*, 239, pp. 162–167. doi: 10.1016/0005-2760(71)90162-7.

Dobrea, G. M., Unnerstall, J. R. and Rao, M. S. (1992). “The expression of CNTF message and immunoreactivity in the central and peripheral nervous system of the rat”. *Developmental Brain Research*, 66, pp. 209–219. doi: 10.1016/0165-3806(92)90082-8.

Domingues, H. S., …, and Relvas, J. B. (2016). “Oligodendrocyte, astrocyte, and microglia crosstalk in myelin development, damage, and repair”. *Frontiers in Cell and Developmental Biology*, 4, p. 71. doi: 10.3389/fcell.2016.00071.

Dopp, J. M., …, and Merrill, J. E. (1997). “Differential expression, cytokine modulation, and specific functions of type-1 and type-2 tumor necrosis factor receptors in rat glia”. *Journal of Neuroimmunology*, 75, pp. 104–112. doi: 10.1016/s0165-5728(97)00009-x.

Dringen, R. and Hamprecht, B. (1993). “Differences in glycogen metabolism in astroglia-rich primary cultures and sorbitol-selected astroglial cultures derived from mouse brain”. *Glia*, 8, pp. 143–149. doi: 10.1002/glia.440080302.

Dringen, R., Gebhardt, R. and Hamprecht, B. (1993a). “Glycogen in astrocytes: possible function as lactate supply for neighboring cells”. *Brain Research*, 623, pp. 208–214. doi: 10.1016/0006-8993(93)91429-V.

Dringen, R., Wiesinger, H. and Hamprecht, B. (1993b). “Uptake of L-lactate by cultured rat brain neurons”. *Neuroscience Letters*, 163, pp. 5–7. doi: 10.1016/0304-3940(93)90215-7.

Dringen, R., Gutterer, J. M. and Hirrlinger, J. (2000). “Glutathione metabolism in brain”. *European Journal of Biochemistry*, 267, pp. 4912–4916. doi: 10.1046/j.1432-1327.2000.01597.x.

Duncan, I. D., …, and Wierenga, L. A. (2018). “The adult oligodendrocyte can participate in remyelination”. *Proceedings of the National Academy of Sciences*, 115, E11807–E11816. doi: 10.1073/pnas.1808064115.

Ebert, D., Haller, R. G. and Walton, M. E. (2003). “Energy contribution of octanoate to intact rat brain metabolism measured by 13C nuclear magnetic resonance spectroscopy”. *Journal of Neuroscience*, 23, pp. 5928–5935. doi: 10.1523/JNEUROSCI.23-13-05928.2003.

Edgar, J. M., …, and Griffiths, I. R. (2004). “Age-related axonal and myelin changes in the rumpshaker mutation of the Plp gene”. *Acta Neuropathologica*, 107, pp. 331–335. doi: 10.1007/s00401-003-0808-9.

Edgar, J. M., …, and Griffiths, I. R. (2009). “Early ultrastructural defects of axons and axon–glia junctions in mice lacking expression of Cnp1”. *Glia*, 57, pp. 1815–1824. doi: 10.1002/glia.20893.

Edgar, J. M. and Griffiths, I. R. (2014). “Chapter 7 - White Matter Structure: A Microscopist’s View”. *Diffusion MRI (Second Edition)*. San Diego: Academic Press, pp. 127–153. isbn: 978-0-12-396460-1. doi: 10.1016/B978-0-12-396460-1.00007-X.

Edgar, J. M., Smith, R. S. and Duncan, I. D. (2020). “Transmission Electron Microscopy and Morphometry of the CNS White Matter”. *Axon Degeneration: Methods and Protocols*. New York, NY: Springer US, pp. 233–261. isbn: 978-1-07-160585-1. doi: 10.1007/978-1-0716-0585-1_18.

Edgar, J. M., …, and Boullerne, A. (2021). “Río-Hortega’s drawings revisited with fluorescent protein defines a cytoplasm-filled channel system of CNS myelin”. *Journal of Anatomy*, 239, pp. 1241–1255. doi: 10.1111/joa.13577.

Edmond, J., …, and Vellis, J. de (1987). “Capacity for substrate utilization in oxidative metabolism by neurons, astrocytes, and oligodendrocytes from developing brain in primary culture”. *Journal of Neuroscience Research*, 18, pp. 551–561. doi: 10.1002/jnr.490180407.

Escartin, C., …, and Verkhratsky, A. (2021). “Reactive astrocyte nomenclature, definitions, and future directions”. *Nature Neuroscience*, 24, pp. 312–325. doi: 10.1038/s41593-020-00783-4.

Etschmaier, K., …, and Panzenboeck, U. (2011). “Adipose triglyceride lipase affects triacylglycerol metabolism at brain barriers”. *Journal of Neurochemistry*, 119, pp. 1016–1028. doi: 10.1111/j.1471-4159.2011.07498.x.

Faber, D. S. and Pereda, A. E. (2018). “Two forms of electrical transmission between neurons”. *Frontiers in Molecular Neuroscience*, 11, p. 427. doi: 10.3389/fnmol.2018.00427.

Fadó, R., Rodríguez-Rodríguez, R. and Casals, N. (2021). “The return of malonyl-CoA to the brain: cognition and other stories”. *Progress in Lipid Research*, 81, p. 101071. doi: 10.1016/j.plipres.2020.101071.

Falkowska, A., …, and Baranowska-Bosiacka, I. (2015). “Energy metabolism of the brain, including the cooperation between astrocytes and neurons, especially in the context of glycogen metabolism”. *International Journal of Molecular Sciences*, 16, pp. 25959–25981. doi: 10.3390/ijms161125939.

Fancy, S. P. J., …, and Rowitch, D. H. (2009). “Dysregulation of the Wnt pathway inhibits timely myelination and remyelination in the mammalian CNS”. *Genes & Development*, 23, pp. 1571–1585. doi: 10.1101/gad.1806309.

Fancy, S. P. J., …, and Rowitch, D. H. (2011). “Axin2 as regulatory and therapeutic target in newborn brain injury and remyelination”. *Nature Neuroscience*, 14, pp. 1009–1016. doi: 10.1038/nn.2855.

Fard, M. K., …, and Simons, M. (2017). “BCAS1 expression defines a population of early myelinating oligodendrocytes in multiple sclerosis lesions”. *Science Translational Medicine*, 9. doi: 10.1126/scitranslmed.aam7816.

Farmer, B. C., Kluemper, J. and Johnson, L. A. (2019). “Apolipoprotein E4 alters astrocyte fatty acid metabolism and lipid droplet formation”. *Cells*, 8, p. 182. doi: 10.3390/cells8020182.

Fields, R. D. (2008). “White matter in learning, cognition and psychiatric disorders”. *Trends in Neurosciences*, 31, pp. 361–370. doi: 10.1016/j.tins.2008.04.001.

Fields, R. D., Woo, D. H. and Basser, P. J. (2015). “Glial regulation of the neuronal connectome through local and long-distant communication”. *Neuron*, 86, pp. 374–386. doi: 10.1016/j.neuron.2015.01.014.

Floriddia, E. M., …, and Castelo-Branco, G. (2020). “Distinct oligodendrocyte populations have spatial preference and different responses to spinal cord injury”. *Nature Communications*, 11, p. 5860. doi: 10.1038/s41467-020-19453-x.

Follett, P. L., …, and Jensen, F. E. (2000). “NBQX attenuates excitotoxic injury in developing white matter”. *The Journal of Neuroscience*, 20, pp. 9235–9241. doi: 10.1523/jneurosci.20-24-09235.2000.

Follett, P. L., …, and Jensen, F. E. (2004). “Glutamate receptor-mediated oligodendrocyte toxicity in periventricular leukomalacia: A protective role for topiramate”. *Journal of Neuroscience*, 24, pp. 4412–4420. doi: 10.1523/JNEUROSCI.0477-04.2004.

Foran, D. R. and Peterson, A. C. (1992). “Myelin acquisition in the central nervous system of the mouse revealed by an MBP-Lac Z transgene”. *Journal of Neuroscience*, 12, pp. 4890–4897. doi: 10.1523/JNEUROSCI.12-12-04890.1992.

Foster, P. C. and Bailey, E. (1976). “Changes in hepatic fatty acid degradation and blood lipid and ketone body content during development of the rat”. *Enzyme*, 21, pp. 397–407. doi: 10.1159/000458889.

Franklin, R. J. M. and ffrench-Constant, C. (2017). “Regenerating CNS myelin — from mechanisms to experimental medicines”. *Nature Reviews Neuroscience*, 18, pp. 753–769. doi: 10.1038/nrn.2017.136.

French, H. M., …, and Grinspan, J. B. (2009). “Oxidative stress disrupts oligodendrocyte maturation”. *Journal of Neuroscience Research*, 87, pp. 3076–3087. doi: 10.1002/jnr.22139.

Froberg, M. K., …, and Drewes, L. R. (2001). “Expression of monocarboxylate transporter MCT1 in normal and neoplastic human CNS tissues”. *NeuroReport*, 12, pp. 761–765. doi: 10.1097/00001756-200103260-00030.

Fu, H., …, and Stiles, C. D. (2009). “A genome-wide screen for spatially restricted expression patterns identifies transcription factors that regulate glial development”. *The Journal of Neuroscience*, 29, pp. 11399–11408. doi: 10.1523/JNEUROSCI.0160-09.2009.

Fünfschilling, U., …, and Nave, K.-A. (2012). “Glycolytic oligodendrocytes maintain myelin and long-term axonal integrity”. *Nature*, 485, pp. 517–521. doi: 10.1038/nature11007.

Garg, S., Syed, M. M. and Kielian, T. (2005). “Staphylococcus aureus-derived peptidoglycan induces Cx43 expression and functional gap junction intercellular communication in microglia”. *Journal of Neurochemistry*, 95, pp. 475–483. doi: 10.1111/j.1471-4159.2005.03384.x.

Gauthier-Coles, G., …, and Bröer, S. (2021). “Quantitative modelling of amino acid transport and homeostasis in mammalian cells”. *Nature Communications*, 12, p. 5282. doi: 10.1038/s41467-021-25563-x.

Gerdes, H.-H., Bukoreshtliev, N. V. and Barroso, J. F. V. (2007). “Tunneling nanotubes: A new route for the exchange of components between animal cells”. *FEBS Letters*, 581, pp. 2194–2201. doi: 10.1016/j.febslet.2007.03.071.

Gerhart, D. Z., …, and Drewes, L. R. (1997). “Expression of monocarboxylate transporter MCT1 by brain endothelium and glia in adult and suckling rats”. *The American Journal of Physiology*, 273 (1 Pt 1), E207–213. doi: 10.1152/ajpendo.1997.273.1.E207.

Geyer, R. P., Matthews, L. W. and Stare, F. J. (1949). “Metabolism of emulsified trilaurin (-C1400-) and octanoic acid (-C1400-) by rat tissue slices”. *The Journal of Biological Chemistry*, 180, pp. 1037–1045.

Ghoumari, A. M., Baulieu, E. E. and Schumacher, M. (2005). “Progesterone increases oligodendroglial cell proliferation in rat cerebellar slice cultures”. *Neuroscience*, 135, pp. 47–58. doi: 10.1016/j.neuroscience.2005.05.023.

Gibson, E. M., …, and Monje, M. (2014). “Neuronal activity promotes oligodendrogenesis and adaptive myelination in the mammalian brain”. *Science*, 344. doi: 10.1126/science.1252304.

Gilles, F. H. (1976). “Myelination in the neonatal brain”. *Human Pathology*, 7, pp. 244–248. doi: 10.1016/S0046-8177(76)80035-4.

Gillilan, L. A. (1958). “The arterial blood supply of the human spinal cord”. *The Journal of Comparative Neurology*, 110, pp. 75–103. doi: 10.1002/cne.901100104.

Ginhoux, F. and Merad, M. (2011). “Les cellules de la microglie - leurs origines extra-embryonnaires enfin révélées”. *Médecine/Sciences*, 27, pp. 719–724. doi: 10.1051/medsci/2011278013.

Ginhoux, F. and Guilliams, M. (2016). “Tissue-resident macrophage ontogeny and homeostasis”. *Immunity*, 44, pp. 439–449. doi: 10.1016/j.immuni.2016.02.024.

Glatz, J. F. C. and van der Vusse, G. J. (1996). “Cellular fatty acid-binding proteins: their function and physiological significance”. *Progress in Lipid Research*, 35, pp. 243–282. doi: 10.1016/S0163-7827(96)00006-9.

Glatz, J. F. C., Luiken, J. J. F. P. and Bonen, A. (2010). “Membrane fatty acid transporters as regulators of lipid metabolism: implications for metabolic disease”. *Physiological Reviews*, 90, pp. 367–417. doi: 10.1152/physrev.00003.2009.

Glick, D., Barth, S. and Macleod, K. F. (2010). “Autophagy: cellular and molecular mechanisms”. *The Journal of Pathology*, 221, pp. 3–12. doi: 10.1002/path.2697.

Goebbels, S., …, and Nave, K.-A. (2017). “A neuronal PI(3,4,5)P3 -dependent program of oligodendrocyte precursor recruitment and myelination”. *Nature Neuroscience*, 20, pp. 10–15. doi: 10.1038/nn.4425.

Goedhart, J. and Luijsterburg, M. S. (2020). “VolcaNoseR is a web app for creating, exploring, labeling and sharing volcano plots”. *Scientific Reports*, 10, p. 20560. doi: 10.1038/s41598-020-76603-3.

Goldberg, M. and Choi, D. (1993). “Combined oxygen and glucose deprivation in cortical cell culture: calcium-dependent and calcium-independent mechanisms of neuronal injury”. *The Journal of Neuroscience*, 13, pp. 3510–3524. doi: 10.1523/JNEUROSCI.13-08-03510.1993.

Gómez-Hernández, J. M., …, and Barrio, L. C. (2003). “Molecular basis of calcium regulation in connexin-32 hemichannels”. *Proceedings of the National Academy of Sciences*, 100, pp. 16030–16035. doi: 10.1073/pnas.2530348100.

Goodenough, D. A. and Paul, D. L. (2009). “Gap junctions”. *Cold Spring Harbor Perspectives in Biology*, 1, a002576. doi: 10.1101/cshperspect.a002576.

Gousset, K., …, and Zurzolo, C. (2009). “Prions hijack tunnelling nanotubes for intercellular spread”. *Nature Cell Biology*, 11, pp. 328–336. doi: 10.1038/ncb1841.

Gray, J. and Ross, M. E. (2011). “Neural tube closure in mouse whole embryo culture”. *Journal of Visualized Experiments: JoVE*, p. 3132. doi: 10.3791/3132.

Griffiths, I., …, and Nave, K. A. (1998). “Axonal swellings and degeneration in mice lacking the major proteolipid of myelin”. *Science*, 280, pp. 1610–1613. doi: 10.1126/science.280.5369.1610.

Gruenenfelder, F. I., …, and Edgar, J. M. (2020). “Neural stem cells restore myelin in a demyelinating model of Pelizaeus-Merzbacher disease”. *Brain*, 143, pp. 1383–1399. doi: 10.1093/brain/awaa080.

Guérout, N., Li, X. and Barnabé-Heider, F. (2014). “Cell fate control in the developing central nervous system”. *Experimental Cell Research*, 321, pp. 77–83. doi: 10.1016/j.yexcr.2013.10.003.

Guo, Y., …, and Walther, T. C. (2009). “Lipid droplets at a glance”. *Journal of Cell Science*, 122, pp. 749–752. doi: 10.1242/jcs.037630.

Guzmán, M. and Blázquez, C. (2004). “Ketone body synthesis in the brain: possible neuroprotective effects”. *Prostaglandins, Leukotrienes and Essential Fatty Acids*, 70, pp. 287–292. doi: 10.1016/j.plefa.2003.05.001.

Haim, L. B. and Rowitch, D. H. (2017). “Functional diversity of astrocytes in neural circuit regulation”. *Nature Reviews Neuroscience*, 18, pp. 31–41. doi: 10.1038/nrn.2016.159.

Hall, E. T., …, and Ogden, S. K. (2021). “Cytoneme delivery of Sonic Hedgehog from ligand-producing cells requires Myosin 10 and a Dispatched-BOC/CDON co-receptor complex”. *eLife*, 10, e61432. doi: 10.7554/eLife.61432.

Hamilton, G. and Gillingwater, T. H. (2013). “Spinal muscular atrophy: going beyond the motor neuron”. *Trends in Molecular Medicine*, 19, pp. 40–50. doi: 10.1016/j.molmed.2012.11.002.

Hampson, E. C. and Robinson, S. R. (1995). “Heterogeneous morphology and tracer coupling patterns of retinal oligodendrocytes”. *Philosophical Transactions of the Royal Society of London. Series B, Biological Sciences*, 349, pp. 353–364. doi: 10.1098/rstb.1995.0124.

Hanrahan, J. D., …, and Edwards, A. D. (1996). “Cerebral metabolism within 18 hours of birth asphyxia: A proton magnetic resonance spectroscopy study”. *Pediatric Research*, 39, pp. 584–590. doi: 10.1203/00006450-199604000-00004.

Harris, J. J., Jolivet, R. and Attwell, D. (2012). “Synaptic energy use and supply”. *Neuron*, 75, pp. 762–777. doi: 10.1016/j.neuron.2012.08.019.

Harrison, R. G., …, and Jackson, C. M. (1907). “Observations of the living developing nerve fiber”. *The Anatomical Record*, 1, pp. 116–128. doi: 10.1002/ar.1090010503.

Harrison, R. G. (1910). “The outgrowth of the nerve fiber as a mode of protoplasmic movement”. *Journal of Experimental Zoology*, 9, pp. 787–846. doi: 10.1002/jez.1400090405.

Hasegawa, M., …, and Ohno, T. (1992). “Development of myelination in the human fetal and infant cerebrum: a myelin basic protein immunohistochemical study”. *Brain & Development*, 14, pp. 1–6. doi: 10.1016/s0387-7604(12)80271-3.

Hawkins, R. A., Williamson, D. H. and Krebs, H. A. (1971). “Ketone-body utilization by adult and suckling rat brain in vivo”. *Biochemical Journal*, 122, pp. 13–18. doi: 10.1042/bj1220013.

He, C. and Klionsky, D. J. (2009). “Regulation mechanisms and signaling pathways of autophagy”. *Annual Review of Genetics*, 43, pp. 67–93. doi: 10.1146/annurev-genet-102808-114910.

Hernández-Fonseca, K., …, and Massieu, L. (2008). “Calcium-dependent production of reactive oxygen species is involved in neuronal damage induced during glycolysis inhibition in cultured hippocampal neurons”. *Journal of Neuroscience Research*, 86, pp. 1768–1780. doi: 10.1002/jnr.21634.

Hernandez-Gerez, E., Fleming, I. N. and Parson, S. H. (2019). “A role for spinal cord hypoxia in neurodegeneration”. *Cell Death & Disease*, 10, pp. 1–8. doi: 10.1038/s41419-019-2104-1.

Hernandez-Gerez, E., …, and Parson, S. H. (2020). “Widespread tissue hypoxia dysregulates cell and metabolic pathways in SMA”. *Annals of Clinical and Translational Neurology*, 7, pp. 1580–1593. doi: 10.1002/acn3.51134.

Herrero-Mendez, A., …, and Bolaños, J. P. (2009). “The bioenergetic and antioxidant status of neurons is controlled by continuous degradation of a key glycolytic enzyme by APC/C-Cdh1”. *Nature Cell Biology*, 11, pp. 747–752. doi: 10.1038/ncb1881.

Hertz, L., Gibbs, M. E. and Dienel, G. A. (2014). “Fluxes of lactate into, from, and among gap junction-coupled astrocytes and their interaction with noradrenaline”. *Frontiers in Neuroscience*, 8, p. 261. doi: 10.3389/fnins.2014.00261.

Herzig, S., …, and Martinou, J.-C. (2012). “Identification and functional expression of the mitochondrial pyruvate carrier”. *Science*, 337, pp. 93–96. doi: 10.1126/science.1218530.

Hesp, Z. C., …, and McTigue, D. M. (2015). “Chronic oligodendrogenesis and remyelination after spinal cord injury in mice and rats”. *Journal of Neuroscience*, 35, pp. 1274–1290. doi: 10.1523/JNEUROSCI.2568-14.2015.

Hildebrand, C., …, and Bjartmar, C. (1993). “Myelinated nerve fibres in the CNS”. *Progress in Neurobiology*, 40, pp. 319–384. doi: 10.1016/0301-0082(93)90015-K.

Hill, R. A., Li, A. M. and Grutzendler, J. (2018). “Lifelong cortical myelin plasticity and age-related degeneration in the live mammalian brain”. *Nature Neuroscience*, 21, pp. 683–695. doi: 10.1038/s41593-018-0120-6.

Himwich, H. E. and Nahum, L. H. (1929). “Respiratory quotient of the brain.” *Proceedings of the Society for Experimental Biology and Medicine*, 26, pp. 496–497. doi: 10.3181/00379727-26-4362.

Hinds, J. W. (1968). “Autoradiographic study of histogenesis in the mouse olfactory bulb. I. Time of origin of neurons and neuroglia”. *The Journal of Comparative Neurology*, 134, pp. 287–304. doi: 10.1002/cne.901340304.

Hines, J. H., …, and Appel, B. (2015). “Neuronal activity biases axon selection for myelination in vivo”. *Nature Neuroscience*, 18, pp. 683–689. doi: 10.1038/nn.3992.

Hirokawa, N., …, and Niwa, S. (2009). “Kinesin superfamily motor proteins and intracellular transport”. *Nature Reviews Molecular Cell Biology*, 10, pp. 682–696. doi: 10.1038/nrm2774.

Hirrlinger, J. and Dringen, R. (2010). “The cytosolic redox state of astrocytes: Maintenance, regulation and functional implications for metabolite trafficking”. *Brain Research Reviews*, 63, pp. 177–188. doi: 10.1016/j.brainresrev.2009.10.003.

Hirrlinger, J. and Nave, K.-A. (2014). “Adapting brain metabolism to myelination and long-range signal transduction”. *Glia*, 62, pp. 1749–1761. doi: 10.1002/glia.22737.

Hisahara, S., …, and Miura, M. (1997). “ICE/CED-3 family executes oligodendrocyte apoptosis by tumor necrosis factor”. *Journal of Neurochemistry*, 69, pp. 10–20. doi: 10.1046/j.1471-4159.1997.69010010.x.

Hochstim, C., …, and Anderson, D. J. (2008). “Identification of positionally distinct astrocyte subtypes whose identities are specified by a homeodomain code”. *Cell*, 133, pp. 510–522. doi: 10.1016/j.cell.2008.02.046.

Hofmann, K., …, and Kuerschner, L. (2017). “Astrocytes and oligodendrocytes in grey and white matter regions of the brain metabolize fatty acids”. *Scientific Reports*, 7, p. 10779. doi: 10.1038/s41598-017-11103-5.

Hosokawa, N., Hara, Y. and Mizushima, N. (2006). “Generation of cell lines with tetracycline-regulated autophagy and a role for autophagy in controlling cell size”. *FEBS Letters*, 580, pp. 2623–2629. doi: 10.1016/j.febslet.2006.04.008.

Howarth, C., Gleeson, P. and Attwell, D. (2012). “Updated energy budgets for neural computation in the neocortex and cerebellum”. *Journal of Cerebral Blood Flow and Metabolism*, 32, pp. 1222–1232. doi: 10.1038/jcbfm.2012.35.

Howarth, C. (2014). “The contribution of astrocytes to the regulation of cerebral blood flow”. *Frontiers in Neuroscience*, 8, p. 103. doi: 10.3389/fnins.2014.00103.

Hughes, A. N. and Appel, B. (2020). “Microglia phagocytose myelin sheaths to modify developmental myelination”. *Nature Neuroscience*, 23, pp. 1055–1066. doi: 10.1038/s41593-020-0654-2.

Hughes, E. G., …, and Bergles, D. E. (2018). “Myelin remodeling through experience-dependent oligodendrogenesis in the adult somatosensory cortex”. *Nature Neuroscience*, 21, pp. 696–706. doi: 10.1038/s41593-018-0121-5.

Hutchins, K. D., …, and Lyman, W. D. (1990). “Localization of morphologically distinct microglial populations in the developing human fetal brain: implications for ontogeny”. *Developmental Brain Research*, 55, pp. 95–102. doi: 10.1016/0165-3806(90)90109-C.

Iadecola, C., …, and Ross, M. E. (1995). “Inducible nitric oxide synthase gene expression in brain following cerebral ischemia”. *Journal of Cerebral Blood Flow and Metabolism*, 15, pp. 378–384. doi: 10.1038/jcbfm.1995.47.

Ikonen, E. (2008). “Cellular cholesterol trafficking and compartmentalization”. *Nature Reviews Molecular Cell Biology*, 9, pp. 125–138. doi: 10.1038/nrm2336.

Ishibashi, T., …, and Fields, R. D. (2009). “Leukemia inhibitory factor regulates the timing of oligodendrocyte development and myelination in the postnatal optic nerve”. *Journal of Neuroscience Research*, 87, pp. 3343–3355. doi: 10.1002/jnr.22173.

Jablonska, B., …, and Gallo, V. (2016). “Sirt1 regulates glial progenitor proliferation and regeneration in white matter after neonatal brain injury”. *Nature Communications*, 7, p. 13866. doi: 10.1038/ncomms13866.

Jagielska, A., Wilhite, K. D. and Vliet, K. J. V. (2013). “Extracellular acidic pH inhibits oligodendrocyte precursor viability, migration, and differentiation”. *PLOS ONE*, 8, e76048. doi: 10.1371/journal.pone.0076048.

Jahn, O., Tenzer, S. and Werner, H. B. (2009). “Myelin proteomics: molecular anatomy of an insulating sheath”. *Molecular Neurobiology*, 40, pp. 55–72. doi: 10.1007/s12035-009-8071-2.

James, O. G., …, and Chandran, S. (2021). “iPSC-derived myelinoids to study myelin biology of humans”. *Developmental Cell*, 56, 1346–1358.e6. doi: 10.1016/j.devcel.2021.04.006.

Jastroch, M., …, and Brand, M. D. (2010). “Mitochondrial proton and electron leaks”. *Essays in Biochemistry*, 47, pp. 53–67. doi: 10.1042/bse0470053.

Jernberg, J. N., …, and Scafidi, S. (2017). “Developmental regulation and localization of carnitine palmitoyltransferases (CPTs) in rat brain”. *Journal of Neurochemistry*, 142, pp. 407–419. doi: 10.1111/jnc.14072.

Jha, M. K., …, and Suk, K. (2018). “Functional dissection of astrocyte-secreted proteins: Implications in brain health and diseases”. *Progress in Neurobiology*, 162, pp. 37–69. doi: 10.1016/j.pneurobio.2017.12.003.

Jurewicz, A., …, and Selmaj, K. (2005). “Tumour necrosis factor-induced death of adult human oligodendrocytes is mediated by apoptosis inducing factor”. *Brain*, 128 (Pt 11), pp. 2675–2688. doi: 10.1093/brain/awh627.

Juurlink, B. H., Hertz, L. and Yager, J. Y. (1992). “Astrocyte maturation and susceptibility to ischaemia or substrate deprivation”. *NeuroReport*, 3, pp. 1135–1137. doi: 10.1097/00001756-199212000-00026.

Juurlink, B. H., Thorburne, S. K. and Hertz, L. (1998). “Peroxide-scavenging deficit underlies oligodendrocyte susceptibility to oxidative stress”. *Glia*, 22, pp. 371–378. doi: 10.1002/(sici)1098-1136(199804)22:4<371::aid-glia6>3.0.co;2-6.

Kabat, H. and Anderson, J. P. (1943). “Acute arrest of cerebral circulation in man”. *Archives of Neurology & Psychiatry*, 50, pp. 510–528. doi: 10.1001/archneurpsyc.1943.02290230022002.

Kadenbach, B. (2003). “Intrinsic and extrinsic uncoupling of oxidative phosphorylation”. *Biochimica Et Biophysica Acta*, 1604, pp. 77–94. doi: 10.1016/s0005-2728(03)00027-6.

Kardon, J. R. and Vale, R. D. (2009). “Regulators of the cytoplasmic dynein motor”. *Nature Reviews Molecular Cell Biology*, 10, pp. 854–865. doi: 10.1038/nrm2804.

Karsai, G., …, and Kurth, I. (2019). “DEGS1-associated aberrant sphingolipid metabolism impairs nervous system function in humans”. *The Journal of Clinical Investigation*, 129, pp. 1229–1239. doi: 10.1172/JCI124159.

Kassmann, C. M., …, and Nave, K.-A. (2011). “A role for myelin-associated peroxisomes in maintaining paranodal loops and axonal integrity”. *FEBS Letters*, 585, pp. 2205–2211. doi: 10.1016/j.febslet.2011.05.032.

Kassmann, C. M. (2014). “Myelin peroxisomes - essential organelles for the maintenance of white matter in the nervous system”. *Biochimie*, 98, pp. 111–118. doi: 10.1016/j.biochi.2013.09.020.

Kessaris, N., …, and Richardson, W. D. (2006). “Competing waves of oligodendrocytes in the forebrain and postnatal elimination of an embryonic lineage”. *Nature Neuroscience*, 9, pp. 173–179. doi: 10.1038/nn1620.

Kety, S. S. and Schmidt, C. F. (1948). “The nitrous oxide method for the quantitative determination of cerebral blood flow in man: theory, procedure and normal values”. *Journal of Clinical Investigation*, 27, pp. 476–483. doi: 10.1172/jci101994.

Kihara, A. (2012). “Very long-chain fatty acids: elongation, physiology and related disorders”. *Journal of Biochemistry*, 152, pp. 387–395. doi: 10.1093/jb/mvs105.

Kim, T.-K., …, and Kim, Y.-B. (2018). “Improvement by human oligodendrocyte progenitor cells of neurobehavioral disorders in an experimental model of neonatal periventricular leukomalacia”. *Cell Transplantation*, 27, pp. 1168–1177. doi: 10.1177/0963689718781330.

Kinney, H. C., …, and Kirschner, D. A. (1994). “Myelination in the developing human brain: biochemical correlates”. *Neurochemical Research*, 19, pp. 983–996. doi: 10.1007/BF00968708.

Kinney, H. C. and Back, S. A. (1998). “Human oligodendroglial development: relationship to periventricular leukomalacia”. *Seminars in Pediatric Neurology*, 5, pp. 180–189. doi: 10.1016/s1071-9091(98)80033-8.

Kirby, B. B., …, and Appel, B. (2006). “In vivo time-lapse imaging shows dynamic oligodendrocyte progenitor behavior during zebrafish development”. *Nature Neuroscience*, 9, pp. 1506–1511. doi: 10.1038/nn1803.

Kirischuk, S., …, and Kettenmann, H. (1995). “Preferential localization of active mitochondria in process tips of immature retinal oligodendrocytes”. *NeuroReport*, 6, pp. 737–741. url: https://journals.lww.com/neuroreport/Abstract/1995/03270/Preferential_localization_of_active_mitochondria.8.aspx (visited on 06/09/2021).

Kleopa, K. A. and Scherer, S. S. (2006). “Molecular genetics of X-linked Charcot-Marie-Tooth disease”. *Neuromolecular Medicine*, 8, pp. 107–122. doi: 10.1385/nmm:8:1-2:107.

Koehler-Stec, E. M., …, and Landschulz, W. H. (1998). “Monocarboxylate transporter expression in mouse brain”. *American Journal of Physiology. Endocrinology and Metabolism*, 275, E516–E524. doi: 10.1152/ajpendo.1998.275.3.E516.

Kogel, V., …, and Seitz, J. (2021). “Long-term glucose starvation induces inflammatory responses and phenotype switch in primary cortical rat astrocytes”. *Journal of Molecular Neuroscience*. doi: 10.1007/s12031-021-01800-2.

Kotter, M. R., …, and Franklin, R. J. M. (2006). “Myelin impairs CNS remyelination by inhibiting oligodendrocyte precursor cell differentiation”. *The Journal of Neuroscience*, 26, pp. 328–332. doi: 10.1523/JNEUROSCI.2615-05.2006.

Kounakis, K., …, and Tavernarakis, N. (2019). “Emerging roles of lipophagy in health and disease”. *Frontiers in Cell and Developmental Biology*, 7, p. 185. doi: 10.3389/fcell.2019.00185.

Kralingen, C. van, …, and Graham, E. S. (2013). “Exposure to inflammatory cytokines IL-1β and TNFα induces compromise and death of astrocytes; implications for chronic neuroinflammation”. *PLOS ONE*, 8, e84269. doi: 10.1371/journal.pone.0084269.

Krupinski, J., …, and Wang, J. M. (1994). “Role of angiogenesis in patients with cerebral ischemic stroke”. *Stroke*, 25, pp. 1794–1798. doi: 10.1161/01.str.25.9.1794.

Kuhn, S., …, and Dombrowski, Y. (2019). “Oligodendrocytes in development, myelin generation and beyond”. *Cells*, 8, p. 1424. doi: 10.3390/cells8111424.

Kuno, R., …, and Suzumura, A. (2005). “Autocrine activation of microglia by tumor necrosis factor-alpha”. *Journal of Neuroimmunology*, 162, pp. 89–96. doi: 10.1016/j.jneuroim.2005.01.015.

Lauritzen, F., Eid, T. and Bergersen, L. H. (2015). “Monocarboxylate transporters in temporal lobe epilepsy: roles of lactate and ketogenic diet”. *Brain Structure & Function*, 220, pp. 1–12. doi: 10.1007/s00429-013-0672-x.

Lawson, L. J., …, and Gordon, S. (1990). “Heterogeneity in the distribution and morphology of microglia in the normal adult mouse brain”. *Neuroscience*, 39, pp. 151–170. doi: 10.1016/0306-4522(90)90229-W.

Lebrun-Julien, F., …, and Suter, U. (2014). “Balanced mTORC1 activity in oligodendrocytes is required for accurate CNS myelination”. *The Journal of Neuroscience*, 34, pp. 8432–8448. doi: 10.1523/JNEUROSCI.1105-14.2014.

Lee, H. K., …, and Deneen, B. (2015). “Daam2-PIP5K is a regulatory pathway for Wnt signaling and therapeutic target for remyelination in the CNS”. *Neuron*, 85, pp. 1227–1243. doi: 10.1016/j.neuron.2015.02.024.

Lee, J. C., Mayer-Proschel, M. and Rao, M. S. (2000). “Gliogenesis in the central nervous system”. *Glia*, 30, pp. 105–121. doi: 10.1002/(SICI)1098-1136(200004)30:2<105::AID-GLIA1>3.0.CO;2-H.

Lee, J. A., …, and Allen, S. P. (2021). “Lipid metabolism in astrocytic structure and function”. *Seminars in Cell & Developmental Biology*, 112, pp. 123–136. doi: 10.1016/j.semcdb.2020.07.017.

Lee, S. C., …, and Raine, C. S. (1990). “Multiple sclerosis: a role for astroglia in active demyelination suggested by class II MHC expression and ultrastructural study”. *Journal of*

Neuropathology and Experimental Neurology, 49, pp. 122–136. doi: 10.1097/00005072-199003000-00005.

Lee, S., …, and Chan, J. R. (2012). “A culture system to study oligodendrocyte myelination processes using engineered nanofibers”. *Nature Methods*, 9, pp. 917–922. doi: 10.1038/nmeth.2105.

Lee, S., …, and Chan, J. R. (2013). “A rapid and reproducible assay for modeling myelination by oligodendrocytes using engineered nanofibers”. *Nature Protocols*, 8, pp. 771–782. doi: 10.1038/nprot.2013.039.

Leino, R. L., Gerhart, D. Z. and Drewes, L. R. (1999). “Monocarboxylate transporter (MCT1) abundance in brains of suckling and adult rats: a quantitative electron microscopic immunogold study”. *Brain Research. Developmental Brain Research*, 113, pp. 47–54. doi: 10.1016/s0165-3806(98)00188-6.

Leone, D. P., …, and Suter, U. (2003). “Tamoxifen-inducible glia-specific Cre mice for somatic mutagenesis in oligodendrocytes and Schwann cells”. *Molecular and Cellular Neuroscience*, 22, pp. 430–440. doi: 10.1016/S1044-7431(03)00029-0.

Levine, J. M., Reynolds, R. and Fawcett, J. W. (2001). “The oligodendrocyte precursor cell in health and disease”. *Trends in Neurosciences*, 24, pp. 39–47. doi: 10.1016/S0166-2236(00)01691-X.

Li, L., …, and Stary, C. M. (2021). “MicroRNA-338 inhibition protects against focal cerebral ischemia and preserves mitochondrial function in vitro in astrocytes and neurons via COX4I1”. *Mitochondrion*, 59, pp. 105–112. doi: 10.1016/j.mito.2021.04.013.

Li, Y., …, and Yao, L. (2014). “Nanofibers support oligodendrocyte precursor cell growth and function as a neuron-free model for myelination study”. *Biomacromolecules*, 15, pp. 319–326. doi: 10.1021/bm401558c.

Liedtke, W., …, and Raine, C. S. (1996). “GFAP is necessary for the integrity of CNS white matter architecture and long-term maintenance of myelination”. *Neuron*, 17, pp. 607–615. doi: 10.1016/s0896-6273(00)80194-4.

Lin, S.-T., …, and Fu, Y.-H. (2013). “MicroRNA-23a promotes myelination in the central nervous system”. *Proceedings of the National Academy of Sciences*, 110, pp. 17468–17473. doi: 10.1073/pnas.1317182110.

Liu, L., …, and Wang, R. (2016). “Proinflammatory signal suppresses proliferation and shifts macrophage metabolism from Myc-dependent to HIF1α-dependent”. *Proceedings of the National Academy of Sciences*, 113, pp. 1564–1569. doi: 10.1073/pnas.1518000113.

Liu, P., Du, J.-L. and He, C. (2013a). “Developmental pruning of early-stage myelin segments during CNS myelination in vivo”. *Cell Research*, 23, pp. 962–964. doi: 10.1038/cr.2013.62.

Liu, X.-B., …, and Deng, W. (2013b). “Vulnerability of premyelinating oligodendrocytes to white-matter damage in neonatal brain injury”. *Neuroscience Bulletin*, 29, pp. 229–238. doi: 10.1007/s12264-013-1311-5.

Loewenstein, W. R. (1981). “Junctional intercellular communication: the cell-to-cell membrane channel”. *Physiological Reviews*, 61, pp. 829–913. doi: 10.1152/physrev.1981.61.4.829.

Lord, S. J., …, and Fritz-Laylin, L. K. (2020). “SuperPlots: communicating reproducibility and variability in cell biology”. *Journal of Cell Biology*, 219. doi: 10.1083/jcb.202001064.

Lorek, A., …, and Reynolds, E. O. R. (1994). “Delayed (“secondary”) cerebral energy failure after acute hypoxia-ischemia in the newborn piglet: continuous 48-hour studies by phosphorus magnetic resonance spectroscopy”. *Pediatric Research*, 36, pp. 699–706. doi: 10.1203/00006450-199412000-00003.

Lu, Q. R., …, and Rowitch, D. H. (2002). “Common developmental requirement for olig function indicates a motor Neuron/Oligodendrocyte connection”. *Cell*, 109, pp. 75–86. doi: 10.1016/S0092-8674(02)00678-5.

Lum, J. J., …, and Thompson, C. B. (2005). “Growth factor regulation of autophagy and cell survival in the absence of apoptosis”. *Cell*, 120, pp. 237–248. doi: 10.1016/j.cell.2004.11.046.

Luse, S. A. (1956). “Formation of myelin in the central nervous system of mice and rats, as studied with the electron microscope”. *The Journal of Biophysical and Biochemical Cytology*, 2, pp. 777–784. doi: 10.1083/jcb.2.6.777.

Lyons, S. A. and Kettenmann, H. (1998). “Oligodendrocytes and microglia are selectively vulnerable to combined hypoxia and hypoglycemia injury in vitro”. *Journal of Cerebral Blood Flow and Metabolism*, 18, pp. 521–530. doi: 10.1097/00004647-199805000-00007.

Madisen, L., …, and Zeng, H. (2010). “A robust and high-throughput Cre reporting and characterization system for the whole mouse brain”. *Nature Neuroscience*, 13, pp. 133–40. doi: 10.1038/nn.2467.

Magistretti, P. J. and Pellerin, L. (1999). “Astrocytes couple synaptic activity to glucose utilization in the brain”. *Physiology*, 14, pp. 177–182. doi: 10.1152/physiologyonline.1999.14.5.177.

Magistretti, P. J. and Allaman, I. (2015). “A cellular perspective on brain energy metabolism and functional imaging”. *Neuron*, 86, pp. 883–901. doi: 10.1016/j.neuron.2015.03.035.

Maglione, M., …, and Kettenmann, H. (2010). “Oligodendrocytes in mouse corpus callosum are coupled via gap junction channels formed by connexin47 and connexin32”. *Glia*, 58, pp. 1104–1117. doi: 10.1002/glia.20991.

Maher, F., Vannucci, S. J. and Simpson, I. A. (1994). “Glucose transporter proteins in brain”. *FASEB Journal*, 8, pp. 1003–1011. doi: 10.1096/fasebj.8.13.7926364.

Marschallinger, J., …, and Wyss-Coray, T. (2020). “Lipid-droplet-accumulating microglia represent a dysfunctional and proinflammatory state in the aging brain”. *Nature Neuroscience*, 23, pp. 194–208. doi: 10.1038/s41593-019-0566-1.

Martirosyan, N. L., …, and Preul, M. C. (2011). “Blood supply and vascular reactivity of the spinal cord under normal and pathological conditions”. *Journal of Neurosurgery. Spine*, 15, pp. 238–251. doi: 10.3171/2011.4.SPINE10543.

Matcovitch-Natan, O., …, and Amit, I. (2016). “Microglia development follows a stepwise program to regulate brain homeostasis”. *Science*, 353. doi: 10.1126/science.aad8670.

Matthews, M. A. and Duncan, D. (1971). “A quantitative study of morphological changes accompanying the initiation and progress of myelin production in the dorsal funiculus of the rat spinal cord”. *Journal of Comparative Neurology*, 142, pp. 1–22. doi: 10.1002/cne.901420102.

Mayer-Pröschel, M. (1998). “Isolation and generation of oligodendrocytes by immunopanning”. *Current Protocols in Neuroscience*, 3, pp. 3.13.1–3.13.11. doi: 10.1002/0471142301.ns0313s00.

Mazumder, R., …, and Ochoa, S. (1961). “A new enzyme in the conversion of propionyl coenzyme A to succinyl coenzyme A”. *The Journal of Biological Chemistry*, 236, PC53–55.

McCarthy, K. D. and de Vellis, J. (1980). “Preparation of separate astroglial and oligodendroglial cell cultures from rat cerebral tissue”. *The Journal of Cell Biology*, 85, pp. 890–902. doi: 10.1083/jcb.85.3.890.

McGarry, J. D., Mannaerts, G. P. and Foster, D. W. (1977). “A possible role for malonyl-CoA in the regulation of hepatic fatty acid oxidation and ketogenesis.” *The Journal of Clinical Investigation*, 60, pp. 265–270. doi: 10.1172/JCI108764.

McKimmie, C. S. and Fazakerley, J. K. (2005). “In response to pathogens, glial cells dynamically and differentially regulate Toll-like receptor gene expression”. *Journal of Neuroimmunology*, 169, pp. 116–125. doi: 10.1016/j.jneuroim.2005.08.006.

Mensch, S., …, and Lyons, D. A. (2015). “Synaptic vesicle release regulates myelin sheath number of individual oligodendrocytes in vivo”. *Nature Neuroscience*, 18, pp. 628–630. doi: 10.1038/nn.3991.

Meschkat, M., …, and Möbius, W. (2020). “White matter integrity requires continuous myelin synthesis at the inner tongue”. *bioRxiv Preprint Server*. doi: 10.1101/2020.09.02.279612.

Meyer, N. and Rinholm, J. E. (2021). “Mitochondria in myelinating oligodendrocytes: slow and out of breath?” *Metabolites*, 11, p. 359. doi: 10.3390/metabo11060359.

Mi, S., …, and Pepinsky, R. B. (2005). “LINGO-1 negatively regulates myelination by oligodendrocytes”. *Nature Neuroscience*, 8, pp. 745–751. doi: 10.1038/nn1460.

Miller, R. H. (2002). “Regulation of oligodendrocyte development in the vertebrate CNS”. *Progress in Neurobiology*, 67, pp. 451–467. doi: 10.1016/s0301-0082(02)00058-8.

Minhas, G., …, and Anand, A. (2017). “Hypoxia in CNS pathologies: emerging role of miRNA-based neurotherapeutics and yoga based alternative therapies”. *Frontiers in Neuroscience*, 11. doi: 10.3389/fnins.2017.00386.

Miron, V. E., Kuhlmann, T. and Antel, J. P. (2011). “Cells of the oligodendroglial lineage, myelination, and remyelination”. *Biochimica et Biophysica Acta (BBA) - Molecular Basis of Disease*, 1812, pp. 184–193. doi: 10.1016/j.bbadis.2010.09.010.

Mitchell, P. (1961). “Coupling of phosphorylation to electron and hydrogen transfer by a chemi-osmotic type of mechanism”. *Nature*, 191, pp. 144–148. doi: 10.1038/191144a0.

Mitchell, R. W., …, and Hatch, G. M. (2011). “Fatty acid transport protein expression in human brain and potential role in fatty acid transport across human brain microvessel endothelial cells”. *Journal of Neurochemistry*, 117, pp. 735–746. doi: 10.1111/j.1471-4159.2011.07245.x.

Mitew, S., …, and Emery, B. (2018). “Pharmacogenetic stimulation of neuronal activity increases myelination in an axon-specific manner”. *Nature Communications*, 9, p. 306. doi: 10.1038/s41467-017-02719-2.

Miyazawa, H., …, and Miura, M. (2017). “Rewiring of embryonic glucose metabolism via suppression of PFK-1 and aldolase during mouse chorioallantoic branching”. *Development*, 144, pp. 63–73. doi: 10.1242/dev.138545.

Moccia, M., …, and Ciccarelli, O. (2019). “Advances in spinal cord imaging in multiple sclerosis”. *Therapeutic Advances in Neurological Disorders*, 12, p. 1756286419840593. doi: 10.1177/1756286419840593.

Moon, J.-S., …, and Choi, A. M. K. (2015). “mTORC1-induced HK1-dependent glycolysis regulates NLRP3 inflammasome activation”. *Cell Reports*, 12, pp. 102–115. doi: 10.1016/j.celrep.2015.05.046.

Morcos, Y., Lee, S. M. and Levin, M. C. (2003). “A role for hypertrophic astrocytes and astrocyte precursors in a case of rapidly progressive multiple sclerosis”. *Multiple Sclerosis*, 9, pp. 332–341. doi: 10.1191/1352458503ms931oa.

Morell, P. and Jurevics, H. (1996). “Origin of cholesterol in myelin”. *Neurochemical Research*, 21, pp. 463–470. doi: 10.1007/BF02527711.

Morgello, S., …, and Haber, R. S. (1995). “The human blood-brain barrier glucose transporter (GLUT1) is a glucose transporter of gray matter astrocytes”. *Glia*, 14, pp. 43–54. doi: 10.1002/glia.440140107.

Morris, L., Graham, C. F. and Gordon, S. (1991). “Macrophages in haemopoietic and other tissues of the developing mouse detected by the monoclonal antibody F4/80”. *Development*, 112, pp. 517–526.

Mukandala, G., …, and O’Connor, J. J. (2016). “The effects of hypoxia and inflammation on synaptic signaling in the CNS”. *Brain Sciences*, 6, p. 6. doi: 10.3390/brainsci6010006.

Nagy, J. I. and Rash, J. E. (2003). “Astrocyte and oligodendrocyte connexins of the glial syncytium in relation to astrocyte anatomical domains and spatial buffering”. *Cell Communication & Adhesion*, 10, pp. 401–406. doi: 10.1080/cac.10.4-6.401.406.

Nakazawa, T., …, and Benowitz, L. I. (2006). “Tumor necrosis factor-alpha mediates oligodendrocyte death and delayed retinal ganglion cell loss in a mouse model of glaucoma”. *The Journal of Neuroscience*, 26, pp. 12633–12641. doi: 10.1523/JNEUROSCI.2801-06.2006.

Nave, K.-A. (2010a). “Myelination and support of axonal integrity by glia”. *Nature*, 468, pp. 244–252. doi: 10.1038/nature09614.

Nave, K.-A. (2010b). “Myelination and the trophic support of long axons”. *Nature Reviews Neuroscience*, 11, pp. 275–283. doi: 10.1038/nrn2797.

Nave, K.-A. and Werner, H. B. (2014). “Myelination of the nervous system: mechanisms and functions”. *Annual Review of Cell and Developmental Biology*, 30, pp. 503–533. doi: 10.1146/annurev-cellbio-100913-013101.

Nehlig, A. and Pereira de Vasconcelos, A. (1993). “Glucose and ketone body utilization by the brain of neonatal rats”. *Progress in Neurobiology*, 40, pp. 163–221. doi: 10.1016/0301-0082(93)90022-k.

Neijssen, J., …, and Neefjes, J. (2005). “Cross-presentation by intercellular peptide transfer through gap junctions”. *Nature*, 434, pp. 83–88. doi: 10.1038/nature03290.

Neumann, H., Kotter, M. R. and Franklin, R. J. M. (2009). “Debris clearance by microglia: an essential link between degeneration and regeneration”. *Brain*, 132 (Pt 2), pp. 288–295. doi: 10.1093/brain/awn109.

Nikolakopoulou, P., …, and Herland, A. (2020). “Recent progress in translational engineered in vitro models of the central nervous system”. *Brain*, 143, pp. 3181–3213. doi: 10.1093/brain/awaa268.

Nimmerjahn, A., Kirchhoff, F. and Helmchen, F. (2005). “Resting microglial cells are highly dynamic surveillants of brain parenchyma in vivo”. *Science*, 308, pp. 1314–1318. doi: 10.1126/science.1110647.

Nobes, C. D., …, and Brand, M. D. (1990). “Non-ohmic proton conductance of the mitochondrial inner membrane in hepatocytes”. *The Journal of Biological Chemistry*, 265, pp. 12903–12909.

Nodin, C., Nilsson, M. and Blomstrand, F. (2005). “Gap junction blockage limits intercellular spreading of astrocytic apoptosis induced by metabolic depression”. *Journal of Neurochemistry*, 94, pp. 1111–1123. doi: 10.1111/j.1471-4159.2005.03241.x.

Norenberg, M. D., …, and Norenberg, L.-O. B. (1987). “Effects of lactic acid on astrocytes in primary culture”. *Journal of Neuropathology and Experimental Neurology*, 46, pp. 154–166. doi: 10.1097/00005072-198703000-00004.

Norton, W. T. and Poduslo, S. E. (1973). “Myelination in rat brain: changes in myelin composition during brain maturation”. *Journal of Neurochemistry*, 21, pp. 759–773. doi: 10.1111/j.1471-4159.1973.tb07520.x.

Norton, W. T. and Cammer, W. (1984). “Isolation and Characterization of Myelin”. *Myelin*. Boston, MA: Springer US, pp. 147–195. isbn: 978-1-4757-1830-0. url: https://doi.org/10.1007/978-1-4757-1830-0_5.

Nualart-Marti, A., Solsona, C. and Fields, R. D. (2013). “Gap junction communication in myelinating glia”. *Biochimica et Biophysica Acta (BBA) - Biomembranes*, 1828, pp. 69–78. doi: 10.1016/j.bbamem.2012.01.024.

O’Connor, R. S., …, and Milone, M. C. (2018). “The CPT1a inhibitor, etomoxir induces severe oxidative stress at commonly used concentrations”. *Scientific Reports*, 8, p. 6289. doi: 10.1038/s41598-018-24676-6.

O'Meara, R. W., …, and Kothary, R. (2017). "Oligodendrocyte development and CNS myelination are unaffected in a mouse model of severe spinal muscular atrophy". *Human Molecular Genetics*, 26, pp. 282–292. doi: 10.1093/hmg/ddw385.

Obrenovitch, T. P. (1995). "The ischaemic penumbra: twenty years on". *Cerebrovascular and Brain Metabolism Reviews*, 7, pp. 297–323.

Ogata, T., …, and Kataoka, K. (1995). "A possible mechanism for the hypoxia-hypoglycemia-induced release of excitatory amino acids from cultured hippocampal astrocytes". *Neurochemical Research*, 20, pp. 737–743. doi: 10.1007/BF01705543.

Orthmann-Murphy, J. L., …, and Scherer, S. S. (2007). "Loss-of-function GJA12/connexin47 mutations cause Pelizaeus-Merzbacher-like disease". *Molecular and Cellular Neurosciences*, 34, pp. 629–641. doi: 10.1016/j.mcn.2007.01.010.

Orthmann-Murphy, J. L., Abrams, C. K. and Scherer, S. S. (2008). "Gap junctions couple astrocytes and oligodendrocytes". *Journal of Molecular Neuroscience*, 35, pp. 101–116. doi: 10.1007/s12031-007-9027-5.

Osellame, L. D., Blacker, T. S. and Duchen, M. R. (2012). "Cellular and molecular mechanisms of mitochondrial function". *Best Practice & Research. Clinical Endocrinology & Metabolism*, 26, pp. 711–723. doi: 10.1016/j.beem.2012.05.003.

Owen, O. E. (2005). "Ketone bodies as a fuel for the brain during starvation". *Biochemistry and Molecular Biology Education*, 33, pp. 246–251. doi: 10.1002/bmb.2005.49403304246.

Paller, A., …, and Siegel, N. (2002). *Rudolph's Pediatrics: 21st Edition*. Appleton & Lange.

Palmer, C., Roberts, R. L. and Young, P. I. (2004). "Timing of neutrophil depletion influences long-term neuroprotection in neonatal rat hypoxic-ischemic brain injury". *Pediatric Research*, 55, pp. 549–556. doi: 10.1203/01.PDR.0000113546.03897.FC.

Pang, R., …, and Robertson, N. J. (2020). "Proton magnetic resonance spectroscopy lactate/N-acetylaspartate within 48 h predicts cell death following varied neuroprotective interventions in a piglet model of hypoxia-ischemia with and without inflammation-sensitization". *Frontiers in Neurology*, 11, p. 883. doi: 10.3389/fneur.2020.00883.

Papaneophytou, C., Georgiou, E. and Kleopa, K. A. (2019). "The role of oligodendrocyte gap junctions in neuroinflammation". *Channels*, 13, pp. 247–263. doi: 10.1080/19336950.2019.1631107.

Pardridge, W. M. and Mietus, L. J. (1980). "Palmitate and cholesterol transport through the blood-brain barrier". *Journal of Neurochemistry*, 34, pp. 463–466. doi: 10.1111/j.1471-4159.1980.tb06621.x.

Paridaen, J. T. and Huttner, W. B. (2014). “Neurogenesis during development of the vertebrate central nervous system”. *EMBO Reports*, 15, pp. 351–364. doi: 10.1002/embr.201438447.

Pedraza, L., Huang, J. K. and Colman, D. (2009). “Disposition of axonal caspr with respect to glial cell membranes: Implications for the process of myelination”. *Journal of Neuroscience Research*, 87, pp. 3480–3491. doi: 10.1002/jnr.22004.

Peinado, A., Yuste, R. and Katz, L. C. (1993). “Extensive dye coupling between rat neocortical neurons during the period of circuit formation”. *Neuron*, 10, pp. 103–114. doi: 10.1016/0896-6273(93)90246-N.

Pellerin, L. and Magistretti, P. J. (1994). “Glutamate uptake into astrocytes stimulates aerobic glycolysis: a mechanism coupling neuronal activity to glucose utilization”. *Proceedings of the National Academy of Sciences*, 91, pp. 10625–10629. doi: 10.1073/pnas.91.22.10625.

Pellerin, L., …, and Magistretti, P. J. (1998a). “Evidence supporting the existence of an activity-dependent astrocyte-neuron lactate shuttle”. *Developmental Neuroscience*, 20, pp. 291–299. doi: 10.1159/000017324.

Pellerin, L., …, and Magistretti, P. J. (1998b). “Expression of monocarboxylate transporter mRNAs in mouse brain: Support for a distinct role of lactate as an energy substrate for the neonatal vs. adult brain”. *Proceedings of the National Academy of Sciences*, 95, pp. 3990–3995. doi: 10.1073/pnas.95.7.3990.

Pellerin, L. and Magistretti, P. J. (2012). “Sweet sixteen for ANLS”. *Journal of Cerebral Blood Flow and Metabolism*, 32, pp. 1152–1166. doi: 10.1038/jcbfm.2011.149.

Pérez-Cerdá, F., Sánchez-Gómez, M. V. and Matute, C. (2015). “Pío del Río Hortega and the discovery of the oligodendrocytes”. *Frontiers in Neuroanatomy*, 9, p. 92. doi: 10.3389/fnana.2015.00092.

Pfeiffer, S. E., Warrington, A. E. and Bansal, R. (1993). “The oligodendrocyte and its many cellular processes”. *Trends in Cell Biology*, 3, pp. 191–197. doi: 10.1016/0962-8924(93)90213-K.

Philips, T. and Rothstein, J. D. (2017). “Oligodendroglia: metabolic supporters of neurons”. *The Journal of Clinical Investigation*, 127, pp. 3271–3280. doi: 10.1172/JCI90610.

Philips, T., …, and Rothstein, J. D. (2021). “MCT1 deletion in oligodendrocyte lineage cells causes late-onset hypomyelination and axonal degeneration”. *Cell Reports*, 34. doi: 10.1016/j.celrep.2020.108610.

Poitelon, Y., Kopec, A. M. and Belin, S. (2020). “Myelin fat facts: an overview of lipids and fatty acid metabolism”. *Cells*, 9, p. 812. doi: 10.3390/cells9040812.

Ponath, G., …, and Pitt, D. (2017). “Myelin phagocytosis by astrocytes after myelin damage promotes lesion pathology”. *Brain*, 140, pp. 399–413. doi: 10.1093/brain/aww298.

Pouly, S., …, and Antel, J. P. (2000). “Interferon-gamma modulates human oligodendrocyte susceptibility to Fas-mediated apoptosis”. *Journal of Neuropathology and Experimental Neurology*, 59, pp. 280–286. doi: 10.1093/jnen/59.4.280.

Pringle, N. P. and Richardson, W. D. (1993). “A singularity of PDGF alpha-receptor expression in the dorsoventral axis of the neural tube may define the origin of the oligodendrocyte lineage”. *Development*, 117, pp. 525–533. url: https://dev.biologists.org/content/117/2/525 (visited on 01/10/2021).

Probert, L., …, and Kollias, G. (1995). “Spontaneous inflammatory demyelinating disease in transgenic mice showing central nervous system-specific expression of tumor necrosis factor alpha”. *Proceedings of the National Academy of Sciences*, 92, pp. 11294–11298. doi: 10.1073/pnas.92.24.11294.

Purves, D., …, and Williams, S. M. (2001). “Increased conduction velocity as a result of myelination”. *Neuorscience*. 2nd edition. url: https://www.ncbi.nlm.nih.gov/books/NBK10921/.

Quastel, J. H. and Wheatley, A. H. M. (1933). “Oxidation of fatty acids in the liver”. *Biochemical Journal*, 27, pp. 1752.1–1762. doi: https://dx.doi.org/10.1042%2Fbj0271752.

Rae-Grant, A. D., …, and Fox, R. J. (2014). “Observations on the brain vasculature in multiple sclerosis: A historical perspective”. *Multiple Sclerosis and Related Disorders*, 3, pp. 156–162. doi: 10.1016/j.msard.2013.08.005.

Raff, M. C., …, and Noble, M. D. (1988). “Platelet-derived growth factor from astrocytes drives the clock that times oligodendrocyte development in culture”. *Nature*, 333, pp. 562–565. doi: 10.1038/333562a0.

Ralhan, I., …, and Ioannou, M. S. (2021). “Lipid droplets in the nervous system”. *Journal of Cell Biology*, 220. doi: 10.1083/jcb.202102136.

Ransom, B. R. and Kettenmann, H. (1990). “Electrical coupling, without dye coupling, between mammalian astrocytes and oligodendrocytes in cell culture”. *Glia*, 3, pp. 258–266. doi: 10.1002/glia.440030405.

Ransom, B. R., Butt, A. M. and Black, J. A. (1991). “Ultrastructural identification of HRP-injected oligodendrocytes in the intact rat optic nerve”. *Glia*, 4, pp. 37–45. doi: 10.1002/glia.440040105.

Rao, V. T. S., …, and Antel, J. P. (2017). “Distinct age and differentiation-state dependent metabolic profiles of oligodendrocytes under optimal and stress conditions”. *PLOS ONE*, 12, e0182372. doi: 10.1371/journal.pone.0182372.

Rash, J. E., …, and Yasumura, T. (1997). “Grid-mapped freeze-fracture analysis of gap junctions in gray and white matter of adult rat central nervous system, with evidence for a ”panglial syncytium” that is not coupled to neurons”. *The Journal of Comparative Neurology*, 388, pp. 265–292.

Ratcliffe, P. J., …, and Pugh, C. W. (1998). “Oxygen sensing, hypoxia-inducible factor-1 and the regulation of mammalian gene expression”. *The Journal of Experimental Biology*, 201 (Pt 8), pp. 1153–1162.

Reddy, J. K. and Hashimoto, T. (2001). “Peroxisomal beta-oxidation and peroxisome proliferator-activated receptor alpha: an adaptive metabolic system”. *Annual Review of Nutrition*, 21, pp. 193–230. doi: 10.1146/annurev.nutr.21.1.193.

Rehncrona, S., Rosén, I. and Siesjö, B. K. (1981). “Brain lactic acidosis and ischemic cell damage: 1. Biochemistry and neurophysiology”. *Journal of Cerebral Blood Flow and Metabolism*, 1, pp. 297–311. doi: 10.1038/jcbfm.1981.34.

Rehncrona, S. (1985). “Brain acidosis”. *Annals of Emergency Medicine*, 14, pp. 770–776. doi: 10.1016/S0196-0644(85)80055-X.

Rezaie, P. and Male, D. (1999). “Colonisation of the developing human brain and spinal cord by microglia: a review”. *Microscopy Research and Technique*, 45, pp. 359–382. doi: 10.1002/(SICI)1097-0029(19990615)45:6<359::AID-JEMT4>3.0.CO;2-D.

Rich, P. (2003). “The molecular machinery of Keilin’s respiratory chain”. *Biochemical Society Transactions*, 31, pp. 1095–1105. doi: 10.1042/bst0311095.

Richardson, W. D., …, and Dubois-Dalcg, M. (1988). “A role for platelet-derived growth factor in normal gliogenesis in the central nervous system”. *Cell*, 53, pp. 309–319. doi: 10.1016/0092-8674(88)90392-3.

Richardson, W. D., Kessaris, N. and Pringle, N. (2006). “Oligodendrocyte wars”. *Nature Reviews Neuroscience*, 7, pp. 11–18. doi: 10.1038/nrn1826.

Richert, S., …, and Kassmann, C. M. (2014). “In vivo labeling of peroxisomes by photoconvertible mEos2 in myelinating glia of mice”. *Biochimie*, 98, pp. 127–34. doi: 10.1016/j.biochi.2013.10.022.

Rinholm, J. E., …, and Attwell, D. (2011). “Regulation of oligodendrocyte development and myelination by glucose and lactate”. *Journal of Neuroscience*, 31, pp. 538–548. doi: 10.1523/JNEUROSCI.3516-10.2011.

Rinholm, J. E., …, and Clayton, D. A. (2016). “Movement and structure of mitochondria in oligodendrocytes and their myelin sheaths”. *Glia*, 64, pp. 810–825. doi: 10.1002/glia.22965.

Ritzel, R. M., …, and Wu, J. (2021). “Proton extrusion during oxidative burst in microglia exacerbates pathological acidosis following traumatic brain injury”. *Glia*, 69, pp. 746–764. doi: 10.1002/glia.23926.

Robinson, …, and Vaney, D. I. (1993). “Unidirectional coupling of gap junctions between neuroglia”. *Science*, 262, pp. 1072–1074. doi: 10.1126/science.8093125.

Rolfe, D. F. and Brown, G. C. (1997). “Cellular energy utilization and molecular origin of standard metabolic rate in mammals”. *Physiological Reviews*, 77, pp. 731–758. doi: 10.1152/physrev.1997.77.3.731.

Rone, M. B., …, and Antel, J. P. (2016). “Oligodendrogliopathy in multiple sclerosis: low glycolytic metabolic rate promotes oligodendrocyte survival”. *Journal of Neuroscience*, 36, pp. 4698–4707. doi: 10.1523/JNEUROSCI.4077-15.2016.

Rosenberg, S. S., …, and Chan, J. R. (2008). “The geometric and spatial constraints of the microenvironment induce oligodendrocyte differentiation”. *Proceedings of the National Academy of Sciences*, 105, pp. 14662–14667. doi: 10.1073/pnas.0805640105.

Rosenbluth, J. (1999). “A brief history of myelinated nerve fibers: one hundred and fifty years of controversy”. *Journal of Neurocytology*, 28, pp. 251–262. doi: 10.1023/A:1007083409850.

Roy, C. S. and Sherrington, C. S. (1890). “On the regulation of the blood-supply of the brain”. *The Journal of Physiology*, 11, pp. 85–158.17. doi: 10.1113/jphysiol.1890.sp000321.

Ruggieri, M. and Pike, M. (1999). “Spinal cord insults in the prenatal, perinatal, and neonatal periods”. *Developmental Medicine & Child Neurology*, 41, pp. 311–317. doi: 10.1111/j.1469-8749.1999.tb00608.x.

Rushton, W. A. H. (1951). “A theory of the effects of fibre size in medullated nerve”. *The Journal of Physiology*, 115, pp. 101–122. doi: 10.1113/jphysiol.1951.sp004655.

Rustom, A. (2004). “Nanotubular highways for intercellular organelle transport”. *Science*, 303, pp. 1007–1010. doi: 10.1126/science.1093133.

Saab, A. S., …, and Nave, K.-A. (2016). “Oligodendroglial NMDA receptors regulate glucose import and axonal energy metabolism”. *Neuron*, 91, pp. 119–132. doi: 10.1016/j.neuron.2016.05.016.

Sabri, M. I. and Ochs, S. (1971). “Inhibition of glyceraldehyde-3-phosphate dehydrogenase in mammalian nerve by iodoacetic acid”. *Journal of Neurochemistry*, 18, pp. 1509–1514. doi: 10.1111/j.1471-4159.1971.tb00013.x.

Sadler, T. W. (2005). “Embryology of neural tube development”. *American Journal of Medical Genetics*, 135C, pp. 2–8. doi: 10.1002/ajmg.c.30049.

Saher, G., …, and Nave, K.-A. (2005). “High cholesterol level is essential for myelin membrane growth”. *Nature Neuroscience*, 8, pp. 468–475. doi: 10.1038/nn1426.

Saher, G. and Stumpf, S. K. (2015). “Cholesterol in myelin biogenesis and hypomyelinating disorders”. *Biochimica Et Biophysica Acta*, 1851, pp. 1083–1094. doi: 10.1016/j.bbalip.2015.02.010.

Sánchez-Abarca, L. I., Tabernero, A. and Medina, J. M. (2001). “Oligodendrocytes use lactate as a source of energy and as a precursor of lipids”. *Glia*, 36, pp. 321–329. doi: 10.1002/glia.1119.

Sanders, T. A., Llagostera, E. and Barna, M. (2013). “Specialized filopodia direct long-range transport of SHH during vertebrate tissue patterning”. *Nature*, 497, pp. 628–632. doi: 10.1038/nature12157.

Sato, K., …, and Okajima, F. (2020). “The protective role of proton-sensing TDAG8 in the brain injury in a mouse ischemia reperfusion model”. *Scientific Reports*, 10, p. 17193. doi: 10.1038/s41598-020-74372-7.

Schindelin, J., …, and Cardona, A. (2012). “Fiji: an open-source platform for biological-image analysis”. *Nature Methods*, 9, pp. 676–82. doi: 10.1038/nmeth.2019.

Schmidt, M. and Dringen, R. (2009). “Differential effects of iodoacetamide and iodoacetate on glycolysis and glutathione metabolism of cultured astrocytes”. *Frontiers in Neuroenergetics*, 1. doi: 10.3389/neuro.14.001.2009.

Schoenfeld, R., …, and Cortopassi, G. (2010). “Oligodendroglial differentiation induces mitochondrial genes and inhibition of mitochondrial function represses oligodendroglial differentiation”. *Mitochondrion*, 10, pp. 143–150. doi: 10.1016/j.mito.2009.12.141.

Schönfeld, P. and Reiser, G. (2013). “Why does brain metabolism not favor burning of fatty acids to provide energy? - Reflections on disadvantages of the use of free fatty acids as fuel for brain”. *Journal of Cerebral Blood Flow and Metabolism*, 33, pp. 1493–1499. doi: 10.1038/jcbfm.2013.128.

Schönfeld, P. and Wojtczak, L. (2016). “Short- and medium-chain fatty acids in energy metabolism: the cellular perspective”. *Journal of Lipid Research*, 57, pp. 943–954. doi: 10.1194/jlr.R067629.

Schrader, M., …, and Fahimi, H. (1996). “Interaction of microtubules with peroxisomes. Tubular and spherical peroxisomes in HepG2 cells and their alterations induced by microtubule-active drugs”. *European Journal of Cell Biology*, 69, pp. 24–35.

Schultz, V., …, and Edgar, J. M. (2021). “Oligodendrocytes are susceptible to Zika virus infection in a mouse model of perinatal exposure: implications for CNS complications”. *Glia*, 69, pp. 2023–2036. doi: 10.1002/glia.24010.

Selmaj, K. W. and Raine, C. S. (1988). “Tumor necrosis factor mediates myelin and oligodendrocyte damage in vitro”. *Annals of Neurology*, 23, pp. 339–346. doi: 10.1002/ana.410230405.

Semenza, G. L., …, and Giallongo, A. (1996). “Hypoxia response elements in the aldolase A, enolase 1, and lactate dehydrogenase A gene promoters contain essential binding sites for hypoxia-inducible factor 1”. *The Journal of Biological Chemistry*, 271, pp. 32529–32537. doi: 10.1074/jbc.271.51.32529.

Shalak, L. and Perlman, J. M. (2004). “Hypoxic–ischemic brain injury in the term infant-current concepts”. *Early Human Development*, 80, pp. 125–141. doi: 10.1016/j.earlhumdev.2004.06.003.

Sharp, F. R. and Bernaudin, M. (2004). “HIF1 and oxygen sensing in the brain”. *Nature Reviews Neuroscience*, 5, pp. 437–448. doi: 10.1038/nrn1408.

Shi, L. Z., …, and Chi, H. (2011). “HIF1α–dependent glycolytic pathway orchestrates a metabolic checkpoint for the differentiation of TH17 and Treg cells”. *Journal of Experimental Medicine*, 208, pp. 1367–1376. doi: 10.1084/jem.20110278.

Sleigh, J. N., Gillingwater, T. H. and Talbot, K. (2011). “The contribution of mouse models to understanding the pathogenesis of spinal muscular atrophy”. *Disease Models & Mechanisms*, 4, pp. 457–467. doi: 10.1242/dmm.007245.

Smith, C. M., Mayer, J. A. and Duncan, I. D. (2013). “Autophagy promotes oligodendrocyte survival and function following dysmyelination in a long-lived myelin mutant”. *Journal of Neuroscience*, 33, pp. 8088–8100. doi: 10.1523/JNEUROSCI.0233-13.2013.

Smolič, T., …, and Vardjan, N. (2021). “Astrocytes in stress accumulate lipid droplets”. *Glia*, 69, pp. 1540–1562. doi: 10.1002/glia.23978.

Snaidero, N., …, and Simons, M. (2014). “Myelin membrane wrapping of CNS axons by PI(3,4,5)P3-dependent polarized growth at the inner tongue”. *Cell*, 156, pp. 277–290. doi: 10.1016/j.cell.2013.11.044.

Snaidero, N., …, and Simons, M. (2017). “Antagonistic functions of MBP and CNP establish cytosolic channels in CNS myelin”. *Cell Reports*, 18, pp. 314–323. doi: 10.1016/j.celrep.2016.12.053.

Snell, K. and Walker, D. G. (1973). “Glucose metabolism in the newborn rat. Temporal studies in vivo”. *Biochemical Journal*, 132, pp. 739–752. doi: 10.1042/bj1320739.

Sofroniew, M. V. and Vinters, H. V. (2010). “Astrocytes: biology and pathology”. *Acta Neuropathologica*, 119, pp. 7–35. doi: 10.1007/s00401-009-0619-8.

Sokoloff, L. (1960). *The Metabolism of the Central Nervous System in Vivo.* Vol. 3. Washington, D.C.: American Physiological Society. 1843-1864.

Somers, E., …, and Parson, S. H. (2012). “Density, calibre and ramification of muscle capillaries are altered in a mouse model of severe spinal muscular atrophy”. *Neuromuscular Disorders*, 22, pp. 435–442. doi: 10.1016/j.nmd.2011.10.021.

Somers, E., …, and Parson, S. H. (2016). “Vascular defects and spinal cord hypoxia in spinal muscular atrophy”. *Annals of Neurology*, 79, pp. 217–230. doi: 10.1002/ana.24549.

Sowinski, S., …, and Davis, D. M. (2008). “Membrane nanotubes physically connect T cells over long distances presenting a novel route for HIV-1 transmission”. *Nature Cell Biology*, 10, pp. 211–219. doi: 10.1038/ncb1682.

Stanganello, E., …, and Scholpp, S. (2015). “Filopodia-based Wnt transport during vertebrate tissue patterning”. *Nature Communications*, 6, p. 5846. doi: 10.1038/ncomms6846.

Stassart, R. M., …, and Edgar, J. M. (2018). “The axon-myelin unit in development and degenerative disease”. *Frontiers in Neuroscience*, 12, p. 467. doi: 10.3389/fnins.2018.00467.

Stöckli, K. A., …, and Sendtner, M. (1991). “Regional distribution, developmental changes, and cellular localization of CNTF-mRNA and protein in the rat brain.” *Journal of Cell Biology*, 115, pp. 447–459. doi: 10.1083/jcb.115.2.447.

Stolfi, A., …, and Levine, M. (2011). “Neural tube patterning by Ephrin, FGF and Notch signaling relays”. *Development*, 138, pp. 5429–5439. doi: 10.1242/dev.072108.

Stone, S., …, and Lin, W. (2020). “The UPR preserves mature oligodendrocyte viability and function in adults by regulating autophagy of PLP”. *JCI Insight*, 5. doi: 10.1172/jci.insight.132364.

Supplie, L. M., …, and Nave, K.-A. (2017). “Respiration-deficient astrocytes survive as glycolytic cells in vivo”. *The Journal of Neuroscience*, 37, pp. 4231–4242. doi: 10.1523/JNEUROSCI.0756-16.2017.

Susuki, K., …, and Rasband, M. N. (2013). “Three mechanisms assemble central nervous system nodes of Ranvier”. *Neuron*, 78, pp. 469–482. doi: 10.1016/j.neuron.2013.03.005.

Sutor, B. and Hagerty, T. (2005). “Involvement of gap junctions in the development of the neocortex”. *Biochimica et Biophysica Acta (BBA) - Biomembranes*, 1719, pp. 59–68. doi: 10.1016/j.bbamem.2005.09.005.

Swanson, R. A. (1992). “Astrocyte glutamate uptake during chemical hypoxia in vitro”. *Neuroscience Letters*, 147, pp. 143–146. doi: 10.1016/0304-3940(92)90580-Z.

Swanson, R. A., Farrell, K. and Stein, B. A. (1997). “Astrocyte energetics, function, and death under conditions of incomplete ischemia: A mechanism of glial death in the penumbra”. *Glia*, 21, pp. 142–153. doi: 10.1002/(SICI)1098-1136(199709)21:1<142::AID-GLIA16>3.0.CO;2-S.

Swigonová, Z., Mohsen, A.-W. and Vockley, J. (2009). “Acyl-CoA dehydrogenases: Dynamic history of protein family evolution”. *Journal of Molecular Evolution*, 69, pp. 176–193. doi: 10.1007/s00239-009-9263-0.

Takebayashi, H., …, and Nabeshima, Y.-i. (2002). “The basic helix-loop-helix factor Olig2 is essential for the development of motoneuron and oligodendrocyte lineages”. *Current Biology*, 12, pp. 1157–1163. doi: 10.1016/S0960-9822(02)00926-0.

Tasaki, I. (1939). “The electro-saltatory transmission of the nerve impulse and the effect of narcosis upon the nerve fiber”. *American Journal of Physiology*, 127, pp. 211–227. doi: 10.1152/ajplegacy.1939.127.2.211.

Tauchi-Sato, K., …, and Fujimoto, T. (2002). “The surface of lipid droplets is a phospholipid monolayer with a unique fatty acid composition”. *Journal of Biological Chemistry*, 277, pp. 44507–44512. doi: 10.1074/jbc.M207712200.

Tawk, M., …, and Massaad, C. (2011). “Wnt/beta-catenin signaling is an essential and direct driver of myelin gene expression and myelinogenesis”. *The Journal of Neuroscience*, 31, pp. 3729–3742. doi: 10.1523/JNEUROSCI.4270-10.2011.

Tekkök, S. B., …, and Ransom, B. R. (2005). “Transfer of glycogen-derived lactate from astrocytes to axons via specific monocarboxylate transporters supports mouse optic nerve activity”. *Journal of Neuroscience Research*, 81, pp. 644–652. doi: 10.1002/jnr.20573.

Tepavčević, V. (2021). “Oligodendroglial energy metabolism and (re)myelination”. *Life*, 11, p. 238. doi: 10.3390/life11030238.

Thomson, C. E., …, and McCulloch, M. C. (2006). “Murine spinal cord explants: A model for evaluating axonal growth and myelination in vitro”. *Journal of Neuroscience Research*, 84, pp. 1703–1715. doi: 10.1002/jnr.21084.

Thomson, C. E., …, and McLaughlin, M. (2008). “Myelinated, synapsing cultures of murine spinal cord – validation as an in vitro model of the central nervous system”. *European Journal of Neuroscience*, 28, pp. 1518–1535. doi: 10.1111/j.1460-9568.2008.06415.x.

Timmerman, R., Burm, S. M. and Bajramovic, J. J. (2018). “An overview of in vitro methods to study microglia”. *Frontiers in Cellular Neuroscience*, 12, p. 242. doi: 10.3389/fncel.2018.00242.

Toloe, J., …, and Mironov, S. L. (2014). “Metabolic differences in hippocampal ‘Rett’ neurons revealed by ATP imaging”. *Molecular and Cellular Neuroscience*, 59, pp. 47–56. doi: 10.1016/j.mcn.2013.12.008.

Traiffort, E., …, and Laouarem, Y. (2020). “Astrocytes and microglia as major players of myelin production in normal and pathological conditions”. *Frontiers in Cellular Neuroscience*, 14. doi: 10.3389/fncel.2020.00079.

Trapp, B. D. and Stys, P. K. (2009). “Virtual hypoxia and chronic necrosis of demyelinated axons in multiple sclerosis”. *The Lancet Neurology*, 8, pp. 280–291. doi: 10.1016/S1474-4422(09)70043-2.

Tress, O., …, and Willecke, K. (2011). “Pathologic and phenotypic alterations in a mouse expressing a connexin47 missense mutation that causes Pelizaeus-Merzbacher-like disease in humans”. *PLOS Genetics*, 7, e1002146. doi: 10.1371/journal.pgen.1002146.

Trevisiol, A., …, and Hirrlinger, J. (2020). “Structural myelin defects are associated with low axonal ATP levels but rapid recovery from energy deprivation in a mouse model of spastic paraplegia”. *PLOS Biology*, 18, e3000943. doi: 10.1371/journal.pbio.3000943.

Truett, G. e, …, and Warman, M. l (2000). “Preparation of PCR-quality mouse genomic DNA with hot sodium hydroxide and Tris (HotSHOT)”. *BioTechniques*, 29, pp. 52–54. doi: 10.2144/00291bm09.

Uhlenberg, B., …, and Gärtner, J. (2004). “Mutations in the gene encoding gap junction protein alpha 12 (connexin 46.6) cause Pelizaeus-Merzbacher-like disease”. *American Journal of Human Genetics*, 75, pp. 251–260. doi: 10.1086/422763.

Valério-Gomes, B., …, and Lent, R. (2018). “The absolute number of oligodendrocytes in the adult mouse brain”. *Frontiers in Neuroanatomy*, 12. doi: 10.3389/fnana.2018.00090.

Vaney, D. I. (1991). “Many diverse types of retinal neurons show tracer coupling when injected with biocytin or Neurobiotin”. *Neuroscience Letters*, 125, pp. 187–190. doi: 10.1016/0304-3940(91)90024-N.

Van Tilborg, E., …, and Nijboer, C. H. (2018). “Origin and dynamics of oligodendrocytes in the developing brain: Implications for perinatal white matter injury”. *Glia*, 66, pp. 221–238. doi: 10.1002/glia.23256.

Vartanian, T., …, and Stefansson, K. (1995). “Interferon-gamma-induced oligodendrocyte cell death: implications for the pathogenesis of multiple sclerosis”. *Molecular Medicine*, 1, pp. 732–743.

Vasenkova, I., Luginbuhl, D. and Chiba, A. (2006). “Gliopodia extend the range of direct glia-neuron communication during the CNS development in Drosophila”. *Molecular and Cellular Neurosciences*, 31, pp. 123–130. doi: 10.1016/j.mcn.2005.10.001.

Verkhratsky, A. and Butt, A. (2013). *Glial Physiology and Pathophysiology*. John Wiley & Sons. 556 pp. isbn: 978-1-118-40205-4. url: 10.1002/9781118402061.

Vignais, P. M., Gallagher, C. H. and Zabin, I. (1958). “Activation and oxidation of long chain fatty acids by rat brain”. *Journal of Neurochemistry*, 2, pp. 283–287. doi: 10.1111/j.1471-4159.1958.tb12375.x.

Vinken, P. J., Bruyn, G. W. and Moser, H. W. (1996). *Neurodystrophies and Neurolipidoses*. Vol. 22. Elsevier Health Sciences.

Volk, M. E., Millington, R. H. and Weinhouse, S. (1952). “Oxidation of endogenous fatty acids of rat tissues in vitro”. *The Journal of Biological Chemistry*, 195, pp. 493–501.

Volpe, J. J. (2001). “Neurobiology of periventricular leukomalacia in the premature infant”. *Pediatric Research*, 50, pp. 553–562. doi: 10.1203/00006450-200111000-00003.

Volpe, J. J. (2009). “Brain injury in premature infants: a complex amalgam of destructive and developmental disturbances”. *The Lancet Neurology*, 8, pp. 110–124. doi: 10.1016/S1474-4422(08)70294-1.

Waak, J. and Dringen, R. (2006). “Formation and rapid export of the monochlorobimane–glutathione conjugate in cultured rat astrocytes”. *Neurochemical Research*, 31, pp. 1409–1416. doi: 10.1007/s11064-006-9192-x.

Waitt, A. E., …, and Brown, A. M. (2017). “Emerging roles for glycogen in the CNS”. *Frontiers in Molecular Neuroscience*, 10, p. 73. doi: 10.3389/fnmol.2017.00073.

Wallraff, A., …, and Steinhäuser, C. (2004). “Distinct types of astroglial cells in the hippocampus differ in gap junction coupling”. *Glia*, 48, pp. 36–43. doi: 10.1002/glia.20040.

Wang, S., …, and Barres, B. A. (1998). “Notch receptor activation inhibits oligodendrocyte differentiation”. *Neuron*, 21, pp. 63–75. doi: 10.1016/s0896-6273(00)80515-2.

Wang, Y., …, and Zhang, Y. (2011). “Tunneling-nanotube development in astrocytes depends on p53 activation”. *Cell Death & Differentiation*, 18, pp. 732–742. doi: 10.1038/cdd.2010.147.

Warshaw, J. B. and Terry, M. L. (1976). “Cellular energy metabolism during fetal development: VI. Fatty acid oxidation by developing brain”. *Developmental Biology*, 52, pp. 161–166. doi: 10.1016/0012-1606(76)90016-6.

Wasseff, S. K. and Scherer, S. S. (2011). “Cx32 and Cx47 mediate oligodendrocyte:astrocyte and oligodendrocyte: oligodendrocyte gap junction coupling”. *Neurobiology of disease*, 42, pp. 506–513. doi: 10.1016/j.nbd.2011.03.003.

Wegner, M. (2008). “A matter of identity: transcriptional control in oligodendrocytes”. *Journal of Molecular Neuroscience*, 35, pp. 3–12. doi: 10.1007/s12031-007-9008-8.

Weinhouse, S., Millington, R. H. and Volk, M. E. (1950). “Oxidation of isotopic palmitic acid in animal tissues”. *The Journal of Biological Chemistry*, 185, pp. 191–200.

Welte, M. A. and Gould, A. P. (2017). “Lipid droplet functions beyond energy storage”. *Biochimica Et Biophysica Acta (BBA) - Molecular and Cell Biology of Lipids*, 1862 (10 Pt B), pp. 1260–1272. doi: 10.1016/j.bbalip.2017.07.006.

Wender, R., …, and Ransom, B. R. (2000). “Astrocytic glycogen influences axon function and survival during glucose deprivation in central white matter”. *The Journal of Neuroscience*, 20, pp. 6804–6810. doi: 10.1523/jneurosci.20-18-06804.2000.

White, C. J., …, and Wolfgang, M. J. (2020). “Determining the bioenergetic capacity for fatty acid oxidation in the mammalian nervous system”. *Molecular and Cellular Biology*, 40. doi: 10.1128/MCB.00037-20.

Wiemer, E., …, and Subramani, S. (1997). “Visualization of the peroxisomal compartment in living mammalian cells: dynamic behavior and association with microtubules”. *Journal of Cell Biology*, 136, pp. 71–80. doi: 10.1083/jcb.136.1.71.

Willecke, K., …, and Söhl, G. (2002). “Structural and functional diversity of connexin genes in the mouse and human genome”. *Biological Chemistry*, 383, pp. 725–737. doi: 10.1515/BC.2002.076.

Williams, L. R. and Leggett, R. W. (1989). “Reference values for resting blood flow to organs of man”. *Clinical Physics and Physiological Measurement*, 10, pp. 187–217. doi: 10.1088/0143-0815/10/3/001.

Wu, Y., …, and Stevens, B. (2015). “Microglia: dynamic mediators of synapse development and plasticity”. *Trends in Immunology*, 36, pp. 605–613. doi: 10.1016/j.it.2015.08.008.

Wyss, M. T., …, and Weber, B. (2011). “In vivo evidence for lactate as a neuronal energy source”. *Journal of Neuroscience*, 31, pp. 7477–7485. doi: 10.1523/JNEUROSCI.0415-11.2011.

Yan, H. and Rivkees, S. A. (2006). “Hypoglycemia influences oligodendrocyte development and myelin formation”. *NeuroReport*, 17, pp. 55–59. doi: 10.1097/01.wnr.0000192733.00535.b6.

Ye, F., …, and Lu, Q. R. (2009). “HDAC1 and HDAC2 regulate oligodendrocyte differentiation by disrupting the β-catenin–TCF interaction”. *Nature Neuroscience*, 12, pp. 829–838. doi: 10.1038/nn.2333.

Ye, J., …, and Madden, T. L. (2012). “Primer-BLAST: a tool to design target-specific primers for polymerase chain reaction”. *BMC Bioinformatics*, 13, p. 134. doi: 10.1186/1471-2105-13-134.

Ye, P. and D’Ercole, A. J. (1999). “Insulin-like growth factor I protects oligodendrocytes from tumor necrosis factor-α-induced injury”. *Endocrinology*, 140, pp. 3063–3072. doi: 10.1210/endo.140.7.6754.

Yeung, M. S. Y., …, and Frisén, J. (2014). “Dynamics of oligodendrocyte generation and myelination in the human brain”. *Cell*, 159, pp. 766–774. doi: 10.1016/j.cell.2014.10.011.

Young, K. E., …, and Reynolds, J. M. (2017). “Fatty acid synthase regulates the pathogenicity of Th17 cells”. *Journal of Leukocyte Biology*, 102, pp. 1229–1235. doi: 10.1189/jlb.3AB0417-159RR.

Young, K. M., …, and Richardson, W. D. (2013). “Oligodendrocyte dynamics in the healthy adult CNS: evidence for myelin remodeling”. *Neuron*, 77, pp. 873–885. doi: 10.1016/j.neuron.2013.01.006.

Yuen, T. J., …, and Rowitch, D. H. (2014). “Oligodendrocyte-encoded HIF function couples postnatal myelination and white matter angiogenesis”. *Cell*, 158, pp. 383–396. doi: 10.1016/j.cell.2014.04.052.

Zawadzka, M., …, and Franklin, R. J. M. (2010). “CNS-resident glial progenitor/stem cells produce Schwann cells as well as oligodendrocytes during repair of CNS demyelination”. *Cell Stem Cell*, 6, pp. 578–590. doi: 10.1016/j.stem.2010.04.002.

Zhang, Z.-A., Nonaka, H. and Hatori, T. (1997). “The microvasculature of the spinal cord in the human adult”. *Neuropathology*, 17, pp. 32–42. doi: 10.1111/j.1440-1789.1997.tb00008.x.

Zhang, Y., …, and Wu, J. Q. (2014). “An RNA-sequencing transcriptome and splicing database of glia, neurons, and vascular cells of the cerebral cortex”. *Journal of Neuroscience*, 34, pp. 11929–11947. doi: 10.1523/jneurosci.1860-14.2014.

Zhao, X., …, and Lu, Q. R. (2010). “MicroRNA-mediated control of oligodendrocyte differentiation”. *Neuron*, 65, pp. 612–626. doi: 10.1016/j.neuron.2010.02.018.

Zhou, Q., Choi, G. and Anderson, D. J. (2001). “The bHLH transcription factor Olig2 promotes oligodendrocyte differentiation in collaboration with Nkx2.2”. *Neuron*, 31, pp. 791–807. doi: 10.1016/s0896-6273(01)00414-7.

Ziabreva, I., …, and Mahad, D. (2010). “Injury and differentiation following inhibition of mitochondrial respiratory chain complex IV in rat oligodendrocytes”. *Glia*, 58, pp. 1827–1837. doi: 10.1002/glia.21052.

Ziemka-Nalecz, M., …, and Sypecka, J. (2018). “Impact of neonatal hypoxia-ischaemia on oligodendrocyte survival, maturation and myelinating potential”. *Journal of Cellular and Molecular Medicine*, 22, pp. 207–222. doi: 10.1111/jcmm.13309.

Zonta, B., …, and Brophy, P. J. (2008). “Glial and neuronal isoforms of Neurofascin have distinct roles in the assembly of nodes of Ranvier in the central nervous system”. *Journal of Cell Biology*, 181, pp. 1169–1177. doi: 10.1083/jcb.200712154.